Understanding UK Air Quality with a Chemistry Transport Model

Luke Fakes

Doctor of Philosophy

University of York

Chemistry

September 2023

Abstract

Ambient air pollution exposure was associated with 4.2 million premature deaths globally in 2019. In the UK, it is considered the single biggest environmental health issue, with particular concern regarding pollution from nitrogen dioxide (NO_2), Ozone (O_3) and Particulate Matter ($PM_{2.5}$). Numerical representations (models) allow us to interrogate our understanding of processes controlling pollution but are inherently simplified representations. This work uses the GEOS-Chem atmospheric chemistry transport model run in both its nested and stretched grid configuration to extend our understanding of air pollution over the UK.

Compared to observations, the model systematically underestimates Nitrogen Oxides (NO_x) in non-rural environments, potentially due to spatial resolution. This underestimate could lead to an overestimation of O_3 concentrations in these environments, but is balanced by a model underestimate in background O_3 flowing into the UK. It is estimated that 78% of UK O_3 comes from outside of the UK. Reducing UK NO_x emissions increases wintertime O_3 by reducing NO titration, and reduces overall summertime O_3 production. Higher spatial resolutions reduce bias and improve correlations with observations for both NO_x and O_3, due to better representation of local emissions and lower O_3 production rates.

Despite capturing the average concentrations of ammonia and sulphur dioxide reasonably, model overestimates in inorganic aerosols lead to an overestimate of $PM_{2.5}$. Changes to Industrial SO_2 emission injection heights improve estimates for SO_2, with small improvements for $PM_{2.5}$ and aerosol sulfate (SO_4^{2-}). Population-weighted $PM_{2.5}$ violates both the WHO 5 μgm^{-3} and UK's 10 μgm^{-3} guidelines in the standard model. Removal of all UK anthropogenic and agricultural emissions reduces the population exceeding the WHO guideline from 95% to 27%, but highlights the challenge of complying with the guideline. Higher spatial resolutions increase $PM_{2.5}$ bias overall, but model-observation correlations continue to improve with higher resolutions.

Contents

List of Tables

List of Figures

Acknowledgements

I first thank my supervisors, Mat Evans and Ally Lewis. Mat, you are the reason I came to do a PhD, it's been great to work with you and I can't thank you enough for the all guidance and support you've given me. I'm thankful for the friendship offered by the Evans group and from everyone in the Wolfson Atmospheric Chemistry Laboratories (WACL), you've made this experience such a great chapter in my life.

To Ryan and Killian, your expertise and patience has got me through many a challenge. Without it, I'm sure I'd still be stuck on any number of problems.

To my esteemed colleague, Lucy. Your company and positivity have made the last few years so much easier. I hope I can offer the same to you and that there are more years to come.

Finally, thanks to my parents for their consistent support and encouragement throughout my long academic journey, it's been invaluable.

This project was undertaken on the Viking Cluster, which is a high performance compute facility provided by the University of York. We are grateful for computational support from the University of York High Performance Computing service, Viking and the Research Computing team. Thank you to NCAS for funding my PhD research, and allowing me this opportunity.

Authors Declaration

I declare that this thesis is a presentation of original work and I am the sole author. This work has not previously been presented for a degree or other qualification at this University or elsewhere. All sources are acknowledged as references.

1   Introduction

1.1   The importance of Air Quality

Exposure to poor air quality is one of the greatest environmental risks to health globally. The issue is so prevalent that the WHO reported that almost all (99%) of the global population breathe air that exceeds WHO guideline limits, leading to an estimated 4.2 million premature deaths in 2019 (`https://www.who.int/news-room/fact-sheets/detail/ambient-(outdoor)-air-quality-and-health`; last access 06/08/2023). However, air pollution and its health impacts are not a new problem. As early as 400 BC, Hippocrates made the association of illness with poor air quality, observing that the inhabitants of cities exposed to damp westerly winds were "likely to have deep, hoarse voices, because of the atmosphere, since it is usually impure and unhealthy in such places" (Jones et al., 1927). Whilst natural processes and meteorology (transport) also play a role, anthropogenic activity is dominant. These human contributions to air pollution are associated with 28,000 to 36,000 deaths each year in the UK, making it the largest environmental risk to UK public health (`https://www.gov.uk/government/publications/air-pollution-applying-all-our-health/air-pollution-applying-all-our-health`; last access 30/07/2023).

This chapter will first describe the vertical structure of the Earth system (Section 1.2), before discussing the chemistry, sources and sinks of common air pollutants in the UK (Section 1.4). The complexity of these processes requires the use of numerical models to represent them. Section 1.5 broadly discusses these models. However, gaps and errors in our understanding of these processes means model fidelity needs to be assessed to understand their weaknesses. Section 1.6 will introduce some of the UK air quality research undertaken with CTMs. Finally, Section 1.7 will outline the aims and structure of this thesis.

1.2   Atmospheric Structure

The Earth's atmosphere is a layer of gases, predominantly Nitrogen (N_2), Oxygen (O_2), water vapour and Argon (Ar) bound to the planet's surface by gravity. A vast number of trace gases, solid and liquid aerosol particles are also present, but at considerably smaller concentrations. The complex interplay of these trace species is of pivotal concern due to their effects on the climate, human and plant health.

The Earths' atmosphere is vertically partitioned based on its temperature profile (Jacob, 1999), which is shown in Figure 1 along with the atmospheric layers it defines. At the surface, the lowest layer is called the troposphere and extends from the surface to 16-18 km in the tropics and 8-12 km in higher latitudes. Within this layer, temperature is highest at the surface due to solar heating and decreases gradually at a rate of 6.5 K km^{-1} from the combined effect of radiation, convection and heat release from water condensation up until a temperature minimum called the tropopause. The troposphere is further divided into the planetary boundary layer (PBL), which extends up to 1-3 km from the surface, and the free troposphere above it (Brasseur and Jacob, 2017). Compressional heating due to a general slow sinking motion in the free troposphere typically creates a subsidence inversion that both limits the height of the PBL and restricts mixing between the PBL and free troposphere. Turbulent eddies from mechanical and buoyant turbulence drive vertical mixing within the PBL. These result in stronger mixing and a less stable boundary layer diurnal profile over land than oceans, where changes in surface temperature are comparatively smaller (Stull, 1988).

The stratosphere lies above the tropopause, extending up to the stratopause at around 50 km altitude and is characterised by temperature increases with height due to the absorption of solar energy by the ozone layer (Manabe and Strickler, 1964). The temperature inversion in the stratosphere makes it stable against vertical transport and limits the mixing with the troposphere below (Holton
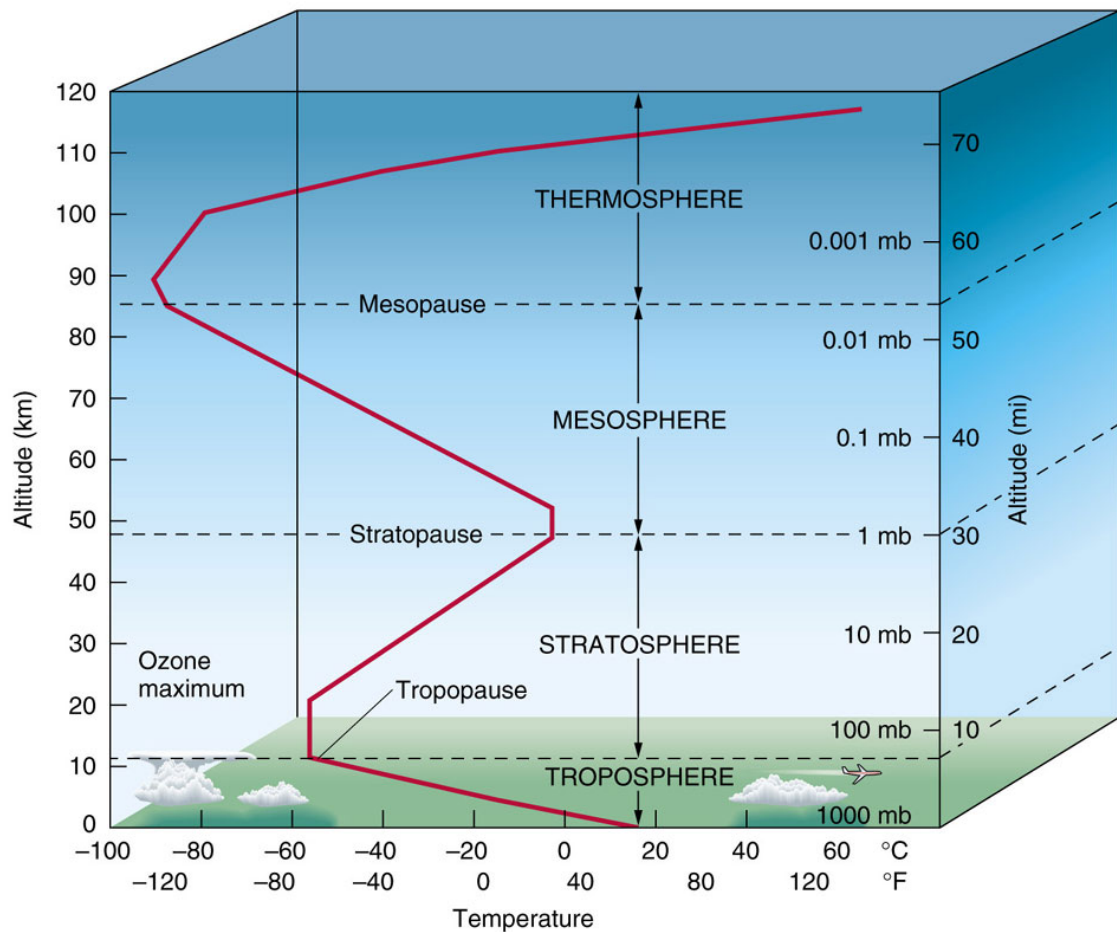
Figure 1: The vertical structure of the atmosphere and mean vertical profile of air temperature (red line). From Aguado and Burt (2013), copyright © Pearson Education.

et al., 1995). The mesosphere sits above the stratopause and extends up to the mesopause at around 100 km altitude. Here, temperature once again decreases with altitude due to radiative cooling by CO_2 when there is little ozone available to absorb solar radiation. Next, temperature increases rapidly with height in the thermosphere due to the absorption of strong UV radiation by O_2, N_2 and O.

Around 80% of the atmosphere's mass lies within the troposphere, so understanding the processes which drive its composition is of central importance for air quality research and all human exposure.

1.3 Emission Processes

Emissions from the land and oceans lead to a large range of gases and particles with varying emission rates based on their sources. Despite the large quantity of non-anthropogenic emission sources, there is little doubt that emissions from human activity (e.g fossil fuel combustion, industrial processes, transport and agriculture) are an important factor in poor ambient air quality (WHO, 2016; Manisalidis et al., 2020; Gaffney and Marley, 2009; Lelieveld et al., 2015). Early awareness of the detrimental effect of human contribution on the atmosphere brought about international protocols and directives such as the Montreal Protocol (1987) and the Gothenburg Protocol (1999). As Figure 2 illustrates for continental Europe and the surrounding regions these interventions have led to substantial reductions in emissions of several significant air pollutants between 1990 and 2016. Whilst there has been significant efforts made over decades to reduce emissions of NO_x, SO_x, and NVMOCs, efforts to reduce NH_3 emissions have been relatively small.
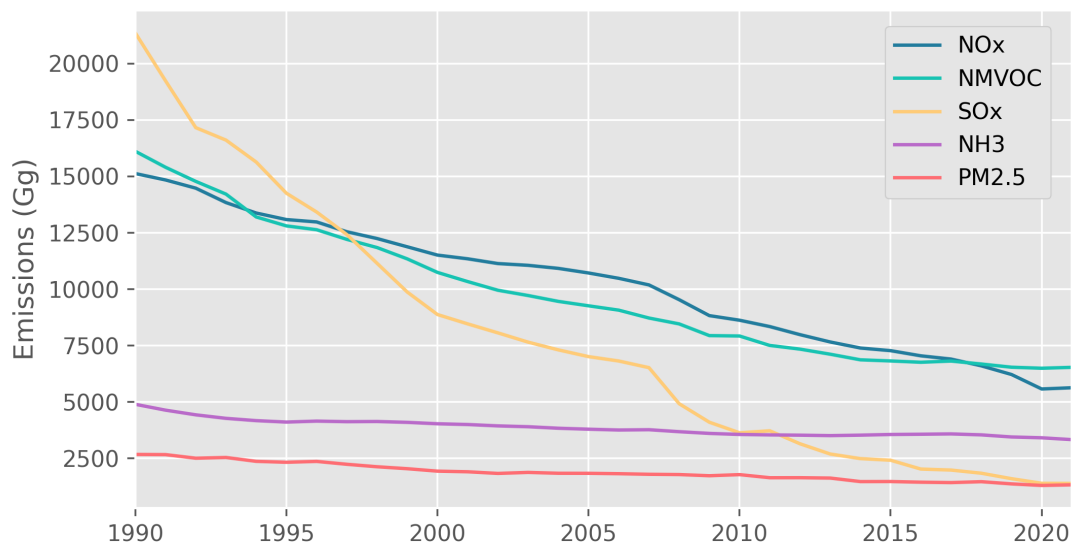
Figure 2: Emission trends for NO_x (blue), Non-Methane Volatile Organic Compounds (green), SO_x (yellow), NH_3 (purple) and $PM_{2.5}$ (red) from the EU27 from 1990 to 2021 period. Data: `www.eea.europa.eu/data-and-maps/`; last access 01/08/2023).

The transport and lifetime of trace gases is impacted by the vertical profile of emissions sources (De Meij et al., 2006; Mailler et al., 2013). Whilst some an-

thropogenic sources such as road transport and domestic combustion are generally considered to be emitted entirely at the surface, others like industrial activity, energy production and aviation have higher effective emission heights (Pregger and Friedrich, 2009). Emission injection height uncertainty varies by emission species, but have been shown to have impact on both air quality and climtate (Guevara et al., 2014; Yang et al., 2019).

1.4   Chemical Processes in the Troposphere

Much of atmospheric chemistry is driven by the reactions of radical species. Solar radiation provides a large source of radicals in the atmosphere by photolytic cleavage. The simplest example of this is the formation of the hydroxyl radical (OH) by the reaction of water vapour with electronically excited oxygen ($O(^1D)$) formed from ozone photolysis (R1 and R2) (Lelieveld and Crutzen, 1990). Whilst this is the main source of tropospheric OH, the photolysis of nitrous acid (HONO), formaldehyde and carbonyls are other sources of radicals (Atkinson, 2000).

$$O_3 + h\nu \longrightarrow O(^1D) + O_2 \tag{R1}$$

$$O(^1D) + H_2O \longrightarrow 2\,OH \tag{R2}$$
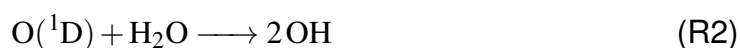
Hydroxyl is a strong oxidant, which reacts with carbon monoxide (CO), methane (CH_4), other organic compounds (RH) and NO_2 to form peroxy radicals (HO_2, RO_2) which go on to oxidise additional species (R3-R5).

$$CO + OH \xrightarrow{O_2} CO_2 + HO_2 \tag{R3}$$

$$CH_4 + OH \xrightarrow{O_2} CH_3O_2 + HO_2 \tag{R4}$$

$$RH + OH \xrightarrow{O_2} RO_2 + HO_2 \tag{R5}$$
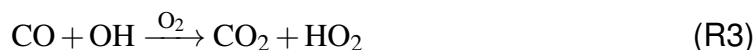
OH can be regenerated from the reaction of nitric oxide (NO) with HO_2 (R6):

$$NO + HO_2 \longrightarrow NO_2 + OH \tag{R6}$$

or indirectly from the reaction of NO with RO_2 (R7) via alkoxy radicals (RO) (Jenkin et al., 2019), followed by oxidation (hydrogen abstraction) by O_2 to form carbonyls (RCHO) and HO_2 (R8). Alternatively, RO can undergo isomerization or decomposition reactions:

$$NO + RO_2 \longrightarrow NO_2 + RO \tag{R7}$$

$$RO \xrightarrow{O_2} RCHO + HO_2 \tag{R8}$$

The dominant HO_x (HO_x = OH + HO_2) sink is the production of hydrogen peroxide H_2O_2 from the HO_2 + HO_2 self-reaction (R9) followed by deposition or conversion to water (R10). Organic peroxides can also be formed in the same way.

$$HO_2 + HO_2 \longrightarrow H_2O_2 \tag{R9}$$

$$H_2O_2 + OH \xrightarrow{M} HO_2 + H_2O \tag{R10}$$
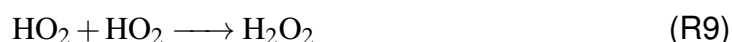
But photolysis of H_2O_2 means it can also act as a HO_x reservoir (R11).

$$H_2O_2 + h\nu \longrightarrow 2\,OH \tag{R11}$$

1.4.1   Nitrogen Oxides

Nitrogen oxides (NO_x = NO + NO_2) are emitted by combustion, lightning (Schumann and Huntrieser, 2007) and microbial processes in soils (Hall et al., 1996). Most NO_x emissions are in the form of NO, although there is a small NO_2 component (EPA, 1999). High-temperature combustion in the presence of oxygen results in the formation of nitric oxide from N_2, which can react with O_3 to form NO_2 (R12). However, during the daytime photolysis of NO_2 results in rapid interconversion back to NO (R13 and R14). These reactions result in a null cycle and an equilibrium between NO and NO_2 during the daytime.

$$NO + O_3 \longrightarrow NO_2 + O_2 \tag{R12}$$

$$NO_2 + h\nu \xrightarrow{\lambda < 400 \text{ nm}} NO + O(^3P) \tag{R13}$$

$$O(^3P) + O_2 \longrightarrow O_3 \tag{R14}$$
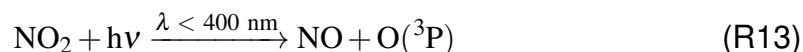
The dominant loss process for NO_x species in the troposphere is conversion to nitric acid (HNO_3) followed by wet or dry deposition, via reaction with OH during the day (reaction R15) (Stavrakou et al., 2013):

$$NO_2 + OH + M \longrightarrow HNO_3 + M \tag{R15}$$
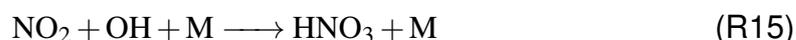
At night, NO_2 oxidation by O_3 to form NO_3 (R16), and subsequent reaction with NO_2 forms dinitrogen pentoxide (N_2O_5) (R17). N_2O_5 can undergo heterogeneous hydrolysis on aerosol particles, forming HNO_3 (R18) (Dentener and Crutzen, 1993; Ehhalt and Drummond, 1982).

$$NO_2 + O_3 \longrightarrow NO_3 + O_2 \tag{R16}$$

$$NO_2 + NO_3 + M \longrightarrow N_2O_5 + M \tag{R17}$$

$$N_2O_5 + H_2O\,(l) \xrightarrow{\text{aerosol}} 2\,HNO_3\,(l) \tag{R18}$$
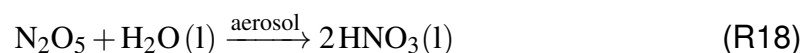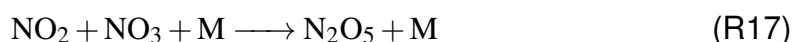
N_2O_5 acts as a nighttime NO_x reservoir, as N_2O_5 can thermally decompose back to NO_3 and NO_2.

NO_2 itself is a respiratory irritant. Acute exposure can lead to coughing and difficulty breathing, whilst chronic exposure may contribute to the development of asthma and increase susceptibility to respiratory infections (Wolfe and Patz, 2002) Additional air quality issues due to NO_x come from the potential to produce other harmful secondary pollutants like O_3 (Section 1.4.3) and aerosols (1.4.6).

1.4.2 VOCs

Atmospheric chemists refer to the vast number of organic species present in the gas phase as volatile organic compounds (VOCs). They are mainly emitted as hydrocarbons from biogenic sources (e.g isoprene, monoterprenes) (Guenther et al., 2012), from industrial processes and from combustion (Pandey and Yadav, 2018), and their main reactions are oxidation to ultimately produce CO and CO_2. Methane (CH_4) is usually considered separately because of it's relatively long lifetime (around 10 years) against oxidation compared to other organic species. The term Non-Methane Volatile Organic Compounds (NMVOCs) is often used to make this distinction. Although oxidation by OH radicals (R5) is their primary sink, NMVOCs also react with other atmospheric oxidants like O_3, NO_3 and halogen atoms, decompose by photolysis, and directly deposit to surfaces (Mellouki et al., 2015).

Air quality issues from VOCs are primarily the result of their ability to form secondary pollutants. An important example is the reaction of RO_2 with NO (R7) to facilitate O_3 production by NO_2 photolysis. This will be further discussed in Section 1.4.3. In addition, atmospheric VOCs can form secondary organic aerosols (SOA), which have significant implications on global climate and health(Section 1.4.6). Reaction R7 is limited by the availability of NO. Thus, at low NO_x concentrations there is an additional sink of RO_2 by reaction with HO_2 (R19) to form organic peroxides, and providing a sink for HO_x radicals.

$$RO_2 + HO_2 \longrightarrow ROOH + O_2 \tag{R19}$$

1.4.3 Ozone

Ozone (O_3) has variable impacts depending on its height in the atmosphere. Stratospheric ozone is produced by photolysis of O_2, and works beneficially to protect life by reducing UV exposure in the "ozone layer" (Henriksen et al., 1990). Net downward transport of high concentrations of stratospheric O_3 provides a

source of tropospheric ozone (Logan, 1985). However, the dominant source of tropospheric O_3 is the HO_x and NO_x-catalyzed photochemical oxidation of VOCs and CO by O_2, exceeding the stratospheric source by a factor of 5-7 (Young et al., 2013). It is because of this behaviour that global increases in background ozone concentrations are mainly attributed to human activity (Volz and Kley, 1988). At the surface, O_3 is a respiratory irritant which is harmful to human health, damaging to plants (Davison and Barnes, 1998) and buildings(Screpanti and De Marco, 2009), and a component of photochemical smog (Sillman, 2003).

O_3 loss occurs by photolysis (R1 and R2) and reactions with HO_x radicals (R20 and R21), or a small contribution from deposition to the surface.

$$O_3 + OH \longrightarrow HO_2 + O_2 \tag{R20}$$

$$O_3 + HO_2 \longrightarrow OH + 2O_2 \tag{R21}$$

Catalytic cycles with halogens (Cl, Br, I, denoted X) provide another route to O_3 destruction (Chameides and Davis, 1980), such as via R22 and R23, where R24 is the net reaction:

$$O_3 + X \longrightarrow XO + O_2 \tag{R22}$$

$$XO + O \longrightarrow X + O_2 \tag{R23}$$

$$Net: O + O_3 \longrightarrow 2O_2 \tag{R24}$$

In most of the troposphere, where NO_x concentrations are low due to its short lifetime, O_3 production by RO_2 + NO (R7 and R6) compete with reactions to form peroxides. In this "NO_x-limited" regime, O_3 production increases linearly with NO_x concentration, with no dependence on VOC concentration. An alternate O_3 production regime occurs at high NO_x concentrations, where the dominant HO_x sink is nitric acid formation. In this "NO_x-saturated" (or "VOC-limited") regime, O_3 production rate increases linearly with VOC concentration and inversely with NO_x concentration. Figure 3 illustrates the relationship between VOC and NO_x con-

centrations and O_3 concentration. VOC-limited regimes are characteristic of urban areas due to the typically higher NO_x concentration, whereas less urbanised and remote areas are often NO_x-limited (Sillman, 1995; Jaeglé et al., 1998).
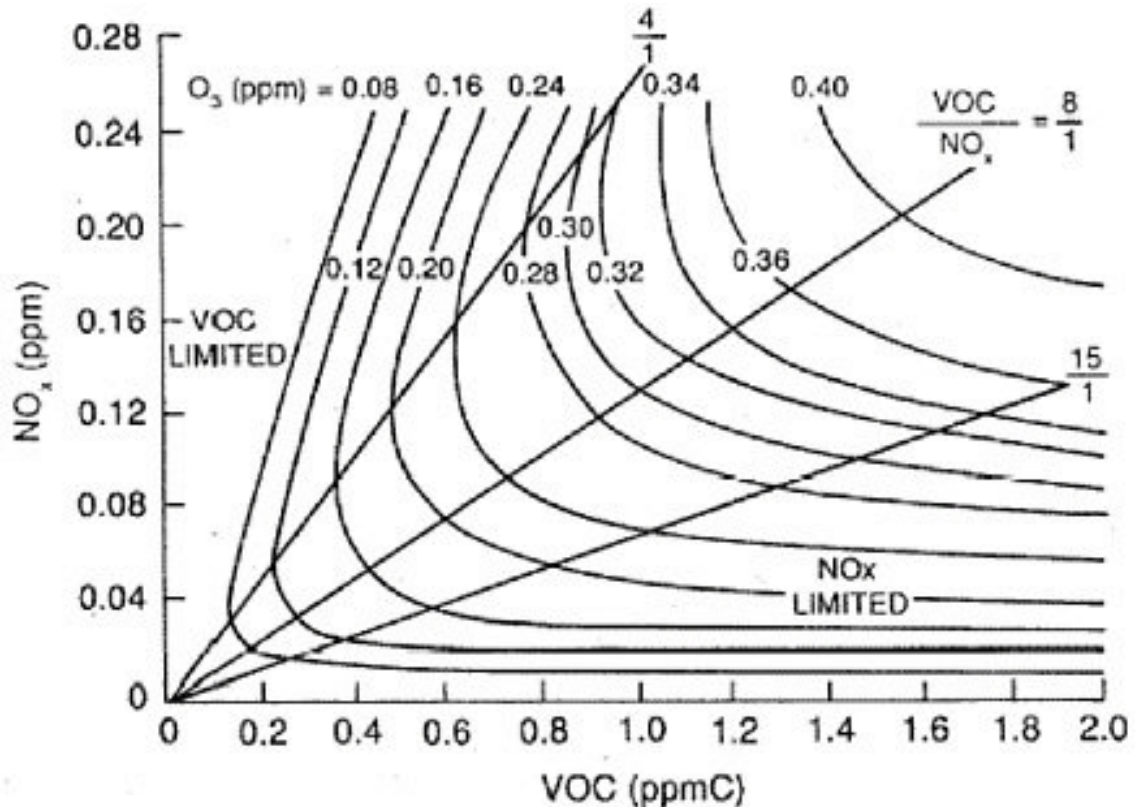
Figure 3: An O_3 isopleth based on box model calculations, showing the dependence of O_3 concentration on NO_x and VOC concentrations. Source: National Research Council (1992).

1.4.4   Sulfur Dioxide

Air pollution from SO_2 can directly cause harm to human-health with only short-term exposure (Orellano et al., 2021). Oxidation of SO_2 to sulfate provides additional detrimental environmental impacts including the acidification through wet deposition to aquatic and terrestrial ecosystems and climate impacts via acting as cloud-condensation nuclei and interacting with shortwave radiation (Kiehl and Briegleb, 1993). The major global sources of SO_2 are anthropogenic emissions from fossil fuel combustion-namely power generation and shipping- and industrial activity (Cullis and Hirschler, 1980). These sources also emit a small fraction

directly as sulfate (Chin et al., 2000). Although regulations have effectively reduced anthropogenic SO_2 emissions in Europe and the USA in recent decades (Figure 2), emissions are increasing in other parts of the world (Forster et al., 2007). Volcanic emissions of SO_2 and biogenic emissions of dimethylsulfide (DMS, $(CH_3)_2S$) are natural sources of sulfur compounds (Cullis and Hirschler, 1980). Oxidation to sulfate is the major atmospheric sink for SO_2, and proceeds by reaction with OH in the gas phase or with either H_2O_2 or O_3 in the aqueous phase (R25, R26). The aqueous phase reaction is believed to account for in the region of 80% of sulfate production globally (Faloona, 2009). Gaseous sulfuric acid (H_2SO_4) from the gas-phase reaction is a major precursor of new aerosol particles through the reaction with ammonia (NH_3) and amines (Zhang et al., 2012b).

$$HSO_3{}^- + H_2O_2(aq) + H^+ \longrightarrow SO_4{}^{2-} + H_2O + 2\,H^+ \qquad \text{(R25)}$$

$$SO_3{}^{2-} + O_3(aq) \longrightarrow SO_4{}^{2-} + O_2 \qquad \text{(R26)}$$
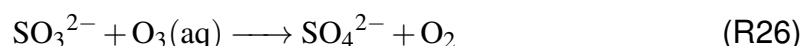
1.4.5   Ammonia

NH_3 is the dominant form of reduced nitrogen in the atmosphere and the most abundant alkaline gas in the atmosphere (Behera et al., 2013). It reacts with acidic aerosols to form $PM_{2.5}$ (Section 1.4.6) (Behera and Sharma, 2010; Sharma et al., 2007). Further, NH_x (sum of NH_3, particulate and aqueous ammonium) negatively affects ecosystems through direct exposure, soil acidification and water eutrophication (Aneja et al., 2001, 2008). Agricultural sources and in particular livestock manure management and mineral fertilizer use, account for around 70% of total global NH_3 emissions (Sutton et al., 2013). In the UK, this figure was 87% in 2021 (`https://www.gov.uk/government/statistical-data-sets/` `env01-emissions-of-air-pollutants`; last access 31/12/2023). Additional anthropogenic sources of NH_3 are from waste management, energy production of from the use of NH_3 or urea precursors in selective catalytic reduction (SCR) systems in vehicle exhausts. Emissions from soils, oceans, biomass burning and sea birds provide natural emissions (Behera et al., 2013). It has been reported

that reducing NH_3 emissions would most effectively reduce $PM_{2.5}$ both in the UK (Vieno et al., 2016b) and globally (Gu et al., 2021). However, there has only been small reductions in NH_3 emissions since 2005 despite reductions in other PM precursors (`https://www.eea.europa.eu/publications/national-emission-red uction-commitments-directive-2023`; last access 06/08/2023). The impact of NH_3 will increase as the climate warms due to increased volatilisation of ammonia emissions (Sutton et al., 2013). NH_3 is removed from the atmosphere by wet or dry deposition or conversion to aerosols.

1.4.6 Particulate Matter and aerosols

As well as gaseous species, aerosols (suspended solid or liquid particles in a gas) are present in the atmosphere with a range of sizes. They are important because of their effects on the climate and public health (Charlson et al., 1992; Tie et al., 2009; Seinfeld, 2004). Whilst atmospheric aerosols can have both primary (direct emission) and secondary (formed in the atmosphere) sources, aerosol loss occurs mostly via wet deposition and some by dry deposition. Depending on aerosol properties and meteorological conditions, aerosol lifetimes can vary from hours to weeks (Pöschl, 2005). From a public health perspective focus is often on Particulate Matter (PM) with a radius of less than 2.5 μm ($PM_{2.5}$).

PM chemical composition, concentration and size distributions vary substantially based on the sources, lifetimes and transport of its component species. Whilst there are minor components such as trace metals and pollen, the predominant components of PM are organic carbon (OC), black carbon (BC), sulfate, nitrate and ammonium aerosol, Dust and Sea Salt (Andreae and Rosenfeld, 2008). Anthropogenic emissions are responsible for the majority of these components, as well as some natural and biogenic sources (Andreae and Rosenfeld, 2008).

Whilst H_2SO_4 can form aerosol particles on it's own, aerosol sulfate and nitrate are often associated with ammonium, and both are important components of

PM that should be considered. These will be referred to collectively as secondary inorganic aerosol (SIA) or sulfate-nitrate-ammonium aerosol (SNA). Secondary inorganic aerosols are formed by the neutralisation of nitric acid (HNO_3) or H_2SO_4 (from SO_2 and NO_x oxidation) by NH_3 to form ammonium nitrate (NH_4NO_3), ammonium bisulfate (NH_4HSO_4) and ammonium sulfate (($NH_4)_2SO_4$) (R27, R28, R29). Neutralisation of H_2SO_4 is preferentially neutralised by NH_3 before HNO_3, so the amount of ammonium nitrate can depend on availability of ammonia.

$$HNO_3(g) + NH_3(g) \rightleftharpoons NH_4NO_3(a) \tag{R27}$$

$$H_2SO_4(a) + NH_3(g) \longrightarrow NH_4HSO_4(a) \tag{R28}$$

$$NH_4HSO_4(a) + NH_3(g) \longrightarrow (NH_4)_2SO_4(a) \tag{R29}$$

In some European cities, SNA is reported to contribute 40% of total $PM_{2.5}$ (Sillanpää et al., 2006). Sulfate aerosol concentrations declined in Europe between 1990 and 2010, attributable to the reductions in precursor SO_2 emissions (Figure 2). However, despite large reductions in NO_x emissions over the same period, aerosol nitrate concentrations did not reduce as much as expected (Ciarelli et al., 2019). This may be due to the inadvertent increase in "free ammonia" which reduced the effect of emissions reductions on aerosol nitrate concentrations. Consequently, the importance of reducing NH_3 emissions to lower aerosol nitrate has been stressed in recent years (Deutsch et al., 2008; Gu et al., 2021; Wyer et al., 2022).

Carbonaceous aerosols are categorised into a black carbon (BC) and organic carbon (OC) component. BC (often described as soot) is emitted into the atmosphere by incomplete combustion of fuels. Road transport, industrial activity, domestic fuel use and shipping were the largest sources of BC in the UK in 2017. BC efficiently absorbs light. As a result, it is thought to be the dominant light absorbing aerosol in many regions (Rosen et al., 1978). OC is composed of an array of compounds with a range of volatilities and sources. It comprises Primary

Organic Aerosol (POA), where particles are directly emitted from the sources and Secondary Organic Aerosol (SOA), where particles are formed in the gas phase. Secondary organic aerosol can be be further categorised intro biogenic and anthropogenic in origin (BSOA and ASOA), although the two are not always mutually exclusive (Kanakidou et al., 2000). POA has both natural sources such as biomass burning, soil resuspension and anthropogenic sources such as agricultural activity, energy, transport and residential combustion (Daellenbach et al., 2020; Samaké et al., 2020). Consequently, emission controls can directly reduce POA, so being able to distinguish between POA and SOA is vital. SOA formation is initiated by the gas-phase oxidation of organic compounds to from semivolatile products with functional groups that reduce their volatility, enabling their uptake to pre-existing organic or aqueous particles. This source of SOA was estimated to be between 140 and 910 Tg yr^{-1} (Goldstein and Galbally, 2007). Approximately 10^6 compounds are thought to be involved (Goldstein and Galbally, 2007), and this combined with the chemical complexity of SOA formation leads to large uncertainties in global SOA yields (Harley et al., 1992; Goldstein and Galbally, 2007; Matsui et al., 2009). Despite this uncertainty, the current consensus appears to be that the biogenic contribution to SOA dominates (Guenther et al., 2012), although biogenic SOA formation can be facilitated by anthropogenic emissions (Goldstein et al., 2009). The climate impacts of SOA are due to the ability to scatter and absorb radiation and to influence the number of cloud condensation nuclei (CCN) particles.

The sea salt aerosol component of particulate matter is mainly produced by bursting bubbles during whitecap formation in the open-ocean and waves breaking in the surface zone (Monahan et al., 1986; Goroch and Geernaert, 1995). Sea salt aerosol is the main source of tropospheric reactive chlorine (Cl_y^*) and bromine (Br_y^*) to the marine boundary layer, which can have impacts on global ozone and OH concentrations and methane lifetime and radiative forcing (Horowitz et al., 2020).

Dust describes a suspension of mineral particles which can influence the Earth's radiative balance, act as efficient cloud condensation nuclei, and contribute to air pollution by direct contribution to PM and indirectly elevating non-dust anthropogenic pollutants by altering atmospheric circulation and influencing the transport and removal of atmospheric pollutants (Yang et al., 2017; Xia et al., 2022). Long-range transport of sand from arid and semi-arid regions is the main natural dust source, with a minor local soil contribution. Because of the emission dependence on meteorology and its subsequent transport, the natural dust contribution to PM varies globally according to meteorological conditions. Anthropogenic dust from human activities (e.g tyre wear, construction, industrial activity) are another source, and are characterised by high concentrations of toxic heavy metals (e.g Pb, Zn, Co, As) (Dytłow and Górka-Kostrubiec, 2021). In the UK, whilst there is an anthropogenic dust source, large natural sources (e.g the Sahara) are farther away. Despite this, natural sources from the Sahara can contribute in part to PM pollution episodes in the UK (Vieno et al., 2016a).

1.5   Chemical Transport Models

Our ability to understand and make predictions of atmospheric composition is challenged by the complexity of the chemical, transport, production (emissions) and loss (e.g wet and dry deposition) processes which take place in the atmosphere. Numerical representations are required to represent the evolution of interacting chemicals in the atmosphere. These systems are known as chemical transport models (CTMs). In essence, this numerical representation is a coupled set of continuity equations that describe the mass conservation for chemical species, in the general form of Equation 1 (Brasseur and Jacob, 2017).

$$\frac{\delta C_i}{\delta t} = E_i - \nabla \cdot p_i v + P_i - L_i - D_i \tag{1}$$

Here, the local evolution of the mixing ratio, *C*, for a species *i*, is sum of the emission (E_i), transport (flux divergence,$\nabla \cdot p_i v$), chemical production P_i and loss L_i, and Deposition (D_i) processes. The production and loss terms can also be affected by meteorological processes. CTMs can be broadly divided into "online" or "offline" models depending on how they handle meteorology. Many CTMs are offline models, such as the Unified European Monitoring and Evaluation, EMEP (Simpson et al., 2012a), and GEOS-Chem (Bey et al., 2001). In offline CTMs, 3-D time dependent meteorology data are provided as a CTM input. In contrast, online models like the Weather Research and Forecasting model with Chemistry, WRF-Chem (Grell et al., 2005), integrate the calculation of meteorology with the solving of the chemical continuity equations, fully coupling chemical transport with dynamics and the hydrological cycle and removing the added error from time-averaging of offline meteorology data. However, using offline meteorology tends to have a lower computational cost and can offer a standardised framework for model intercomparisons (Grell and Baklanov, 2011). Table 1 provides a brief comparison of several of the mentioned online and offline chemical transport models.

Model	Species	Meteorology	Reference
EMEP	70	Offline	Simpson et al. (2012a)
WRF-Chem	117	Online	Grell et al. (2005)
GEOS-Chem	158	Offline	Bey et al. (2001)
MOZART	85	Offline	Emmons et al. (2010)

Table 1: Summary of several online and offline models, with the approximate number of gaseous species simulated by default. Note: The number of simulated species can vary between model versions and configurations.

CTM estimates of the state of the atmosphere can vary due to differences in areas including their inputs (e.g initial conditions, emissions, meteorology, scaling), process parameterization, complexity of chemistry and resolutions. Resolution can vary based on target application-e.g single-country and regional versus global models (Mircea et al., 2019; Lin et al., 2017). Smaller-scale models such as the EMEP4UK model (Vieno et al., 2005) typically operating at a finer horizontal resolution than global models such as the model for ozone and related chemical tracers, MOZART (Brasseur et al., 1998), because of input resolution limitations and concerns for computational resources usage. However, improvements in high performance and parallel computing have made high resolution global simulations more feasible. Model resolution is known to be an important factor when simulating fast processes or those occurring over a small area, so there is a need to run CTMs at a sufficiently fine resolution for each research objective. For example, Wang et al. (2023) simulated urban air pollution in Hong Kong at 33 m resolution by coupling the online WRF-Chem model with a Large Eddy Simulation (LES) model. Nested simulations, where a "fine" resolution simulation is nested within one or multiple regions within a relatively "coarse" global simulation (see Section 2.6) can bridge the resolution gap between regional and global models.

To accurately simulate the introduction of species into the Earth's atmosphere, CTMs incorporate emissions data. This can represent natural sources such as biomass burning, sea salt spray and plant emissions, as well as contributions from anthropogenic activity. However, models are susceptible to biases and uncertainties in these input emissions, which limit their ability to accurately simulate air quality.

Whilst the ability of CTMs to simulate surface air quality continues to improve, a comparative measure of their performance is required. For the UK, this typically involves observation from surface measurement networks or satellites. Although

satellite-derived evaluations can provide enhanced spatial coverage compared to ground-based measurements, observations are restricted by overpass times and can be limited by the obscuring effect of clouds, ground albedo, coarse temporal, horizontal and vertical resolutions, and uncertainties in the retrievals (Vijayaraghavan et al., 2008).

1.6   Modelling UK Air Quality

A range of CTMs have been used to explore air quality in the UK, investigating areas including emissions (Solazzo et al., 2021; Marais et al., 2021), deposition (Dore et al., 2015; Hardacre et al., 2021; Jonson et al., 2022), pollution events (Yu et al., 2008; Vieno et al., 2014) and broader model evaluations (Chemel et al., 2010; Dore et al., 2015; Garstin, 2017; Solazzo et al., 2017).

Dore et al. (2015) evaluated annual mean concentrations at rural and semi-rural UK sites for gaseous NO_2, NH_3, SO_2, HNO_3, and aerosol SO_4^{2-}, NO_3^- and NH_4^+ at resolutions from 5-50 km for 7 CTMs of varying complexity. The models could reasonably capture the spatial distribution of the species assessed (average Pearson correlation, *r*, for all models and species of 0.65-0.93), but normalised mean bias (NMB) varied between models. Overall, they reported that although simpler models could give a good representation of gaseous species concentrations, more complex models which used dynamic meteorology and more detailed photochemistry could better represent aerosol concentrations. They also highlighted the influence of systematic biases in the evaluation due to large uncertainties in measurement techniques.

Quantifying and communicating model uncertainties from model evaluations can be challenging. As a collaboration between the third phase of the Air Quality Model Evaluation International Initiative (AQMEII3) and the Hemispheric Transport of Air Pollutants (HTAP) initiatives, Solazzo et al. (2017) attempt to evaluate

and error apportion an ensemble of CTMs over European and North American domains. Assessing O_3, CO, SO_2, NO, NO_2, PM_{10}, $PM_{2.5}$, wind speed and temperature, they identified sources of model biases. Importantly, they reaffirmed the substantial impacts of model inputs (emissions, meteorology and boundary conditions) and the poor representation of vertical mixing within stable boundary layers on model bias.

Identifying the key drivers of air pollution is an important application for CTMs. Vieno et al. (2014) used the EMEP4UK regional chemical model to assess the contribution of domestic emissions and long-range transport on secondary inorganic aerosols and PM over the UK, both in the long-term (2001-2010) and during three pollution events in 2003. The drivers behind PM and high secondary inorganic aerosol pollution episodes were found to vary for different periods. However, up to 60% of particulate nitrate was estimated to be imported from outside of the UK under specific conditions. Further, the close proximity of the South and South East UK to mainland Europe make them particularly susceptible to these external contributions. Limited frequency and availability of measurements can present a challenge when there is need to validate models to support their findings. Although in this work the EMEP4UK model was shown to reproduce the long-term concentrations of SNA, comparisons were limited to only 4 sites recording monthly measurements. Whilst CTMs can fill in gaps where monitoring networks cannot feasibly cover, lack of appropriate measurements makes it challenging to quantify and communicate model uncertainty.

1.7   Summary

Whilst surface measurements do provide valuable information about the air quality, they have their own issues when trying to understand air quality. Although the UK has a comprehensive surface measurement network its spatial coverage is inherently limited. Simulations with chemical transport models can address this

gap and help to answer other pertinent questions about UK air quality. This thesis will address three such questions using the GEOS-Chem chemical transport model, which is described in Chapter 2. Firstly, how well we can simulate UK surface air quality with GEOS-Chem (Chapter 3)? Secondly, what are the contributions of key emissions sources and source regions on UK air quality, and how linear are their contributions (Chapter 4)? Thirdly, what is the effect of horizontal resolution on model performance over the UK for NO_x, O_3 and $PM_{2.5}$ (Chapter 5)?

2   GEOS-Chem

2.1   The GEOS-Chem Chemical Transort Model

This work will use the GEOS-Chem CTM as described by Bey et al. (2001). The following section will detail the GEOS-Chem Classic (GCC) implementation of GEOS-Chem used in Chapters 3 and 4, whilst Chapter 5 will introduce the GEOS-Chem High Performance implementation. GEOS-Chem uses offline meteorology data from the Goddard Earth Observation System (GEOS) of the NASA Global Modeling Assimilation Office (GMAO). There are two meteorology products available from GEOS (1) the GEOS Forward-Processing (GEOS-FP) operational data, starting in 2012, at $0.25°\times0.3125°$ horizontal resolution (2) the MERRA-2 reanalysis product, available for 1979-present at $0.5°\times0.625°$ horizontal resolution. Both archives have 72 verticals levels, and 3-hourly temporal resolution for 3-D fields and 1-hour resolution for 2-D fields. Default timesteps are optimised to balance speed and accuracy as detailed by Philip et al. (2016). GEOS-Chem simulations can be conducted at either 72 or 47 vertical levels by coarsening the resolution in the stratosphere and mesosphere. Vertical grid centres extend from 0.058 km above the surface to 78.146 km at 72-level resolution and 72.18 km at 47 level-resolution (`http://wiki.seas.harvard.edu/geos-chem/index.php/GEOS-Chem_vertical_grids#Comparisons_of_vertical_grids_used_by_GEOS-Chem;` last access 26/08/2023).

2.2   Emissions

The Harmonised Emission Component (HEMCO, Keller et al. (2014)) handles all model emissions in GEOS-Chem at runtime. HEMCO determines emissions for different sources, regions and species at any spatial and temporal resolution, and applies any scaling factors and masks. GEOS-Chem versions after v13.1.0

use the updated version, HEMCO 3.0 (Lin et al., 2021), which includes improvements to facilitate implementation into other atmospheric chemistry models and improved capability for calculating emissions at any model resolution.

The default anthropogenic emissions in the model are from Community Emissions Data System (CEDS) v2.0 (McDuffie et al., 2020), with Tzompa-Sosa et al. (2017) and Xiao et al. (2008) replacing ethane and propane emissions respectively. Fine anthropogenic dust emissions are from the Anthropogenic, Fugitive, Combustion and Industrial Dust (AFCID) emissions of Philip et al. (2017). Emissions are vertically distributed by sector following the Hemispheric CMAQ model. The Aviation Emissions Inventory Code (AEIC) 2005 inventory of Stettler et al. (2011) provides aviation emissions. To account for O_3 and HNO_3 production within shipping emission plumes, NO_x emissions from shipping are processed by the PARANOx plume-in-grid module of Vinken et al. (2011), updated by Holmes et al. (2014).

The model uses online lightning NO_x emissions (Murray et al., 2012), and grid-independent (offline) emissions for dust (Meng et al., 2021), sea salt and soil NO_x (Weng et al., 2020). Offline biogenic emissions are provided by Model of Emissions of Gases and Aerosols from Nature (MEGAN) v2.1 (Guenther et al., 2012). Emissions from open fires use the GFED4.1 inventory (Randerson et al., 2017). Oceanic emissions of DMS (Breider et al., 2017) and acetaldehyde (Millet et al., 2010) were included, with NH_3 emissions from the ocean adapted from Global Emission InitiAtive (GEIA) (Bouwman et al., 1997) and arctic seabirds (Croft et al., 2016). Table 2 summarises the resolutions for these inventories.

Inventory	Resolution	Reference
CEDS v2.0	0.5°×0.5°	McDuffie et al. (2020)
AFCID	0.25°×0.3125°	Philip et al. (2017)
AEIC	0.625°×0.5°	Stettler et al. (2011)
Dust	0.25°×0.25°	Meng et al. (2021)
Sea Salt	0.25°×0.3125°	Weng et al. (2020)
Soil NO_x	0.25°×0.3125°	Weng et al. (2020)
MEGAN v2.1	0.25°×0.3125°	Guenther et al. (2012)
Oceanic DMS	1°×1°	Breider et al. (2017),
Oceanic Acetaldehyde	1°×1°	Millet et al. (2010)
GFED 4.1	0.25°×0.25°	Randerson et al. (2017)
GEIA oceanic NH_3	1.0°×1.0°	Bouwman et al. (1997)
Arctic seabirds (NH_3)	0.25°×0.25°	Croft et al. (2016)

Table 2: Summary of the resolutions for input emissions of some of the default emissions inventories in GEOS-Chem.

2.3   Transport and Deposition Processes

GCC uses the TPCORE advection algorithm of Lin and Rood (1996) on the meteorological data grid, and calculates convective transport using archived convective mass fluxes from the GEOS met fields (Wu et al., 2007). Planetary boundary layer (PBL) mixing uses the non-local scheme described by Lin and McElroy (2010) and offline PBL height data again from the met fields. Wet deposition for water-soluble aerosols uses the scheme described by Liu et al. (2001), and by Amos et al. (2012) for gases. Dry deposition is based off the resistance-in-series scheme of Wesely, implemented by Wang et al. (1998). Prior to version 13.3.0, aerosol dry deposition uses the scheme from Zhang et al. (2001), whilst more recent versions use revised the size-dependent scheme of Emerson et al. (2020), which captures he importance of interception as a component of dry deposition and accurately considers the role of turbulence on deposition. Additional updates have been made to aerosol deposition to snow and ice (Fisher et al., 2011), gravitational settling for dust (Duncan Fairlie et al., 2007) and coarse sea salt (Alexander et al., 2005), sea salt deposition (Jaeglé et al., 2011), cold-temperature HNO_3 deposition (Jaeglé et al., 2018) and O_3 deposition to the ocean (Pound et al., 2020).

2.4   Gas-phase Chemistry

The gas-phase chemical mechanism in the model represents O_x, HO_x, NO_x, VOC and halogen chemistry in the troposphere and the stratosphere and has 228 species and 724 reactions (Shen et al., 2020). The Kinetics Pre-Processor, KPP (Damian et al., 2002; Sandu and Sander, 2006), generates code for solving chemical kinetics for a given set of reactions and rate constants. GEOS-Chem versions after v14.1.0 use KPP 3.0 (Lin et al., 2023), which includes the option to use an adaptive chemical solver. Chemical kinetics generally follow JPL/UIPAC recommendations but go beyond the recommendations for some aspects e.g tropospheric halogen chemistry (Wang et al., 2021; Sherwen et al., 2016; Chen et al., 2017), isoprene (Bates and Jacob, 2019), aromatics (Bates et al., 2021) and criegees (Millet et al., 2015).

Photolysis rates are calculated using the FAST-JX v7.0 photolysis mechanism (Bian and Prather, 2002), implemented in the troposphere by Mao et al. (2010) and in the stratosphere by Eastham et al. (2014). The approximate random overlap method represents fractional cloud optical depths (Liu et al., 2006, 2009).

2.5   Aerosols in GEOS-Chem

Aerosol representation in GEOS-Chem varies by species (Park et al., 2004). Gas to aerosol phase partitioning for the sulfate-nitrate-ammonium (SNA) aerosols uses the ISORROPIA II thermodynamic model (Fountoukis and Nenes, 2007). Primary organic carbon and black carbon are represented in hydrophilic (OCPI, BCPI) and hydrophobic (OCPO, BCPO) modes. There are two schemes available to represent organic aerosol (OA). In the default "simple SOA" scheme, primary OA is modelled as non-volatile and SOA is approximated by irreversible formation using fixed yields (Pai et al., 2020). The alternative "complex" scheme simulates POA as semi-volatile, uses the volatility basis set approach of (Pye et al., 2010)

for non-isoprene SOA, and includes an aqueous uptake mechanism to model isoprene SOA (Marais et al., 2016). In addition, there is an option to emit marine POA following Gantt et al. (2015). All simulations in this work will use the simple SOA scheme. Sea salt aerosol is represented as either fine or coarse mode (Jaeglé et al., 2011), and dust is represented using four size bins (Duncan Fairlie et al., 2007). In version 13.2.0, 12 aerosol-borne trace metals are also simulated (Xu et al., 2019). Modelled $PM_{2.5}$ is calculated based on aerosol concentration and relative humidity (RH)-dependent hygroscopic growth factors (at 35% by default) based on Latimer and Martin (2019), with the addition of a PM_{10} diagnostic in version 13.4.0 (Zhai et al., 2021).

2.6 Nested Grid Simulations

Chapters 3 and 4 use the nested capability of GEOS-Chem first implemented and described by Wang et al. (2004) and its FlexGrid functionality (`https://wiki.seas.harvard.edu/geos-chem/index.php/FlexGrid#Overview`; last access 22/08/2023). The nested capability enables finer horizontal resolution over a user-defined regional domain with dynamic boundary conditions from a coarser global simulation. FlexGrid allows the use of any defined nested domain without the need for pre-processing of data files at runtime. Figure 4 displays a schematic representation of the nested capability. Nested grid simulations follow a two step process. First, a coarse global simulation (typically $4°\times5°$) is run to output a set of boundary conditions which are fed to the model every 3 hours to provide species concentrations at the boundaries of the nested grid region. Second, the boundary conditions are provided as additional input for the higher resolution simulation over the nested domain. All operations (chemistry, dry deposition, convection and PBL mixing) except TPCORE advection are applied within a 'buffer zone' of 3 grid boxes along each boundary of the nested grid.
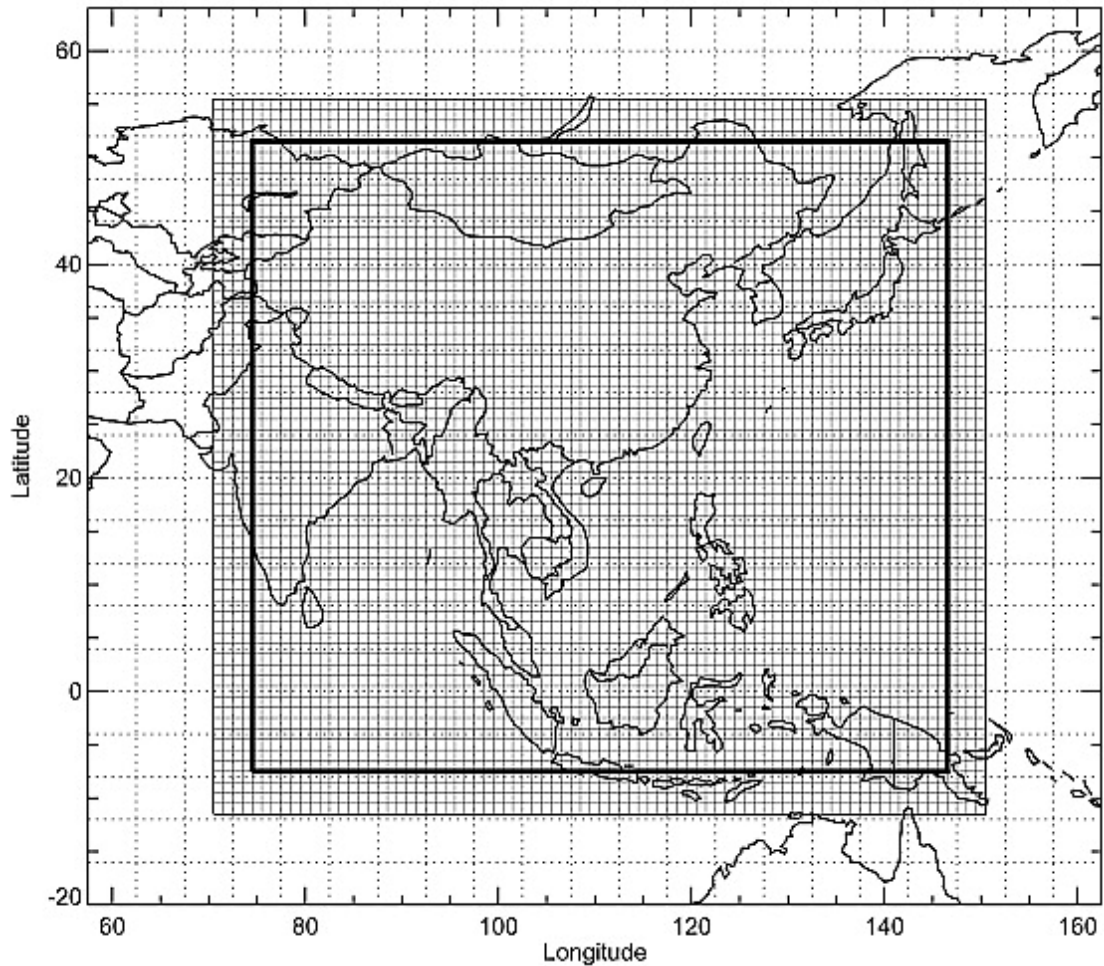
Figure 4: Representation of the GEOS-Chem nested grid over Asia, reproduced from Wang et al. (2004). The coarse global grid at $4°\times5°$ (dotted lines) and higher resolution nested domain spanning 40.5°– 41.5° N, 115.5°–116.5° E at $1°\times1°$ (thin solid lines) are overlayed. The thick black line marks the end of the nested region. Outside of this region, the $1°\times1°$ gridboxes indicate the buffer zone for boundary conditions.

3   Evaluation of the GEOS-Chem model over the UK in 2017

3.1   Introduction

Deaths due to ambient air pollutant exposure in 2016 are calculated at 4,200,000 globally and 21,000 for the United Kingdom (UK) (WHO, 2018). Regulation and emissions control over the last 50 years have brought down the concentration of air pollutants over the UK, but in 2021 the UK government's Department for Environment, Food and Rural Affairs (DEFRA) still reported failures to comply with regulation for some compounds (DEFRA, 2022a). The UK complies with regulations for Sulfur Dioxide (SO_2), Carbon Monoxide (CO), Benzene (C_6H_6), Lead (Pb), Arsenic (As), and Cadmium (Cd). Particulate Matter with diameter less than 10 μm (PM_{10}) and particulate matter less than 2.5 μm ($PM_{2.5}$) concentrations are below current regulatory limits, however, these limits are currently being re-evaluated and concentrations are unlikely to comply with future regulation (House of Lords, 2022; AQEG, 2022; Harrison et al., 2021). All UK monitoring areas complied with the 1-hour limit value of 200 μgm^{-3} for Nitrogen Dioxide (NO_2) concentration, but some exceeded the annual mean limit value of 40 μgm^{-3}. Ozone (O_3) concentrations in the UK meet their short-term targets (less than ten exceedances of maximum daily 8-hour mean (MDA8) > 100 μgm^{-3}), but many areas fail to meet their long-term targets (no more than 25 days where MDA8 $\geq$ 120 μgm^{-3} averaged over 3 years) (AQEG, 2021, 2022). Nickel (Ni) and Benzo[a]pyrene (B[a]P) concentrations also exceed targets at some locations (DEFRA, 2021).

The dominant concern in the UK is the concentration of NO_2 (DEFRA, 2022a). NO_2 exposure causes airway inflammation and decreased immune defence leading to a number of health impacts (WHO, 2021). NO_2, together with nitric oxide (NO), is collectively known as NO_x. NO_x is emitted into the atmosphere, mainly as NO, where it is rapidly oxidised through reaction with O_3 to produce NO_2. Anthro-

pogenic NO_x emissions are mainly from fossil fuel combustion from sources such as vehicles, power plants and industrial sources (McDuffie et al., 2020), while non-anthropogenic sources include lightning, soil and biomass burning (Delmas et al., 1997). Chemical loss of NO_x leads to the production of nitric acid (HNO_3), either through the reaction of NO_2 with OH during the day, or through the production of N_2O_5 at night followed by its hydrolysis on aerosol surfaces. There is also a minor dry deposition loss (Stavrakou et al., 2008; Zhang et al., 2012a). The relatively short chemical lifetime of NO_x (on the order of a few hours (Sillman, 1999)) limits its transport, leading to large spatiotemporal heterogeneity.

NO_x can also lead to the production of other harmful air pollutants. The oxidation of volatile organic compounds (VOCs), methane (CH_4) and carbon monoxide (CO) can produce peroxy radicals (HO_2, RO_2), which in the presence of NO, leads to the production of O_3. O_3 is a respiratory irritant of concern (DEFRA, 2022a). With no primary emission sources, tropospheric O_3 concentrations are determined by photochemical production and loss rates, transport and deposition processes. Although O_3 pollution is a major concern in some parts of the world (Wang et al., 2022), the low solar flux over the UK results in relatively low concentration over the UK hence compliance with its short-term standards (DEFRA, 2022a). However, the relatively long lifetime of O_3 (months) means that its long-range (> 1000 km) transport can be important for meeting air quality guidelines (Derwent and Parrish, 2022). Compliance with the UK long-term concentration regulations may require consideration of emissions well beyond the UK.

The nitric acid (HNO_3) produced from NO_x emissions, can result in the production of fine mode nitrate aerosol (NO_3^-) especially when gas-to-particle partitioning is favoured by the presence of ammonia to produce ammonium nitrate. On average, 16% of UK $PM_{2.5}$ mass is attributed to nitrate, and 7% to ammonium (AQEG, 2015). Another important source of $PM_{2.5}$ comes from the conversion of SO_2 into sulfuric acid (H_2SO_4). SO_2 emissions have dropped rapidly in the UK due to de-

sulfurization technology on coal power stations, the replacement of coal power stations by gas and renewables, and by the reduction in the domestic burning of coal. This has resulted in the UK complying with its SO_2 air quality standards (DEFRA, 2022a). However, although SO_2 emissions have reduced substantially, the sulfuric acid that it produces still constitutes 8% of the $PM_{2.5}$ mass over the UK as aerosol sulfate (AQEG, 2015). Again NH_3 supports this partitioning due to the production of ammonium sulfate. Agricultural emissions accounted for 87.8 % of UK ammonia (NH_3) emissions in 2017, with small contributions from waste and fuel combustion activities (`https://naei.beis.gov.uk/data`; last access 10/07/2023). These agricultural emissions are associated with animal management practices and nitrogen fertilizer use (Hellsten et al., 2008). The aerosol sulfate-nitrate-ammonia system is complex thermodynamically, resulting in sulfuric acid uptake being preferred over nitric acid and the potential for uptake to be limited by available ammonia (Fountoukis and Nenes, 2007).

Another important source of $PM_{2.5}$ comes from organic compounds. Over the UK, organic mass is thought to constitute about 33-44% of total $PM_{2.5}$ (AQEG, 2015). The emission and oxidation of volatile organic compounds (VOCs, typically hydrocarbons) results in the production of oxygenated compounds often with a significantly lower volatility than the parent VOC. As this oxidation continues, the oxidation products have a sufficiently low volatility that the aerosol phase is favoured over the gas. Both anthropogenic (petrochemicals and combustion) and biogenic (mainly associated with trees) emission is thought to contribute to the organic fraction of $PM_{2.5}$ (Donahue et al., 2009; Derwent et al., 2010; Redington and Derwent, 2013). Biogenic emissions are highly temperature and sunlight dependent resulting in larger summer time emissions than winter (Simpson et al., 1995; Wagner and Kuttler, 2014).

The chemical coupling of the NO_2, O_3 and PM air quality problems makes understanding the processes controlling concentration in both the gas and aerosol

phase difficult. The system has a number of non-linear components with local, regional and long-range influences on concentration. Atmospheric Chemistry Transport Models (CTMs) have been developed to consider this complexity (Simpson et al., 2003; Bey et al., 2001; Byun, 1999). They combine emissions, meteorology, chemistry and physics to provide a representation of atmospheric composition at varying spatial and temporal timescales. This makes them a useful tool for improving understanding of atmospheric processes, exploring potential policy options, and advising policy decisions. However, the predictions of these models need to be tested against observations to ensure their veracity. They can also be vulnerable to uncertainties in the model inputs (e.g emissions, meteorology), and the resolution-dependent representativity of processes on the model grid (Solazzo et al., 2017; Kushta et al., 2018; Hood et al., 2018). CTMs need be capable of simulating the interaction of air pollutants in largely urban areas like the UK due to their immediate impact on a large portion of the population (82.9% of the UK population resided in urban areas in 2019, (DEFRA, 2022b)) and the need to accurately simulate the transport of longer-lived pollutants from these regions.

Several previous studies have compared CTMs with UK measurements. Dore et al. (2015) compared Rural UK measurements with a range of CTMs of varying complexity and resolutions from 5-50 km. While the spatial variability was reasonably well-captured for NO_x, SO_2, NH_3 and aerosol SO_4^{2-}, NO_3^-, and NH_4^+, more complex models performed better for aerosol species and performance for each species varied between models, particularly for SO_2. More recent comparisons by Lin et al. (2017); Syrakov et al. (2016); Hood et al. (2018) identified that CTMs perform worse in urban environments than in rural ones, resulting in underestimates of urban NO_x and $PM_{2.5}$, and overestimates for O_3. They attributed this to underestimates in NO_x and PM emissions and model difficulties capturing the sub-grid variability of emissions. Emission representativity has also been proposed to account for modelled NH_3 underestimates (Dore et al., 2015; Ge et al.,

2021a). Concentrations of UK $PM_{2.5}$, Sulphate/Nitrate/Ammonium aerosols and O_3 have been shown to be significantly influenced by transboundary long-range transport contributions (Hood et al., 2018; Dore et al., 2015; Vieno et al., 2014; Derwent and Parrish, 2022). These become particularly important during PM pollution episodes, which are dominated by enhanced transport of $PM_{2.5}$ from continental Europe (Yin and Harrison, 2008; Vieno et al., 2016b).

Most CTMs are able to capture the spatial distribution of primary species relatively well, but performance for secondary species varies more between models. CTMs also display some shared weaknesses such as poorer performance in urban environments, which some evaluations attribute to model resolution (Mircea et al., 2019; Lin et al., 2017). Underestimates of precursor emissions have also been suggested as a potential cause (Oikonomakis et al., 2018; Kuik et al., 2018), providing further support for the findings from measurement studies (Vaughan et al., 2016; Karl et al., 2017). Evaluations have also provided insights into some of the sources of air pollution in the UK e.g. transported contributions from Europe during some pollution episodes (Vieno et al., 2016b). Despite the valuable insights gained from prior evaluations, the existing literature lacks a comprehensive assessment of CTM estimates for a broad range of air pollutants over the UK. Without such an evaluation, it is challenging to obtain a holistic understanding of CTM performance and how it relates to the interaction among different chemical species, particularly when differences between model inputs (emissions, meteorology) and configuration (model resolution, complexity of chemistry, transport and loss processes) must be taken into account.

To address this gap, this chapter will conduct an extensive evaluation of the performance of a CTM for a broad range of gaseous and aerosol species. It will use version 13.1.0 (GC13.1.1, 2021) the GEOS-Chem model (`https://geos-chem.seas.harvard.edu`, last access 10/07/2023, Chapter 2) run in a regional configuration over the UK and compare against observations made by

the DEFRA air quality monitoring network and observations made on the west coast of Ireland at Mace Head, for 2017. This work builds upon the similar assessment by Garstin (2017), which evaluated GEOS-Chem performance for a smaller range of species. The model is updated to use anthropogenic emissions from the European Monitoring and Evaluation Programme (EMEP, `https://www.ceip.at/webdab-emission-database/reported-emissiondata`; last access 03/04/2023) for 2017. Details of the model, emissions and observations are described in sections 3.2.1, 3.2.2 and 3.2.3, respectively. In Section 3.3, modelled concentrations are evaluated against the observations at the annual, daily and hourly timescale, Section 3.3.8 summarises the performance evaluation, and we discuss the results in Section 3.4.

3.2 Methods

3.2.1 Model

This Chapter used Version 13.1.2 (GCv13.1.2, 2021) of the GEOS-Chem model first described by Bey et al. (2001), with meteorological data from the Goddard Earth Observing System - Forward Processing (GEOS-FP) product from the NASA Global Modeling and Assimilation Office (GMAO). The meteorological data are available globally at horizontal resolution of 0.25° latitude by 0.3125° longitude but for computationally expediency we initially run globally at a degraded resolution of 4°×5° from 1st January 2016 to 1st January 2018. The first year is to spin the model up and the second year is to provide boundary conditions (every 3 hours) and an initial condition for a nested grid simulation over the United Kingdom (15° W–5° E, 45° N–65° N) with horizontal resolution of 0.25° latitude by 0.3125° longitude (Figure 5). The nested grid simulation is allowed one month of spin-up time from 1st December 2017 to 31st December 2017 before starting comparisons. All simulations were run with 47 vertical levels extending from the surface to 0.01 hPa. Modelled concentrations from the nested grid simulation

were output hourly. For species which are rapidly dry deposited such as O_3 and SO_2, concentrations were corrected from the lowest model grid layer ($\sim$60 m) to 10 m (which is more comparable to the height of the observations) as in Travis and Jacob (2019). This approach infers the concentration at 10 m from the aerodynamic resistance to turbulent vertical transfer at 10 m, and the local deposition velocity and explicit concentration at 65 m (Zhang et al., 2012a).

The chemical mechanism in the model represents O_x, HO_x, NO_x, VOC and halogen chemistry and has 228 species and 724 reactions (Shen et al., 2020). The model represents the multiple aerosol types with modes of fixed size representing sulfate-nitrate-ammonium, primary organic and black carbon in hydrophilic and hydrophobic modes, secondary organic aerosol, fine and coarse mode seasalt, and 4 size bins of mineral dust (Park et al., 2004). Gas to aerosol phase partitioning for sulfate-nitrate-ammonium (SNA) aerosols uses the ISORROPIA II thermodynamic model (Fountoukis and Nenes, 2007). Secondary organic aerosol (SOA) is approximated by irreversible formation using fixed yields of Pai et al. (2020).

Photolysis rates are calculated using the FAST-JX v7.0 photolysis mechanism implemented in the troposphere by Mao et al. (2010) and in the stratosphere by Eastham et al. (2014). The non-local, VDIFF scheme of Planetary Boundary Layer (PBL) mixing was used (Lin et al., 2008), using offline PBL height data from the met fields. If the boundary layer is stable, a local scheme based on eddy-viscosity theory (K-theory) is used. Wet deposition for water-soluble aerosols uses the scheme described by Liu et al. (2001), and by Amos et al. (2012) for gases.

$PM_{2.5}$ is the mass of particulate matter with an aerodynamic radius of less than 2.5 μm. It is composed of a number of compounds and the associated water at a standard relative humidity (RH). In Europe this standard is 50% (EN
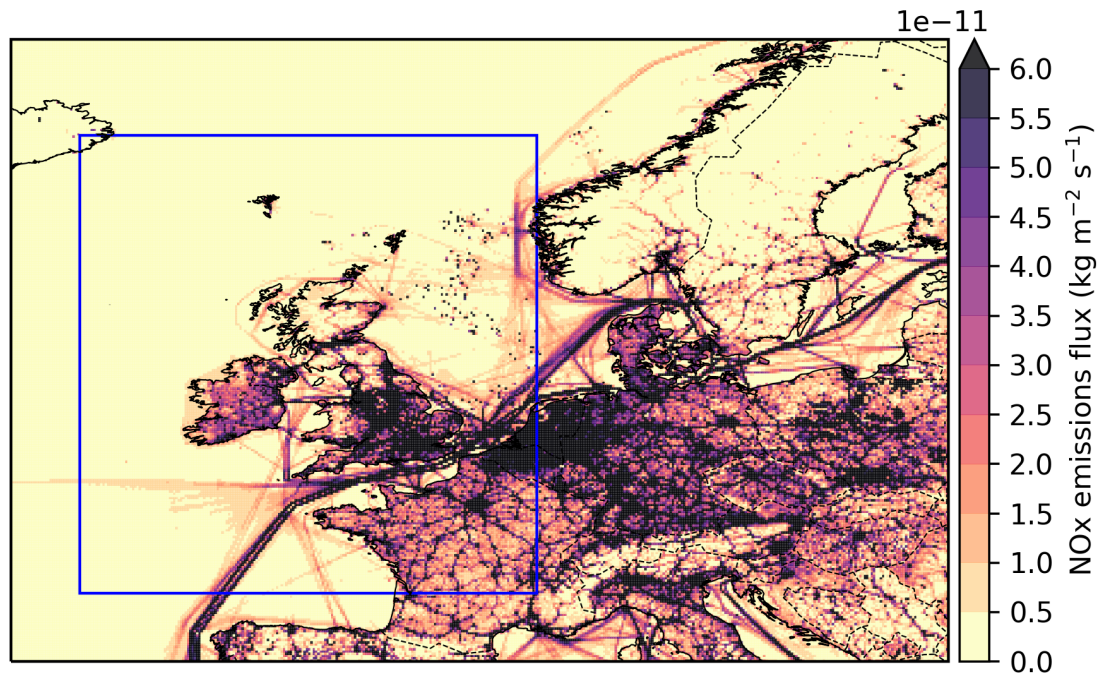
Figure 5: Anthropogenic NO_x emissions flux in 2017 from the EMEP emissions inventory at 0.1°×0.1°, with the nested model domain over the UK (blue box).

12341). $PM_{2.5}$ concentrations were computed from sum of the masses of the different aerosol tracers together with a multiplying factor to convert the dry mass into a wet mass at 50 % relative humidity according to the GEOS-Chem wiki (`http://wiki.seas.harvard.edu/geos-chem/index.php/Particulate_matter _in_GEOS-Chem`; last access 01/04/2022). Equation 2 describes this calculation based on the total mass of sulfate, nitrate, ammonium aerosol (SNA), black carbon (BC), hydrophilic and hydrophobic primary organic carbon (OCPI, OCPO), desert dust, Sea Salt and Secondary Organic Aerosol (SOA). The smallest two dust bins in the model and accumulation mode sea-salt are also included.

$$PM_{2.5} = 1.35 \times SNA + BC + 2.1 \times (OCPO + OCPI \times 1.07) + \text{Dust}$$
$$+ 1.86 \times \text{SeaSalt} + 1.07 \times \text{SOA}$$

(2)

3.2.2 Emissions

Default anthropogenic emissions in the model are from the Community Emissions Data System (CEDS) (McDuffie et al., 2020), with Tzompa-Sosa et al. (2017) and

Xiao et al. (2008) replacing ethane and propane emissions respectively. Over Europe, we replace anthropogenic and shipping emissions with those from EMEP (`https://www.ceip.at/webdab-emission-database/reported-emission` data or `https://www.ceip.at/status-of-reporting-and-review-results/2022-submission`, last access 03/04/2023, (EMEP MSC-W, 2020)). This provides annual average emissions for a number of gas and (primary) aerosol phase compounds at $0.1° \times 0.1°$ resolution, segregated into 13 industrial sectors (Agricultural emissions from livestock, other Agricultural sources, Aviation, Fugitive, Industry, Offroad, Other, Other Stationary Combustion, Public power, Road transport, Shipping, Solvents and Waste). We use the EMEP emissions for all sectors other than aviation, where we use the default Aviation Emissions Inventory Code (AEIC) emissions (Stettler et al., 2011). Sector-specific seasonal and diurnal variability factors were taken from the EMEP/MSC-W model (Ge et al., 2021b)The use of diurnal scale factors for different days of the week is not currently supported by the GEOS-Chem emission component (HEMCO), so the weekday diurnal factors for the UK were used throughout the simulation. Figure 6 shows the emissions diurnal for each of the EMEP sectors.
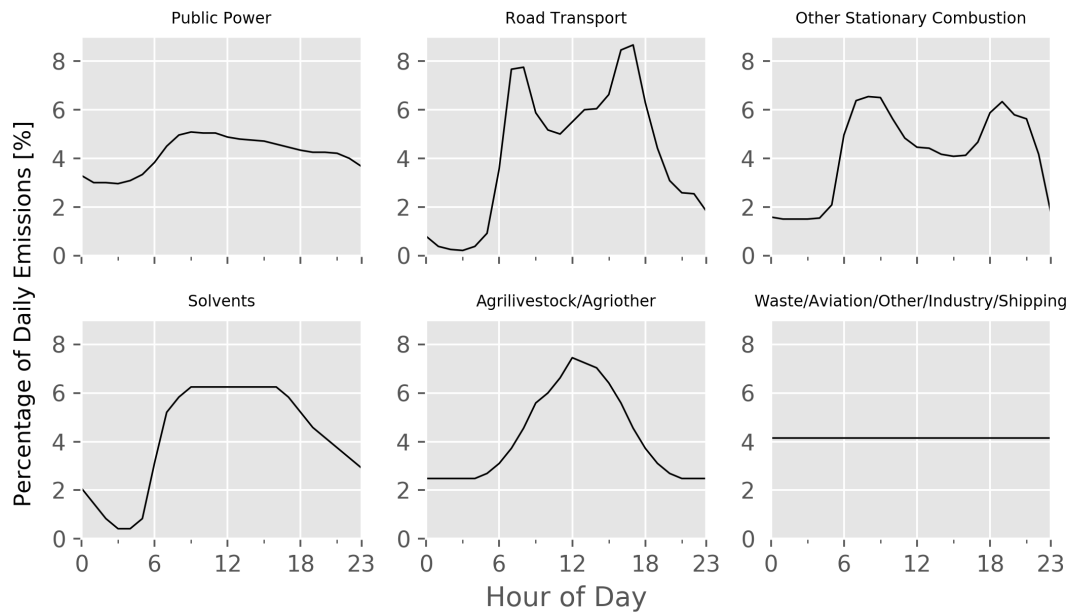
Figure 6: Diurnal profile for anthropogenic emissions from the EMEP sectors implemented. Note: the diurnal emission profile from Waste, Aviation, Other, Industry and Shipping were constant.

Emissions of the EMEP carbon monoxide (CO) and ammonia (NH_3) are relatively straightforward to implement into the model. EMEP emissions of oxides of nitrogen are given in terms of NO_2 mass but were emitted in the model directly as *NO*, conserving nitrogen. EMEP gives the total mass of Non-Methane Volatile Organic Compounds (NMVOCs), which we separate into emissions of ethanol (GEOS-Chem model species *EOH*), ethane (C_2H_6), propane (C_3H_8), alkanes with a carbon number greater than or equal to 4 (*ALK4*), alkenes with a carbon number greater than or equal to 3 (*PRPE*), benzene (*BENZ*), toluene (*TOLU*), grouped xylene isomers (*XYLE*), formaldehyde (CH_2O), acetone (ACET), alcohols with carbon number greater than 2 (*ROH*), aldehydes (lumped, all aldehydes with a carbon number ≥ 3 , RCHO), and methyl ethyl ketone (*MEK*) based on speciation of reported UK total VOC emissions following the method of Passant (2002) (Table 3). This approach applies the same relative speciation of NMVOCs in each gridbox regardless of the sector level activity in that gridbox. Hydrocarbons not included in the model (e.g trimethyl benzene) were excluded, resulting in 10.8% of total NMVOC emissions mass being missed. SO_2 emissions were split into an emissions of SO_2 (98 % by mass) and a direct emissions of aerosol sulfate

(SO_4^{2-}) (2% by mass), (Chin et al., 2000). We emit the EMEP coarse PM, into the largest of GEOS-Chem's dust sizes (Dust aerosol with $r_{eff} = 4.5$ μm , DST4). The EMEP primary $PM_{2.5}$ emission was speciated into carbonaceous and dust components based on the speciation in the EMEP CTM (Simpson et al., 2003). Vertical distributions of emissions were based on sectors from the EMEP Status Report (EMEP, 2019), interpolated to the GEOS-Chem model vertical resolution (Figure 7).
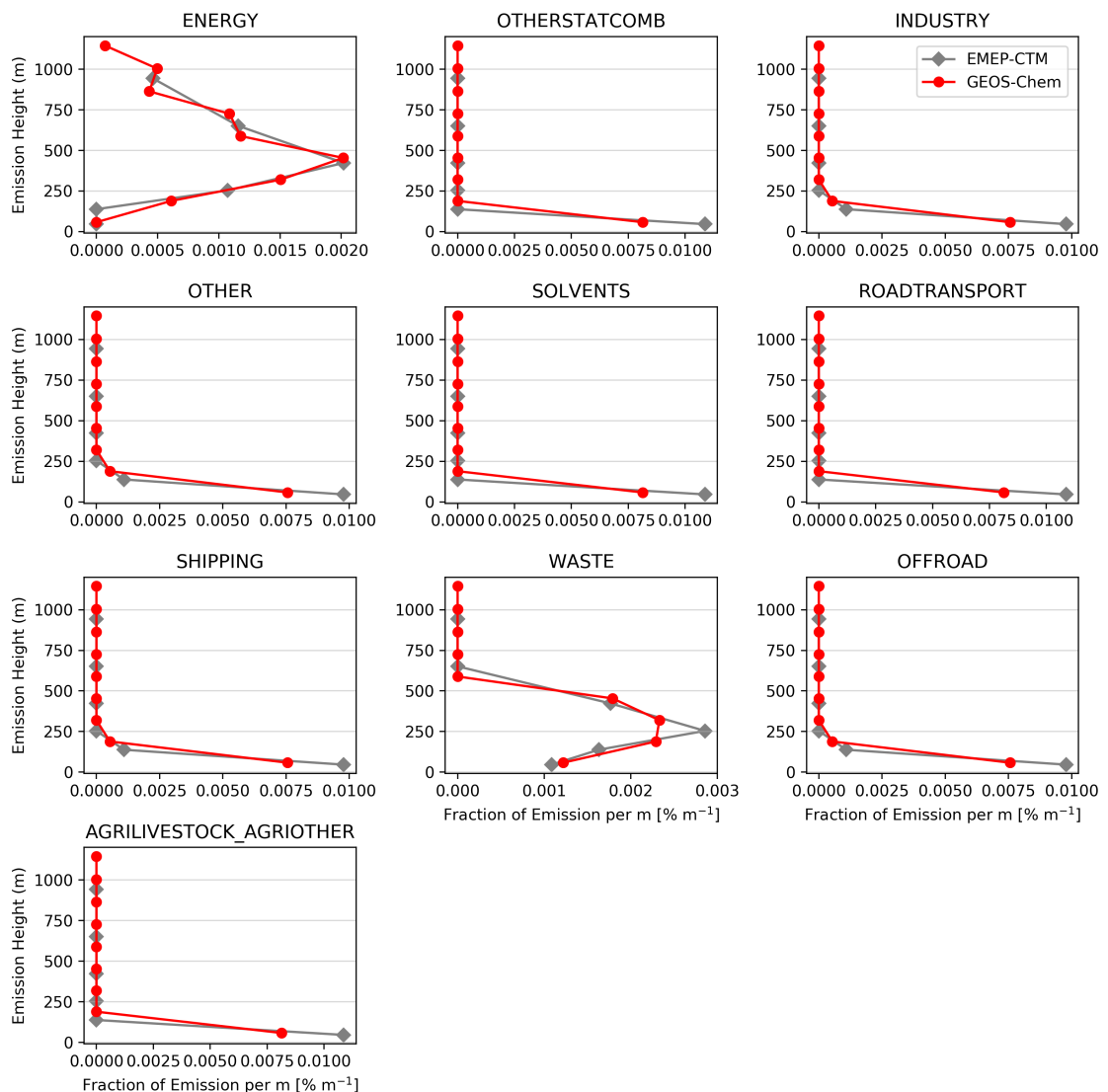
Figure 7: Vertical emissions profiles for the EMEP-CTM ("EMEP-CTM", grey) and re-weighted for use in this work ("GEOS-Chem", red). The percentage of total emissions for a sector are normalised by the height of the EMEP/GEOS-Chem vertical model layer.

Table 3: Speciations applied to anthropogenic NMVOC emissions from the EMEP inventory based on speciated NAEI NMVOC emissions for 2017 with methodology from Passant (2002). Species are given as model species and speciations as fractions of total NMVOC emissions. Note: Reported emissions for species not in the model ("Other") were excluded. Data provided by Alastair Lewis

Species	Speciation
EOH	0.2575
ALK4	0.2852
C2H6	0.0624
C3H8	0.0530
XYLE	0.0256
TOLU	0.0248
AROM	0.0280
BENZ	0.0249
CH2O	0.0181
ACET	0.0166
PRPE	0.0156
ROH	0.0182
TMB	0.0203
XYLO	0.0085
RCHO	0.0090
MEK	0.0143
OTHER	0.1179

Table 4 shows the annual emission of NO, CO, SO_2, NMVOCs, NH_3 and $PM_{2.5}$ for the UK based on EMEP reports (`https://www.ceip.at/webdab-emission-database/emissions-as-used-in-emep-models`; last access 26/06/2022), the UK National Atmospheric Emissions Inventory (`https://naei.beis.gov.uk/data/data-selector?view=air-pollutants`; last access 04/01/2023), CEDS (McDuffie et al., 2020) and by diagnosing the annual model simulation for UK gridboxes. EMEP national emissions are based on the reported emissions from NAEI giving near identical results. The differences between the modelled and EMEP reported values are due to corrections/gap-filling methods (Schindlbacher et al., 2021). The modelled values are within 1% of the EMEP reported values. Remaining model emissions follow the default configuration and are described in Chapter 2.

Table 4: Estimates for 2017 total UK anthropogenic emissions (in kT yr^{-1}) of CO, NO$_x$ (as NO), SO$_2$, NMVOCs, NH$_3$ and PM$_{2.5}$ from the EMEP (*EMEP/CEIP 2022* `https://www.ceip.at/status-of-reporting-and-review-results/2022-submission`, last access 03/04/2023), NAEI (`https://naei.beis.gov.uk/data/`, last access 03/04/2023) and CEDS (McDuffie et al., 2020) inventories, and from this model simulation. (a) estimated with a 0.1°×0.1° UK mask on gridded data. (b) Excludes approximately 12.5 kT aviation emissions.

Species	Inventories			Model
	EMEP	NAEI	CEDS^a	GEOS-Chem^a
CO	1594.8	1590	1559.1	1574.2
NO$_x$	588.6	581.8	533.5	580.2^b
SO$_2$	192.8	193	163.7	191.1
NMVOC	807.1	806	791.3	804.9
NH$_3$	275.5	275	357.4	275.3
PM$_{2.5}$	110.1	110	-	109.9

3.2.3 Observations

We use observations of trace gases and aerosols for 2017 from 132 sites which form parts of the UK national and international monitoring networks (Figure 8). Table 6 describes the measurement methods used and Table 5 describes the number of monitoring sites available for each species in 2017.
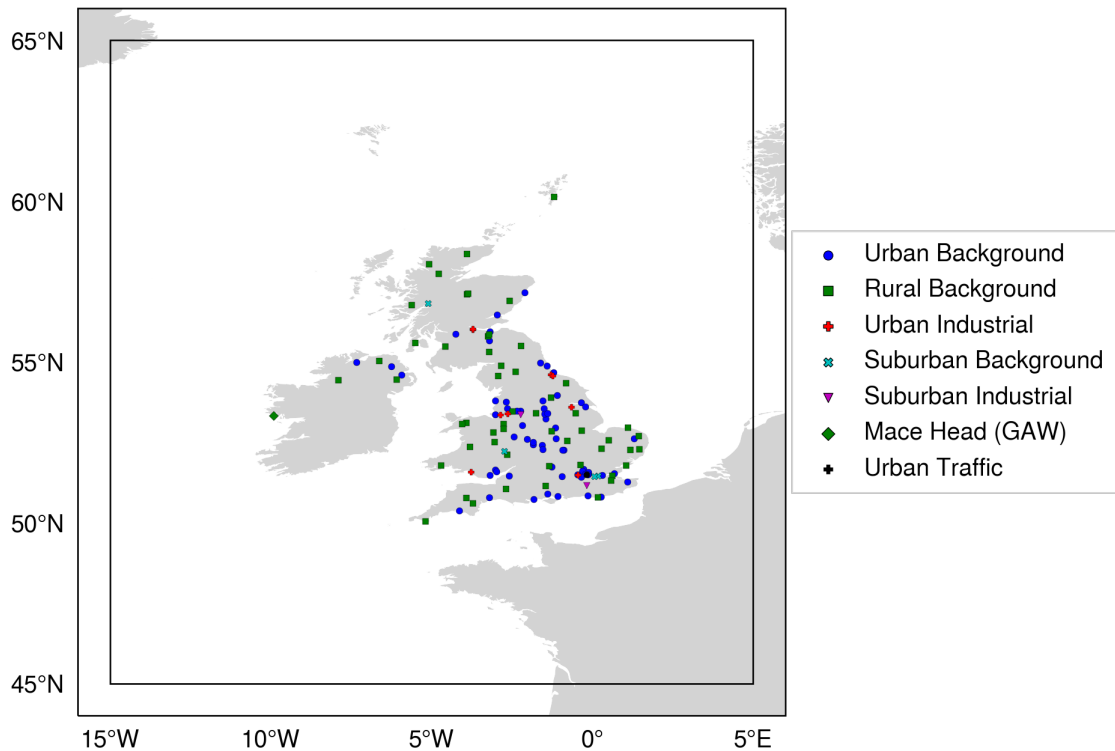
Figure 8: The 0.25° latitude by 0.3125° longitude model domain simulated (black box, 15°W–5°E, 45°N–65°N) and the monitoring sites for which data were used in this work (coloured points).

Continuously measured hourly data timestamped at GMT from the DEFRA AURN network (DEFRA) were obtained for NO, NO_2, O_3, $PM_{2.5}$, CO, SO_2 and for speciated NMVOCs from the Automatic Hydrocarbon Network using the openair *R* package (Carslaw and Ropkins, 2012). The UK Eutrophying and Acidifying Atmospheric Pollutants (UKEAP) network (Tang et al., 2013) provided monthly average concentrations of gaseous ammonia, and aerosol sulfate, nitrate and ammonium. Within the UKEAP network, observations of ammonia from the National Ammonia Monitoring Network (NAMN) and the Acid Gases and Aerosol Network (AGANet) are at a lower temporal resolution (monthly) than measurements from the two EMEP sites at Auchencorth Moss and Chilbolton Observatory, which use the Monitor for AeRosols and Gases in Air (MARGA) instruments and provide hourly measurements. For these two measurement sites we also obtain weekly-averaged measurements for OC from the Particle Numbers and Concentration Network and for BC from the UK Black Carbon Network. The Global Atmosphere Watch (GAW) site at Mace Head has hourly averaged O_3

and fortnightly averaged CO measurements (Prinn et al., 2018). Observations given in μgm^{-3} were converted into mixing ratios with conversion factors calculated at 20 °C and 1013 mb in accordance with the UK Air Quality Archive (`https://uk-air.defra.gov.uk/assets/documents/reports/cat06/050216085 1_Conversion_Factors_Between_ppb_and.pdf`, last access 14/12/2022).

Site environment types across the national measurement network are split into six categories describing the areas and pollution sources expected: Urban Background, Urban Traffic, Urban Industrial, Suburban Background, Suburban Industrial and Rural Background (`https://uk-air.defra.gov.uk/networks/sit e-types`, last access 14/12/2022). Urban areas are characterised by continuously built-up residential and commercial areas, where air quality measurements are representative of a few km^2. Suburban sites are situated in "largely built-up" areas with a mix of non-urbanised areas such as lakes and woods, and with measurements representative of tens of km^2. Rural sites must be more than 20 km from agglomerations and more than 5 km from other built up areas such as industrial installations, motorways and major roads. Traffic stations experience pollution predominantly arising from nearby traffic sources and are representative of street segments longer than 100 m. Urban Traffic sites are representative of areas much smaller than the model horizontal resolution, meaning they cannot be effectively simulated by the model and were excluded from this analysis. Industrial stations are placed in the nearest residential areas downwind of industrial (e.g power generation, incinerators, waste treatment plants) sources and must be representative of 250 m^2 areas. Background stations should not be significantly influenced by individual sources or streets, but by contributions from all upwind sources.

Table 5: Number of UK monitoring sites for each environment type for the species evaluated in this work. Total counts for CO and O_3 exclude Mace Head.

Site Type	NO$_x$	SO$_2$	CO	NMVOC	NH$_3$	O$_3$	PM$_{2.5}$	SO$_4^{2-}$	NH$_4^+$	NO$_3^-$
Urban Background	58	14	5	-	-	43	42	-	-	-
Rural Background	15	6	-	2	37	22	3	26	27	26
Urban Industrial	9	5	1	-	-	4	6	-	-	-
Suburban Background	4	-	-	1	-	3	2	-	-	-
Suburban Industrial	2	-	-	-	-	1	-	-	-	-
Total	88	25	6	3	37	73	53	26	27	26

The model uses a number of lumped NMVOC tracers. "ALK4" represents alkanes with 4 or more carbons, "PRPE" represents alkenes with 3 or more carbons and "XYLE" represents the isomers of xylene. For comparisons with observations we sum the concentrations of *i*-butane, *i*-pentane,*n*-pentante, *n*-hexane, *n*-heptane, 2-methyl-pentane, *i*-octane, *n*-octane to compare with ALK4; propene, 1-butene, 1,3-butadiene, *trans*-2-butene, *cis*-2-butene, 1-pentene, *trans*-2-pentene for comparison with PRPE and *o*-xylene, *m,p*-xylene for comparison with XYLE. Calculated concentrations of lumped tracers were only used where measurements for each of the component species were available. Data capture rates varied for each NMVOC across the 3 Automatic Hydrocarbon Network sites (Auchencorth Moss, Chilbolton Observatory, London Eltham). Although most measurements were available for all species at London Eltham, data capture at Auchencorth Moss and Chilbolton Observatory was poorer. As a percentage of total number of measurements possible for the year across the three sites, ethane had 81.5%, propane had 81.5%, PRPE had 37.1%, ALK4 had 57.8%, benzene had 71.3%, toluene had 81.5%, xylene had 78.1% and isoprene had 78.7%.

Table 6: Measurement methods and temporal frequency for observational data. Method information for AURN, MARGA, Automatic Hydrocarbon and UKEAP sites from (`https://uk-air.defra.gov.uk/networks/index`, last access 6/1/2023), Automatic Hydrocarbon Network, and Mace Head from (`https://agage.mit.edu/stations/mace-head`, last access 6/1/2023). Sampling inlets must be more than 50cm from buildings and trees, and generally placed between 1.5 and 4 m above the ground, or up to 8 m if the station is representative of a large area. Flow around sampling inlets is regularly checked to ensure it's unrestricted (AEA Group, 2009)

.

Species	Technique (measurement frequency)
NO, NO_2, NO_x	Chemiluminescence (Hourly)
SO_2	UV fluorescence (Hourly)
CO	AURN: Non-dispersive infrared (NDIR) analyser (Hourly)
	Mace Head: gas chromatography-mass spectrometry (Hourly)
NMVOCs	Perkin Elmer automatic gas chromatograph (VOCAIR) (Hourly)
NH_3	DEnuder for Long-Term Atmospheric (DELTA) sampling system (Fortnightly)
O_3	UV photometry (Hourly)
	Mace Head: UV photometry (Hourly)
$PM_{2.5}$	Tapered Element Oscillating Microbalance (Hourly)
	Beta Attenuation monitor (Hourly)
	Gravimetric monitor (Hourly)
	Filter Dynamics Measurement System (FDMS) (Hourly)
	Optical light scattering (Hourly)
	Fine Dust Analysis System (FIDAS) (Hourly)
Aerosol SO_4^{2-}, NO_3^-, NH_4^+	MARGA (only Auchencorth Moss, Chilbolton Observatory) (Hourly)
	DEnuder for Long-Term Atmospheric (DELTA) sampling system (Fortnightly)
BC	Transmittance, Magee Aethalometer (AE22) (Weekly)
OC (in $PM_{2.5}$)	Transmittance, Digital DPA14 aerosol sampler (Weekly)

3.2.4 Metrics

A number of metrics can be used to evaluate model performance. For a time series of n points, where M_i and O_i are the modelled and observed values at time i, μ_M and μ_O are the modelled and observed means, and σ_M and σ_O are the modelled and observed standard deviations the Normalised Mean Bias (NMB) is defined as:

$$NMB = \frac{\sum_{i=1}^{n} M_i - O_i}{\sum_{i=1}^{n} O_i} \tag{3}$$

and the Pearson's r correlation coefficient between observed and modelled concentrations is defined as:

$$r = \sum_{i=1}^{n} \frac{(M_i - \mu_M)(O_i - \mu_O)}{n\sigma_M\sigma_O} \tag{4}$$

These summary statistics were calculated based on the mean averages of the modelled and measured data at annual, daily and hourly timescales, except for NO_x, where concentrations are known to be non-normally distributed and the median was used instead.

3.3 Model Evaluation

We now evaluate the model predictions for pollutant concentrations over the UK. We start by analysing the concentration of primary emitted species: oxides of nitrogen (NO_x) (Section 3.3.1), sulfur dioxide (Section 3.3.2), non methane volatile organic compounds (NMVOCs) (Section 3.3.4) and ammonia (Section 3.3.5). We then turn to secondary products. Section 3.3.6 analyses the model performance of ozone (O_3), and Section 3.3.7 analyses $PM_{2.5}$ together with aerosol phase sulfate, nitrate and ammonium concentrations.

3.3.1 NO$_x$

3.3.1.1 Annual median NO$_x$

Figure 9 shows the spatial distribution of the annual median modelled and mea-

sured NO, NO_2 and NO_x ($NO+NO_2$), with Figure 10 comparing the annual median concentrations on a site-by-site basis. The model identifies the general spatial distribution of NO, NO_2 and NO_x, with higher concentrations in the southeast and around population centres, and lower concentrations in Wales, Scotland and Northern Ireland, reflecting the emissions sources and regional population densities (r_{NO}=0.44, r_{NO2}=0.60, r_{NOx}=0.56). The model is biased low, by 1.57 ppbv for NO, 3.96 ppbv for NO_2, and 5.53 ppbv for NO_x (NMB: -0.77, -0.52, -0.56 for NO, NO_2 and NO_x, respectively). If only the rural sites are considered (green dots in Figure 8), the model underestimate is smaller (biases of 0.25 ppbv, 0.24 ppbv, 0.41 ppbv for NO, NO_2 and NO_x, respectively). Many of these NO_2 observations were made using a heated molybdenum converter technique rather than a blue light converter. This is well known to lead to an overestimate in the NO_2 concentration (Steinbacher et al., 2007). If modelled reactive nitrogen, NO_y (NO_y = NO + NO_2 + PAN + HNO_3), is compared to the NO_x measurements, the model underestimate for NO_x measurements only drops from 5.53 ppbv to 4.18 ppbv. This effect would be most important in Urban areas where there are large sources of NO_x emissions. However, uncertainty in the NO_2 measurements cannot fully explain the NO_2 underestimate. Moreover, it fails to elucidate the consistent NO underestimates observed at Urban and Suburban sites, potentially indicating a broader underestimate in NO emissions sources in these regions. In the UK and Europe, studies have suggested underestimates of NO_x emissions from road transport, particularly pointing to diesel vehicle emissions (Vaughan et al., 2016; Karl et al., 2017; Wilson et al., 2023)

3.3.1.2   Daily median NO_x

Figure 11 shows the daily median concentrations for NO_x for all of the Rural and Non-Rural sites (Urban Background, Suburban Background, Urban Industrial and Suburban Industrial). The winter maximum and summer minimum are captured by the model, with the correlation for the rural environments being higher than for the urban ones (r_{Rural}=0.72; $r_{Non-Rural}$=0.58). The model marginally underestimates concentrations at Rural sites (0.63 ppbv, NMB=-0.14) but shows a more
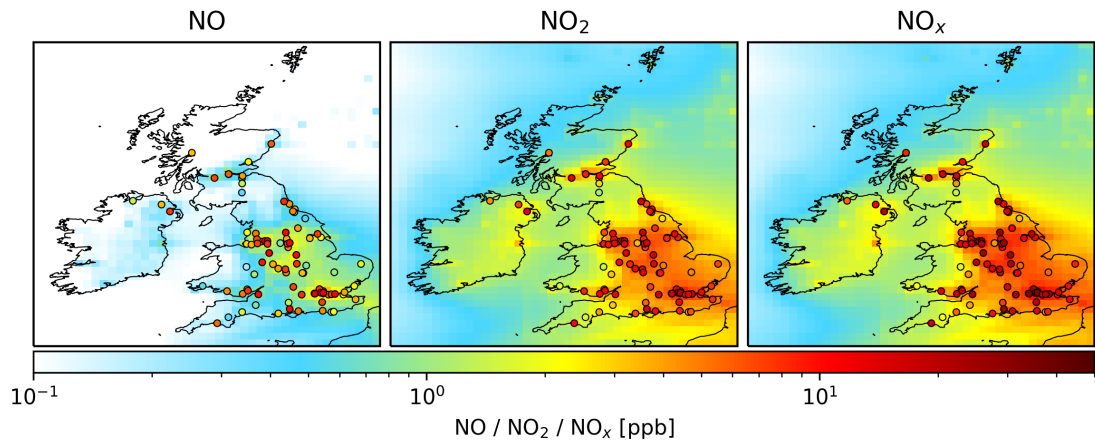
Figure 9: Annual median observed (filled points) and modelled (mapped) concentrations of NO, NO_2 and NO_x.
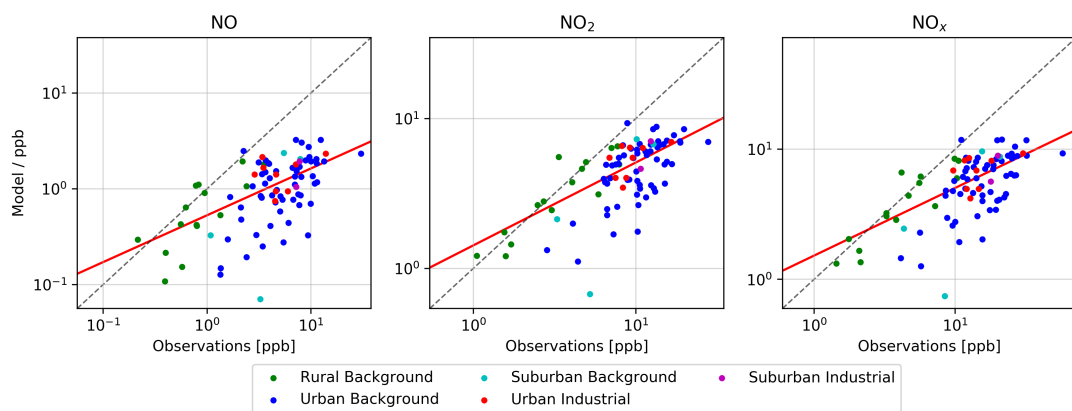
Figure 10: Observed and modelled annual median concentrations for NO, NO_2 and NO_x at each site (points) on a log scale. The best-fit (red line) was determined by Theil-Sen regression and the grey dashed line shows the 1:1 relationship.

significant underestimate at the Non-Rural sites (9.39 ppbv, NMB=-0.58) .

3.3.1.3   Median NO_x diurnal profile

Figure 12 shows the annual median diurnal profile for modelled and observed NO, NO_2, and NO_x at Rural (top) and Non-Rural (bottom) sites. Modelled and measured NO correlate, with both showing a nighttime minimum and daytime maximum (r_{Rural}=0.77; $r_{Non-Rural}$=0.47). However, in both environments, the model underestimates NO concentrations, especially at night (NO: NMB_{Rural}=-0.42, $NMB_{Non-Rural}$=-0.78), although this could be due to instrument detection limits.

Observed NO_2 and NO_x diurnal profiles were similar at Rural and Non-Rural sites, and the peaks at around 0700 and 1800 and a decrease at noon are in-
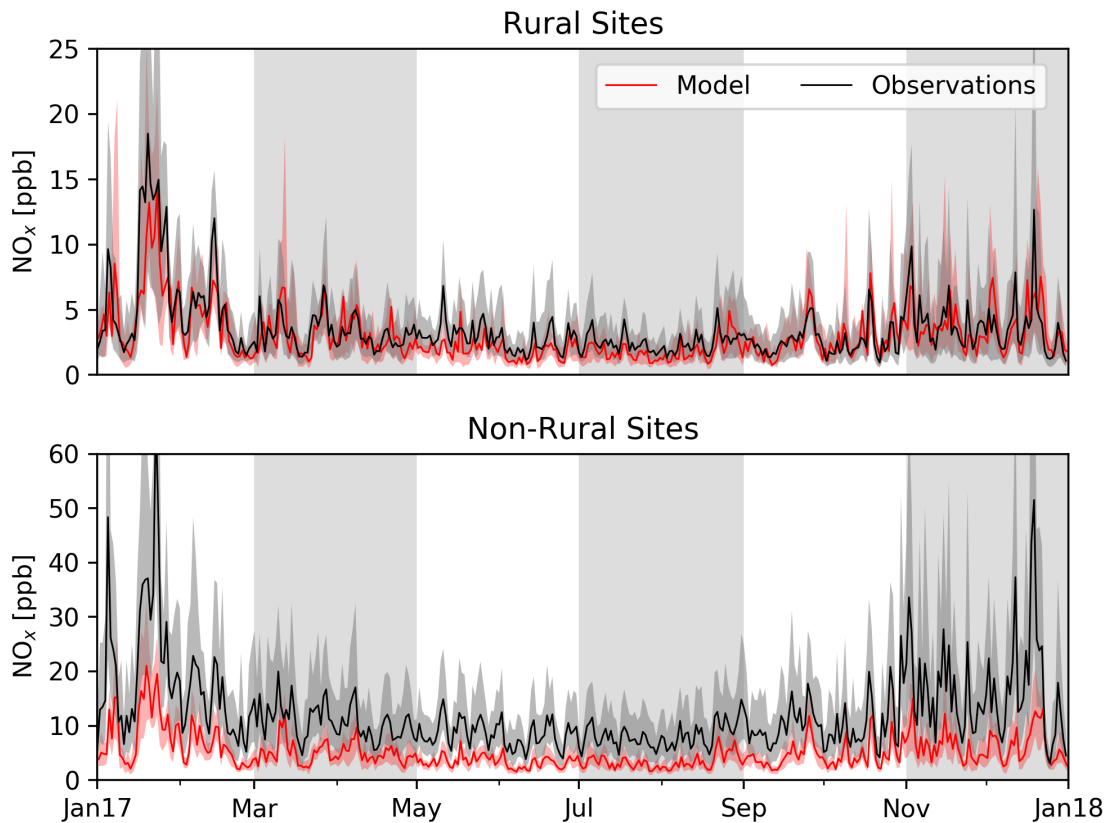
Figure 11: Daily median observed (black) and modelled (red) concentration for NO_x at Rural (top, N=15) and Non-Rural (bottom, N=73) sites. Shaded areas show the inter-quartile ranges. Y-axis limits shortened for clarity, maximum observed upper quantiles were 32.6 and 125.8 ppbv for Rural and Non-Rural sites, respectively.

dicative of rush-hour traffic emissions and NO_2 photolysis, respectively. Modelled NO_2 and NO_x at Rural sites showed smaller underestimates (NO_2 NMB_{Rural}=-0.07, NO_x NMB_{Rural}=-0.11) than at Non-Rural sites (NO_2 $NMB_{Non-Rural}$=-0.57, NO_x $NMB_{Non-Rural}$=-0.59), which might be due to the representation of the higher NO_x emissions in Non-Rural environments. A similar comparison by Hood et al. (2018) compared the regional-scale EMEP4UK model using similar emissions to UK monitoring network measurements in London in 2012. Non-Rural underestimate were attributed to the low resolution of the model input emissions (5 km $\times$ 5 km) compared to local sources. Performance was improved by coupling the model to the fine-scale ADMS-Urban model using increased vehicular NO_x emissions to better represent road sources. We discuss the potential explanations for the model failure simulating NO_x in Section 3.4.
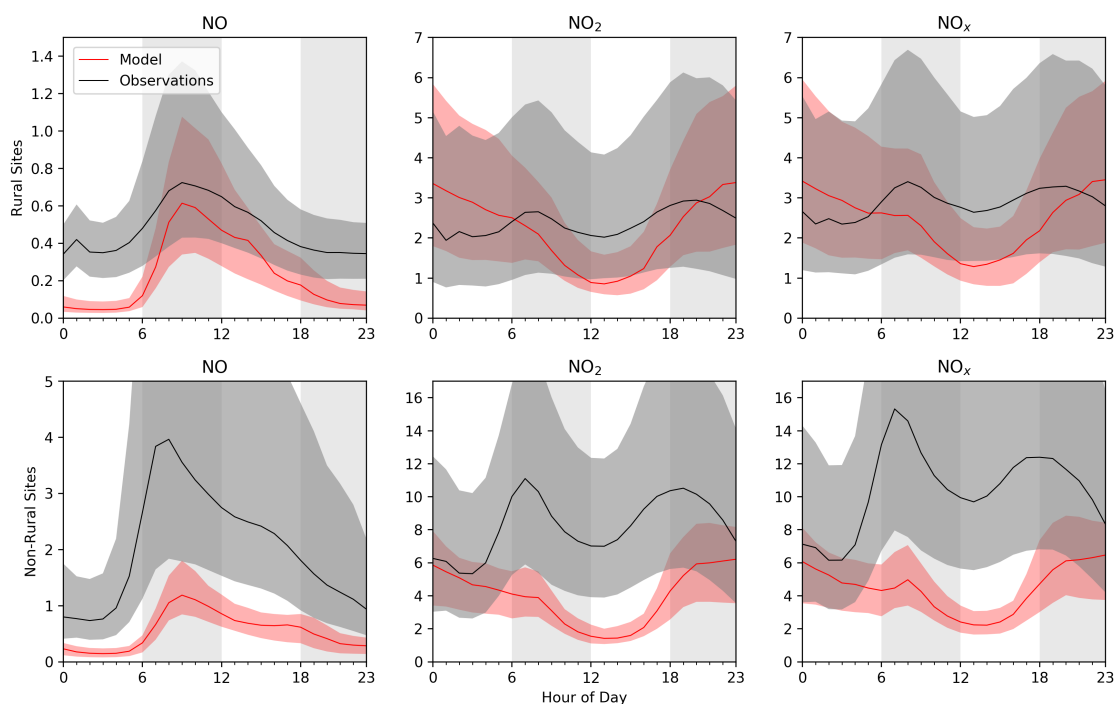
Figure 12: Median observed (black) and modelled (red) diurnal profiles for NO (left), NO_2 (centre) and NO_x (right) at Rural (top, N=15) and Non-Rural (bottom, N=77) sites. Shaded areas show the upper and lower quartile about the medians. Y-axes on the Non-Rural sites were limited for clarity, maximum observed upper quantiles were 10.3, 19.1 and 29.7 ppbv for NO, NO_2 and NO_x, respectively.

3.3.2 SO_2

3.3.2.1   Annual mean SO_2

Figure 13 shows the simulated and measured annual mean concentrations of SO_2 (left), together with the corresponding scatter between model and measurement at each site (right). Modelled and observed SO_2 were moderately well correlated (r=0.48), with an overall overestimate (NMB=0.23). The highest modelled concentrations were found in a band from Liverpool to Hull along the middle of the UK, with small regional increases around large cities such as Cardiff, Belfast and Edinburgh attributable to high local emissions. Some large overestimates occurred near large emissions sources such as power plants, ports and petrochemical refineries (`https://naei.beis.gov.uk/emissionsapp`, last access 14/12/2022). The overestimate is discussed in more detail in Section 3.4.4. The objective of the AURN SO_2 UV-fluorescence analysers is to detect pollutant events (Twigg et al., 2016) rather than to monitor changes in background concentrations. This method

has a reported limit of detection of 1.5 ppbv for SO_2 (Walker et al., 2019). Given the observed concentrations at most measurements sites lower than this limit, it is challenging to reliably assess the performance of GEOS-Chem for SO_2.
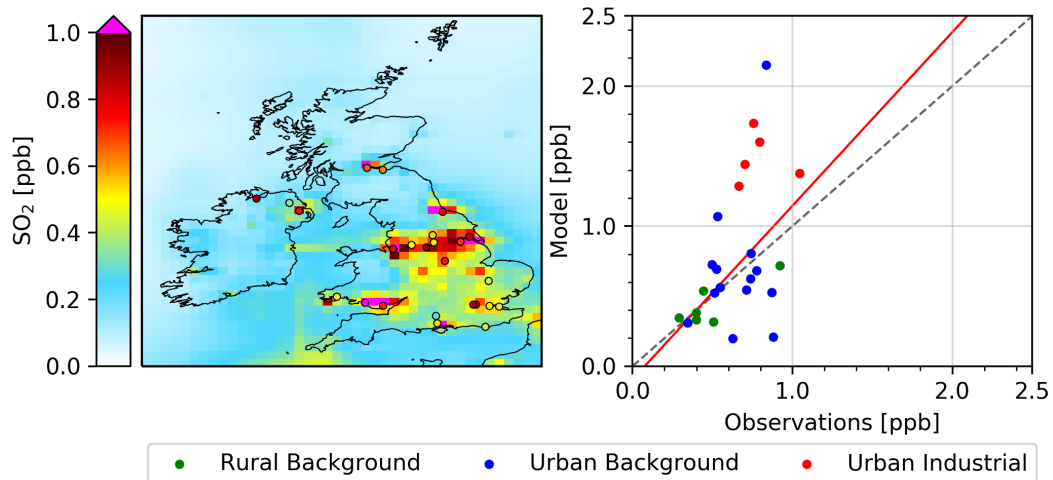
Figure 13: Left: Annual mean observed (filled points) and modelled (mapped) concentrations for SO_2 (N=25). Right: Observed and modelled annual mean SO_2 concentrations. The best fit line (red) was determined by Theil-Sen regression and the grey dashed line shows the 1:1 relationship.

3.3.2.2   Daily mean SO_2

Figure 14 shows the daily mean measured and modelled SO_2 at all sites. Both measured and modelled SO_2 show little seasonality. However, the model struggles to capture much of the day-to-day variability (r=0.16).

3.3.2.3   Mean SO_2 diurnal profile

Figure 15 shows the annual mean modelled and observed SO_2 diurnal cycle. The observed diurnal shows a small morning increase from 0.55 ppbv rising to a daytime maximum of 0.73 ppbv at 09:00, and slowly decreasing throughout the rest of the day. In contrast, modelled SO_2 decreased by half at around midday, and showed a small correlation with the observations (r=0.32).
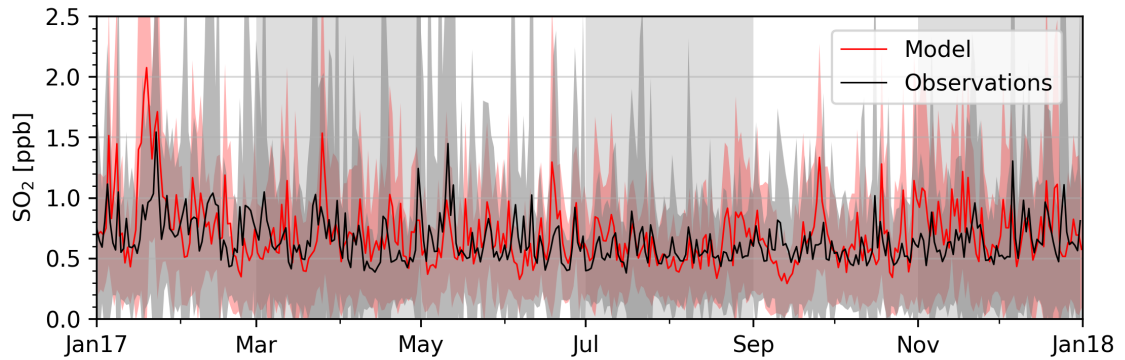
Figure 14: Daily mean observed (black) and modelled (red) SO$_2$ concentrations in ppbv for SO$_2$ (N=25). Shaded regions show the standard deviation about the mean. Y-axis limited for clarity. Maximum values were 5.01 ppbv for the observations and 4.01 ppbv for the model.
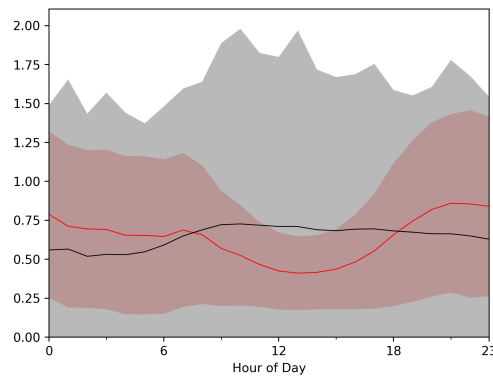
Figure 15: Mean observed (black) and modelled (red) diurnal profile for SO$_2$. Shaded regions show the standard deviation about the mean.

3.3.3   Carbon Monoxide

3.3.3.1   Annual mean CO

Ambient CO concentrations in the UK have remained below the statutory limit value for many years (DEFRA, 2021). Consequently, monitoring for CO is not a priority, with measurements available at only 6 AURN sites in 2017. Figure 16 compares annual median observed and modelled CO at the 6 AURN sites and at the Mace Head observatory (Ireland) with the modelled spatial distribution. Modelled concentrations were highest in the east and south-east of England, with small increases around large cities and industrial regions. The model overestimated the observed median of 90 ppbv by 15 ppbv and displayed a very low correlation coefficient (*r*=-0.09). The Mace Head site was accurately simulated

with a median bias of -0.03 ppbv for the year. Three of the AURN sites show lower annual median concentrations compared to those at Mace Head. Given the relatively long CO lifetime (several months) and the prevailing westerly flow of air, it is hard to reconcile several sites recording lower CO concentrations than the incoming airflow at Mace Head (Khalil and Rasmussen, 1990). This raises concerns about the quality of AURN CO measurements made with these IR absorbance instruments. Whilst this method may be sufficient for assessing whether the UK meets its air quality standards for CO (maximum daily 8-hour mean of 8,600 ppbv), current concentrations are substantially below this. The GC-MS measurements at Mace Head on the other hand, are intended for long-term monitoring of trace gases, and are considered the more accurate method. This raises concerns about the accuracy and precision of the IR instruments used in the DEFRA network for model assessment. Several of these older CO instruments were recently replaced in 2021 due to poor performance (Ricardo, 2021). Given concerns about the performance of these CO instruments, we don't discuss the model's performance for CO any further.
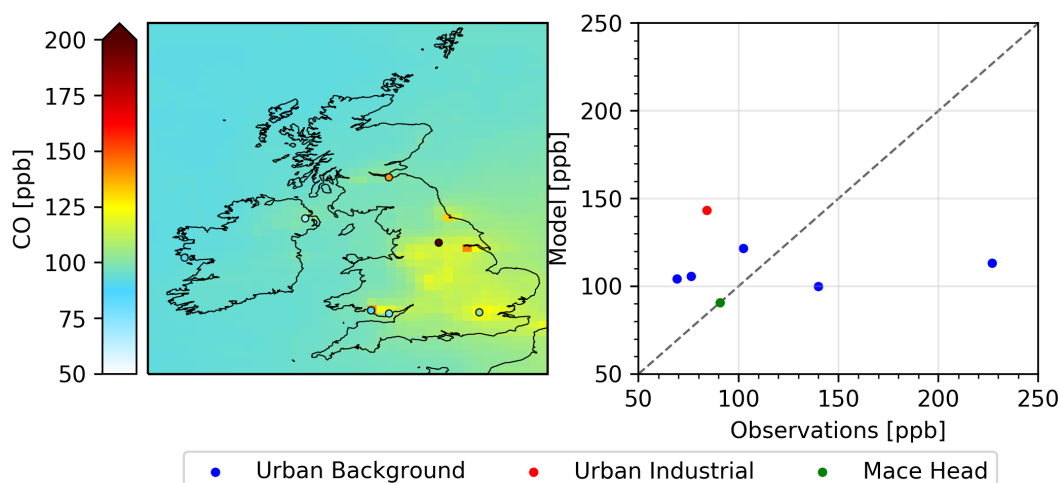
Figure 16: Left: Annual mean observed (filled points) and modelled (mapped) concentrations of CO concentration at the 6 AURN sites and Mace Head. Right: The grey dashed line shows the 1:1 relationship. Theil-Sen regression was not performed due measurement accuracy concerns.

3.3.4   Non methane volatile organic compounds (NMVOCs)

3.3.4.1   Annual mean NMVOC

Figure 17 shows the spatial distribution of the model calculation with the observations superimposed for ethane, propane, PRPE, ALK4, benzene, xylene, toluene and isoprene. Given the prevailing westerly winds, it is evident that there is a sizeable background concentration flowing in the country from the Atlantic for the longer lived species such as ethane, propane, ALK4 and benzene, with essentially no background for the shorter lived propene, xylene, toluene and isoprene. For the anthropogenic species highest concentrations are seen around the south east of the country, in the midlands and between Liverpool and Hull. Isoprene concentrations are high around London, over North Wales and Welsh borders region and in Scotland and Ireland. UK isoprene concentrations are dominated by biogenic contributions, so the spatial distribution reflects this (Khan et al., 2018; AQEG, 2009).
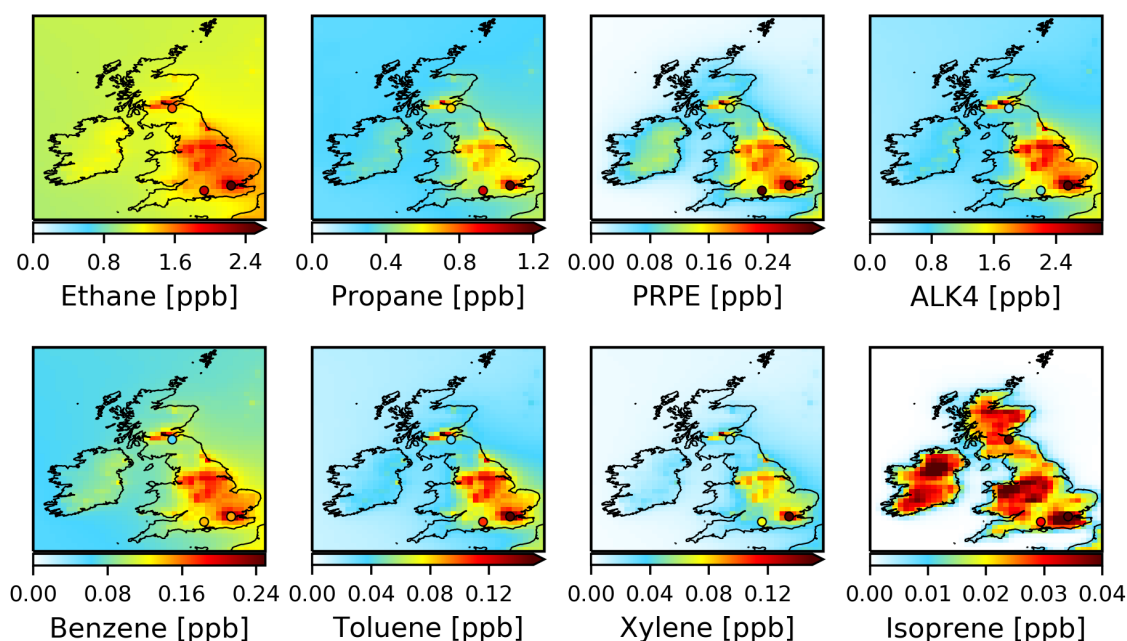
Figure 17: Annual mean observed (filled points) and modelled (mapped) concentrations for ethane, propane, PRPE, ALK4, benzene, xylene and toluene and isoprene. The mean for isoprene is calculated for the period 2017/05/15-2017/09/31.

Figure 18 compares the Normalised Mean Bias for each NMVOC at each of the three measurement sites. Auchencorth Moss (55.79 N, 3.24 W) is a Rural Background site located in Scotland, 18 km South of Edinburgh. Chilbolton Observatory (51.57 N, 1.32 W) is Rural Background site located in South East England, 80 km West of London and 200 m South East of the outskirts of Chilbolton village. London Eltham (51.5 N, 0.07 W) is a suburban background site in Greater London approximately 25 m North of the A210 Bexley Road. The relatively longer lived ethane and propane are generally underestimated, which is consistent with an underestimate in the global emissions for these species (Tzompa-Sosa et al., 2017; Etiope and Ciccioli, 2009; Dals øren et al., 2018). Underestimates of UK inventory emissions from urban natural gas leakage for ethane and propane, and road transport for propane (Derwent et al., 2017) could account for the larger bias at London Eltham compared to the other sites. As the lifetime of the NMVOC reducess a different pattern emerges. For the cleaner site (Auchencorth Moss) the model tends to overestimate concentrations. This might be explained by its proximity to Edinburgh which falls within the same model gridbox as the measurement site. For the more polluted sites (Chilbolton and London) the model

tends to underestimate. For isoprene the model tends to consistently underestimate concentrations by a factor of roughly 2 at all sites. The reported detection limit for these observations is typically 0.1 ppbv (DEFRA, 2011). Thus, observed benzene, toluene, xylene and most significantly, isoprene, were frequently at or below this level thus uncertainties in the measurement of these species may explain some of the biases observed.
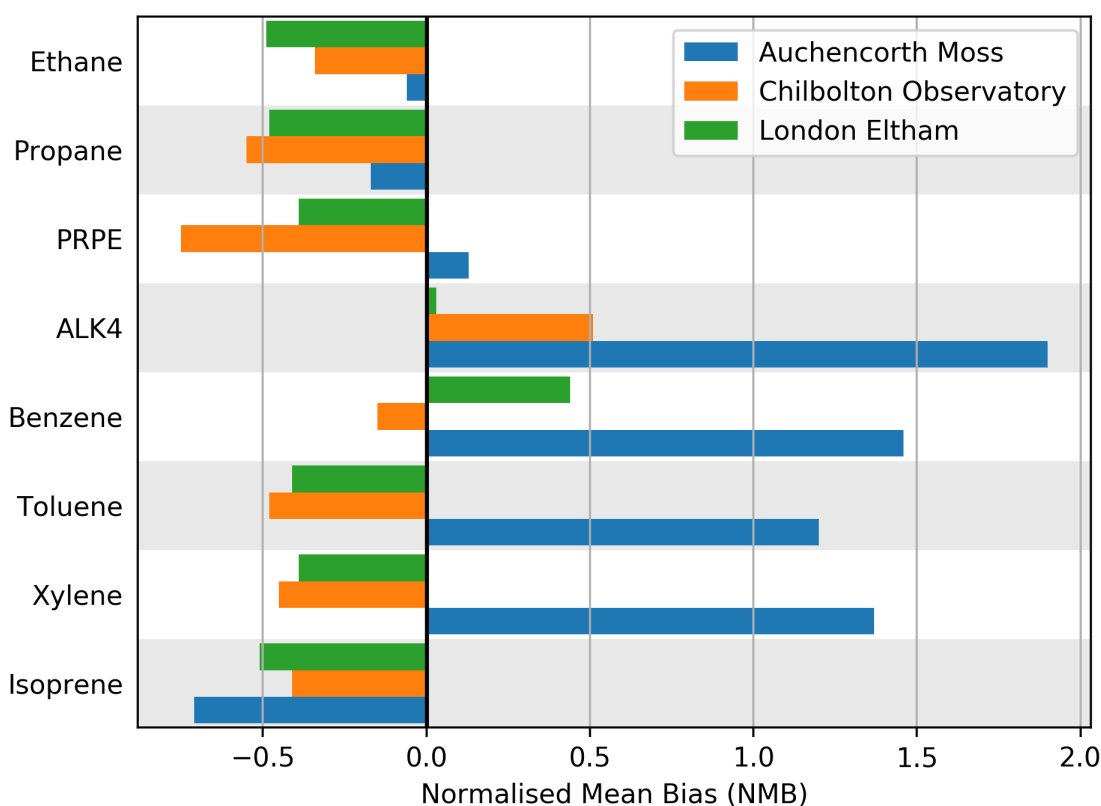
Figure 18: Model-Observation Normalised Mean Bias (NMB) at Auchencorth Moss (Blue), Chilbolton Observatory (Orange) and London Eltham (Green) for ethane, propane, PRPE, ALK4, benzene, toluene, xylene and isoprene.

3.3.4.2   NMVOC Daily mean

Figure 19 compares the annual daily mean NMVOC concentrations for the three sites with Table 7 showing the NMB and Pearson's *r* for each species. Modelled and observed anthropogenic NMVOCs share peak concentrations in the winter and minimums in the summer, consistent with low photochemical loss

and reduced vertical mixing in the winter. Model estimates for NMVOCs was poorest in the winter but more closely captured by ALK4 and Benzene, which were the only anthropogenic NMVOCs to show a positive bias overall. PRPE showed the weakest correlation and largest bias, attributed to most PRPE observations at both Auchencorth Moss and Chilbolton Observatory being available only during the winter (Section 3.2.3). Concurrent overestimates for ethane and benzene in September are discussed in Section 3.4.1. Consistent with the modelled estimates of Stewart et al. (2003), measurable Isoprene concentrations were mostly observed during the summer and early autumn, following the seasonality of light fluxes, temperatures and leaf biomass. Modelled isoprene captured the low/zero concentrations outside of the May-September period, and initially performed well in late May/early June, before significantly underestimating the observed increases later in the summer.

Table 7: Daily mean Normalised Mean Bias (NMB) and Pearson's coefficient *r* for ethane, propane, PRPE, ALK4, benzene, xylene, toluene and isoprene.

	Ethane	Propane	PRPE	ALK4	Benzene	Xylene	Toluene	Isoprene
NMB	-0.36	-0.42	-0.47	0.27	0.33	-0.28	-0.32	-0.40
r	0.69	0.80	0.43	0.76	0.52	0.72	0.74	0.75
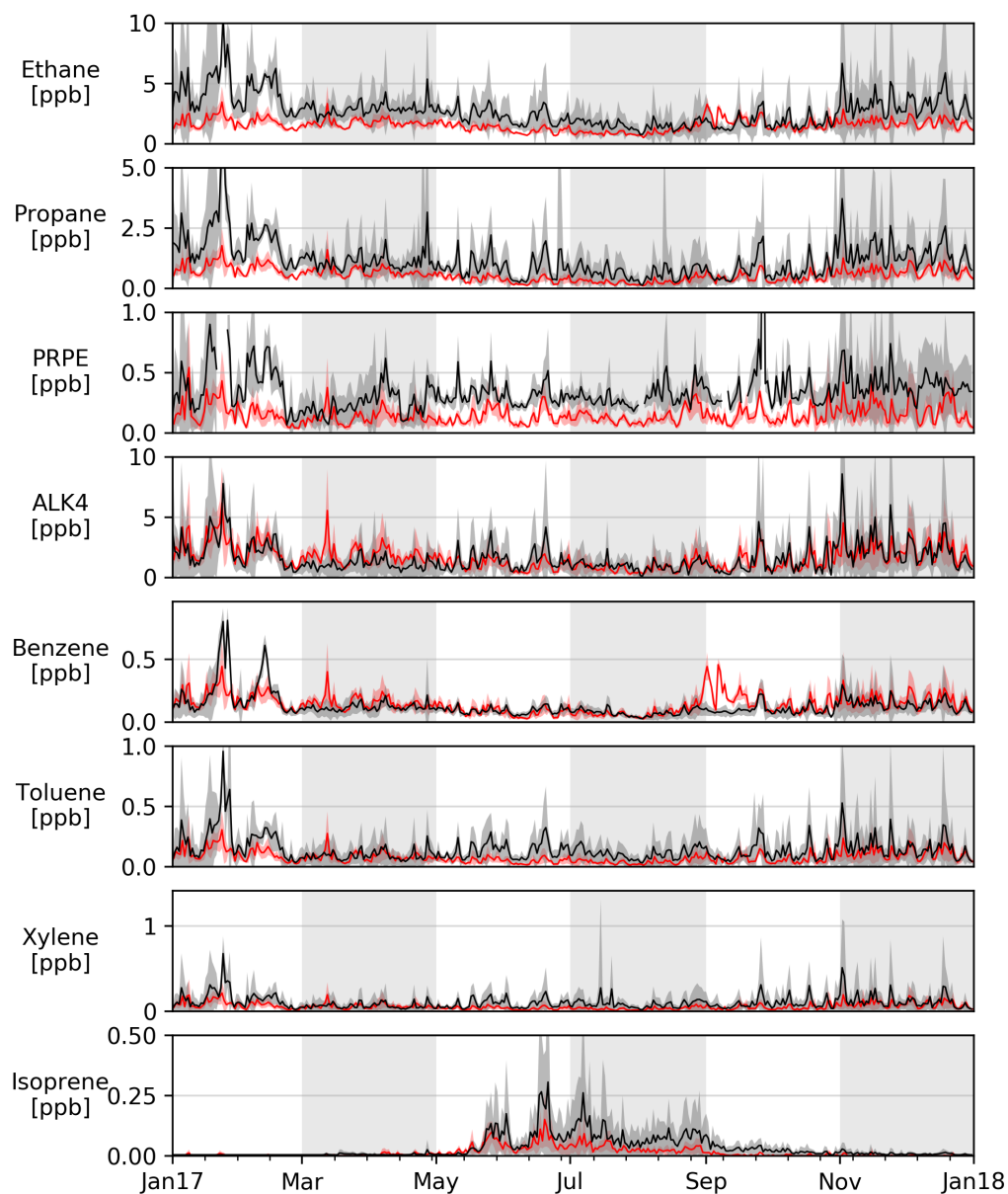
Figure 19: Daily mean observed (black) and modelled (red) concentrations for ethane, propane, PRPE, ALK4, benzene, xylene, toluene and isoprene. Shaded regions show the standard deviation about the mean. Y-axes limits were shortened for clarity.

3.3.4.3 Mean NVMOC Diurnal Profiles

Figure 20 shows the mean observed and modelled diurnals for the NMVOCs. With the exception of isoprene, observed NMVOC mixing ratios were moderately constant throughout the day, with small increases around 07:00 and 18:00 and decreases at midday. Simulated diurnals for ethane and propane showed strong correlations with the measurements (r_{ethane}=0.86; $r_{propane}$=0.84). The model shows a less pronounced daytime decrease compared to the observations, and an overall underestimate (NMB = -0.36 and -0.45 for ethane and propane, respectively). The observed diurnal profile for PRPE, ALK4, benzene, xylene and toluene show evidence of a morning and evening increase consistent with a traffic source. Although the corresponding modelled profiles showed some evidence of these rush-hour increase, they were smaller (r: 0.35, 0.89, 0.50, 0.82, 0.84 for PRPE, ALK4, benzene, xylene and toluene, respectively). Overall the model underestimated the concentrations of PRPE, ALK4, benzene, xylene and toluene (NMB: -0.54, 0.20, 0.32, -0.28, -0.29). Observations of isoprene show significant concentrations at night whereas modelled concentrations are significantly lower (NMB: -0.54, r: 0.80).
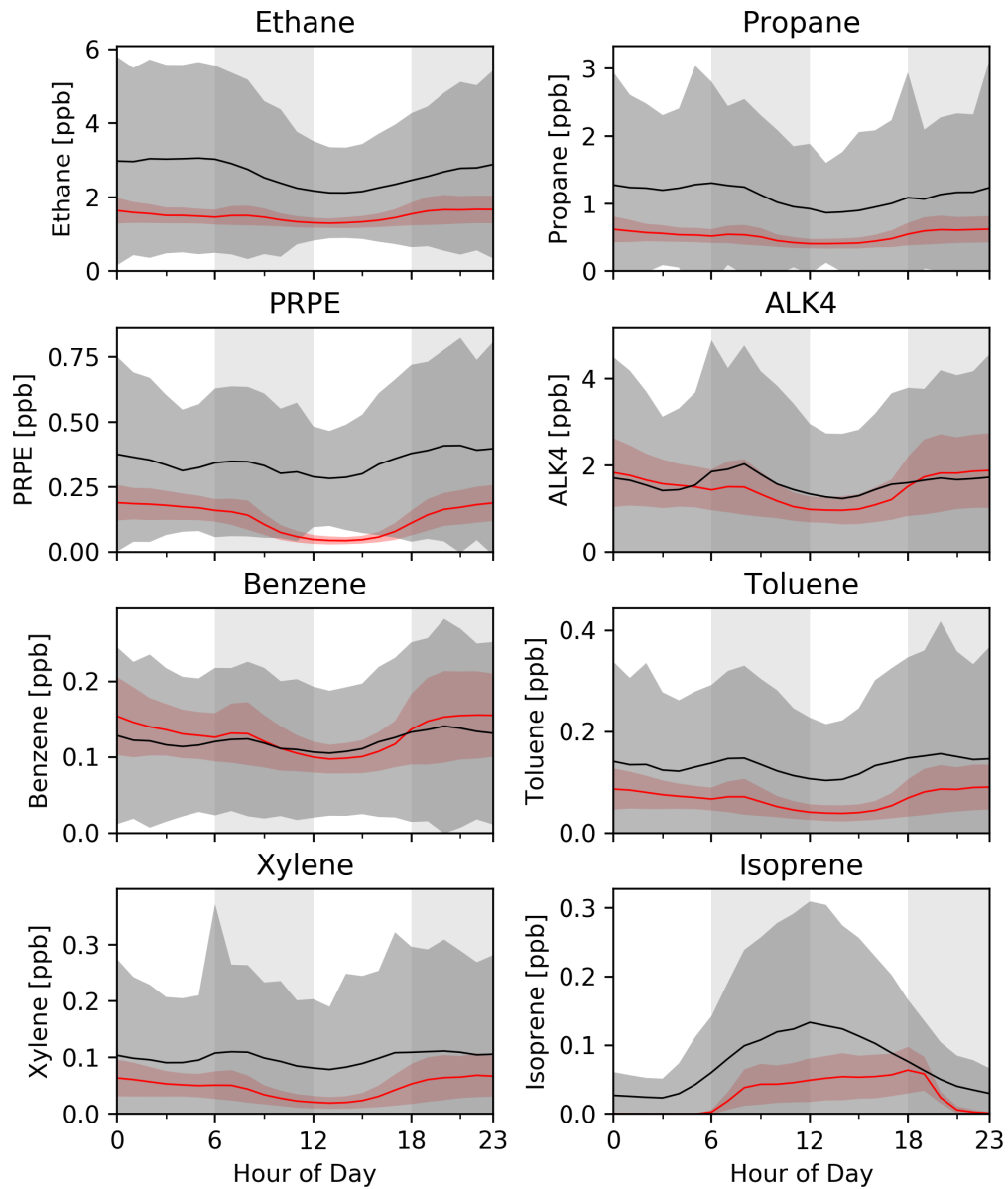
Figure 20: Mean observed (red) and modelled (black) diurnal profiles for ethane, propane, PRPE, ALK4, benzene, toluene and xylene for all of 2017, and for isoprene from 2017/05/15-2017/09/30. Shaded regions show the standard deviation about the mean.

3.3.5   Ammonia

3.3.5.1   Annual mean NH$_3$

Figure 21 compares the spatial distribution of modelled and observed mean ammonia concentration for 2017 on the left, with the annual mean measured and modelled concentration on the right. Modelled NH$_3$ shows the same general spatial distribution as the observations with high concentrations over agriculturally active areas and lower concentrations over mountainous regions of Scotland and Wales. On average the model underestimates concentration by 24% (NMB=-0.24) with a correlation coefficient of 0.53. The largest underestimates occurred in areas of the UK with high emissions, such as West England and the Welsh border,which could be indicative an bias in the input emissions.
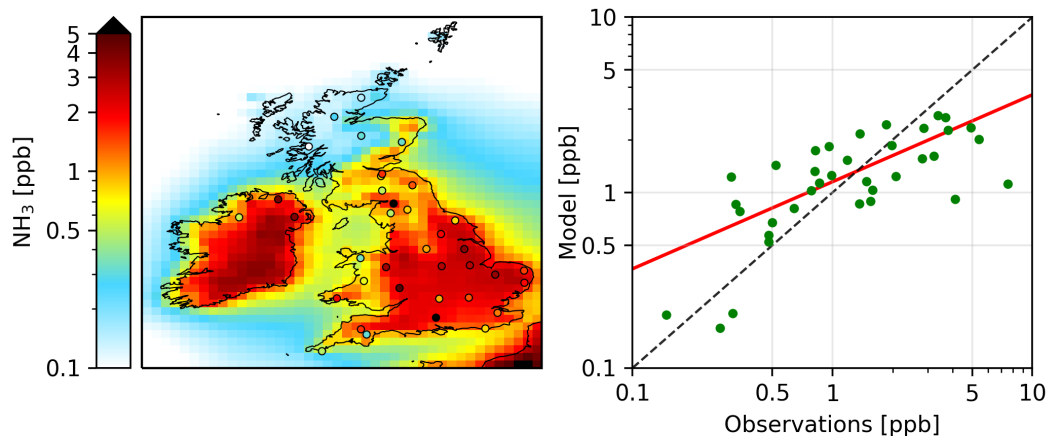
Figure 21: Left: Annual mean observed (filled points) and modelled (mapped) concentrations of NH$_3$. Right: Observed and modelled annual mean concentrations for NH$_3$ at each site, on a logarithmic scale.The best-fit (red line) was determined by Theil-Sen regression,and the dashed line (grey) shows the 1:1 relationship.

3.3.5.2   Daily mean NH$_3$

Comparison of daily mean observed and modelled NH$_3$ (Figure 22) across the sites shows seasonal changes in NH$_3$ concentrations to be fairly well captured by the model (r=0.68). The observed seasonality is small with a peak in March and

April associated with fertiliser and manure use (Hellsten et al., 2007). The model simulates this seasonality relatively well but tends to underestimate in January and February leading to a slightly enhanced seasonal cycle.
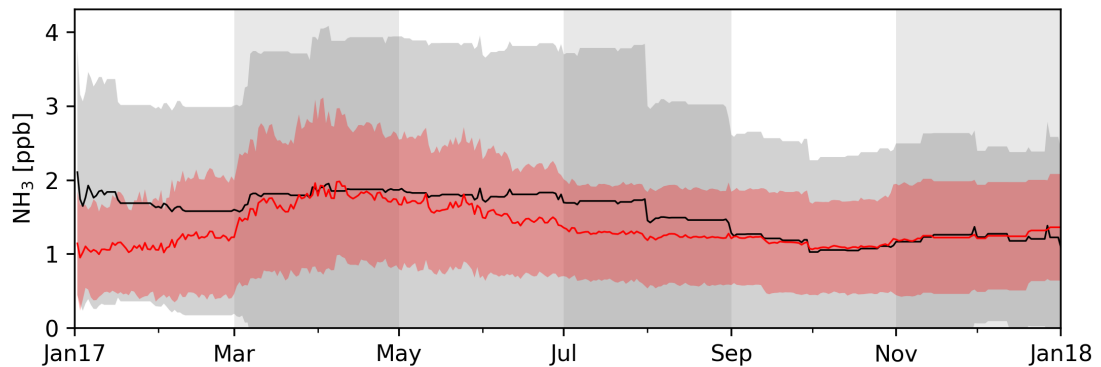
Figure 22: Daily mean observed (black) and modelled (red) concentrations of NH_3. Shaded regions show the standard deviation about the mean.

Comparison of the modelled and observed NH_3 diurnals is not performed due to the relatively low time-resolution of the observations (Table 6).

3.3.6   Ozone

Now that the model performance for primary pollutants has been assessed, we can turn to its ability to simulate secondary species.

3.3.6.1   Annual mean O_3

Figure 23 shows the annual mean concentration of O_3 calculated by the model and from the observations. Highest concentrations are seen over the Atlantic with O_3 concentrations decreasing as the air moves westwards in the prevailing winds. Concentrations are lower around areas with higher population density and NO_x emissions, with the highest mixing ratio of around 30 ppbv in more rural regions such as northern Scotland, South-West England and Western Ireland/Northern Ireland. Overall, the model showed a very small underestimate and reasonable spatial correlation with the observed annual averages (NMB=-0.07, r=0.67). The model error by environment type though varied more signifi-

cantly. Rural sites are biased low (NMB_{Rural}=-0.17) with a relatively high correlation (r_{Rural}=0.84) whereas Non-Rural sites (Urban Industrial, Urban Background, etc...) showed a smaller underestimate ($NMB_{Non-Rural}$=-0.02) with a weaker correlation ($r_{Non-Rural}$=0.56) (see Figure 23, right). There is therefore a degree of compensation in the overall performance. Explanations for the model differences are discussed in Section 3.4.3.
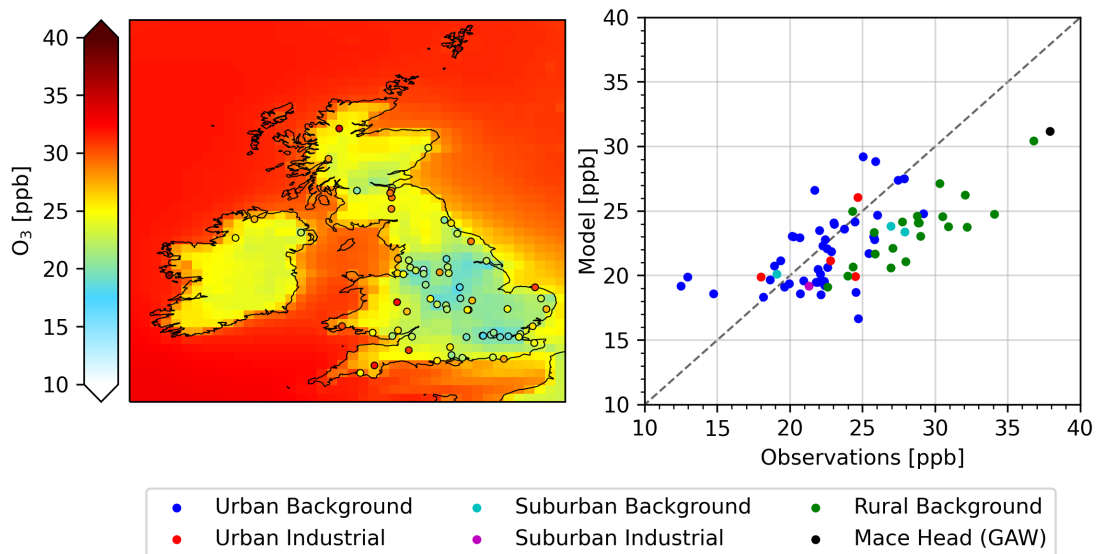
Figure 23: Left: Annual mean observed (filled points) and modelled (mapped) concentrations of O_3. Right: Observed and modelled annual mean concentrations for O_3 at each site.The best-fit (red line) was determined by Theil-Sen regression,and the dashed line (grey) shows the 1:1 relationship

3.3.6.2   Daily mean O_3

Figure 24 shows the daily mean observed and modelled O_3 across all sites and separated into Rural/Non-Rural sites. Observed O_3 reached a minimum in the winter, increasing to a maximum in late spring, then generally decrease into the rest of the year. There are occasional upwards and downwards spikes during pollution events such as in May and June (DEFRA, 2018). This seasonal trend was captured by the model with relatively high values of correlations in all environment types ($r_{AllSites}$=0.73; r_{Rural}=0.73; $r_{Non-Rural}$=0.75). The model underestimates concentrations in the springtime moving to a slight overestimate in the summer and

returning to an underestimate in the winter.
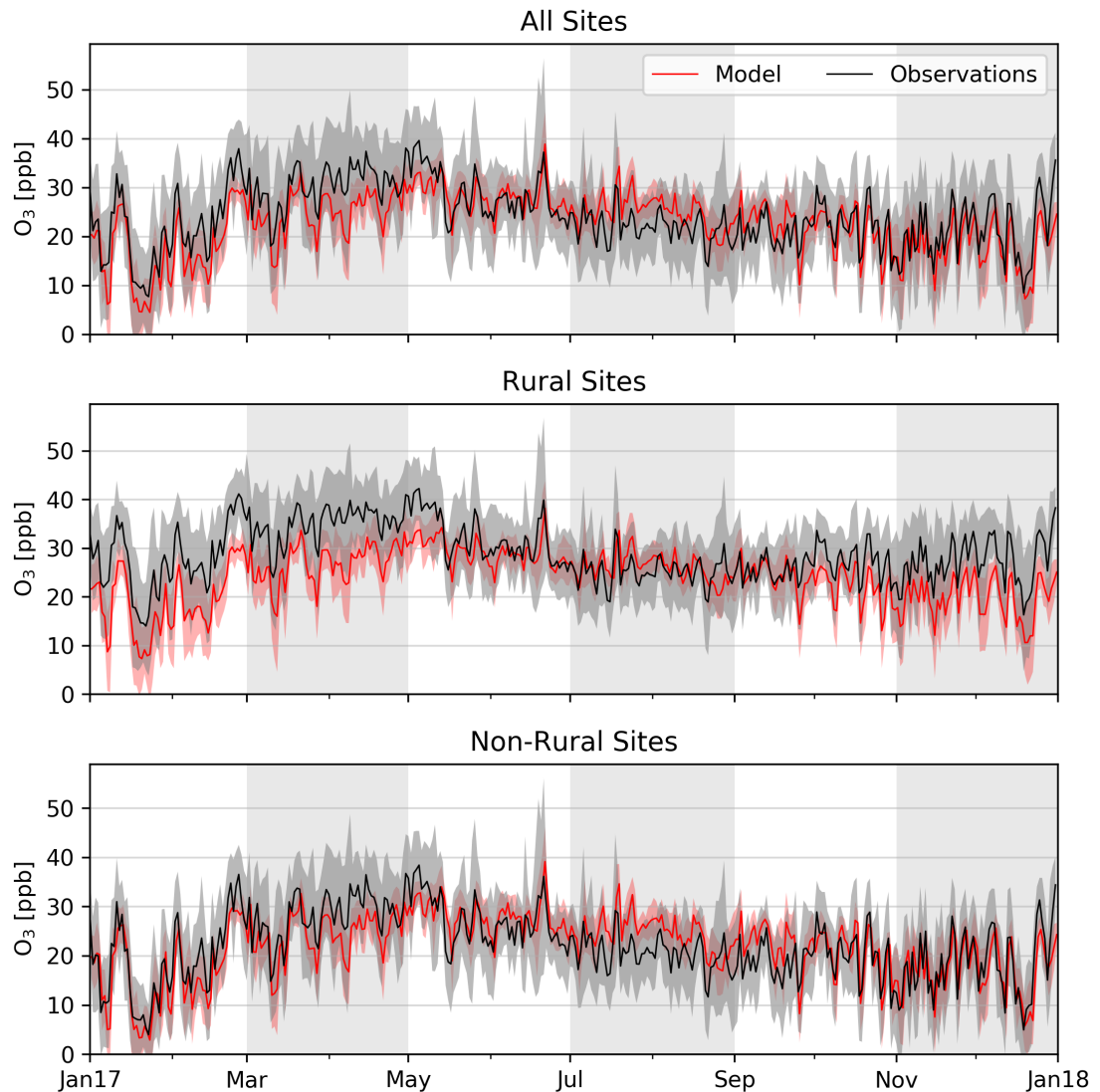
Figure 24: Daily mean observed (black) and modelled (red) concentration of O_3 for all sites (N=73), at Rural sites (N=22) and at Non-Rural sites (N=51). Shaded areas show the standard deviation about the mean.

3.3.6.3   Mean O_3 Diurnal Profile

Figure 25 compares the observed and modelled mean O_3 diurnal for All Sites, and at Rural and Non-Rural sites. When all of the sites are included, the observed O_3 decreases to a minimum at 06:00, then reaches a maximum at 14:00 and decreases into the evening. The overall simulated O_3 profile was similar (r=0.743, but with no morning decrease, and underestimating nighttime concentrations. Modelled Rural O_3 shows a systematic low bias (NMB=-0.17) and a

strong correlation with the observed diurnal profile (r=0.87). Non-Rural observations show pronounced morning decreases in concentration between 06:00 and 07:00, consistent with titration by road traffic NO_x emissions. The same decrease is not present in the model diurnal, which instead increases to an overestimate the daytime maximum by ~2 ppbv, and exaggerated the evening decrease to produce a small nighttime underestimate (NMB=-0.02, r=0.71). We discuss potential explanations for these differences in Section 3.4.3.
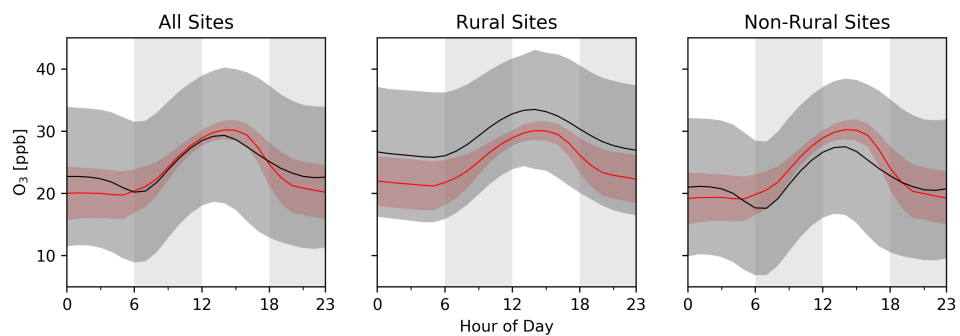
Figure 25: Mean observed (black) and modelled (red) diurnal for O_3 across all sites (N=73), Rural sites (N=22) and non-Rural sites (N=51). Shaded areas show standard deviation about the mean.

3.3.7   PM$_{2.5}$ and Sulfate, Nitrate and Ammonium Aerosol

3.3.7.1   Annual mean PM$_{2.5}$ and Sulfate, Nitrate, Ammonium Aerosol

Figure 26 compares the annual mean observed and modelled PM$_{2.5}$ spatial distribution (on the left) and the annual mean observed and modelled concentrations (on the right). Modelled and observed PM$_{2.5}$ were highest in South-East and central England at around 12 μgm^{-3}, and lowest in Scotland, Wales and Northern Ireland at around 6 μgm^{-3} The highest modelled concentrations in the domain extended over from the South-East of England to France, due to transport of PM$_{2.5}$ across to Europe and shipping emissions (Nawaz et al., 2023).The model is overall biased high by 3.25 μgm^{-3} with a NMB of 0.33, and a moderate correlation with the observations (r=0.70). Nearly all of the sites show this overestimate. Concentrations were underestimated at two measurement sites,

Bournemouth and Derry Rosemount with the largest underestimate at the coast at Bournemouth (obs: 12.86 μgm^{-3}, model: 7.43 μgm^{-3} (-42%)). The underestimate may relate to site position relative to model grid, as both sites are situated in mainly oceanic model gridboxes despite being on land close to cities.
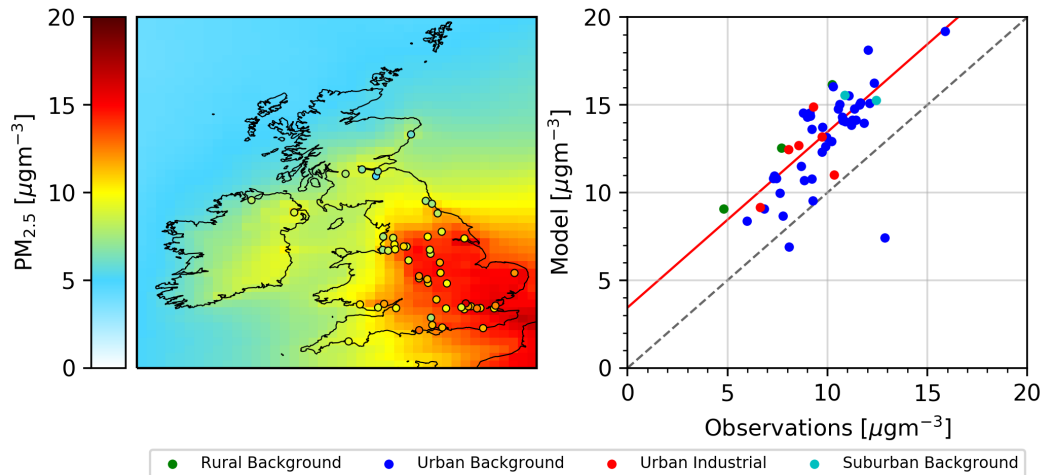
Figure 26: Left: Annual mean observed (filled points) and modelled (mapped) concentration of PM$_{2.5}$. Right: Observed and modelled annual mean concentrations for PM$_{2.5}$ at each site. The best-fit (red line) was determined by Theil-Sen regression,and the dashed line (grey) shows the 1:1 relationship

Figures 27 and 28 compare the modelled annual mean SO$_4^{2-}$, NO$_3^-$ and NH$_4^+$ aerosol concentrations spatially and on a site-by-site basis. The spatial distribution of aerosol SO$_4^{2-}$ was similar to that for SO$_2$ (Figure 13) but less localised around the areas with high SO$_2$ emissions. Simulated SO$_4^{2-}$ concentrations reach minima of 0.5-0.75 μgm^{-3} over oceans and remote areas, whilst central and South-East England show the highest concentrations of 2-2.5 μgm^{-3}. Observed SO$_4^{2-}$ is a factor of three lower than modelled (r=0.37, NMB=1.94). The observed mean SO$_4^{2-}$ for most sites is 0.2-0.9 μgm^{-3}, with higher concentrations in central and southern England and a maximum of 1.4 μgm^{-3} at Chilbolton Observatory.

The highest observed NO$_3^-$ aerosol concentrations of 2.5-3.0 μgm^{-3} occur around cities in central and South-East England, extending over the English Channel,

whilst minimum concentrations of 0.1-0.6 μgm^{-3} occur over oceans and remote regions like Northern Scotland. Simulated NO$_3^-$ captured this spatial variability well but with a consistent overestimate of 1.33 μgm^{-3} (r=0.96, NMB=0.77).

Measured NH$_4^+$ aerosol had a similar spatial distribution to aerosol NO$_3^-$, with maximums of 2.0 μgm^{-3} in central and South-East England and minimums of 0.1-0.5 μgm^{-3} in Northern Scotland. Modelled NH$_4^+$ concentrations were substantially higher than the measurements (NMB=1.24) but captured most of the spatial distribution (r=0.80).

Low volume denuder samplers used have been found to collect less than half the amount of particle phase secondary organic aerosol compared to high volume samplers (Kristensen et al., 2016). This negative measurement bias has been used to account for similar model overestimates (roughly 100%) of aerosol NO$_3^-$ and NH$_4^+$ in previous studies and may explain some of the issues here (Ge et al., 2021a), but PM$_{2.5}$ may still be too high.
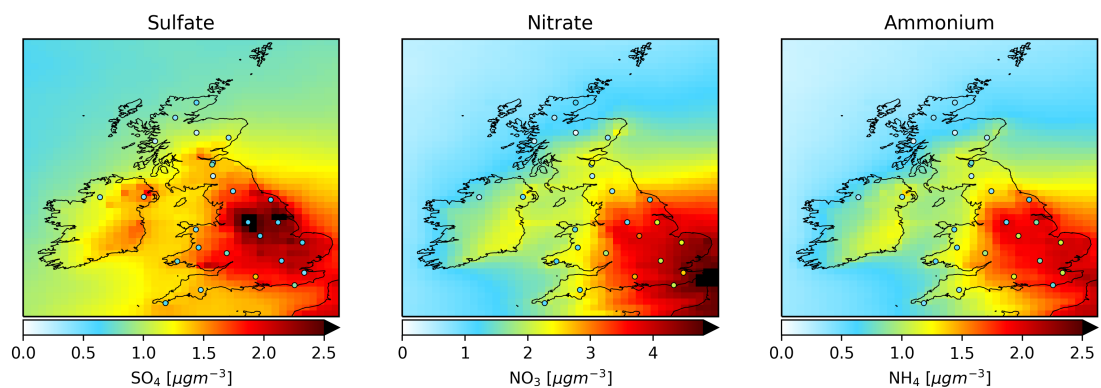
Figure 27: Annual mean observed (filled points) and modelled (mapped) concentrations of aerosol SO$_4^{2-}$ (left), NO$_3^-$ (center) and NH$_4^+$ (right).
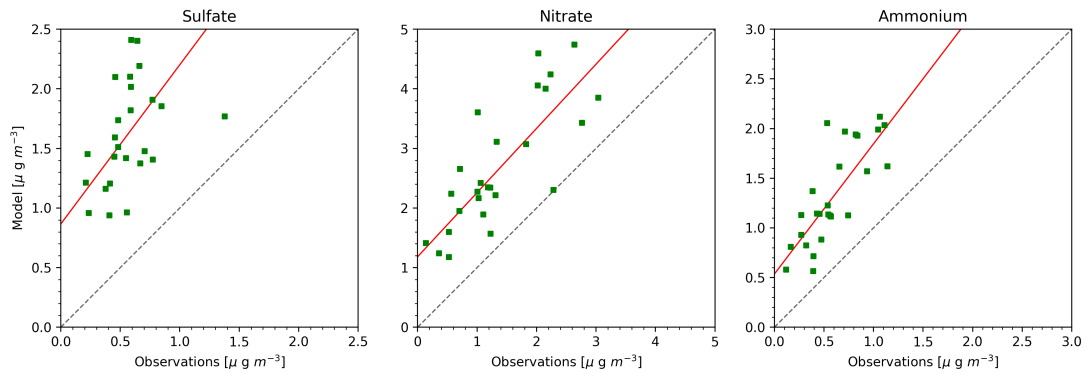
Figure 28: Observed and modelled annual mean concentration of aerosol SO_4^{2-} (left), NO_3^- (center) and NH_4^+ (right). The best-fit (red line) was determined by Theil-Sen regression, and the dashed line (grey) shows the 1:1 relationship

3.3.7.2   PM$_{2.5}$ Composition at AURN and MARGA measurement sites

Figure 29 shows the annual mean composition of modelled PM$_{2.5}$ at the 53 PM$_{2.5}$ measurement sites. Wet mass was determined by scaling as in equation 2. Inorganic aerosols made the largest contribution (65.3%) with NO_3^- (28.9%), SO_4^{2-} (21.6%) and NH_4^+ (14.8%). This is comparable to the reported range of 50-75% in ambient and high pollution conditions in the UK (Graham, 2021). The remaining composition was Sea Salt (14.9%), Organic Aerosol (15.5%), Dust (2.6%) and Black Carbon (2.4%). Given model overestimate of PM$_{2.5}$ and the major contribution of Sulphate/Nitrate/Ammonium to PM$_{2.5}$, it seems likely that the PM2.5 overestimate is strongly influenced by the SNA overestimate. There are only two sites in the sample with regular (hourly) measurements for both PM$_{2.5}$ and SNA aerosol, so evaluating the spatial changes in PM$_{2.5}$ composition over the whole UK was not possible.
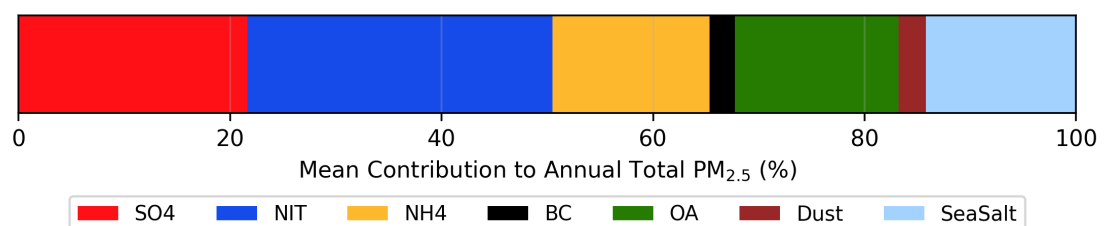
Figure 29: Annual mean contribution of model PM$_{2.5}$ components to total PM$_{2.5}$ wet mass across all PM$_{2.5}$ measurement sites for the year (N=53).

Figure 30 compares the annual mean measured and modelled dry mass concentrations of aerosol SO_4^{2-}, NO_3^-, NH_4^+, BC and OA at these two sites, Auchencorth Moss (ACTH) and Chilbolton Observatory (CHBO), with the remaining modelled $PM_{2.5}$ components also shown. The model correctly identifies that concentrations are higher at CHBO than at ACTH, and that the dominant contribution to $PM_{2.5}$ dry mass comes from the inorganic aerosol component also. At CHBO, BC concentration is overestimated by 0.05 μgm^{-3} (28%) and OA is underestimated by 0.18 μgm^{-3} (14%). Although the model shows large overestimates at ACTH for both BC (0.07 μgm^{-3}, 103%) and OA (0.25 μgm^{-3}, 58%), there were far fewer measurements for the year at this site (see Figure fig:OCBCMARGA).
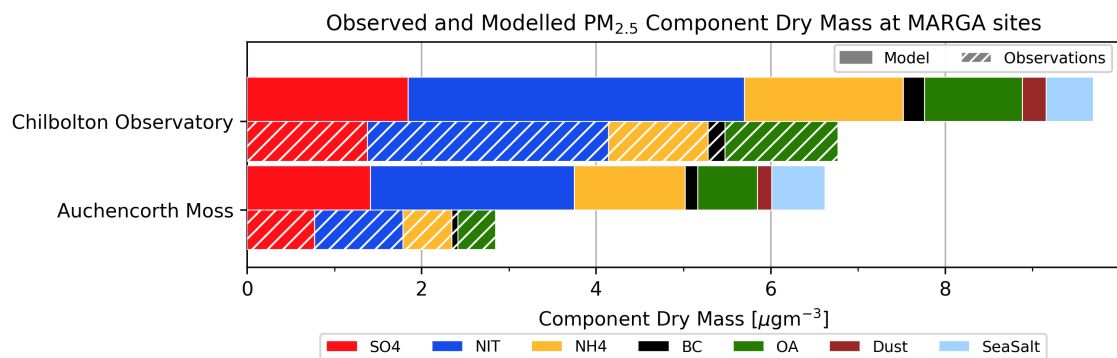
Figure 30: Annual mean observed (hatched) and modelled (solid) dry mass of SO_4^{2-}, NO_3^-, NH_4^+, BC and OA at Auchencorth Moss and Chilbolton Observatory. Modelled bars also show the dry mass of modelled Dust and SeaSalt, which are not measured.

3.3.7.3   Daily mean $PM_{2.5}$, Sulfate, Nitrate, Ammonium Aerosol , Organic Carbon and Black Carbon

Figure 31 compares the daily mean concentrations of observed and modelled $PM_{2.5}$ (NMB=0.36; *r*=0.72). Both show the highest spikes during the winter, with smaller maxima in the summer. These rapid increases in concentration were correctly captured in simulated $PM_{2.5}$ but with a tendency to overestimate the magnitude of the increases (the 90th percentiles for the observations was 16.93 μgm^{-3} whereas the modelled was 24.07 μgm^{-3}).
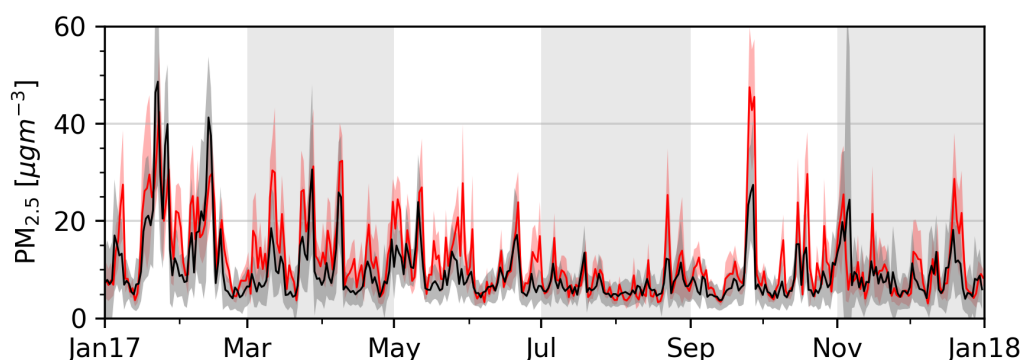
Figure 31: Daily mean observed (black) and modelled (red) concentration of $PM_{2.5}$. Shaded areas show the standard deviation about the mean.

Figure 32 compares daily mean Sulphate/Nitrate/Ammonium concentration at the two MARGA sites, Auchencorth Moss and Chilbolton Observatory. The UKEAP sites were excluded as they only provide monthly average measurements (Section 3.2.3). Measured SO_4^{2-} showed large, brief increases in January, February and September, with maximum of 7.54 μgm^{-3} in mid-February and concentrations around 1.06 μgm^{-3} during the rest of the year. Modelled SO_4^{2-} identified these increases reasonably well (r=0.55) but overestimated the lower concentrations during the rest of the year, particularly in the summer. Between January and May, measured NO_3^- had several large increases from a low baseline concentration of 1.81 μgm^{-3}, and a maximum in late September of 24.8 μgm^{-3}. NO_3^- was modelled well at low concentrations, and the model correctly identified the periods of increased concentration (r=0.76), but overestimated during periods of higher concentration. Measured NH_4^+ showed similar increases in the first half of the year to NO_3^-, reaching a maximum of 10.44 μgm^{-3} in March, and lower concentrations of around 0.86 μgm^{-3} throughout the rest of the year. These changes were well represented in simulated NH_4^+ (r=0.77), with the positive bias occurring when the model overestimates increases in concentration later in the year.

Figure 33 and 34 compare the modelled daily mean concentrations of OA and BC with the weekly averaged measurements at each of the two MARGA sites. The model reasonably captures the changes observed for both species at either

site. Further interrogation of the performance will not be performed for OA and

BC due to the coarse time resolution of the available measurements.
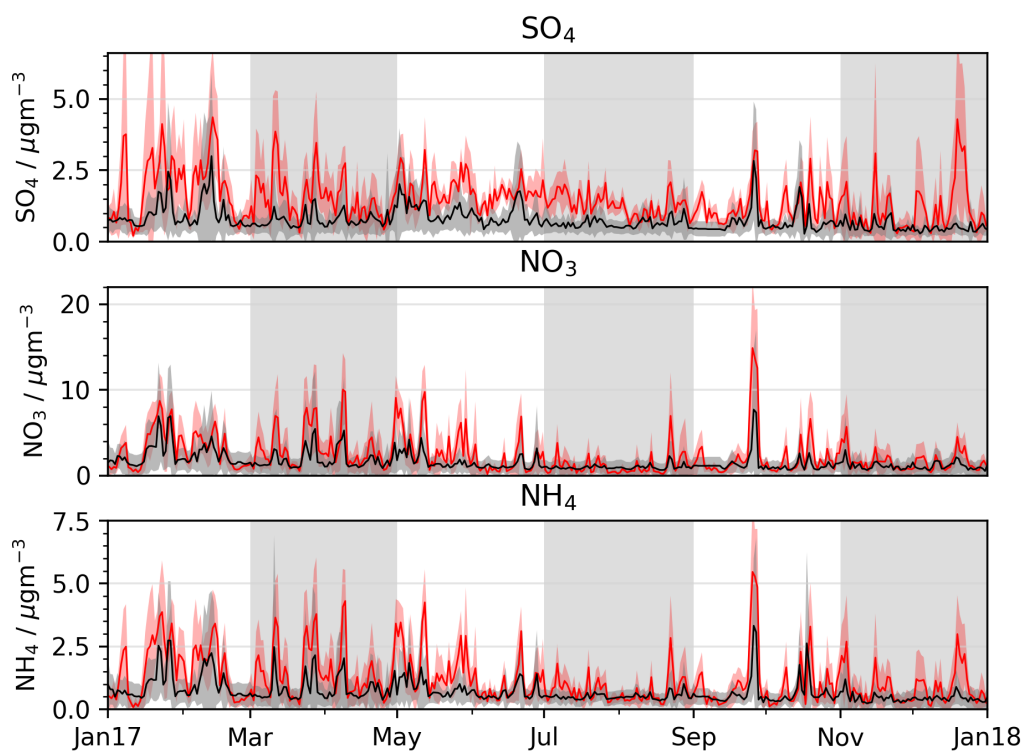
Figure 32: Daily mean observed (black) and modelled (red) concentration of of aerosol SO_4^{2-} (left), NO_3^- (centre) and NH_4^+ (right) at the two MARGA sites, Auchencorth Moss and Chilbolton Observatory. Shaded areas show the standard deviation about the mean.

OA in PM$_{2.5}$
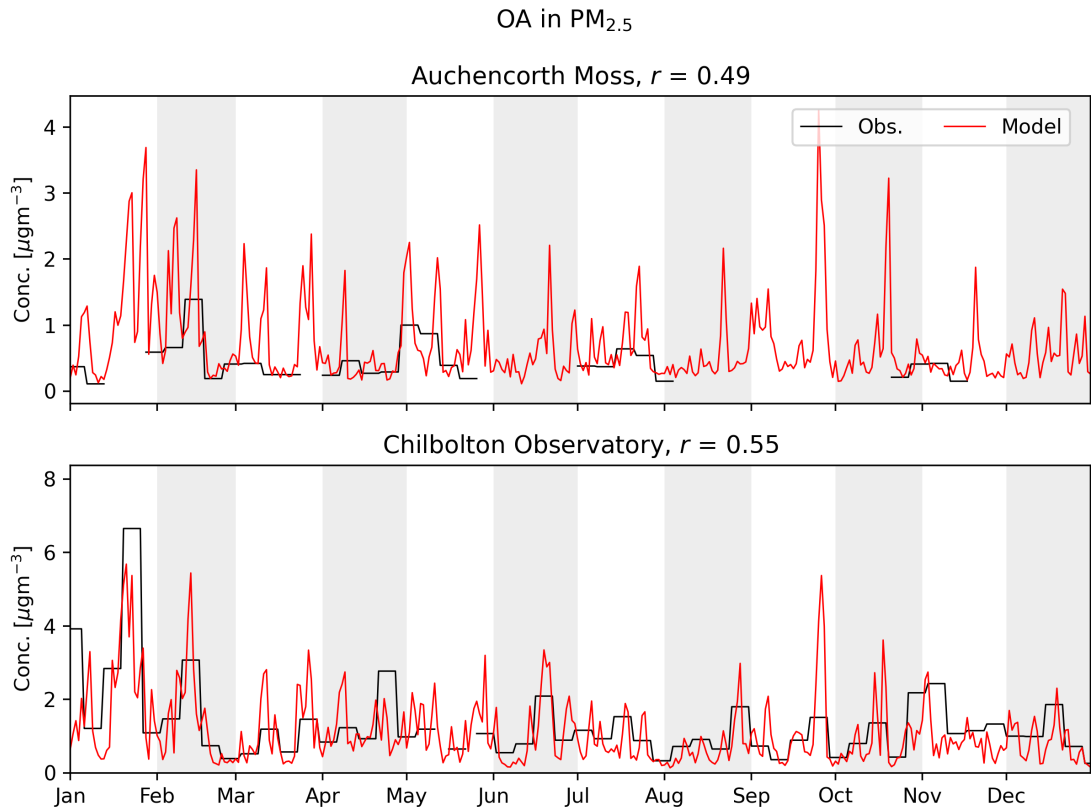
Figure 33: Mean weekly observed (black line) and daily modelled (red line) OA at at Auchencorth Moss and Chilbolton Observatory from 2017/01/01-2018/01/01.

BC in PM$_{2.5}$
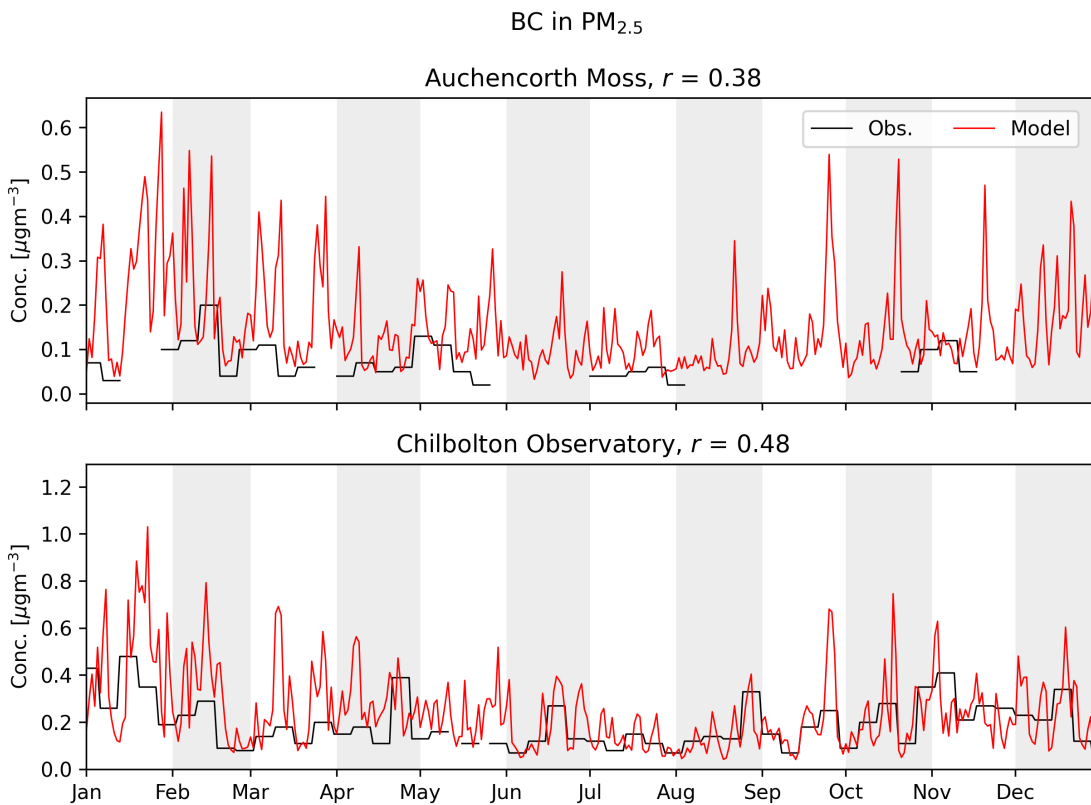
Figure 34: Mean weekly observed (black line) and daily modelled (red line) BC at at Auchencorth Moss and Chilbolton Observatory from 2017/01/01-2018/01/01.

3.3.7.4   Mean PM$_{2.5}$ and Sulfate, Nitrate, Ammonium Aerosol Diurnal Profiles

Figure 35 compares the mean observed and modelled PM$_{2.5}$ diurnals for the year. Observed PM$_{2.5}$ are generally flat throughout the day. In comparison, starting from the afternoon minimum of 6.1 μgm^{-3}, modelled PM$_{2.5}$ increased steadily throughout the night to a morning maximum of 11.7 μgm^{-3} at 0500, with a decrease towards the afternoon minimum (r=0.50).
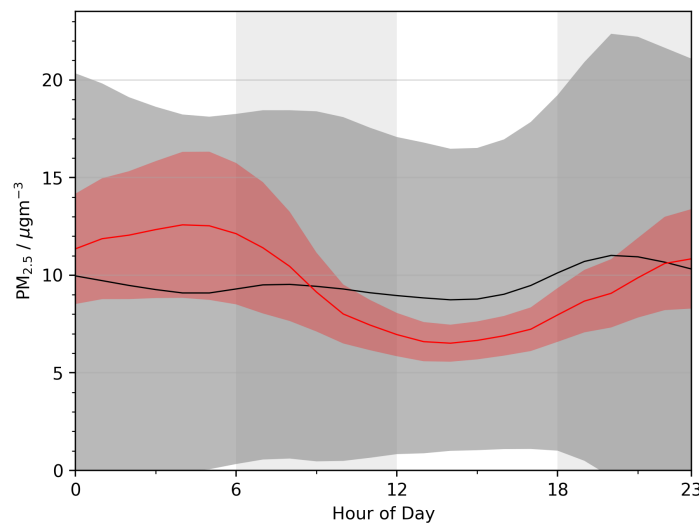
Figure 35: Mean observed (black) and modelled (red) diurnal profile for PM$_{2.5}$ across all sites. Shaded areas show standard deviation about the mean.

As in Section 3.3.7.3, model performance for estimating Sulphate/Nitrate/Ammonium diurnals focuses on the two MARGA sites: Auchencorth Moss (ACTH), in Scotland, and Chilbolton Observatory (CHBO), in South East England. As the two sites are well separated and both observed and modelled concentrations were substantially different at each (Figure 27), we separately evaluate the diurnals at either site in Figure 36. Modelled diurnals showed very similar profiles: a morning maximum at 0500 and an afternoon minimum around 15:00. This profile was more pronounced at CHBO than ACTH. Observed SNA diurnals at ACTH showed a small midday decrease of $\sim$0.1 μgm^{-3} for SO$_4$, and a mid-afternoon decreases

for NO_3^- and NH_4^+, where the model overestimated (NMB_{ACTH}=0.82, 1.25, 1.00; r_{ACTH}=0.5, 0.97, 0.89 for SO_4^{2-}, NO_3^- and NH_4, respectively). Observed concentrations at CHBO were roughly twice those at ACTH and showed smaller overestimates for SO_4^{2-} (29%), NO_3^- (24%) and NH_4^+ (42%). Whilst the model overestimated the amplitude of daytime changes, they were reasonably well represented for SO_4^{2-} (r_{CHBO}=0.50), NO_3^- (r_{CHBO}=0.97) and NH_4^+ (r_{CHBO}=0.89).
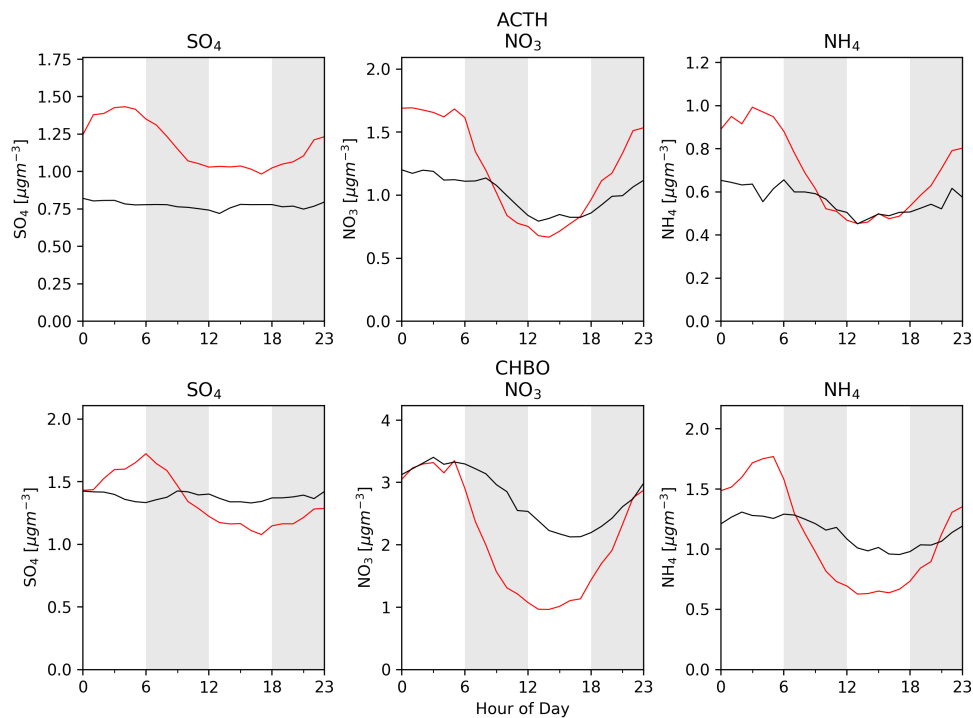
Figure 36: Mean observed (black) and modelled (red) diurnals for aerosol SO_4, NO_3^- and NH_4^+ at Auchencorth Moss (ACTH, top row) and Chilbolton Observatory (CHBO, bottom row). Shaded areas show standard deviation about the mean.

Modelled $PM_{2.5}$ and Sulphate/Nitrate/Ammonium showed diurnal profiles (Figure 35, 36) with a maximum around 06:00, a mid-afternoon minimum and evening increase, which could be attributed to a sensitivity to changes in planetary boundary layer height (PBLH). This has previously been identified as a source of error for PM diurnals in GEOS-Chem (Li et al., 2023b) as well as in other CTMs (Du et al., 2020; Lin et al., 2017). In this case, a shallow boundary layer and weak vertical mixing at night facilitate buildup, and a daytime increase in PBLH produces a drop in concentration. This effect would be strongest in warmer months, when

changes in PBLH are larger (Liu and Liang, 2010). This weakness in model is driven by the meteorological fields used to drive the model.

3.3.8   Model Performance Summary

Tables 8 and 9 summarise model performance. Estimates for NO_x species showed reasonable spatial and synoptic correlations with observations but were underestimated by around 50%.These underestimates were smaller when only Rural sites were considered, and larger for Non-Rural sites. Model NO_x diurnals underestimated the prominent traffic-induced morning and evening increases. SO_2 performance was marred by large overestimates for some sites coinciding with areas with high local emissions, while other, lower emission sites were more accurately represented and typically underestimated slightly. Although the average SO_2 concentration was reasonably estimated (NMB=0.22), synoptic and diurnal changes in the observations were not well identified by the model. Modelled anthropogenic NMVOCs were highest around large cities, but the accuracy of their spatial distribution could not be assessed due to the small number of monitoring sites available. Synoptic and diurnal changes were well captured in observed concentrations across the three measurement sites. Benzene and ALK4 were overestimated by $\sim$30%, and the remaining NMVOCs were underestimated by $\sim$50%. The spatial distribution of model NH_3 was captured with a small underestimate of 18%. Considering the relatively low measurement frequency and constituency of the UKEAP network NH_3 measurements throughout the year, the seasonality was captured well, with underestimates early in the year being the largest cause for error.

Spatial, seasonal and diurnal profiles were well correlated for O_3. O_3 was most accurately simulated in the summer months, and underestimated for the rest of the year. As with NO_x, there was a distinction between performance in Rural and Non-Rural environments. Rural sites showed a constant underestimate of 11%, whereas Non-Rural concentrations showed a smaller overestimate of 4%,

but with rush-hour decreases not represented in the model diurnal profile. Synoptic changes in $PM_{2.5}$ were accurately captured by the model but overestimated by 24%. Given inorganic aerosols were the largest component of simulated $PM_{2.5}$ mass across the sample sites, and showed large overestimates of 173%, 77% and 104 % for SO_4^{2-}, NO_3^- and NH_4^+, respectively, the $PM_{2.5}$ overestimate can be largely attributed to model bias in these species.

Table 8: Summary of model Normalised Mean Bias (NMB) and Pearson's *r* for all sites for NO, NO_2, NO_x, NO_y, SO_2, CO, NH_3, O_3, Ethane, Propane, PRPE, ALK4, Benzene, Toluene, Xylene, Isoprene, NH_3, O_3, $PM_{2.5}$, Corrected $PM_{2.5}$ ($PM_{2.5}$*, see Section 3.4.2) and SO_4, NO_3^- and NH_4 aerosol.

Species	Annual		Daily		Diurnal	
	NMB	*r*	NMB	*r*	NMB	*r*
NO	-0.77	0.44	-0.77	0.43	-0.76	0.48
NO_2	-0.52	0.6	-0.53	0.65	-0.52	0.48
NO_x	-0.42	0.56	-0.59	0.59	-0.57	0.43
NO_y	-0.43	0.57	-0.47	0.56	-0.43	0.43
SO_2	0.23	0.48	0.23	0.16	0.23	0.32
CO	-	-0.09	-	-	-	-
NH_3	-0.24	0.53	-0.12	0.65	-	-
O_3	-0.07	0.67	-0.07	0.73	-0.07	0.73
O_X	-0.19	0.18	-0.19	0.49	-0.19	0.72
$PM_{2.5}$	0.33	0.7	0.36	0.72	0.33	0.5
$PM_{2.5}$*	-0.2	0.72	-0.19	0.74	-0.2	0.55
SO_4^{2-}	1.94	0.37	0.52	0.55	0.48	0.6
NO_3^-	0.77	0.96	0.67	0.76	0.67	0.84
NH_4^+	1.24	0.8	0.8	0.77	0.8	0.81
Ethane	-0.36	-	-0.36	0.69	-0.36	0.86
Propane	-0.42	-	-0.42	0.8	-0.42	0.84
PRPE	-0.47	-	-0.47	0.43	-0.47	0.35
ALK4	0.27	-	0.27	0.76	0.27	0.89
Benzene	0.33	-	0.33	0.52	0.33	0.5
Xylene	-0.28	-	-0.28	0.72	-0.28	0.82
Toluene	-0.32	-	-0.32	0.74	-0.32	0.84
Isoprene	-0.4	-	-0.4	0.75	-0.4	0.8

Table 9: Summary of model Normalised Mean Bias (NMB) and Pearson's *r* (daily and diurnal) for SO_4^{2-}, NO_3^-, NH_4, OA and BC at Auchencorth Moss and Chilbolton Observatory for 2017. Summary statistics correspond to sections 3.3.7.3 and 3.3.7.4.

	ACTH			CHBO		
Species	NMB	r_{day}	r_{hour}	NMB	r_{day}	r_{hour}
SO_4^{2-}	0.82	0.48	0.50	0.29	0.55	0.14
NO_3^-	1.25	0.70	0.97	0.24	0.78	0.97
NH_4^+	1.00	0.70	0.89	0.42	0.80	0.95
OA	0.58	0.49	-	-0.18	0.55	-
BC	1.03	0.38	-	0.28	0.48	-

3.4   Discussion

This section will discuss some of the potential explanations for the differences between the model and measurements shown in Section 3.3. Very often the failure of a model to simulate concentration is attributed to errors in emissions. Often, this is linked to errors in the estimates of local emissions and there is strong experimental evidence to support this (see for example Karl et al. (2017)). However, there are potentially other explanations and we explore some of these here. For longer-lived species, errors in the boundary conditions used in the model may provide an explanation (Section 3.4.1). In Section 3.4.2, we correct the model $PM_{2.5}$ bias by accounting for biases in the inorganic aerosol component of $PM_{2.5}$. The model horizontal resolution could account for some of the differences seen (Section 3.4.3). Finally, uncertainties in the heights of emissions for industrial and energy generation activities are explored in 3.4.4.

3.4.1   Model Boundary Conditions

For longer-lived species, long-range transport from outside of the model domain can be a significant contributor to the concentrations calculated within the domain. For example, Romero-Alvarez et al. (2022) reports that 71% of UK O_3 is sourced outside of the country. Thus model errors on the global distribution of these species can lead to errors in our calculations for the UK. From the perspec-

tive of a model run in a regional configuration, this error is often associated with the boundary conditions used in the model.

Much of the air over the UK is transported in the prevailing Westerly winds from the Atlantic. Thus, a bias in the modelled O_3 concentration in that air may lead to an underestimate in the O_3 concentrations calculated over the UK. The measurements site at Mace Head, Republic of Ireland (53.326 °N, -9.904 °E) experiences predominant ($\sim$51 %) westerly winds from across the Atlantic (Jennings et al., 2003). It is thus well suited to assess the model's ability to simulate background concentrations of O_3 entering the UK. Figure 37 shows the daily mean observed and modelled O_3 at Mace Head.
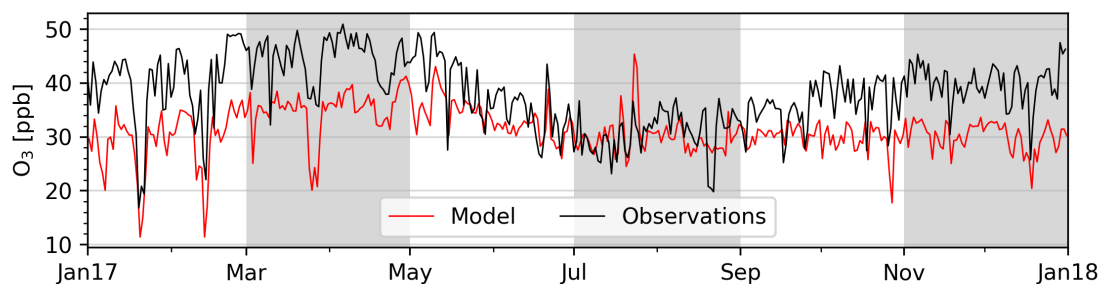
Figure 37: Daily mean observed (black) and modelled (red) concentration of O_3 at Mace Head, Ireland, from 2017-01-01 to 2017-12-31. Shaded areas show the standard deviation about the mean.

The observed annual mean O_3 at Mace Head was the highest of any site in the domain, at 37.89 ppbv, with a model bias of -6.7 ppbv (17.6%) (see Figure 23). Figure 37 looks similar to the mean O_3 in the rural sites shown in Figure 19. Both show a model underestimate in the winter, spring and autumn, with almost no bias in the summer time. Thus it would appear that the model underestimate in O_3 concentrations at the rural sites is linked to the underestimate in the O_3 flowing into the UK. This underestimate in background O_3 concentrations is thought to be an issue in this version of the model (GEOS-Chem Steering Committee, 2022; Wang et al., 2022) occurring over oceanic regions and may be a result of errors in the representation of halogen chemistry in the model. Thus, accurate simulation of the concentration of long lived species will require improvements in

the accuracy of the simulated boundary conditions.

Other long-lived species such as ethane and propane also show underestimates in the model (see Figure 19). These species are also known to show a global underestimate in GEOS-Chem and other models (Tzompa-Sosa et al., 2017; Etiope and Ciccioli, 2009). This is likely due to underestimates in their global emissions. Thus to address the problems associated with these species, a global rather than regional perspective should be taken.

3.4.2   PM$_{2.5}$ bias correction

Overestimates or underestimates for individual PM$_{2.5}$ components will contribute to biases seen in modelled PM$_{2.5}$ composition and concentration. Section 3.3.7 showed that inorganic aerosols made large contributions to total PM$_{2.5}$ mass, but also that this contribution was overestimated. Figure 38 compares the annual mean measurements to those with modelled PM$_{2.5}$ determined with inorganic aerosol concentrations reduced, accounting for overestimates of SO$_4^{2-}$ (193.61%) NO$_3^-$ (95.81%) and NH$_4^+$ (123.85%) (Figure 28). Although Section 3.3.7 also also evaluated to OA and BC components, this was based on comparisons for only two measurement sites and so we do not attempt to account for these errors in modelled PM$_{2.5}$. We note that the SO$_4^{2-}$ bias correction is roughly comparable to the approach of (Marais et al., 2021), where UK anthropogenic SO$_2$ and SO$_4^{2-}$ emissions from land-based point sources were reduced by a factor of 3 to account for possible bias in SO$_2$ emissions on the GEOS-Chem simulation. The modelled PM$_{2.5}$ overestimate of 66% at Rural sites reduces to 0.0%, and the 32% overestimate at Non-Rural sites reduces to a 21% underestimate. This overcompensation for error in Urban environments could be due to (1) failure to account for other PM components which may have larger Urban contributions and errors . (2) The SO$_4^{2-}$, NO$_3^-$ and NH$_4^+$ biases being determined from Rural Background sites only, and so may not correctly capture bias in Urban environments. (3) Poor

representativity between SO_4^{2-}, NO_3^- and NH_4^+ error and $PM_{2.5}$ error due to different measurement locations and difficulties resolving Urban concentrations at this model horizontal resolution.
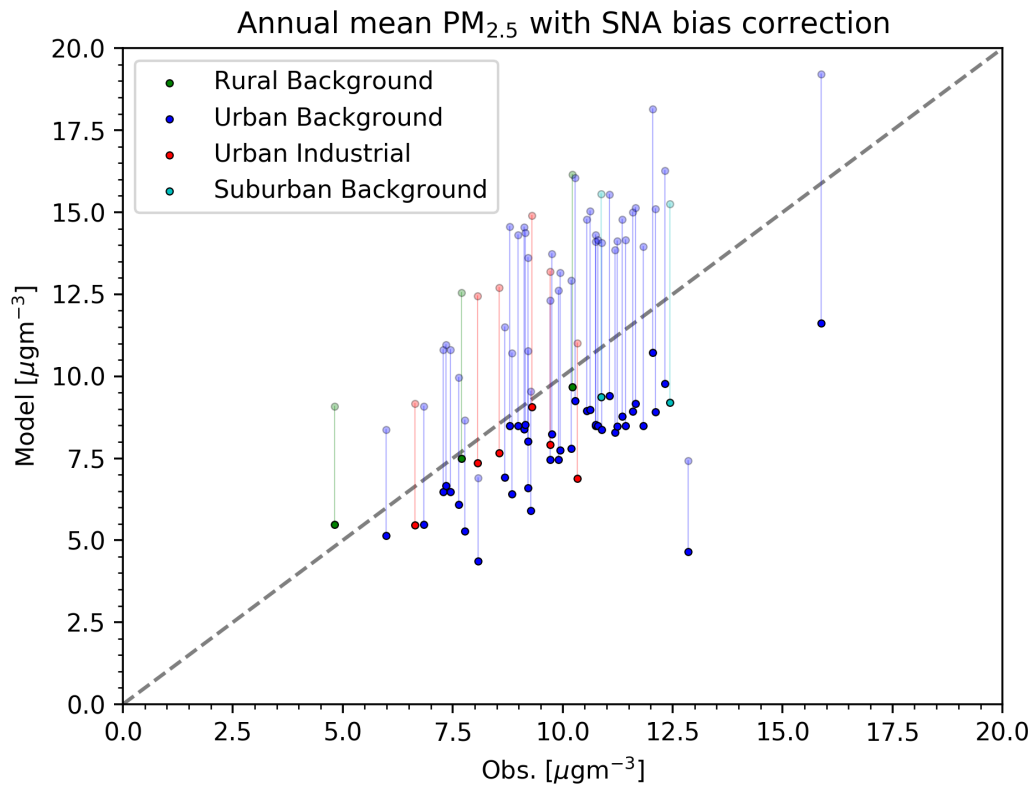
Figure 38: Comparison of the annual mean observed $PM_{2.5}$ with standard model $PM_{2.5}$(faded points) and bias corrected $PM_{2.5}$ (solid points).

This result suggests that the inorganic aerosol bias in the model is a large contributor to surface $PM_{2.5}$ error in the model. However, there are remaining sources of $PM_{2.5}$ error that this adjustment cannot account for, such as the differences in the simulated diurnal profile.

3.4.3   Model Horizontal Resolution

NO_x concentrations in Rural sites were relatively well modelled, but those in non-Rural sites showed a significant underestimate compared to the observations . It was also notable that the observations at the non-Rural sites show a significant

traffic rush-hour signal which was almost completely absent from the model (Figure 12). Thus the observations suggest emissions which are higher than those used, with more of a "traffic" character.

A complementary explanation may come from a consideration of the model horizontal grid resolution. Observation sites are chosen to reflect areas substantially smaller than the almost 800 km^2 of the model grid box, and due to their regulatory role, are likely to target areas of high rather than low emissions. This may have an impact on the comparison between the model and the measurements.

To explore this potential impact we use the annual UK National Atmospheric Emissions Inventory (NAEI) (https://naei.beis.gov.uk/; last access 14/01/2023) which provides emissions at a 1 km$\times$1 km resolution over the UK. It also forms the basis of the EMEP emissions for the UK (see Table 4). For each observation site we calculate the emission from the appropriate NAEI 1 km$\times$1 km grid box (E_{site}) and the equivalent emissions averaged over the GEOS-Chem model grid-box ($\sim$30 km resolution) ($\bar{E}_{model}$). Figure 39 shows the relationship between these values.
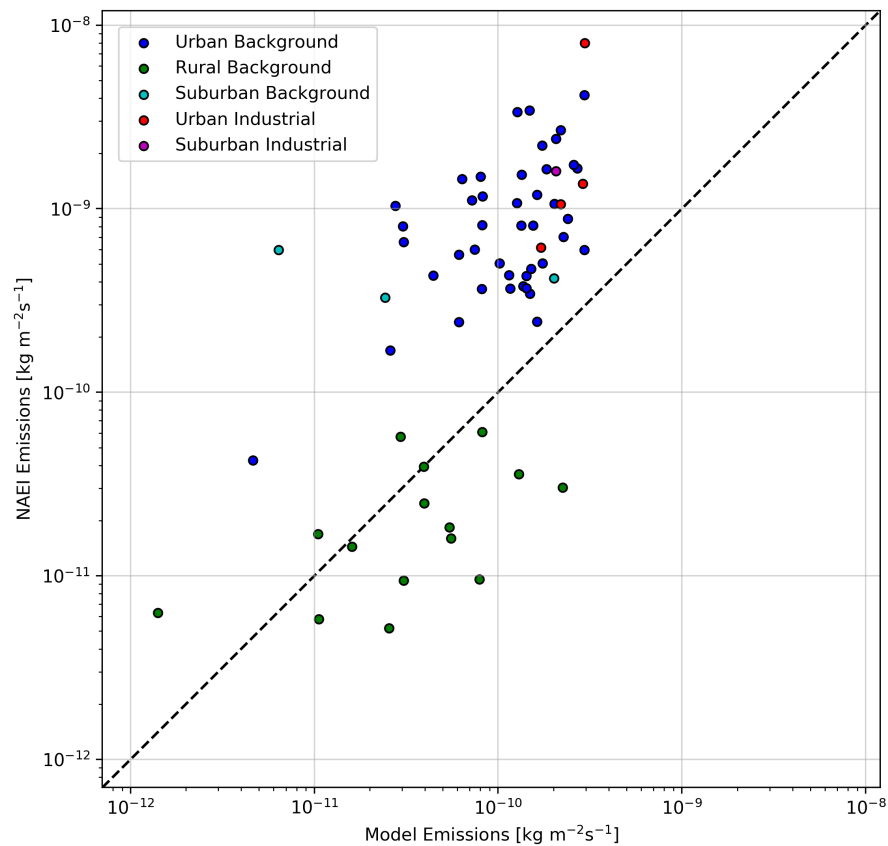
Figure 39: Comparison of NAEI and modelled anthropogenic NO_x emissions in 2017 for each measurement site (points), coloured according to site type. The dashed black line marks the 1:1 relationship between the two emissions sources, and R_{NOx} is the perpendicular distance of each site from the 1:1 line.

For the rural gridboxes (green) the local 1 km×1 km NAEI emission is, in general, less than that in the GEOS-Chem gridbox (median of the ratiosindividual points is 0.23) i.e the measurement sites are cleaner than the model gridbox. However, for the non-rural gridboxes the NAEI emissions are typically higher than those in the model with a median ratio of 3.11. This would suggest that at the GEOS-Chem model resolutions used here, there would always be an expectation of the model underestimating the non-rural NO_x concentrations compared to the observational network. The non-rural measurement sites are located in areas which have higher emissions than the GEOS-Chem grid-box in which they are located. This would also explain some of the model underestimate in the traffic signal observed in the NO_x diurnals. The observational sites are closer to roads (the largest emissions source for NO_x in the UK) than the average over the grid-box. Again this would suggest that some component of the model underestimate

in the NO_x diurnal may be indicative of this resolution impact. Other species may suffer from this problem. Simulated SO_2 concentrations showed opposite biases in Rural (-11%) and Non-Rural (30%) environments, which could be due again to resolution-dependent errors.

This resolution impact on simulated NO_x concentrations may also have an impact on O_3. The model underestimate of UK rural O_3 concentrations is likely due to the model's underestimate of global O_3 concentrations (Section 3.4.1). However, non-rural O_3 concentrations are surprisingly better simulated. One explanation for this could be that the underestimate in the O_3 flowing into the domain is being off-set by an underestimate in the titration of O_3 by NO emissions due to the location of the observational sites with the GEOS-Chem domain. One way to explore this is to compare the model calculated O_x (O_3+NO_2) to that observed, as the O_x concentration should be independent of the amount of titration. Figure 40 compares the annual mean modelled and measured O_x in the same way as in Figure 23 for O_3. The model O_x underestimate of 6.32 ppbv (-19.0%) is comparable to that at Mace Head (6.22 ppbv, -16.4%). Compared to O_3, annual mean performance for both the rural and non-rural points show similar biases and fall around the line indicated as Mace Head bias. Thus the model's ability to reasonably accurately simulate non-Rural O_3 is two wrongs making a right with the underestimate in O_3 flowing into the region being offset by the model-grid related underestimates of NO_x concentrations.
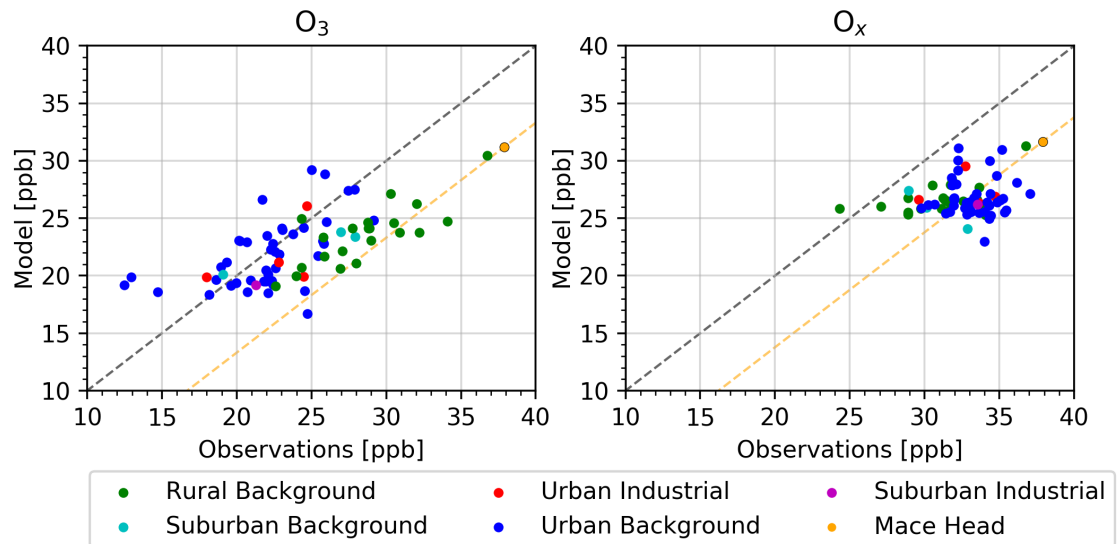
Figure 40: Annual Mean Observed (x-axis) and Modelled (y-axis) concentrations of O_3 (left, as in Figure 23) and O_x (right) for all the O_3 measurement sites. NO_2 at Rural measurement sites which do not record NO_2 (e.g Mace Head) was assumed to be 0 ppbv. The dashed lines show the 1:1 relationship (black) and the 1:1 relationship with a bias equal to that at Mace Head (orange).

3.4.4 Emissions height

The injection height of anthropogenic emissions can have a profound impact on surface air quality (Yang et al., 2019; Mailler et al., 2013). For most activity sectors, emissions occur close to the surface (domestic combustion, road traffic, etc) and so emissions are released into the bottom-most level of the model. However, for some (industrial, energy generation, etc), long chimneys are often used to move pollution away from the surface. In addition, the heat of the emitted gas can then cause those emitted air masses to be buoyant and reach even higher altitudes in the atmosphere (Thomas et al., 1963). Sulfur dioxide (SO_2) emissions are particularly associated with industrial and energy generation and so the emission height associated with that species is particularly important. Previous work has shown large differences in emission height-sensitivities depending on the emission source and pollutants (Guevara et al., 2014). Mailler et al. (2013) showed regionally calculated vertical emissions profiles from plume rise models could produce significant bias reductions for SO_2 and NO_2, with consequences for sulfate aerosol production. Further, (Ahsan et al., 2023) found SO_2 surface lifetime and concentration to be highly sensitive to emissions height, making un-

certainty a significant source of error in CTMs.

Figure 13 shows a model overestimate in the concentration of SO_2 in urban industrial sites. This may be a result of error in the emissions heights for SO_2. The vertical profile of industrial emissions used in the model follows that of the EMEP-CTM (Simpson et al., 2012b) (Figure 7). In Figure 41 we evaluate the impact of increasing SO_2 industrial emissions heights by comparing the original model simulation with one where all anthropogenic industrial SO_2 emissions are emitted in the 9th model vertical layer ($\sim$ 1146 m from the surface). Increasing the industrial SO_2 emission heights reduced NMB from 0.35 to -0.23 for SO_2, from 2.24 to 1.64 for SO_4, and from 0.58 to 0.49 for $PM_{2.5}$ (-58%, -60% and -9%, respectively). The NMB reductions were greater at Urban Industrial sites: from 1.02 to 0.65 for SO_2 and from 0.55 to 0.45 for $PM_{2.5}$. The substantial changes at sites near large industrial emissions sources and relatively small changes at others support vertical placement of emissions as an error component for SO_2, SO_4^{2-} and $PM_{2.5}$ near industrial sources. Whilst emitting all industrial SO_2 at 1 km above the surface is an extreme case and will not be representative for all emissions sources, plume rise models have simulated final plume heights above this for tall stacks (Gillani and Godowitch, 1999), so this may suggest current emissions height are too low or plume rise needs to be accounted for from these sources. Despite a large bias reduction in SO_2, SO_4^{2-} is still overestimated, suggesting other or additional error components such as emission or deposition rates, the representation of plumes, transport into the domain could be responsible.
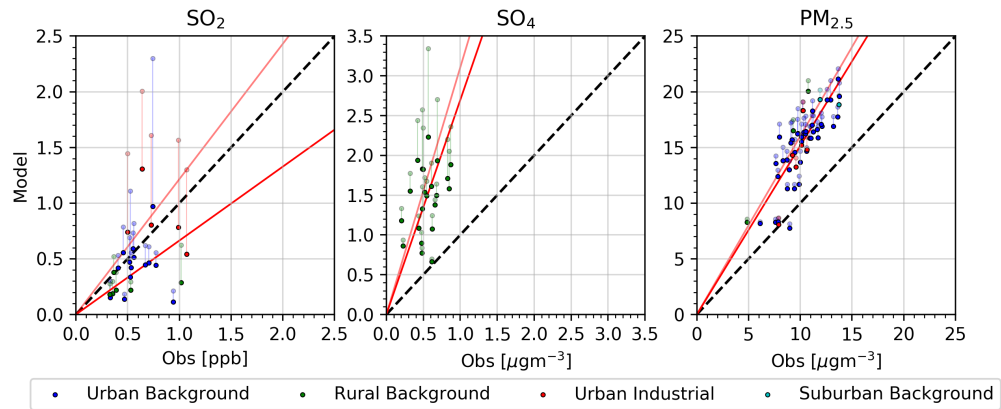
Figure 41: Mean concentration of SO_2, SO_4^{2-} and $PM_{2.5}$ for the available observations (x-axis) and the original model (faded, y-axis) and with industrial SO_2 emissions in the 9th model vertical layer (solid, y-axis), from 2017/03/08 to 2017/04/26, with one week prior spin-up time. Theil-Sen regression best fit lines are shown for the original model (faded, red) and with emissions in the 9th model layer (solid, red), along with the 1:1 line (black dashed line).

3.5   Conclusions

This chapter has evaluated surface concentration estimates of NO_x, CO, SO_2, NMVOCs, NH_3, O_3, $PM_{2.5}$ and aerosol SO_4, NO_3, NH_4 from the nested grid GEOS-Chem model (v13.1.2) at $0.25° \times 0.3125°$ over the UK. The evaluation used surface observations from the UK AURN, UKEAP and Automatic Hydrocarbon monitoring networks for the year 2017. Model performance was assessed at three timescales (annual, daily and diurnal) relevant to the representation of different chemical and physical processes, with normalised mean bias (NMB) and Pearson's correlation (r) metrics.

Comparisons of annual average surface concentrations show that the spatial distributions of measured species were generally well captured, except for CO (r=-0.09) where we find issues with the AURN IR absorbance measurements to be problematic, and for SO_4^{2-} (r=0.37), where uncertainties in model processes like deposition and gas-aerosol partitioning could be sources of error.

The model systematically underestimates the background O_3 contribution coming from the West of the UK, whilst errors in the European contributions may

contribute to the overestimates of $PM_{2.5}$ and aerosol Sulphate, Nitrate and Ammonium (Yin and Harrison, 2008; Vieno et al., 2016b).

Errors arising due to model horizontal resolution may explain the performance differences for NO_x in Rural (NMB=-0.14) and Non-Rural (NMB=-0.58) environments. The reduced NO_x titration that follows produced the counteracting effect on O_3, with smaller errors for Non-Rural (NMB=0.05) than Rural (-0.11) environments. Evaluating total oxidant, O_x (O_x=O_3+NO_2), brought Non-Rural estimates into agreement with the background O_3 underestimate at Mace Head, confirming two counteracting sources of error for O_3.

Increasing the industrial SO_2 emission height (in a short simulation) reduced the model NMB overestimate at Urban Industrial sites from 1.02 to 0.65 for SO_2, from 0.55 to 0.45 for $PM_{2.5}$ and from 2.24 to 1.64 across all (Rural Background) SO_4^{2-} sites. This potentially shows that either increases to the vertical distribution of industrial SO_2 emissions or the more detailed estimated of plume rise could reduce errors for SO_2, SO_4 and $PM_{2.5}$. However, model biases for these species are still large, so other explanations (e.g resolution impacts, emission uncertainties, chemistry and transport biases) should be investigated.

This chapter demonstrates that GEOS-Chem can accurately simulate a range of primary and secondary species over the UK. However, there are two areas where the model exhibits errors, which will be explored in detail in the subsequent chapters. Firstly, emissions sources and source regions can significantly impact species concentrations. For instance, the background contribution's effect on O_3 estimates and the reported European contributions to UK $PM_{2.5}$ are notable examples. In Chapter 4, we will delve into the influence of emissions sources from the UK and continental Europe on these two species. This analysis aims to improve our understanding of their sensitivities to different emission sources. Secondly, considering the evidence of a resolution effect, Chapter 5 will investi-

gate whether higher resolution simulations can enhance model performance for NO_x, O_3, and $PM_{2.5}$. By conducting these investigations, we aim to identify potential improvements in the model's predictive capabilities for these important air pollutants.

4   Sensitivity of O_3 and $PM_{2.5}$ to Emissions from the UK and Europe

4.1   Introduction

Chapter 3 showed the GEOS-Chem CTM with recent EMEP emissions was able to reasonably reproduce to the temporal and spatial distributions for a range of air pollutants. The influence of emissions from different sources on pollutant concentration was discussed in Chapter 1. In the UK, the main air pollutants of concern for human health are NO_2, O_3 and $PM_{2.5}$ (DEFRA, 2022a). This chapter will focus on the impact of 13 hypothetical emission changes over the UK and Europe on the concentrations of O_3 and $PM_{2.5}$ in the UK. The impact of emission changes on NO_2 was not explored as Section 3.3.1 showed the model to systematically underestimate NO_2 concentrations by 57%. This could likely be due to resolution, requiring a higher resolution simulation to simulate NO_2.

To make effective decisions, policy makers need be aware of how policy changes affecting emissions could impact air quality, and CTMs provide a means of estimating these impacts.Approaches to improve air quality through emission controls have been implemented at varying spatial scales, from the national (e.g Gothenburg protocol, National Emissions Ceiling Regulations 2018) to local (e.g low emission zones) scales. Understanding the potential impact of emission reductions can be straightforward for primary pollutants, whose concentrations are proportional to their emissions. However, the situation becomes more complicated when secondary pollutants are considered, as emission reductions may not always produce proportional changes in concentration. Sensitivity studies can be an effective means to inform policy makers on the most effective course of action to improve air quality. Typically, these apply fractional reductions to reported emissions or projections of future emissions for specific species and sectors, followed by the evaluation of the model response. Numerous such studies have looked at

the sensitivities of O$_3$ (e.g Gabusi and Volta (2005); Liu (2022); Tran et al. (2023)) and PM$_{2.5}$ (e.g Vieno et al. (2015); Clappier et al. (2021); Dai and Wang (2021)).

The concentration of O$_3$ can be impacted by a range of factors including meteorology, solar radiation and the local emissions of NO$_x$ and VOCs (Section 1.4.3). Further, the ratio of NO$_x$ to VOCs can determine the effectiveness of emission reductions in an area (Sillman, 1999), where O$_3$ production is typically characterised as falling into either NO$_x$-limited or NO$_x$-saturated regimes. For example, continued reductions in NO$_x$ emissions have contributed gradual increases in urban concentrations of O$_3$ in the UK since 1990 (Jenkin, 2008). A third, 'aerosol inhibited' regime, where HO$_2$ uptake onto aerosol particles is the controlling termination step for O$_3$ production has also been proposed (Jacob, 2000; Sakamoto et al., 2019; Song et al., 2020). In this regime, high levels of particulate pollution result in aerosol uptake of HO$_2$, reducing the availability of HO$_x$ (OH and peroxy) radicals availability and consequently inhibiting the short-term photochemical production of O$_3$. Whilst this is not currently the dominant regime in North America and Europe, it is important in parts of Asia where particulate pollution is high (Ivatt et al., 2022). Using the same approach as Ivatt et al. (2022), Figure 42 shows the dominant chain termination step for O$_3$ production over the domain for each season. With the exception of lower-emission, rural areas during the winter, the HO$_2$ uptake route has only a minor role for most of the year, with the rest of the UK falling into either NO$_x$-limited or NO$_x$-saturated regimes. For most of the year, the $NO_2 + OH$ reaction is the controlling chain termination step for O$_3$ production over most of the UK(NO$_x$-saturated, red). However, in the winter the importance of aerosol uptake of HO$_2$ increases (aerosol-inhibited, pink). In the Summer, the peroxy-self reactions (NO$_x$-limited, green) play a greater role. This highlights how the response of O$_3$ to emissions changes can vary by season. Liu (2022) demonstrated that in future scenarios where North American and European NO$_x$ emissions were significantly reduced, daytime concentrations of O$_3$ decreased in the summer, but winter increases were similar at both day and night

as RO$_2$ concentrations are very low.
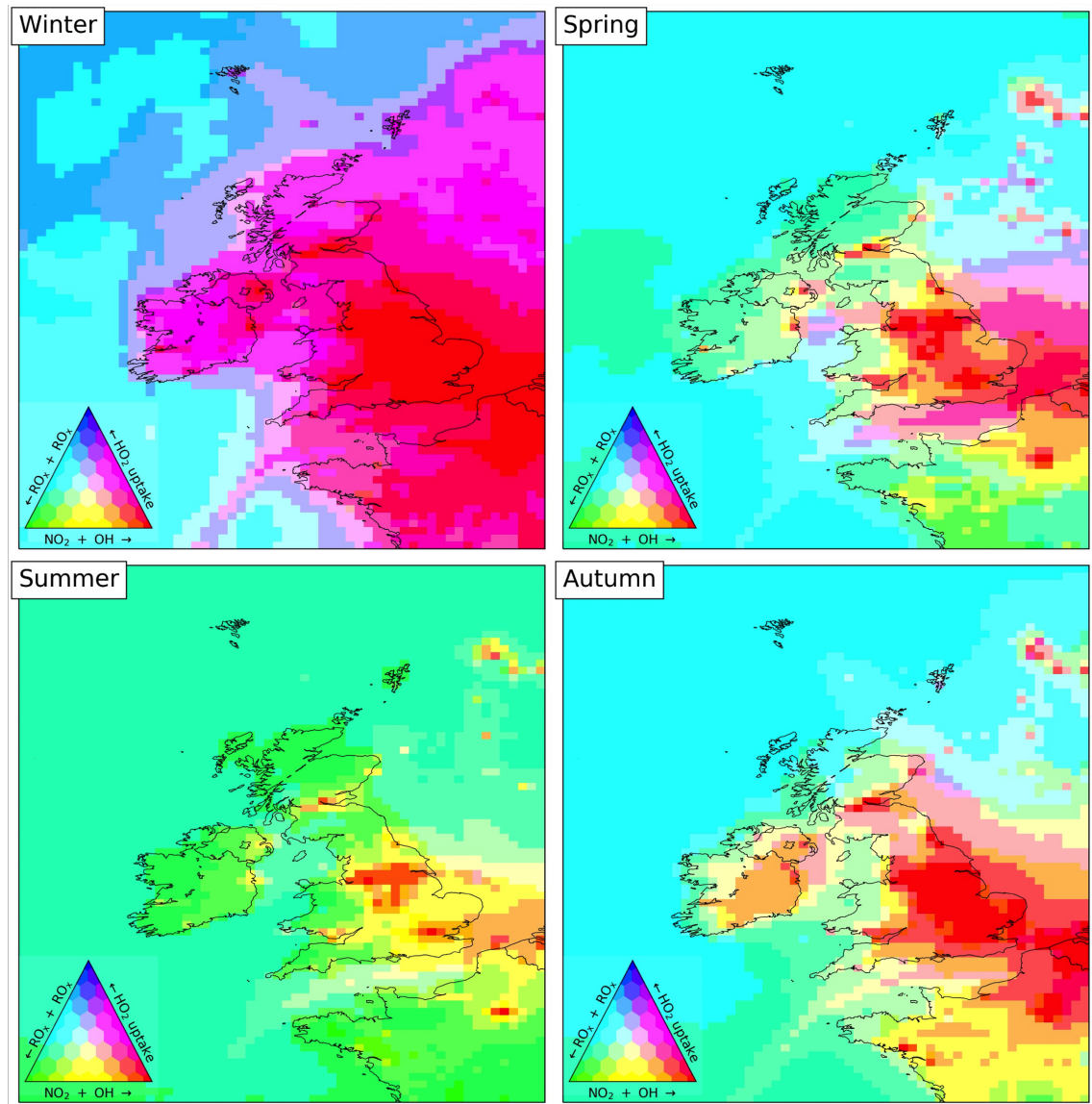
Figure 42: Mean simulated seasonal noon-time fraction of radical termination step at the surface that occurs through OH+NO$_2$ (red), peroxyl-radical self-reactions (green) and aerosol uptake of HO$_2$ (blue).

PM$_{2.5}$ is composed of both primary emitted species (e.g Sea Salt, Dust) and secondary species (e.g secondary inorganic aerosol, secondary organic aerosol) formed through reactions of primary emitted compounds like NO$_x$, SO$_2$, NH$_3$ and NMVOCs. This adds further complexity to establishing the impact of emission changes on PM$_{2.5}$ concentrations. Various approaches using CTMs have tried to evaluate the non-linear effects of sources on PM$_{2.5}$ and its related health impacts. Many of these have found NH$_3$ emissions from the agricultural sector to

be a significant contributor to PM$_{2.5}$ pollution. For example, GEOS-Chem nested grid simulations by Kelly et al. (2023) found agricultural NH$_3$ emissions made the largest contribution to annual mean PM$_{2.5}$ in Leicester, UK. Gu et al. (2023) additionally used the GEOS-Chem adjoint to analyse the emission contributions of various sources and species on PM$_{2.5}$-related health impacts. They found the largest single-sector contributions to PM$_{2.5}$-related health risks were from residential (23.5%), agricultural (23%) and ground transport (19.4%) sources. Sensitivity studies have shown the response of PM$_{2.5}$ concentrations to emission reductions to be non-linear. Thunis et al. (2021) evaluated the effect of incremental single and combined NO$_x$ and NH$_3$ reductions of 25-100% response of PM$_{2.5}$ over the Po Basin region of Italy with the EMEP CTM, and found slight wintertime PM$_{2.5}$ increases following small NO$_x$ reductions in NO$_x$ rich areas due to increased atmospheric oxidative capacity.

For longer lived species, trans-boundary contributions can also play a significant role in determining UK surface concentrations for both O$_3$ (e.g Derwent and Parrish (2022); Romero-Alvarez et al. (2022)) and PM$_{2.5}$ (e.g Vieno et al. (2014); Graham et al. (2020)). This contribution is heavily influenced by the meteorological conditions (Pope et al., 2016; Vieno et al., 2016a).

The UK Air Quality Standards Regulations sets out limit values and target values for air pollutants. Limit values are legally binding standards established by regulatory authorities for air pollutants. Target values are non-binding goals to be met where possible and typically aiming to achieve higher levels of reductions beyond the legal requirements of limits values to improve environmental or public health. In the UK in 2021, the annual mean limit value of 40 μgm^{-3} for NO$_2$ was met at 33 of 43 monitoring zones, although some of this was associated with reduced emissions due to COVID lockdown restrictions. Alongside limit values set out in UK legislation, the World Health Organisation (WHO) also sets out non-binding air quality guidelines for air quality, which were most recently updated in

2021. The new annual mean guideline limit for NO_2 is 10 μgm^{-3}(Organization, 2021).

Section 4.2 will set out the emission scenarios investigated in this work. Sections 4.3 and 4.4 will then explore the impact of the emission scenarios on UK annual mean O_3 and $PM_{2.5}$ spatial concentrations, the seasonal changes for the scenarios on O_3 concentration, and how the scenarios affect the UK's compliance with the latest WHO guidelines. Finally, the degree to which independent emission reduction scenarios can be linearly combined to achieve similar results to when implemented concurrently in model simulations is then assessed in Section 4.5, to provide some guidance on when additional simulations may be necessary to evaluate new scenarios.

4.2   Experiment Setup

4.2.1   Model Configuration

As in Chapter 3, this work used version 13.1.1 (GC13.1.1, 2021) of the GEOS-Chem global chemical transport model (Bey et al., 2001) in its nested grid capability, driven by meteorology from the Goddard Earth Observing System GEOS-FP product. Boundary conditions and initial concentrations were produced from a global $4° \times 5°$ simulations from 1st January 2016 to 1st January 2018, using the first year as model spin-up. The second year provided boundary conditions (every 3 hours) for a nested grid simulation over the United Kingdom (shown in Figure 43, 15°W-5°E, 45°N-65°N) at 0.25°x0.3125°horizontal resolution. Each nested simulation was given one month spin-up time from 2016-12-01 to 2017-01-01 and then run from 2017-01-01 to 2018-01-01. As recommended by the GEOS-Chem nested grid documentation (`http://wiki.seas.harvard.edu/geos-chem/index.php/FlexGrid`), the nested simulation uses a buffer boundary region of 3 fine resolution model grid cells. Details regarding the model chemistry, transport are discussed in Chapter 2.

We use the same emissions configuration as described in Chapter 3 for all scenarios, where anthropogenic emissions over Europe were replaced with emissions from the EMEP inventory.
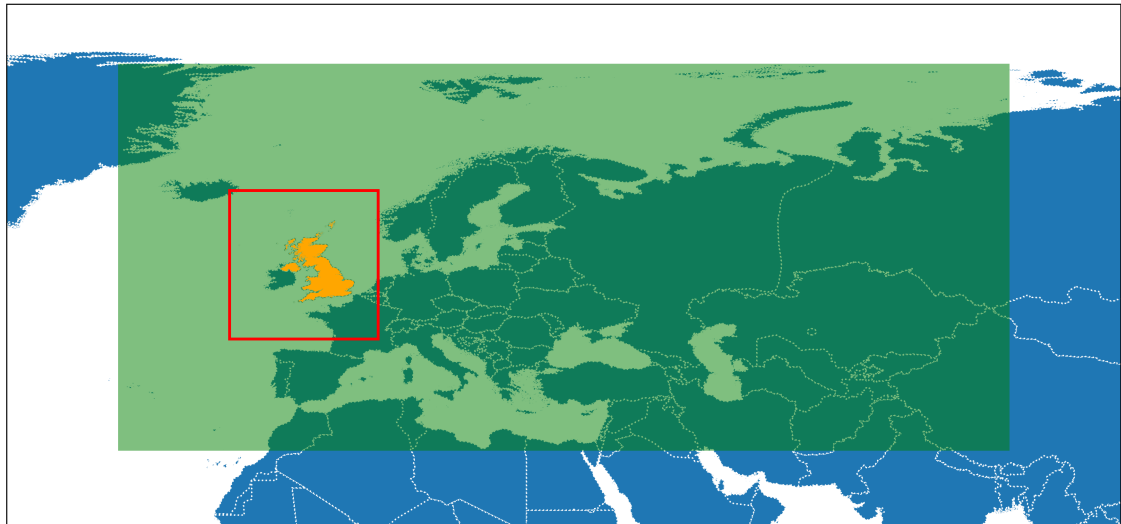
Figure 43: Coverage of EMEP emissions (green, 30°W-90°E 30°N-82°N) in relation to the model nested grid domain (outlined in red). Outside of the EMEP emissions domain, default model emissions were used. Regional EMEP emissions were separated into either the UK (orange), EU (green).

4.2.2 PM$_{2.5}$ Correction

Chapter 3 showed the model to overestimate UK PM$_{2.5}$ by 2.56 μgm^{-3}, with a large component of the error attributed to overestimates of aerosol sulfate, nitrate and ammonium (SO$_4$: 176%, NO$_3$: +77%, NH$_4$: 104%). In Chapter 3 we corrected for the effect of this bias on modelled PM$_{2.5}$ by scaling aerosol sulfate, nitrate and ammonium by their model-observation biases. This reduced PM$_{2.5}$ bias from a 24% overestimate to a 13% underestimate (against annual mean observations, Figure 38), comparable to the 11% underestimate obtained by Kelly et al. (2023) with modified EMEP emissions. Modelled PM$_{2.5}$ and inorganic aerosol concentrations shown in this chapter will incorporate these corrections. A preliminary comparison showed a similar sensitivity of PM$_{2.5}$ changes following emissions perturbations with and without this scaling.

4.2.3   Emission Scenarios

A baseline simulation and a set of 14 sensitivity scenarios were simulated for 2017. Each sensitivity experiment reduced emissions to zero over combinations of the UK, continental Europe ("EU"), or over the ocean within the nested domain. Figure 43 highlights the regions where emission changes were implemented. Emissions sources were categorised as:

- **Anthro**: EMEP Anthropogenic emissions from the energy, road transport, fugtive, industry, offroad, other stationary combustion, other, solvents, waste sectors. Aviation emissions were not changed as these were defined by the default model inventory (AEIC) at 1°×1°.

- **Agri**: EMEP Anthropogenic emissions from the agrilivestock and agriother sectors.

- **Ship**: International shipping emissions. Emissions from EMEP were used within the boundary of 30N-82N, 10W-90E and from the CEDS inventory for the rest of the world. NO$_x$ emissions from shipping are processed using the PARANO$_x$ module (Vinken et al., 2011; Holmes et al., 2014), which accounts for O$_3$ and HNO$_3$ production within plumes.

- **Biogenic**: Offline biogenic emissions of VOC tracers (acetone, acetaldehyde, ethylene, ethanol, isoprene, lumped sesquiterpenes, Secondary Organic Aerosol and Secondary Organic Aerosol Precursor (SOAS and SOAP), etc...) from the Model of Emissions of Gases and Aerosols from Nature (MEGAN) v2.1 (Guenther et al., 2012) inventory were turned off over the UK or continental Europe.

Thus, in the context of this work, anthropogenic emissions will describe all human emissions sources excluding international shipping and agriculture. Table 10 summarises the emissions sources and regions changed for each scenario both within the nested domain and externally through the boundary conditions. The in-domain and global percentage emission changes of NO, CO, SO$_2$, NH$_3$,

ethanol (EOH) and biogenic isoprene (ISOP) for each scenario are summarised in Table 11.

NH$_3$ is the largest mass component of agricultural emissions from the UK and EU. However, there are differences in the emissions of other species which might impact the model response to agricultural emissions changes (Figure 44). These are due to the differences between the emissions reporting procedures and agricultural activities between countries. In 2017 EMEP emissions, the UK reportedly emitted no CO from agriculture, while France emitted 40 kT (`https://www.ceip.at/webdab-emission-database/emissions-as-used-in-emep-models`, last access 2023/03/17). However, within the UK 23 kT of CO emissions from agricultural mobile machinery use were assigned to the industrial combustion sector (`http://www.naei.beis.gov.uk/data/`, last access 2023/03/17). The variation in species emitted from agricultural sources from different countries implies that the potential impact of removing agricultural emissions (and potentially also from other sectors) from either the UK or EU will differ depending on the specific species considered.
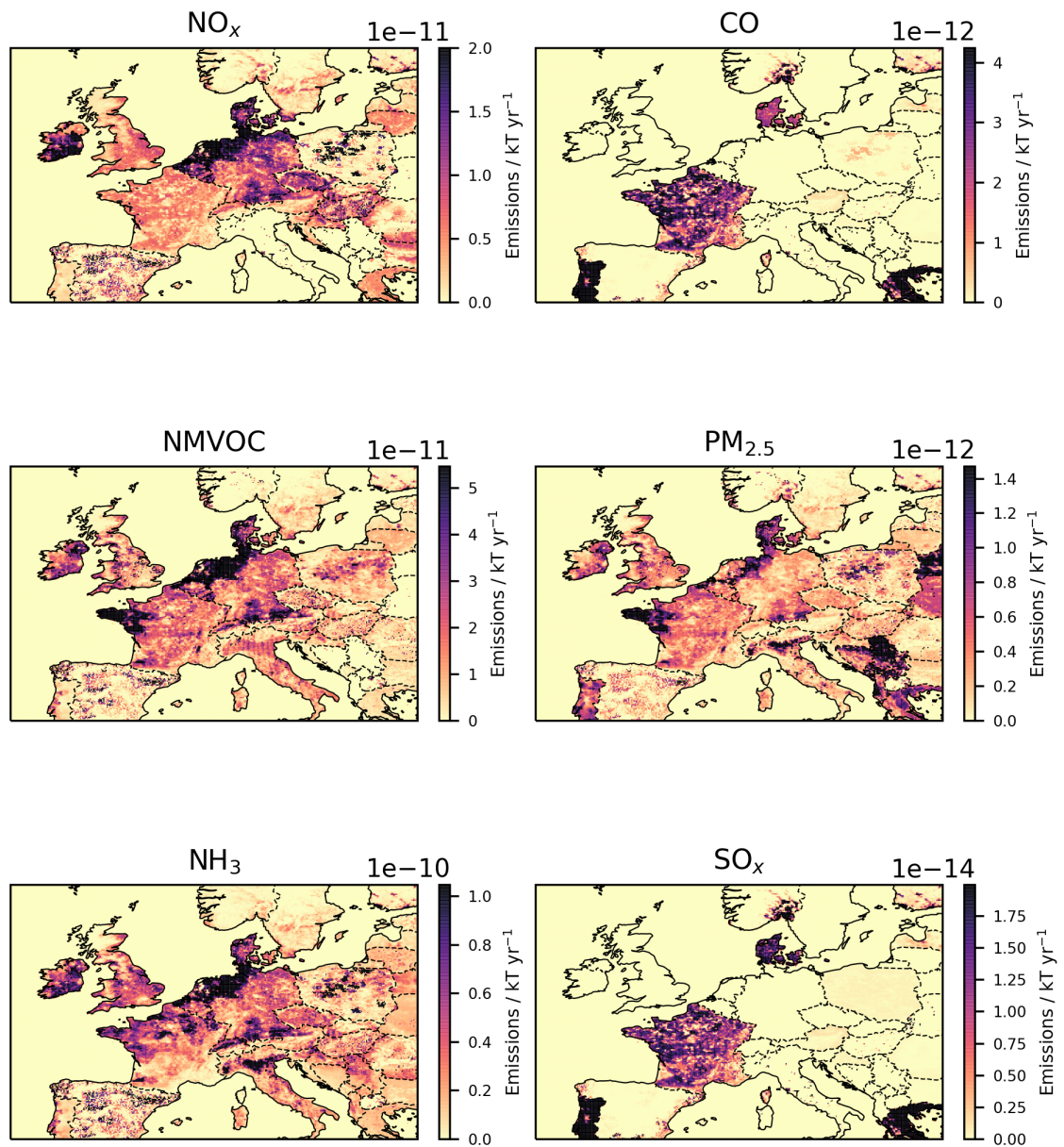
Figure 44: Agricultural emissions of NO_x, CO, NMVOCs, $PM_{2.5}$, NH_3, SO_x over Western Europe for 2017, in kT yr^{-1}.

Table 10: Outline of the Boundary Conditions used, areas and source where emissions were removed for each emission scenario.

Scenario	Boundary Condition	Source(s) removed	Region
1. Baseline	1	None	None
2. noUKAnthro	1	Anthro	UK
3. noUKAgri	1	Agri	UK
4. noUKAnthroAgri	1	Anthro, Agri	UK
5. noEUAnthro	5	Anthro	EU
6. noEUAgri	6	Agri	EU
7. noEUAnthroAgri	7	Anthro, Agri	EU
8. noShip	1	International Shipping*	Nested Domain
9. noUKnoEUAnthro	9	Anthro	UK, EU
10. noUKnoEUAgri	10	Agri	UK, EU
11. noUKnoEUAnthroAgri	11	Anthro, Agri	UK, EU
12. noUKnoEUAnthroAgriShip	11	Anthro, Agri, International Shipping*	UK, EU, Nested Domain
13. noUKBiogenic	1	Biogenic	UK
14. noEUBiogenic	13	Biogenic	EU

Table 11: Percentage decrease in total emissions under each emission scenario within the nested Domain ("Domain") and globally ("Global") compared to the model baseline (Scenario 1, Table 10) for NO, CO, SO_2, NH_3, ethanol (EOH, an example of anthropogenic VOC emissions), and *biogenic* isoprene (ISOP).

Scenario	NO		CO		SO_2		NH_3		EOH		ISOP	
	Domain	Global	Domain	Global	Domain	Global	Domain	Global	Domain	Global	Domain	Global
noUKAnthro	38.9	0.5	42.6	0.2	35.8	0.2	3.3	0.0	35.0	0.6	0.0	0.0
noEUAnthro	37.8	10.5	52.4	7.0	45.9	14.3	3.0	0.7	27.4	15.1	0.0	0.0
noUKnoEUAnthro	76.7	11.0	95.0	7.2	81.7	14.5	6.3	0.7	62.5	15.7	0.0	0.0
noUKAgri	1.6	0.0	0.0	0.0	0.0	0.0	23.5	0.3	5.6	0.1	0.0	0.0
noEUAgri	5.0	0.7	0.7	0.2	0.0	0.0	59.5	9.8	18.9	2.5	0.0	0.0
noUKnoEUAgri	6.6	0.7	0.7	0.2	0.0	0.0	82.9	10.1	24.6	2.6	0.0	0.0
noUKAnthroAgri	40.6	0.5	42.6	0.2	35.8	0.2	26.8	0.3	40.7	0.7	0.0	0.0
noEUAnthroAgri	42.8	11.2	53.0	7.3	45.9	14.3	62.5	10.5	46.4	17.6	0.0	0.0
noUKBiogenic	0.0	0.0	0.0	0.0	0.0	0.0	0.0	0.0	1.3	0.0	22.5	1.3
noEUBiogenic	0.1	0.0	0.0	0.0	0.0	0.0	0.0	0.0	3.0	2.1	77.3	3.2
noShip	3.4	0.0	4.2	0.0	39.4	0.2	0.0	0.0	1.1	0.0	0.0	0.0
noUKnoEUAnthroAgri	83.4	11.7	95.7	7.5	81.7	14.5	89.3	10.8	87.1	18.3	0.0	0.0

Ship stack emissions can be considered as large point sources of gases such as NO$_x$, and chemistry occurs within the emission plumes to form ozone (Lawrence and Crutzen, 1999; Song et al., 2003). Typically, Eulerian CTMs handle point source emissions by instantly diluting them over the entire grid cell. But this treatment can cause problems when the reactive species with non-linear chemistry are emitted into unpolluted areas, leading to unrealistically high concentrations (Davis et al., 2001). To mitigate this, GEOS-Chem handles shipping NO$_x$ emissions differently to other emission sectors, using the PARANOx Gaussian plume dispersion model of Vinken et al. (2011) to account for non-linear effects during the dispersion of ship exhaust plumes. This reduces the effective emissions of shipping NO$_x$ slightly by accounting for the delayed release of HNO$_3$ and O$_3$. Non-NO$_x$ emissions from shipping such as SO$_2$ are handled normally by the GEOS-Chem emissions component.

4.2.4   Area and Population Weighting

For each model gridbox, *i* with species concentration *c*, the area and population weighted concentration were calculated as in 5 and 6.

$$\text{Area-Weighting} = \frac{\sum_i c_i \text{area}_i}{\sum_i \text{area}_i} \tag{5}$$

$$\text{Population-Weighting} = \frac{\sum_i c_i \text{population}_i}{\sum_i \text{population}_i} \tag{6}$$

Grid box area came from the model output diagnostics at 0.25°x0.3125° and residential population data came from the 2011 UK census (source: `https://www.data.gov.uk/dataset/ca2daae8-8f36-4279-b15d-78b0463c61db/uk-gridded-population-2011-based-on-census-2011-and-land-cover-map-2015`, last access 2023/03/16). This was reprojected from 1 km×1 km OSGB36 to WGS84 projection and regridded to the model horizontal resolution (0.25°×0.3125°). Figure 45 compares the population data at these two resolutions. As UK population is heavily concentrated in England and London in particular, population weight-

ing will accentuate concentration changes in these areas at the expense of more rural parts of the UK.
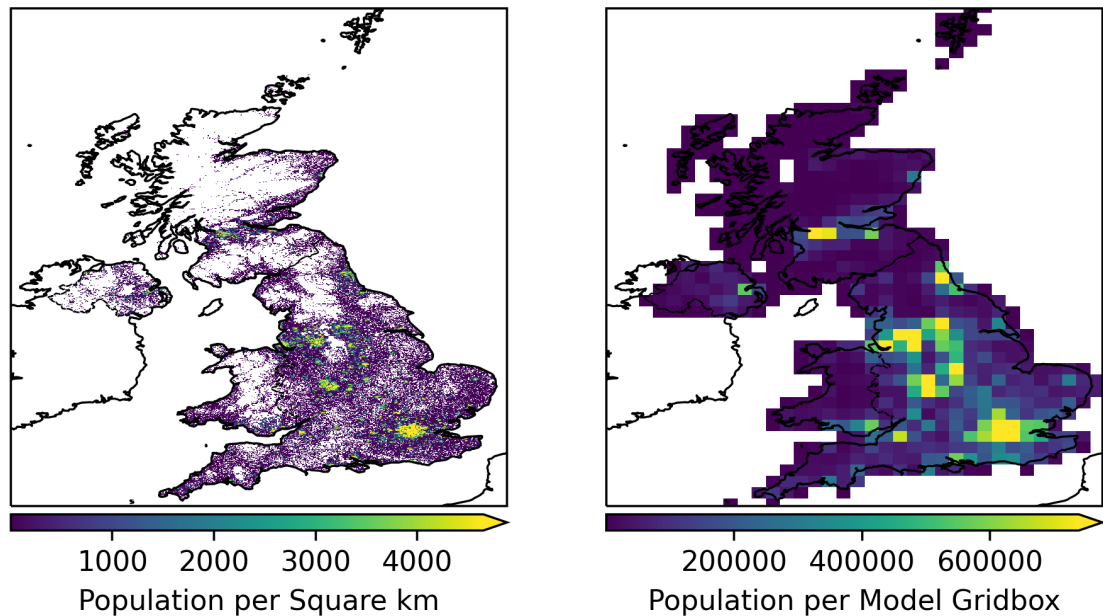
Figure 45: UK 2011 population mapped at 1x1 km (left), and population per 0.25° × 0.3125° model grid box (right).

4.2.5   WHO Air Quality Guidelines

The relative improvements in air quality for O$_3$ and PM$_{2.5}$ from the implemented emission changes are assessed using the WHO air quality guidelines (Organization, 2021) for these species:

- **O$_3$**: A Peak Season average daily maximum 8-hour mean O$_3$ concentration below 60 μgm^{-3}, where "Peak Season" refers to the six consecutive months with the highest running average O$_3$ concentration.

- **PM$_{2.5}$**: An annual mean concentration of PM$_{2.5}$ below 5 μgm^{-3}.

For each species, the extent of compliance with these guidelines was determined as the fraction of the UK area or population in exceedance, as in (7) and (8).

$$\text{Area in Exceedance (\%)} = \frac{\text{Total Area Exceeding WHO guideline}}{\text{Total Area of UK gridboxes}} \quad (7)$$

$$\text{Population in Exceedance (\%)} = \frac{\text{Total Population Exceeding WHO guideline}}{\text{Total UK Population}} \quad (8)$$

4.3   Ozone

This section examines the changes in UK surface O_3 concentrations from the emissions changes described in Section 4.2.3. The analysis occurs from both an area- and population-weighted perspective, and from an annual and peak 6-month season perspective (ie. the basis of the WHO O_3 regulation). The months forming the peak season are shown in Figure 46. For locations in the west of the UK, the peak 6-month season occurs in spring (January-June) due to the spring O_3 maximum typically seen for background sites (Monks, 2000). Moving eastwards, the peak season moves toward the summer time (April-September), which is typical of more polluted continental sites (Parrish et al., 2013; Cooper et al., 2014).

Six month period with the highest
rolling average O3 concentration
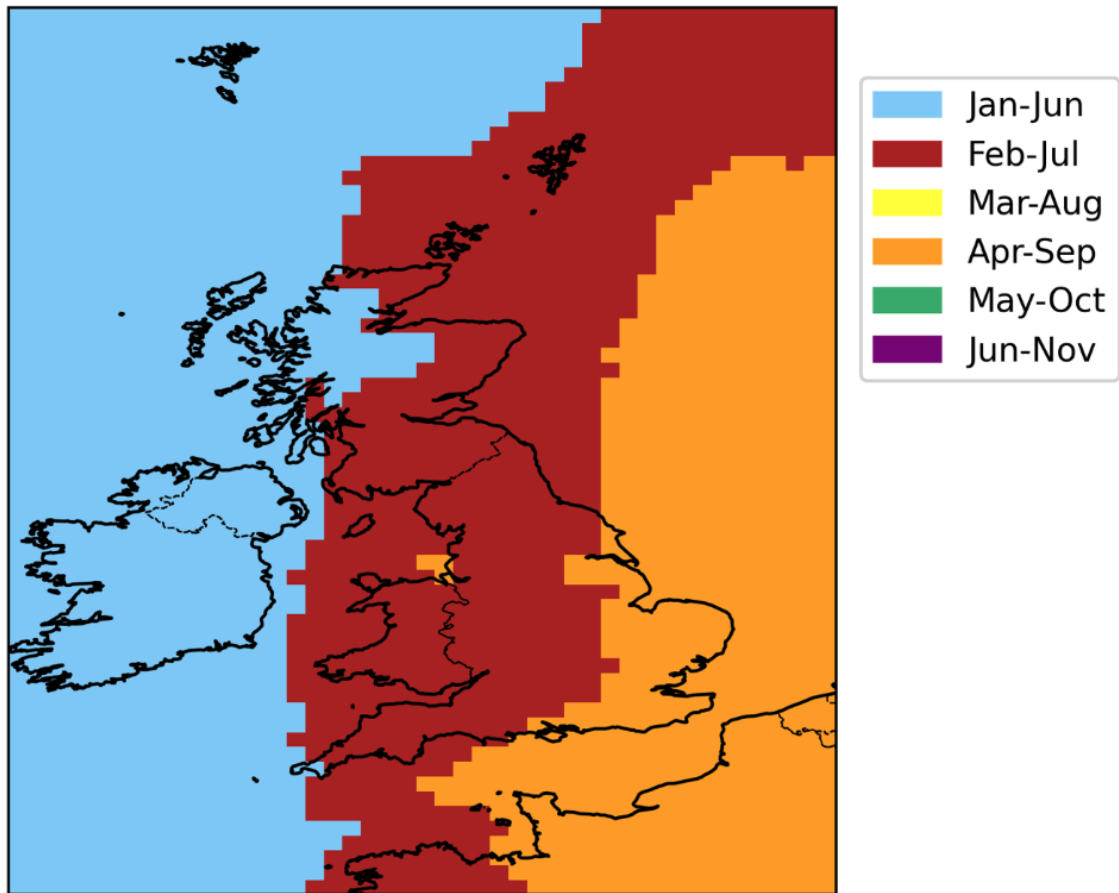
Figure 46: Six-month period with the highest rolling average MDA8 O_3 concentration over the model domain for 2017. This is used to calculate the statistics for WHO O_3 metrics

Figure 47 summarises these simulations. It shows the annual mean O_3 concentrations in the baseline (no emission changes) simulation (blue) and then the perturbations from the emission scenarios for the annual mean (top) and peak 6-month season mean (bottom), and for the area-weighted (left) and population-weight metrics (right). Red and green bars indicate increased or decreased concentration. Tables of these data are given in the Appendix as Table 17. The spatial and temporal complexities of these changes are discussed in Sections 4.3.1-4.3.5, with implications for compliance with the WHO standard discussed in Section 4.3.6.
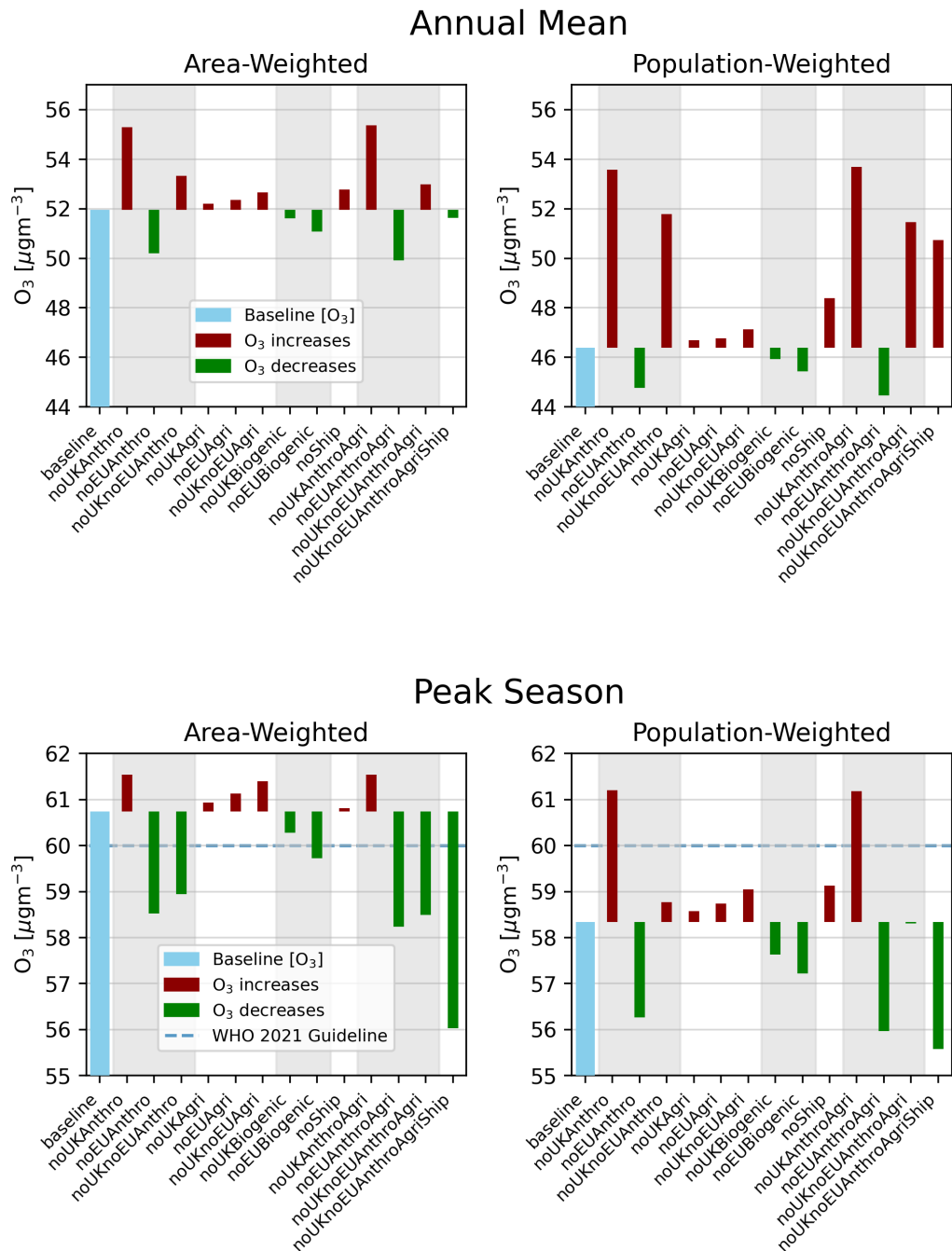
Figure 47: Summary of Area-Weighted (left) and Population-Weighted (right) changes in Annual Mean (top) and Peak Season (bottom) UK surface O$_3$ from the baseline (blue bar) for each emission scenario. Scenarios resulting in an overall increase are given red bars, and decreases given green bars. For Peak Season MDA8 O$_3$, the 2021 WHO guideline for Peak Season O$_3$ (60 μgm^{-3}) is annotated (blue dashed line).

Removing anthropogenic emissions from the UK (noUKAnthro) increases UK O_3 concentrations in all metrics. Lower NO_x emissions reduce $NO+O_3$ titration, increasing O_3 concentration but can also change photochemical O_3 production depending on the photochemical regime (See Figure 42). This was significantly larger in the population-weighted metrics than in the area-weighted ones, reflecting the correlation between anthropogenic NO_x emissions and population density (see Figure 47). The increase in O_3 was smaller for the Peak Season MDA8 O_3, reflecting increased photochemical activity in the summer.

Removing EU anthropogenic emissions (noEUAnthro) led to the opposite effect. UK O_3 concentrations decreased in all metrics. This was due to a decrease in the northern hemispheric background O_3 concentration from the reduced global NO_x emissions. For the UK, the O_3 background is typified by concentrations at Mace Head (see Table 16) which reduce on removal of anthropogenic EU emissions (see Figure 48).

When both the UK and EU anthropogenic emissions were removed (noUK-noEUAnthro), there was an increase in O_3 for all metrics, other than the area-weighted peak season MDA8 O_3). In general, the local increase in O_3 due to reduced titration is larger than the reduced photochemical O_3 production on a local and global O_3 scale (see Figure 48). However, in peak season, for rural areas of the UK, this balance changes. The impacts of these anthropogenic changes are discussed in Section 4.3.1.

Agricultural emissions changes for the UK alone (noUKAgri), the EU alone (EUAgri) and both (noUKnoEUAgri) led to small positive increases in O_3 concentration for all metrics. This is due to both NO_x emission reductions, with an additional contribution from changes to the aerosol burden. This is discussed in more detail in Section 4.3.2.

Removal of biogenic emissions from both the UK (noUKBiogenics) and EU (noEUBiogenics) lead to small decreases in O$_3$ production which were more pronounced in the Peak-Season MDA8 O$_3$ than in the annual mean due to their (predominantly isoprene's) high O$_3$ production efficiencies (Sharkey et al., 2008). This is discussed in more detail in Section 4.3.3.

Removal of in-domain international shipping emissions (noShip) led to increases in O$_3$ concentrations. These were rather small in the area-weighted mean but more significant in the population-weighted mean. This reflects the high population densities in the south-east of England and in port cities like Liverpool and Aberdeen close to the major shipping lanes. Although this resulted in winter increases and summer decreases, the changes were not due to reductions in NO$_x$ titration of O$_3$ but rather the emissions of O$_3$ from the model PARANOx module and how it parameterises ship plumes. The influence of shipping emissions on the UK is discussed in more detail in Section 4.3.4.

The simultaneous removal of emissions from both the UK and EU was essentially equivalent to their summed effects. Similarly, the simultaneous removal of anthropogenic and agricultural emissions was equivalent to their summed effect. This is discussed further in Section 4.5.

Whilst area-weighted changes give perspective regarding the changes over UK land, the population-weighted changes are more important when considering human exposure, and the absolute concentrations could differ by 5-10% depending on whether annual mean or peak season MDA8 concentrations were used. Although this doesn't change the overarching conclusions, it can accentuate or downplay the model responses. For example, O$_3$ changes from shipping removal (noShip) more than doubled with population weighting (from +0.83 μgm^{-3} for Area-Weighted O$_3$ to 2.00 μgm^{-3} for Population-Weighted O$_3$) due to the regions most affected being in the SE of England, which have the highest population

(Section 4.3.4).

The choice of metric can lead the interpreter to draw vastly different conclusions from the result, as is the case when comparing annual mean and peak season results in Figure 47. Differences arise here because "Peak Season MDA8 O$_3$" is a metric intended to measure maximum exposure, so ignores changes outside of the "peak season". As a result, when an emission scenario produced varying changes throughout the year (e.g increases in the winter and decreases in the summer), changes outside of the peak-season can be ignored. This was significant for scenarios where UK anthropogenic or shipping emissions were removed (noUKAnthro, noUKAnthroAgri, noUKnoEUAnthro, noUKnoEUAnthroAgri, noShip). For example, the annual mean captured summertime O$_3$ decreases being outweighed by increases during the rest of the year (Figure 48), whereas these increase for peak season MDA8 concentrations which and suggests the opposite model response overall. Further, the timing of the "Peak Season" for O$_3$ varied depending on the part of the UK considered: for most of the UK the six-month period starts in January or February, but for SE England Peak Season began in April (Appendix Figure 46). These issues highlight the importance of the choice of weighting and time-averaging for sensitivity studies.

The spatial and temporal impacts of these perturbations is now discussed in more detail.

4.3.1   Anthropogenic Emissions

Figure 48 shows the annual mean surface O$_3$ in the baselines model (far left), with then the perturbation caused by removing anthropogenic emissions from the UK, EU and both to the right. Annual area-weighted mean O$_3$ concentration over the UK increased by 3.26 μgm^{-3} following the removal of UK anthropogenic emissions. The impact is largest over cities with a maximum of around 14 μgm^{-3}.

Thus, the population-weighted average increases by 5.50 μgm^{-3}. This increase is indicative of a reduction in O_3 titration due to reduced NO_x emissions. Similar responses have been reported in other cities including Beijing (Liu, 2022), New York City (Tran et al., 2023) and Milan (Gabusi and Volta, 2005).
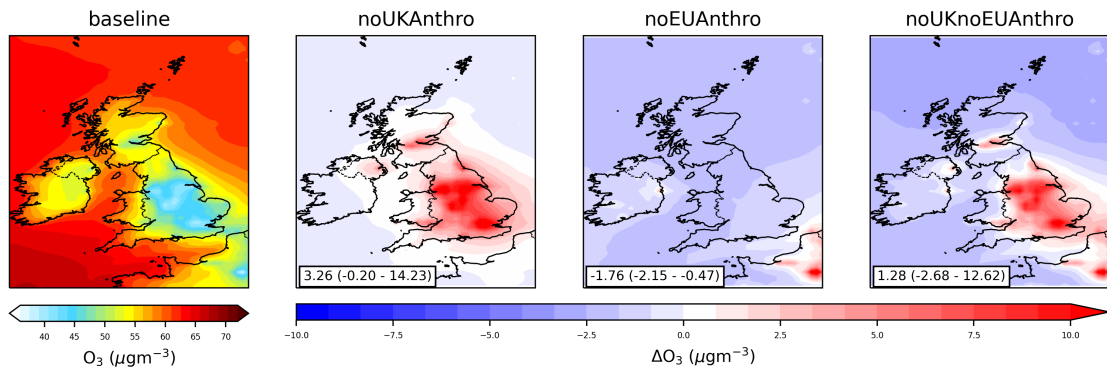
Figure 48: Annual mean O_3 concentration in the baseline scenario (far left), compared to the absolute difference in annual mean O_3 concentration (scenario - baseline) for the three anthropogenic emission scenarios. Annotations show the mean change, minimum and maximum over UK gridboxes for each difference comparison.

Removing the UK anthropogenic emissions leads to a small reduction over the UK (0.2 μgm^{-3}) in background O_3 concentrations at sites such as Mace Head and at the tip of Cornwall (Jennings et al., 2003). The impact on the background O_3 is larger from switching off EU anthropogenic emissions (on average 1.76 μgm^{-3}) with almost no spatial variability. The global impact of this perturbation can be seen from the coarse resolution boundary condition simulation where switching off the anthropogenic emissions from the EU leads to a reduction of up to -5 μgm^{-3} (Figure 49). This creates a band of lower O_3 around the Northern Hemisphere. The UK is at the end of that band and so removal of EU emissions leads to a small decrease in the O_3 imported into the UK.
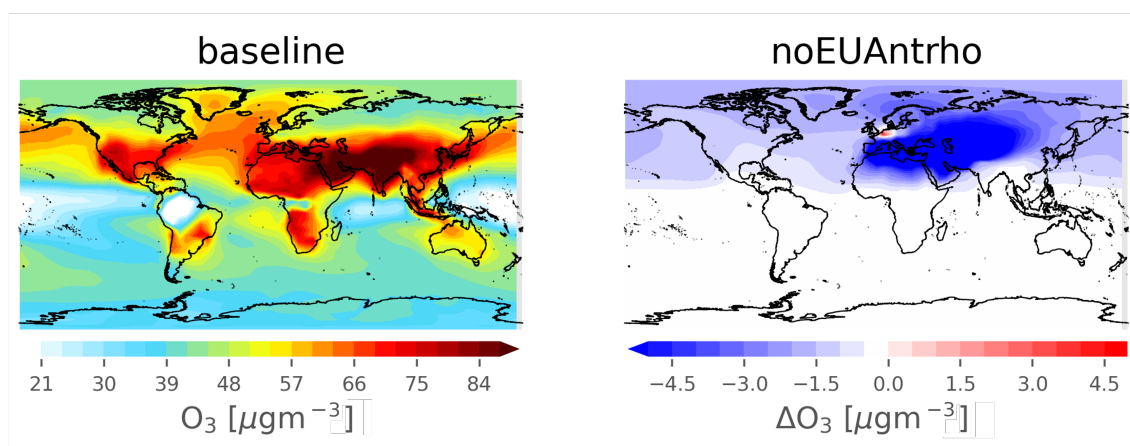
Figure 49: Annual mean surface O$_3$ in the model baseline simulation (left) and the difference in annual mean surface O$_3$ between the baseline and noEUAnthro scenario (right), at 4°×5° horizontal resolution.

Figure 50 shows the monthly daytime (1000-1400 GMT) and night-time (2200-0200 GMT) change in area-weighted UK O$_3$ and O$_x$ (NO$_2$+O$_3$) concentrations for removal of UK anthropogenic emissions (noUKAnthro) and EU anthropogenic emissions (noEUAnthro).
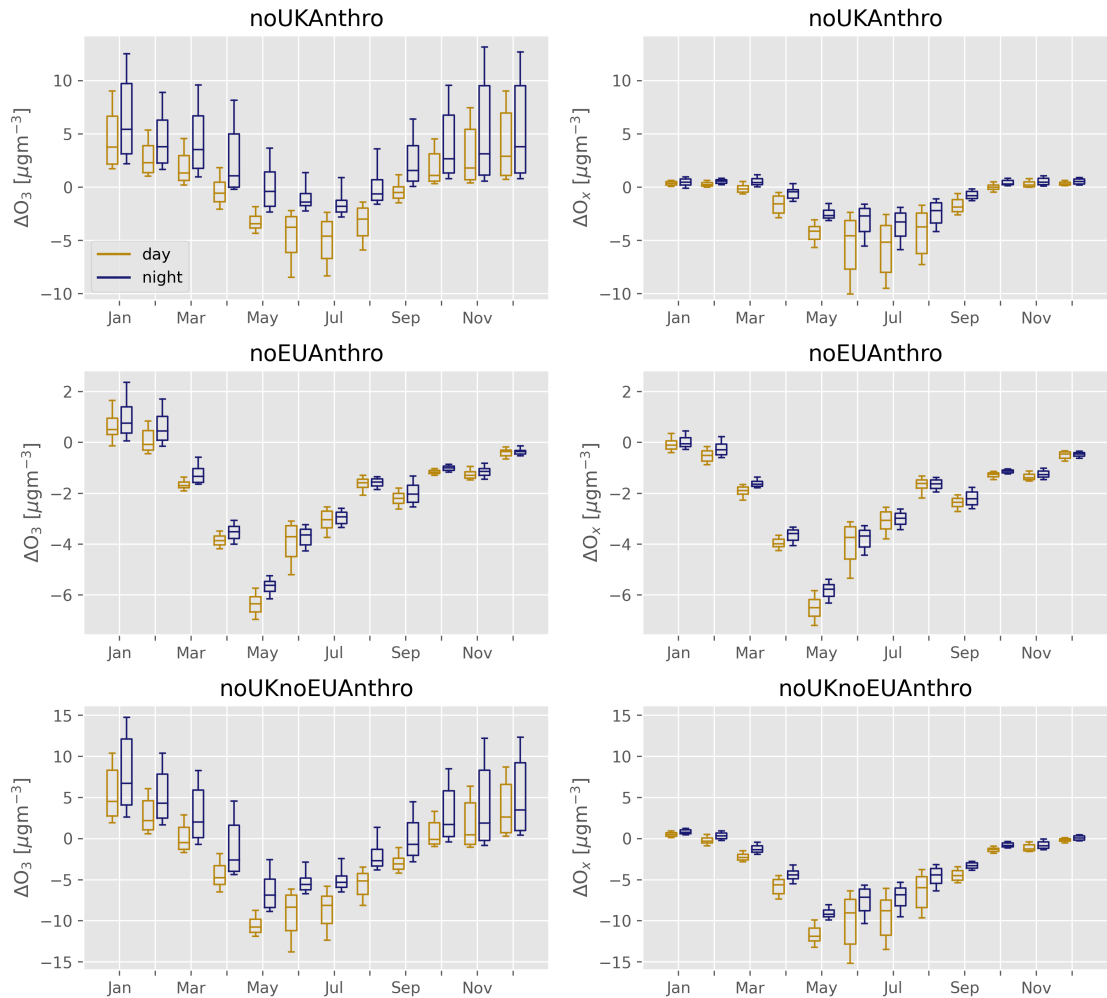
Figure 50: Monthly Day and Night O_3 (left) and O_x (right) changes for the anthropogenic emission scenarios compared to the baseline.

In the winter months, switching off UK Anthropogenic emissions, leads to increased O_3 concentrations (3.5 μgm^{-3}), but has little impact on O_x concentrations. This suggests that the wintertime increases in O_3 are due to the impact of NO titration which reduces O_3 concentrations but has no impact on O_x. In the summer months, switching off UK anthropogenic emissions leads to a reduction in both O_3 and O_x concentrations, suggesting a reduction in the local photochemical production of O_3. These factors (titration and O_3 production) are not cumulative. If they were, summer-to-winter changes in O_3 would be the same as summer-to-winter changes in O_x. The summer to winter change in O_3 is 8.0 μgm^{-3}, whereas for O_x the change is only 5.5 μgm^{-3}. Thus, it seems likely that the titration effect varies throughout the year, with less of an impact in the summer than in the winter.

Removal of the EU emissions shows a different seasonal trend, with the largest decrease (6 μgm^{-3}) occurring in late Spring, consistent with the expected seasonal maximum contribution from the northern hemispheric background (Monks, 2000). The changes in O$_3$ and O$_x$ are almost identical showing that the titration process isn't occurring.

Removal of both UK and EU anthropogenic emissions leads to a combined effect. For O$_3$, wintertime concentrations increase due to the titration effect but this rapidly leads to a reduction in O$_3$ concentrations so that by April O$_3$ concentrations are lower. This continues until September when O$_3$ concentrations turn over to lead to increased O$_3$ concentrations from decreased emissions.

The complexity of these changes explains the difference seen in the average metrics discussed in section 4.3. The combined impact of removing UK and EU anthropogenic emissions lead to a decrease in the area-weighted average, but an increase in the population weighted. This can be understood from the differing balance between titration effect which will be largest where there is the most emissions and the highest population, and the background effect which is more pervasive. Thus the area-weighted effect of removing the anthropogenic emissions leads to lower O$_3$ concentrations, but this is overwhelmed by the titration effect where people actually live.

4.3.2   Agricultural Emissions

Figure 51 shows the annual mean impact of removing agricultural emissions over the UK (noUKAgrid), over the EU (noEUAgri) and from both regions (noUK-noEUAgri). Removal of UK agricultural emissions had a small positive impact of 0.24 μgm^{-3} on UK O$_3$, reaching a maximum of 0.54 μgm^{-3} over South East England where UK emissions from agriculture are at their highest (`https://naei.beis.gov.uk/emissionsapp`, last access 23/03/23) (Figure 51). Eliminating

European agricultural emissions produced larger increases of 0.40 μgm^{-3}, which showed a tendency to be higher towards the East of England. Increases of 0.77 μgm^{-3} occurred near the Ireland-Northern Ireland border. Combined agricultural emission removal from both regions produced the largest average increase of 0.70 μgm^{-3}, which shared the spatial characteristic of both the UK agricultural and EU agricultural emissions changes.
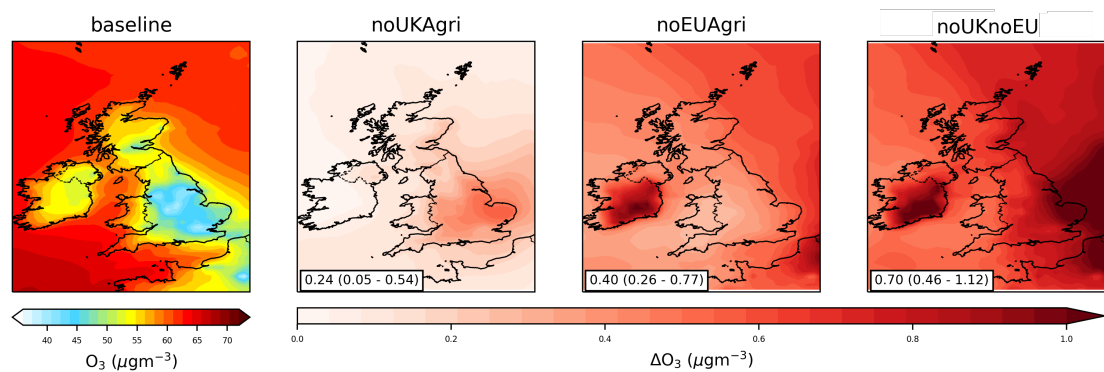
Figure 51: Annual mean O_3 concentration in the baseline scenario, compared to the absolute difference in annual mean O_3 concentration (scenario - baseline) for the agricultural emission scenarios. Annotations show the mean change (minimum - maximum) over UK gridboxes for each difference comparison.

The seasonal variation in O_3 and O_x concentrations are shown in Figure 52. The changes here are much smaller those from anthropogenic emission changes in the previous section (up to 0.5 μgm^{-3} compared to 5 μgm^{-3}. For the removal of UK agricultural emissions, the maximum increase in O_3 occurred in September, with another increase in April and a small summertime decrease. The O_x shows a similar April peak to the O_3 but doesn't show a September peak. This suggests different explanations for the peaks. The April increase in both O_3 and O_x suggests a change in photochemical production. This may be due to changes in agricultural emissions causing changes in aerosol loadings (see Section 4.4) which can impact O_3 concentrations through heterogeneous uptake of HO_2 and N_2O_5 onto aerosols (Jacob, 2000; Song et al., 2022). The uptake of both lead to a reduction in O_3 photochemical production. The September peak in O_3 is not accompanied by a peak in O_x and so suggest that there is titration of O_3 by agricultural NO emissions which follows the seasonality of agricultural practice

(Hellsten et al., 2007).
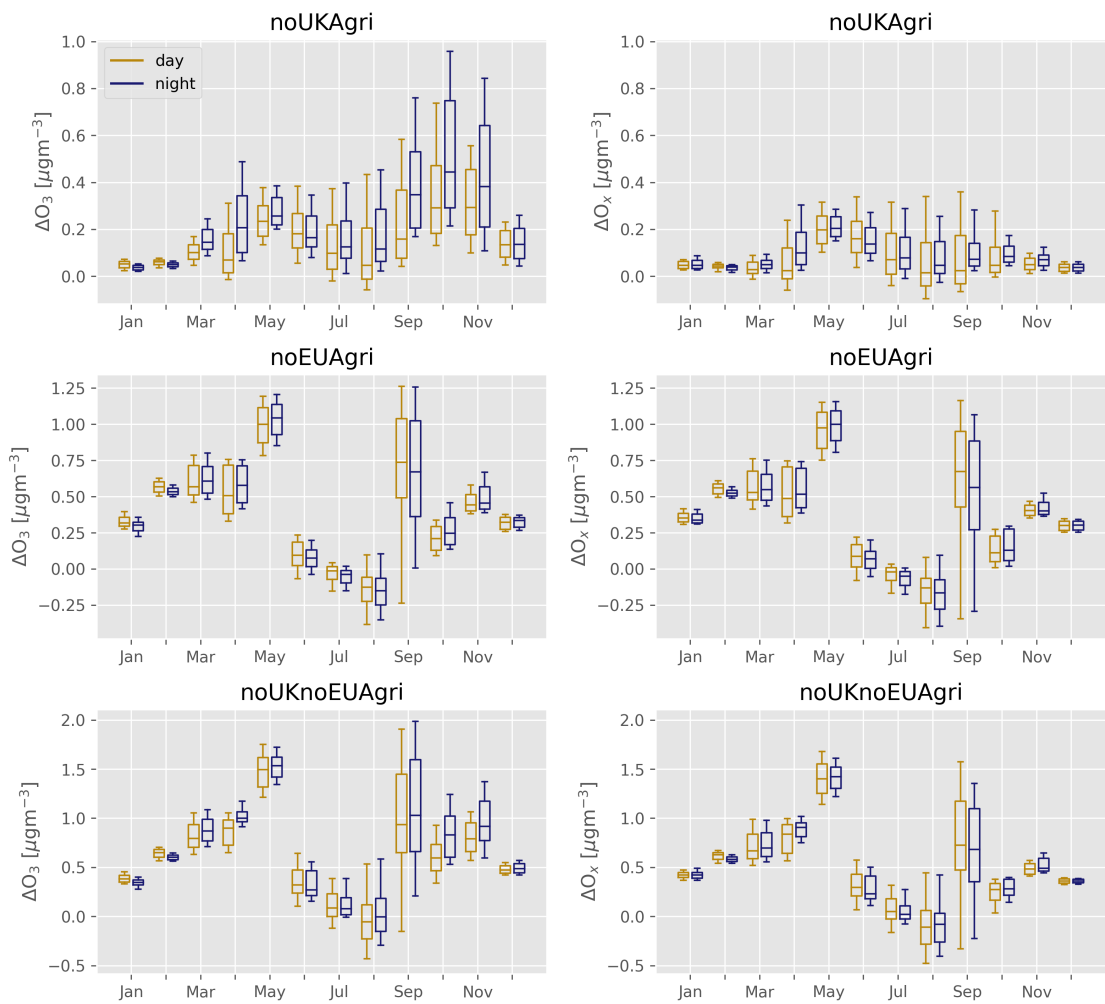
Figure 52: Monthly Day/Night O$_3$ and O$_x$ changes for the agricultural emission scenarios compared to the baseline

Removal of EU agricultural emissions has a mixed impact. In the winter months this leads to an increase in O$_3$ and O$_x$ and in the summer months there is little change. There is no titration effect from EU emissions and thus this impact is likely due to reduced aerosol surface areas. This leads to higher concentrations of HO$_2$ and NO$_x$, and subsequently higher O$_3$ concentrations downwind of Europe. O$_3$ concentrations at Mace Head increase by 0.36 μgm^{-3} on removal of EU Agricultural emissions (Table 16) consistent with the changes seen over the year. The coupled impact is dominated by the EU emissions with a spring and autumn maxima, and winter and summer minima.

4.3.3   Biogenic VOC Emissions

Figure 53 shows the changes in annual mean O$_3$ from removing UK biogenic VOC emissions (noUKBiogenic) and from removing EU biogenic VOC emissions (noEUBiogenic). UK biogenic emissions removal (predominantly isoprene) decreased O$_3$ by 0.33 μgm^{-3} on average, and by up to 0.71 μgm^{-3} in central and southeast England. There were smaller reductions of around 0.1 μgm^{-3} over the rest of the UK. The largest decreases occurred in central and southern England. Cities such as Birmingham and London have high NO$_x$ concentrations and are thus likely to be VOC-limited (Zhang and Stevenson, 2022). Reducing the VOC concentrations would likely lead to lower O$_3$ production in these regions. However, overall for the UK biogenics contribute only a small fraction of the total UK VOC emissions (DEFRA, 2015) compared to from anthropogenic contributions of VOCs such as ethene, propene and xylenes.

European biogenic emissions removal produced a larger annual mean decrease (0.88 μgm^{-3}), than seen from removing UK biogenic VOCs emission. This decrease is largest around the south east of the UK (1.64 μgm^{-3}) but is pervasive throughout the domain. Some of the impact will occur through short range transport of air from Europe towards the south east of the UK but some will be through changes to the hemispheric background. Isoprene emissions increase with both temperature and sunlight (Monson et al., 1992), leading to the EU emitting substantially more isoprene than the UK (Table 11).Further work could look at alternative scenarios where biogenic isoprene emissions increase in response to a warming climate, but this was beyond the scope of this project.
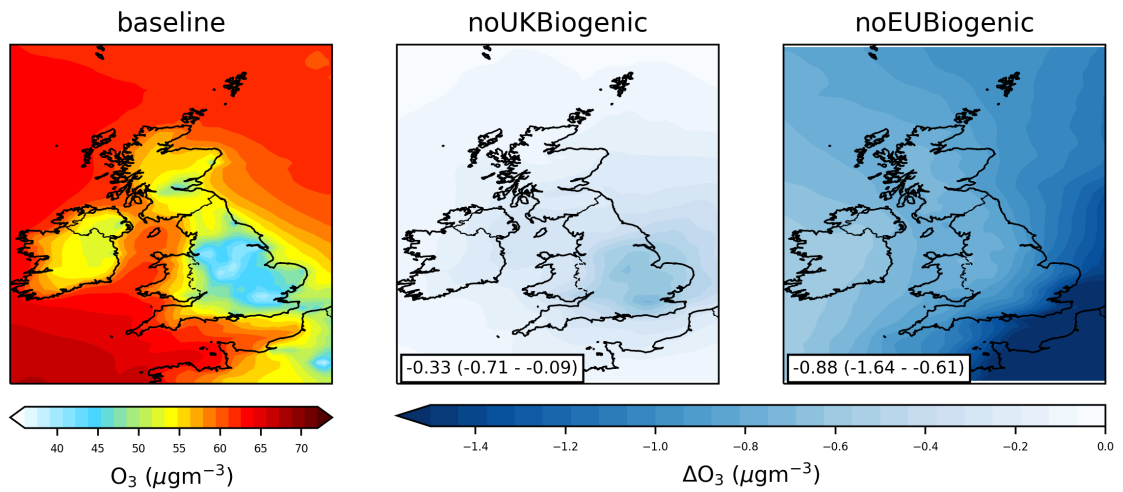
Figure 53: Annual mean O_3 concentration in the baseline scenario, compared to the absolute difference in annual mean O_3 concentration (scenario - baseline) for the biogenic emission scenarios. Annotations show the mean change (minimum - maximum) over UK gridboxes for each difference comparison.

The seasonal changes for removal of UK and EU biogenic VOC emissions are shown in Figure 54. Both show a maximum impact in late Spring and Summer, in line with the seasonality of biogenic emissions (Guenther, 1997) and photochemical ozone production (Pope et al., 2016). The European decreases showed more variability due to variability in the short-range transport of air from Europe to the UK.
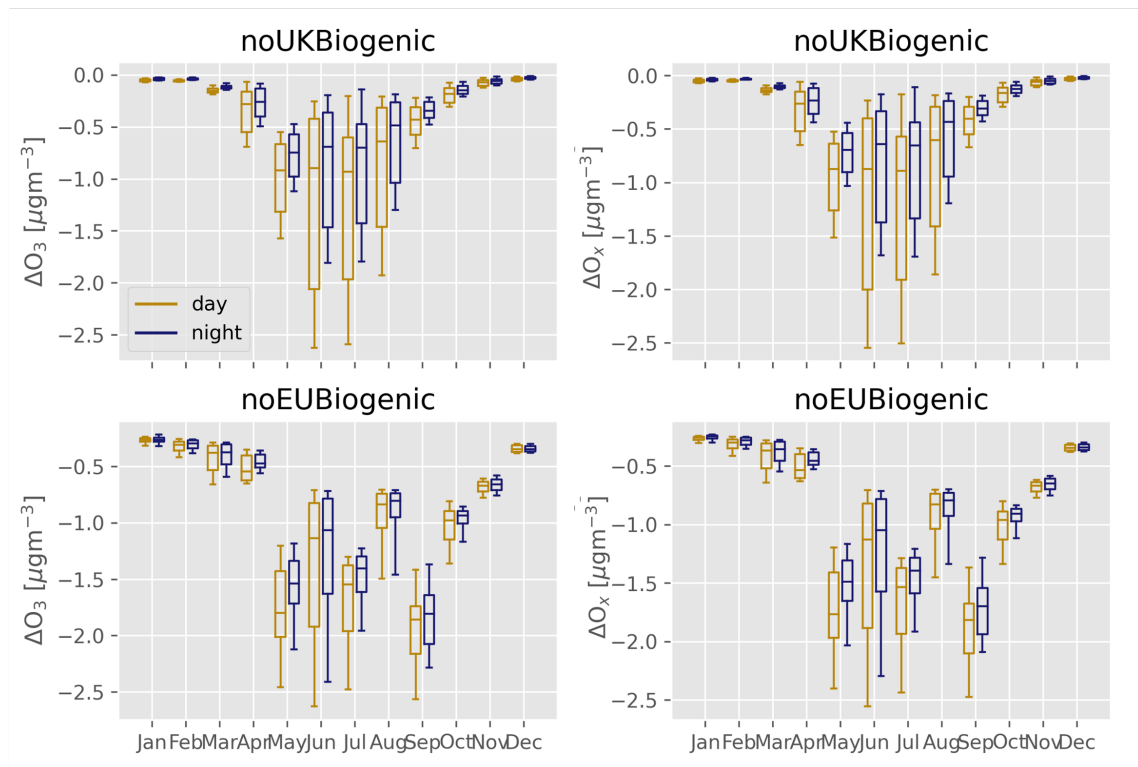
Figure 54: Monthly Day/Night O$_3$ and O$_X$ changes for the biogenic emission scenarios compared to the baseline. Note the different y-axis scales for O$_3$ and OX.

4.3.4 Shipping Emissions

Figure 55 shows the impact of removal of in-domain international shipping emissions from the model (boundary conditions were the same as the baseline simulation, see Table 10). Shipping emissions in the model use the PARANOx module (Vinken et al., 2011; Holmes et al., 2014) to pre-process emissions to account for plume chemistry (see Section 2.2). This results in NO$_x$ emissions from shipping being processed to give a reduced direct emissions of NO$_x$ which is compensated for by direct emissions of HNO$_3$ and O$_3$.
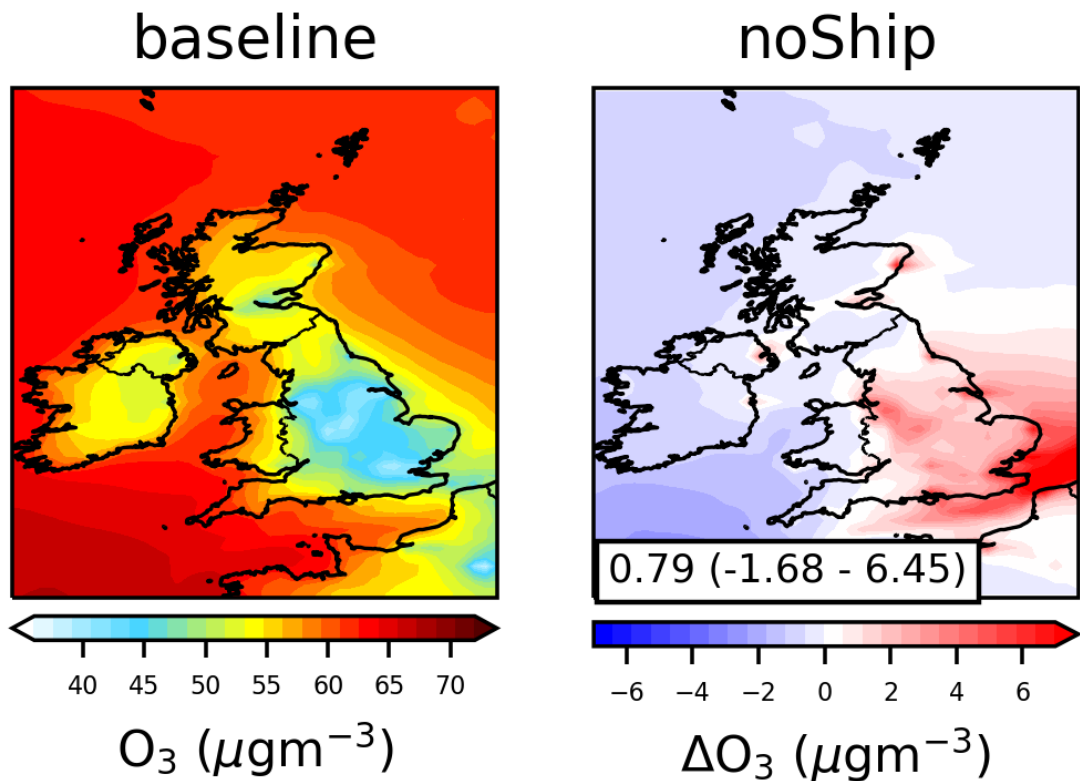
Figure 55: Annual mean O$_3$ concentration in the baseline scenario, compared to the absolute difference in annual mean O$_3$ concentration (scenario - baseline) for the shipping emission scenario. Annotations show the mean change (minimum - maximum) over UK gridboxes for each difference comparison.

The largest O$_3$ changes occur over the English Channel and the North Sea and at the major ports such as Belfast, Liverpool, Hull and Aberdeen. Removal of shipping emissions leads to increases of up to 6.45 μgm^{-3} in coastal SE England. Port cities experienced smaller increases of 3.00 μgm^{-3} which extend inland from Liverpool. Western parts of the UK (Wales, Northern Ireland, SW England) and north Scotland experienced decreases of up to 1.68 μgm^{-3}.

It seems likely that shipping is having multiple impacts. Over clean oceanic regions, removal of shipping reduces NO$_x$ concentrations thereby reducing O$_3$ concentrations, and the removal of the direct emission of O$_3$ from the plume parametrization also leads to lower O$_3$ concentrations. However, reducing the NO$_x$ concentration in places with already high NO$_x$ concentrations (e.g cities and the English channel) has the opposite effect.

The seasonal sensitivity of O$_3$ and O$_x$ to emissions changes is shown in Figure 56. The seasonality in O$_3$ shows a similar trend to anthropogenic emission changes (Figure 50). During the winter months removal of shipping emissions increases O$_3$ concentrations whereas in summer months it tends to decrease concentrations. However, unlike in the anthropogenic emission scenarios (Figure 50), the impact of the emissions reduction on O$_x$ is almost exactly the same as the impact on O$_3$. This would suggest a different mechanism is responsible for the O$_3$ and O$_x$ concentration changes for the removal of shipping emissions than for anthropogenic emissions. In high NO$_x$ conditions above the English Channel PARANOx estimates negative O$_3$ production (O$_3$ removal), so it follows that by removing shipping emissions O$_3$ production should increase when NO$_x$ is highest. This could explain why O$_3$ increased in the winter when UK NO$_x$ is highest (Section 3.3.6) and decreases in the summer, when NO$_x$ concentrations are low and the removal of shipping emissions reduces O$_3$ production. However, it should be noted that PARANOx was designed for use with a coarse (2°×2.5°) model horizontal resolution over fairly remote ocean areas, so there is the question of whether it paramaterizing shipping NO$_x$ emissions in higher emission areas and like coastal regions in western Europe is the correct approach. At the comparatively high resolutions used here it may make sense to switch off PARANOx altogether.
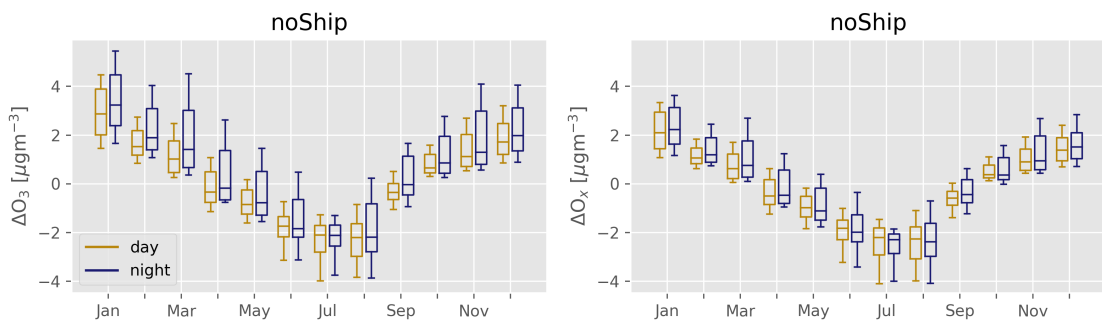
Figure 56: Monthly Day/Night O$_3$ and O$_X$ changes for the shipping emission scenario compared to the baseline. Note the different y-axis scales for O$_3$ and O$_X$.

4.3.5   All UK and EU Anthropogenic, Agricultural and Shipping Emissions

This simulation removes all UK and EU anthropogenic, agricultural and shipping emissions. This would essentially remove all human activity from the continent of Europe. Figure 57 compares the absolute and percentage O_3 changes for this scenario compared to the model baseline. Spatial features were similar to those observed after removing UK and EU anthropogenic emissions (Figure 48). In urban areas, concentrations increased by up to 11.4 μgm^{-3} (69%) due to the removal of the titration effects. For rural areas, concentrations decrease by up to -6.43 μgm^{-3} (8%) reflecting changes in the hemispheric background.
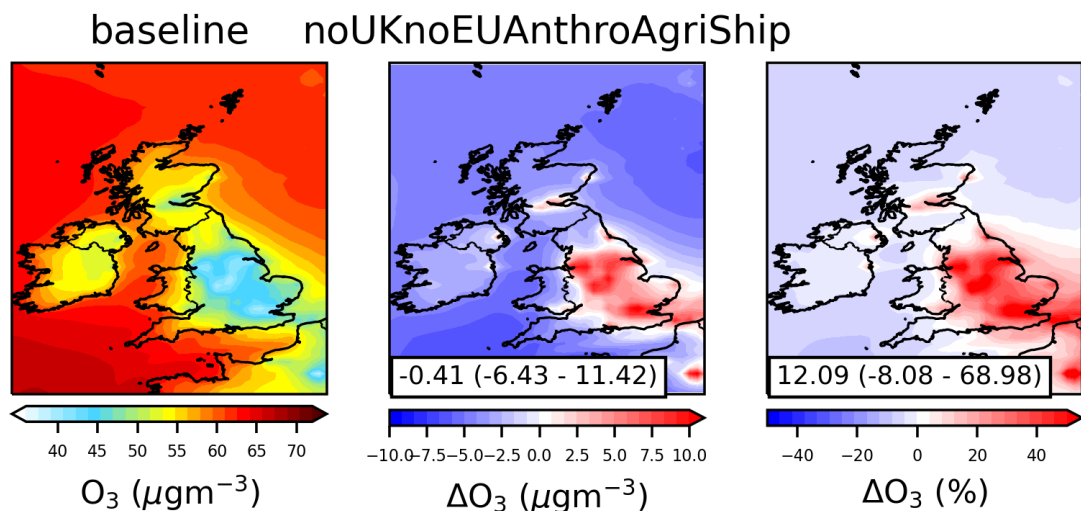
Figure 57: Annual mean O_3 concentration in the baseline scenario, compared to the absolute difference in annual mean O_3 concentration (scenario - baseline) for the emission scenario removing all UK and EU Anthropogenic, Agricultural and Shipping emissions. Annotations show the mean change (minimum - maximum) over UK gridboxes for each difference comparison.

Figure 58 compares the monthly mean UK O_3 and O_x for the base simulation and this "no European human" simulation. Both O_3 and O_X changes showed the same pattern of summer decreases which were larger during the daytime and winter decreases which were same during the day and the night. This shows little difference compared to the noUKnoEUAnthro seasonal changes 50, despite the additional emission reductions, suggesting that most of the changes are due to wintertime reductions in NO_x titration and summertime reductions in O_3 produc-

tion.
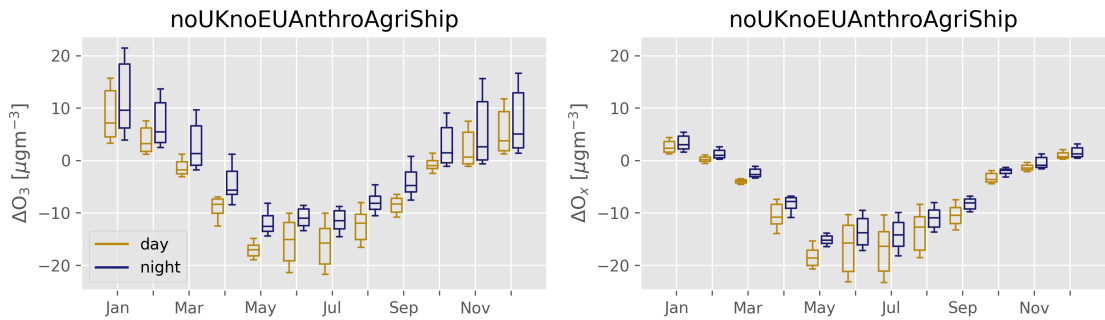
Figure 58: Monthly Day/Night O$_3$ and O$_X$ changes for the noUKnoEUAnthroAgri-Ship emission scenario compared to the baseline.

This "no-European human" simulation can be used to assess the background O$_3$ experienced by the UK. This suggests that over the year, much of the O$_3$ concentrations in the UK are controlled by sources external to the UK. Tagged O$_3$ WRF-Chem simulations by (Romero-Alvarez et al., 2022) estimated the hemispheric background makes a 71% contribution to UK O$_3$ from May-August in 2015. We approximate the same contribution as the change in area-weighted O$_x$ over the UK in the noUKnoEUAnthroAgriShip scenario compared to the baseline. This approach estimates that the hemispheric background contribution was 77.8% over the same period, which is similar given the differences between the two approaches.

4.3.6   O$_3$: Compliance with WHO guidelines

WHO regulation for O$_3$ depends on the average 'peak season' MDA8 concentration. Average concentrations in that period needs to remain below 60 μgm^{-3} to be compliant (Section 4.2.5). Figure 59 shows the "peak season" modelled MDA8 O$_3$ for 2017 for each emission scenario, with the red line indicating the boundary between areas above and below the WHO O$_3$ guideline of 60 μgm^{-3}. The model estimated 59% of the UK area and 22% of the population currently live in locations exceeding the WHO guideline for O$_3$ in 2017.
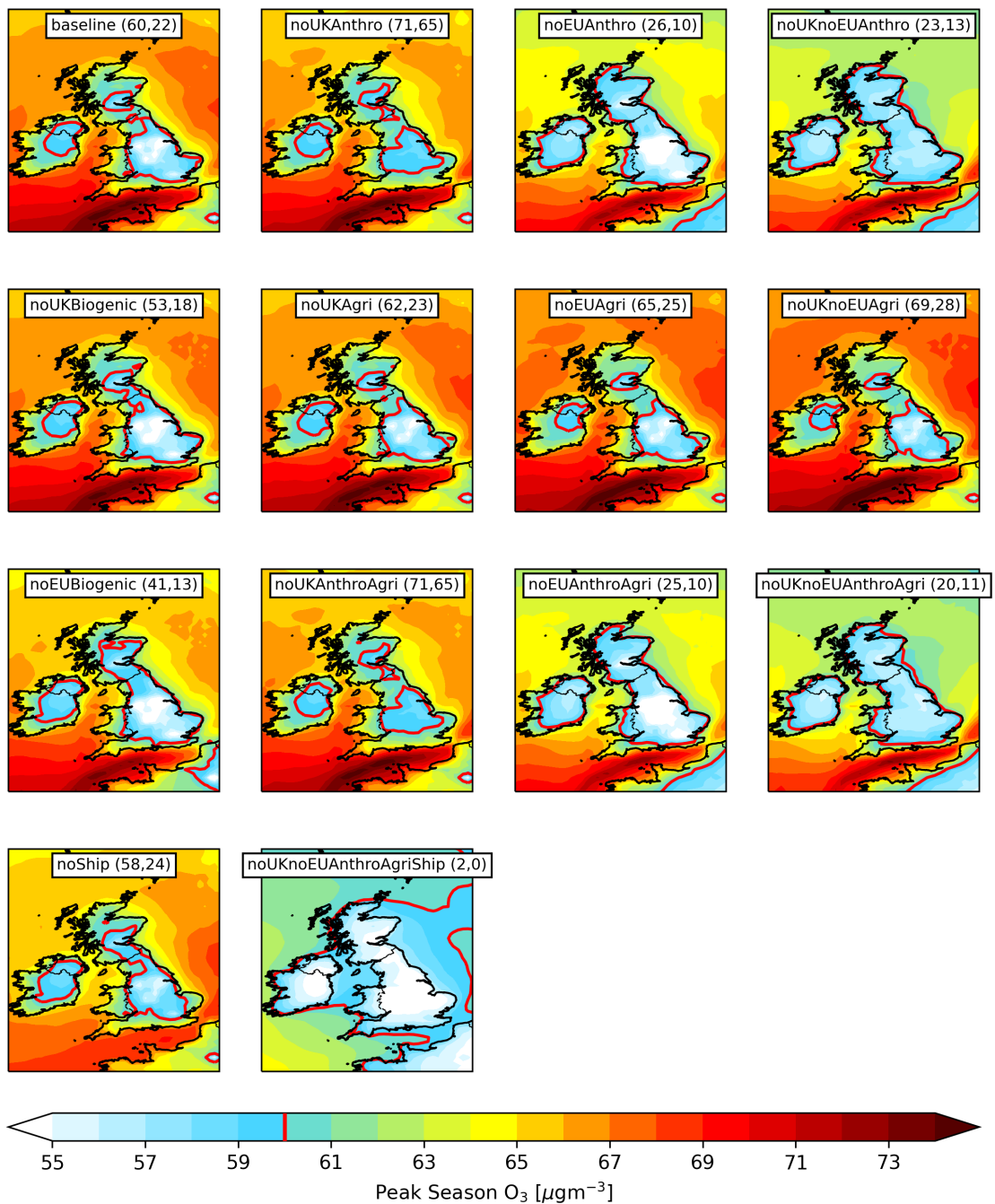
Figure 59: Peak Season MDA8 O_3 for each emission scenario scenario. The number in brackets indicates the percentage of the UK area exceeding the WHO 60 μgm^{-3} guideline for O_3. The red contour distinguishes the boundary between area's exceeding and below the guideline.

The air flowing into the UK exceeds the WHO regulation and it is the effect of the NO titration of O$_3$ in populated regions which brings regions into compliance. Thus regions typically considered "clean" like Wales, the South West of England and Scotland are in violation of this standard. Most of this high O$_3$ air reflects the hemispheric background concentrations, with some due to local emissions from shipping (in the English Channel).

Removing UK anthropogenic emissions triples the non-compliant population (to 65%), removing European anthropogenic reductions from Europe halves it (to 10%), and the combined effect is smaller (to 13%). This reflects the balance between local titration of O$_3$, driven by UK emissions, and the global production of O$_3$ driven by the emissions from the EU and a reduction in short-range transport of pollution from Europe.

Removing agricultural emissions (both from UK and EU) has little impact (increasing the percentage compliant by 1-3%).

Removing International shipping emissions has a small positive (1%) impact on UK O$_3$ exposure, despite large increases in concentration with reduced shipping emissions.

Removal of Biogenic emission from the EU and UK reduces the population exceeding the limit from 22% to 13% and 18%, respectively, despite only small reductions in average O$_3$ concentration.

Wales and SW England showed a relative insensitivity to all of the emission changes implemented, highlighting the importance of the hemispheric background concentration for determining exposure in these regions.

Given the decreasing trend in UK NO$_x$ emissions (DEFRA, 2022a) and the

rest of the world the likely future on UK O$_3$ is complex. Reduction in the titration effect of UK NO$_x$ emission on O$_3$ concentration appear to be larger than the reduction in O$_3$ production even in the peak season. Thus if UK NO$_x$ emissions reduce further we would expect an increasing fraction of the population to be out of compliance. However, this reduction trend will not occur in isolation. If European NO$_x$ emissions also continue to decrease, the background O$_3$ concentration flowing into the UK will also reduce. This will lead to fewer people living in regions out of compliance. Simulations here have only explored the impact of removal of European anthropogenic emissions. It is also likely that North America and Asia will also reduce their NO$_x$ emission, reducing background O$_3$ even further.

Thus future UK O$_3$ concentrations are not entirely under the control of the UK. The control of emissions from other countries can have a significant impact on UK O$_3$ through the background O$_3$ concentration and need to be considered at the same time.

4.4 PM$_{2.5}$

This section will look at the sensitivity of UK PM$_{2.5}$ to the emission reduction scenarios. The mean average mass of PM$_{2.5}$ (including water) and the dry mass of its components under each emission scenario over the UK is compared with area-weighting in Figure 60 and with population-weighting in Figure 61. Values for the figures are given in Appendix Tables 18-24.
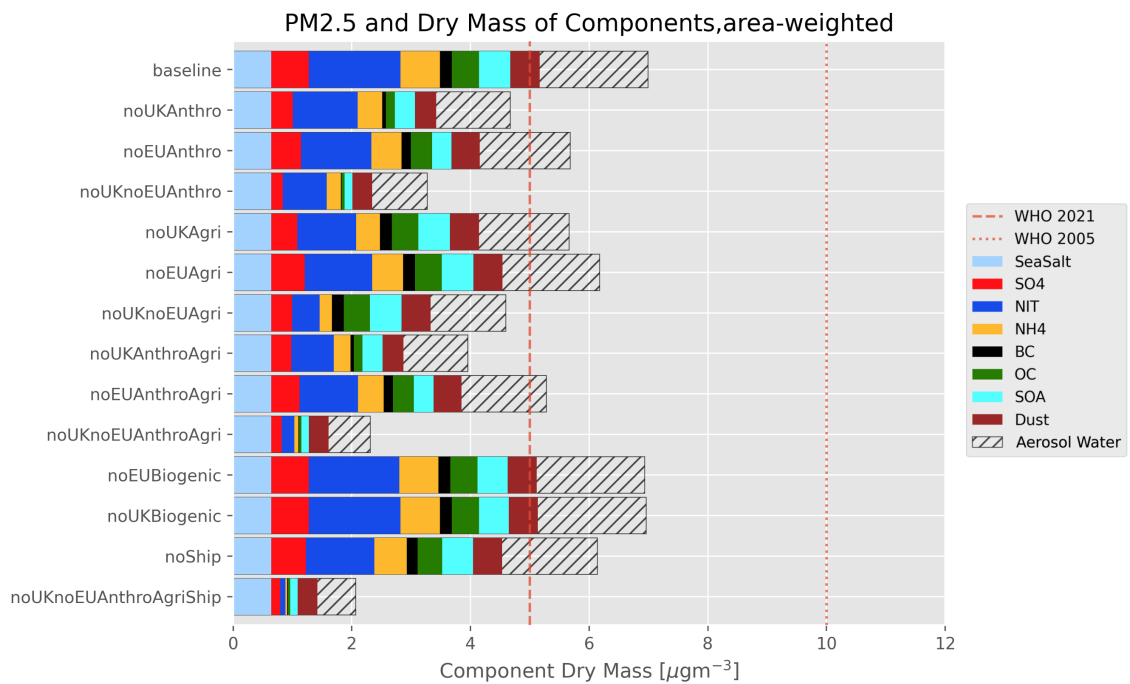
Figure 60: Annual mean area-weighted dry mass of PM$_{2.5}$ components (solid) and PM$_{2.5}$, accounting for water content (hatched) over the UK for each condition. The dotted and dashed lines show the 2005 and 2021 WHO guidelines for annual mean PM$_{2.5}$ concentration
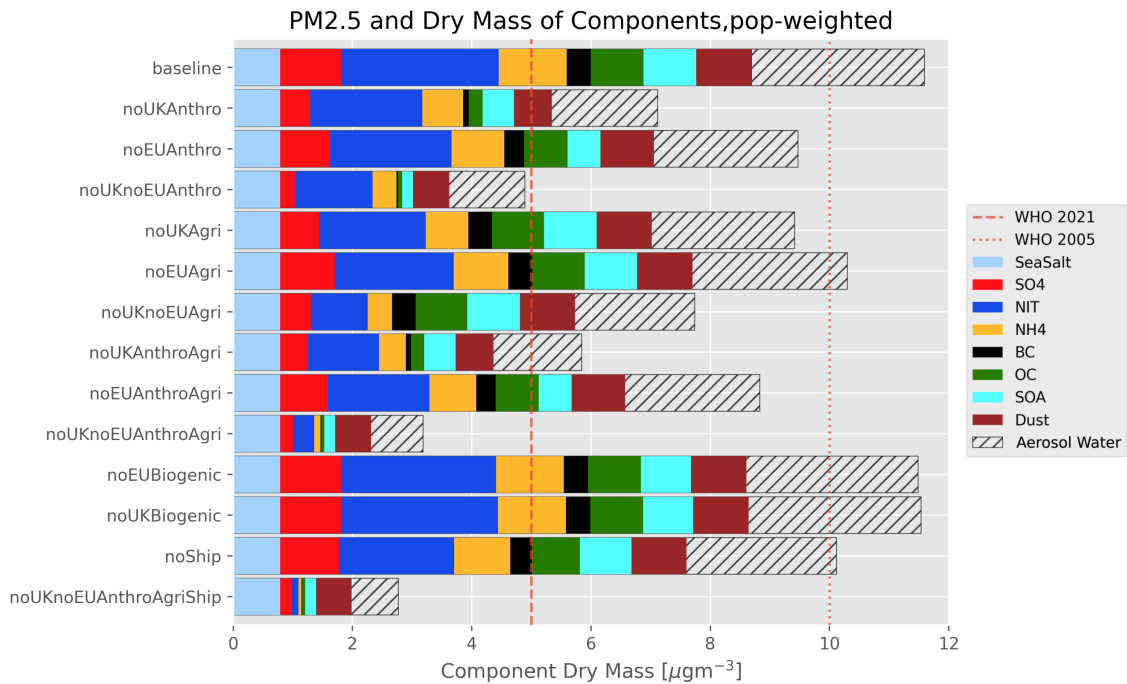
Figure 61: Annual mean population-weighted dry mass of PM$_{2.5}$ components (solid) and PM$_{2.5}$, accounting for water content (hatched) over the UK for each condition. The dotted and dashed lines show the 2005 and 2021 WHO guidelines for annual mean PM$_{2.5}$ concentration

Area-weighted PM$_{2.5}$ mass in the base model (6.99 μgm^{-3}) was well below the previous WHO guideline of 10 μgm^{-3} for annual mean PM$_{2.5}$ but exceeded the latest 5 μgm^{-3} guideline. Population-weighting substantially increased the mean concentration up to 11.75 μgm^{-3}, due to collocation of high PM$_{2.5}$ concentrations with densely populated areas (Figure 45). The estimated population-weighted PM$_{2.5}$ dry mass was 8.70 μgm^{-3} in the baseline, which is lower than the 10.5 μgm^{-3} value reported by McDuffie et al. (2021) for the same year using different anthropogenic emissions and a coarser model horizontal resolution, but consistent with us after the re-weighting (Section 4.2.2).

In the area weighted mean, the contribution from sea salt was 0.65 μgm^{-3} and remained constant throughout all scenarios. In the baseline model the largest contribution was from the inorganic aerosol components (SO$_4^{2-}$, NO$_3^-$ and NH$_4^+$) at 2.81 μgm^{-3}. Black Carbon, Organic Carbon and Secondary Organic Aerosol (SOA) contributed 0.20μgm^{-3}, 0.46μgm^{-3} and 0.53μgm^{-3} and dust contributed 0.49μgm^{-3}. Water associated with the PM$_{2.5}$ (1.81 μgm^{-3}) made a substantial

contribution.

In the population weighted mean, the sea-salt contribution didn't change much (0.78 μgm^{-3}) but the mass of the other contributions increased substantially to 7.8 μgm^{-3}, 0.41 μgm^{-3}, 0.89 μgm^{-3}, 0.88 μgm^{-3} and 0.93 μgm^{-3} for the inorganic aerosol components, black carbon and organic components, SOA and dust respectively.

Eliminating UK anthropogenic emissions reduced area weighted mean UK PM$_{2.5}$ concentrations from 6.99 μgm^{-3} to 4.62 μgm^{-3}, bringing them below the WHO guideline level but the population weighted mean was still above the 5 μgm^{-3} at 7.11 μgm^{-3}. Removing EU anthropogenic emissions reduced the concentrations for both the area- (from 6.99 μgm^{-3} to 5.62 μgm^{-3}) and population- (from 11.59 μgm^{-3} to 9.47 μgm^{-3}) weighted averages. Removing emissions from both regions resulted in average concentrations lower than the WHO guideline in both the area- (3.27 μgm^{-3}) and population- (4.89 μgm^{-3}) weighted averages. Remaining PM mass was due to agricultural emissions, international shipping and natural sources (sea-salt, BVOCs, dust and wildfires).

Eliminating agricultural emissions from the UK and EU halved the overall concentration of inorganic ions (sulphate, nitrate and ammonium), reducing the area- (from 6.99 to 4.59 μgm^{-3}) and population weighted (from 11.59 μgm^{-3} to 7.74 μgm^{-3}) PM$_{2.5}$ concentrations. Most of this change was in the concentration of the inorganic ions due to reduced ammonia concentration. Area weighted ammonia concentrations drop by 1.53 μgm^{-3} (91%), and the inorganic ions (aerosol SO$_4{}^{2-}$, NO$_3{}^{-}$, NH$_4{}^{+}$) drop in total by 1.61 μgm^{-3} (61%).

Shipping emission removal reduced PM$_{2.5}$ by 0.85 μgm^{-3}(12%) in the area weighted average and 1.47 μgm^{-3}(13%) in the population weighted average, comparable to the 10% contribution estimated by Jonson et al. (2020). This

mostly affected concentrations in SE England and near port cities. The bulk of these changes came from lower levels of NH_4^+ (0.12 μgm^{-3}) and NO_3^- (0.38 μgm^{-3}), alongside a smaller decrease in SO_4^{2-} (0.05 μgm^{-3}) due to reduced NO_x and SO_x emissions.

In the most extreme scenario, removing all UK and EU anthropogenic and agricultural emissions, along with in-domain shipping emissions, reduced $PM_{2.5}$ from 6.99 μgm^{-3} to 2.07 μgm^{-3} in the area weighted average and from 11.59 μgm^{-3} to 2.77 μgm^{-3} in the population weighted average. The remaining contributions at this point are predominantly natural, from sea-salt, oxidation of DMS, natural soil emissions and lightning, natural ammonia emissions, biogenic VOC emissions and natural dust emissions. This suggests that there can only be a roughly 2-3 μgm^{-3} anthropogenic enhancement of particulate matter before the WHO guidelines would be broken.

The following sections now assess the spatial changes of $PM_{2.5}$ and its components when the emission scenarios were implemented. Unlike O_3, where the changes in concentration were smaller compared to the absolute concentration, $PM_{2.5}$ concentrations vary more significantly over the UK, so the percentage change in annual concentrations are also given. Seasonal changes in $PM_{2.5}$ and its components were much smaller than those seen for O_3 and so are not discussed.

4.4.1   Anthropogenic Emissions

Figure 62 shows the change in annual mean $PM_{2.5}$ for the anthropogenic emission scenarios compared to the baseline model. UK anthropogenic emissions removal reduced $PM_{2.5}$ by 2.29 μgm^{-3} (26.8%), with the largest reductions of almost 5 μgm^{-3} in central England and peaking around Hull (53.768 N, 0.327 E). In Chapter 3, this area showed a 57% overestimate for $PM_{2.5}$, attributed to an overestimate in SO_4^{2-} and NH_4^+. The SIA results shown here have been scaled by the values from Chapter 3, but even this after scaling these inorganic species saw the largest reductions of any $PM_{2.5}$ component (0.86 μgm^{-3} (54%) for SO_4^{2-} and 0.82 μgm^{-3} (44%) for NO_3^-). Large decreases also occurred over other major cities like Cardiff and London. Rural regions like north Scotland and west Northern Ireland experienced the smallest reductions of 0.40 μgm^{-3}.
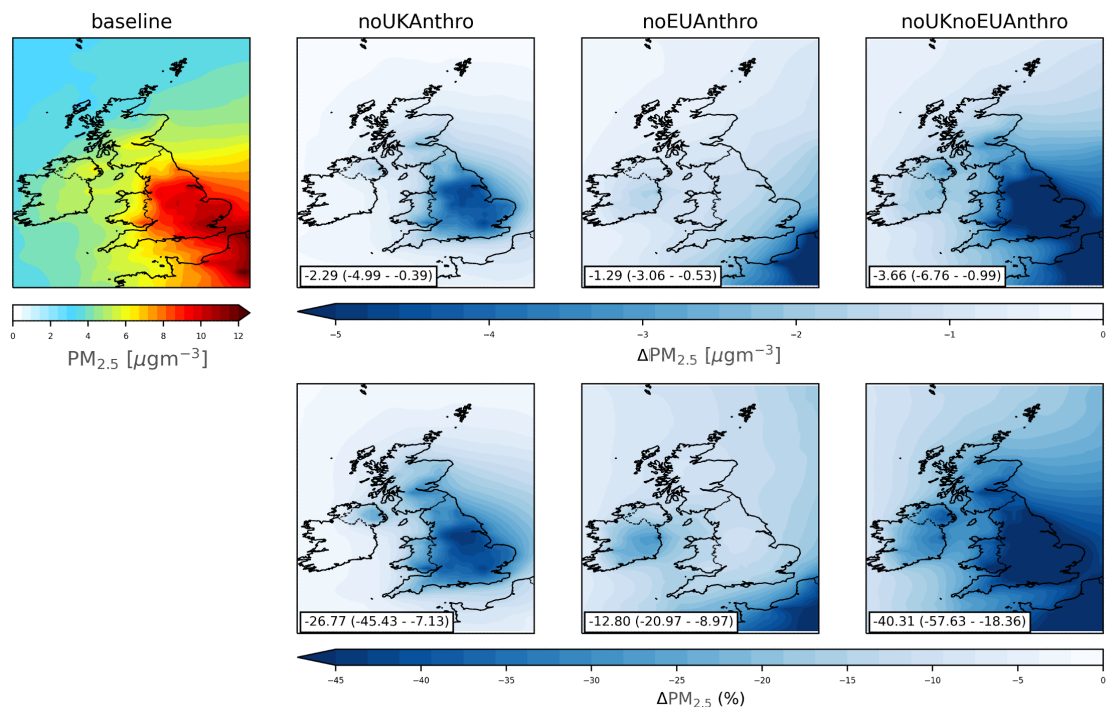
Figure 62: Annual mean surface concentration of $PM_{2.5}$ in the baseline (upper left), compared to the absolute change (top row) and percentage change (bottom row) in $PM_{2.5}$ from implementing the Anthropogenic emission scenarios. Annotations show the average change (minimum-maximum change) over UK grid boxes

The response to eliminating European anthropogenic emissions decreased rapidly north westerly from a maximum decrease of 3.06 μgm^{-3} in coastal SE

England to a minimum decrease of 0.53 μgm^{-3} in North Scotland. The changes were driven by large decreases of SO$_4$ (21%), NO$_3^-$ (8.3%) and NH$_4^+$ (19.9%) transported from continental Europe.

Removing all anthropogenic emissions (UK and EU) has a significant impact on UK PM$_{2.5}$. Reducing concentration by 3.66 μgm^{-3} (40%) on an area weighted basis, with some areas showing reductions of up to 58%.

4.4.2 Agricultural Emissions

Figure 63 shows the spatial changes in annual mean PM$_{2.5}$ for the agricultural emission removal scenarios. PM$_{2.5}$ reduced by 1.31 μgm^{-3} (14.7%), 0.81 μgm^{-3} (7.5%) and 2.37 μgm^{-3}, (24.3%) following removal of agricultural emissions from the UK, EU and both the UK and EU, respectively as an area average. East England showed the largest sensitivity to UK agricultural emissions removal, with a maximum PM$_{2.5}$ reduction of 2.90 μgm^{-3} on the North-East coast of England, whereas the smallest changes occurred in Northern Ireland and North Scotland. The short chemical lifetime of NH$_3$ means the spatial distribution of changes closely follow the UK agricultural NH$_3$ emissions. PM$_{2.5}$ changes were driven by large decreases in aerosol NH$_4^+$ (38%) leading to reduction in the aerosol SO$_4^{2-}$ (28%) and NO$_3^-$ (35%) concentrations. There were also relatively small decreases for OC (2%), BC (2%) and Dust (1%) (Figure 60).
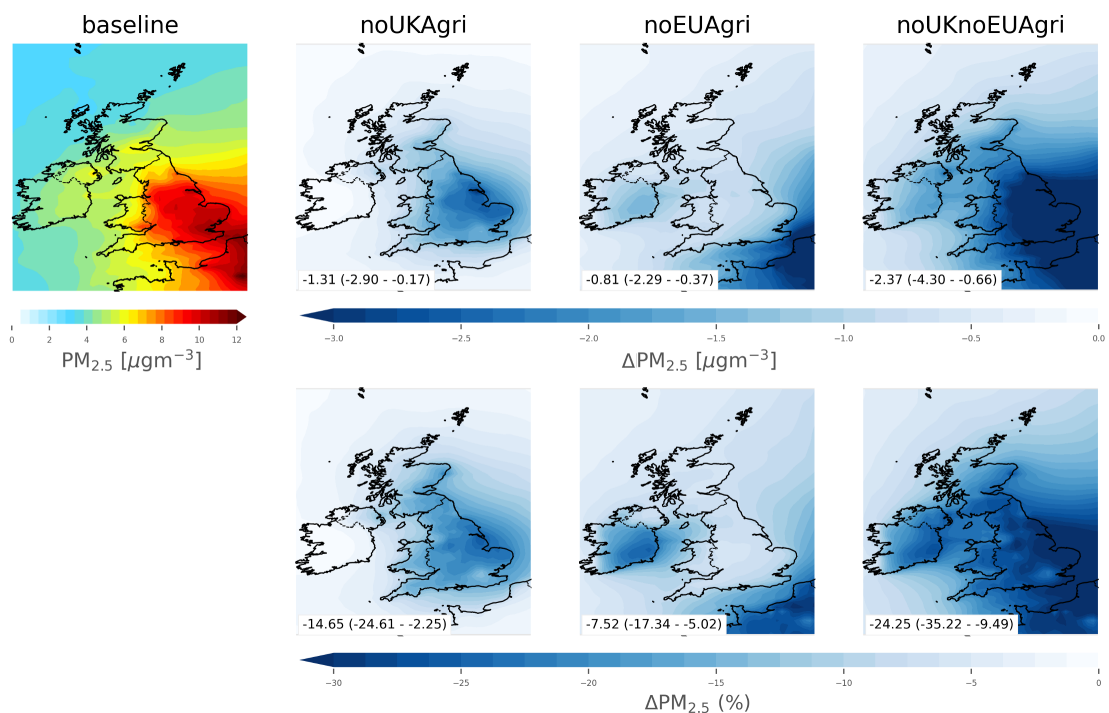
Figure 63: Annual mean surface concentration of PM$_{2.5}$ in the baseline (upper left), compared to the absolute change (top row) and percentage change (bottom row) in PM$_{2.5}$ from implementing the Agricultural emission scenarios. Annotations show the average change (minimum-maximum change) over UK grid boxes.

The spatial sensitivity to European agricultural emission removal was simi-

lar to the anthropogenic equivalent with the maximum change occurring closest to continental Europe in South East England and reduced moving north-west to north Scotland. The order of importance for PM component changes were slightly different to the UK Anthropogenic removal scenario; the largest reductions were for NO_3^- (29%) followed by NH_4^+ (24%), SO_4^{2-} (11%), BC (1%), OC (1%), Dust (0.3%) and SOA (0.3%). Under certain meteorological conditions, import of pollution from continental Europe and in particular aerosol nitrate from European agriculture has been reported to make large contributions to UK $PM_{2.5}$ during pollution episodes (Vieno et al., 2014, 2016b). In both noUKAgri and noEUAgri cases, the model response was largest for inorganic aerosols and produced larger nitrate aerosol changes than sulphate, in agreement with the sensitivity experiments of Redington et al. (2009) and reflecting the preferential irreversible reaction between available NH_4^+ and SO_4^{2-} than between NH_4 and NO_3.

4.4.3   Biogenic Emissions

Figure 64 shows the PM$_{2.5}$ changes from removing biogenic emissions from either the UK or the EU. Changes due to emissions reductions from either region were both predominantly from reductions in SOA concentrations (Figure 60).
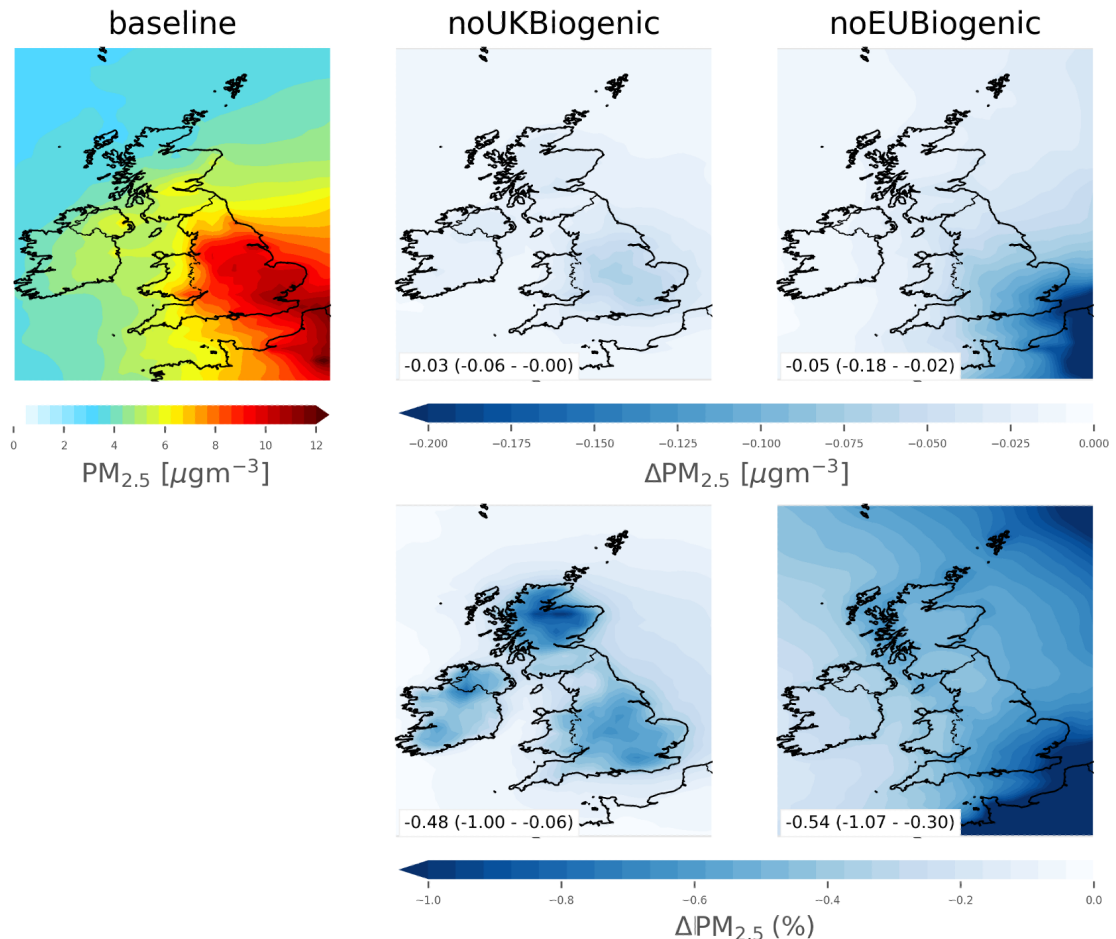
Figure 64: Annual mean surface concentration of PM$_{2.5}$ in the baseline (upper left), compared to the absolute change (top row) and percentage change (bottom row) in PM$_{2.5}$ from removing biogenic emissions from the UK (center) or Europe (right). Annotations show the average change (minimum-maximum change) over UK grid boxes

The changes in PM$_{2.5}$ due to removal of UK biogenic VOC emissions are small with an area weighted average of -0.03 μgm^{-3}. The impact was at a maximum in central England and the North of Scotland, similar to the distribution of UK biogenic emissions (Redington and Derwent, 2013). Changes were overwhelmingly due to reductions in the SOA concentrations.

Removal of EU Biogenic VOC emissions had a larger response on area averaged PM$_{2.5}$ at -0.05 μgm^{-3}. The geographical distribution of the impact is different from that from the removal of UK biogenic emissions with the largest impacts over the south east of England and it reducing towards Scotland.

These results contrast with the modelling study of Redington and Derwent (2013) who reported that the biogenic sources contributed 9-32% to UK PM$_{10}$, substantially larger than the numbers found here. This is likely due to uncertainties in the emissions of biogenic VOCs (Hogrefe et al., 2011) and in the yields of SOA from these biogenics (Pun et al., 2003; Zhang et al., 2007). This highlights the large uncertainties that exist in understanding the role of the natural system on air quality.

4.4.4   Shipping Emissions

Figure 65 shows the PM$_{2.5}$ changes when shipping emissions were removed. A strong signature of the shipping lanes can be seen with the highest percentage reductions occurring over the shipping lanes in the English Channel, and Irish Sea. UK Area-weighted PM$_{2.5}$ reduced on average by 0.84 μgm^{-3} (12%), with the largest reductions of around 2 μgm^{-3} (24 %) in SE England and around UK port cities. This highlights the regions most likely to be affected by shipping emissions around the UK: parts of SE England, Liverpool and Aberdeen. The influence generally decreased northward towards Scotland. The largest driver behind the changes were reductions in nitrate (25%) and ammonium (19%), with additional reductions from BC (10%), OC (11%), sulfate (8%), SOA (2%) and Dust (1%). The greater sensitivity of nitrate than sulfate likely due to the preferential uptake of sulfate to the aerosol phase compared to with ammonium.
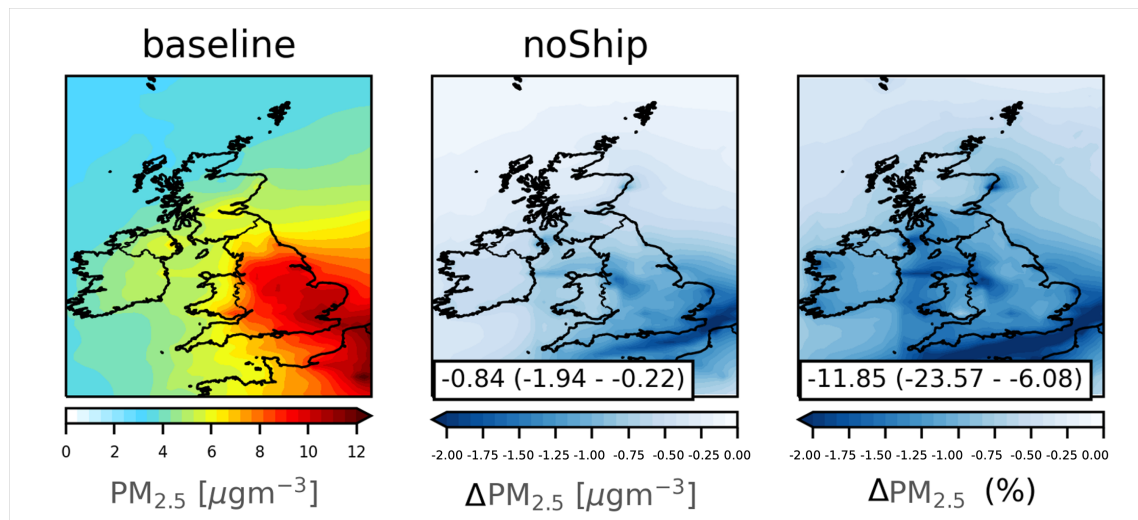
Figure 65: Annual mean surface concentration of PM$_{2.5}$ in the baseline (upper left), compared to the absolute change (top row) and percentage change (bottom row) in PM$_{2.5}$ from removing international shipping emissions within the nested domain. Annotations show the average change (minimum-maximum change) over UK grid boxes

4.4.5 All UK and EU Anthropogenic, Agricultural and Shipping Emissions

Figure 66 shows the absolute and relative changes following the removal of all UK and EU anthropogenic, agricultural and shipping emissions. With these sources removed, remaining $PM_{2.5}$ should be overwhelmingly from natural sources like sea salt, dust, biogenic VOC emissions, DMS, lightning, soil NOx etc. The compositional changes shown in Figure 60 shows that Sea Salt and Dust constituted most of $PM_{2.5}$ dry mass, with minor contributions from inorganic aerosol, OC and BC. The largest decreases of up to 8.97 μgm^{-3} (73%) occurred over central and SE England, also extending over the channel towards continental Europe.
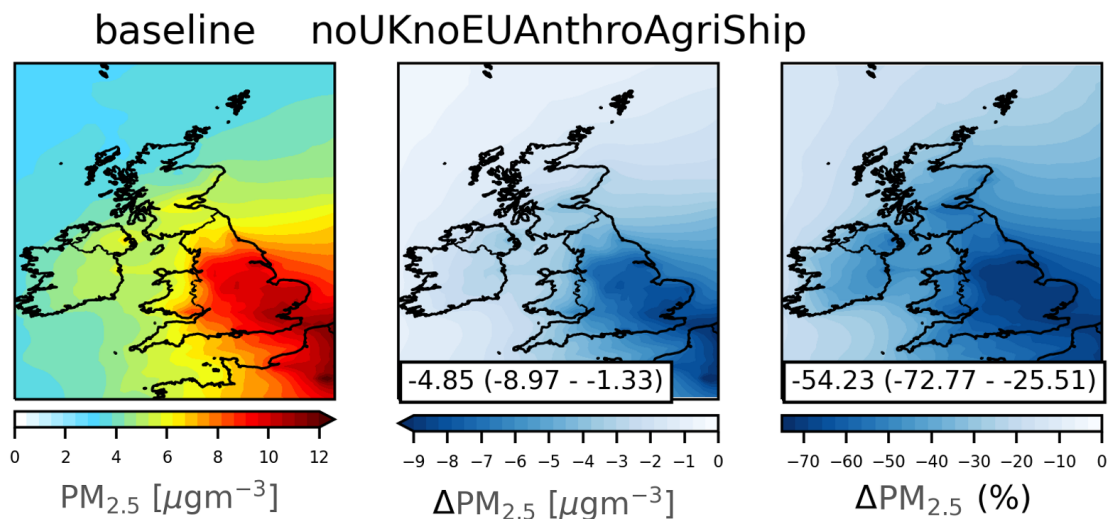
Figure 66: Annual mean surface concentration of $PM_{2.5}$ in the baseline (left), compared to the absolute change (center) and percentage change (right) in $PM_{2.5}$ from removing all UK and EU anthropogenic and agricultural emissions, and international shipping emissions within the nested domain. Annotations show the average change (minimum-maximum change) over UK grid boxes

4.4.6 $PM_{2.5}$: Compliance with WHO guidelines

This section will evaluate the changes in compliance with the previous (10 μgm^{-3}) and updated (5 μgm^{-3}) WHO $PM_{2.5}$ guideline limits. Figure 67 shows the annual mean concentration of $PM_{2.5}$ over the UK in each simulation, highlighting the WHO 2021 guideline of 5 μgm^{-3}.
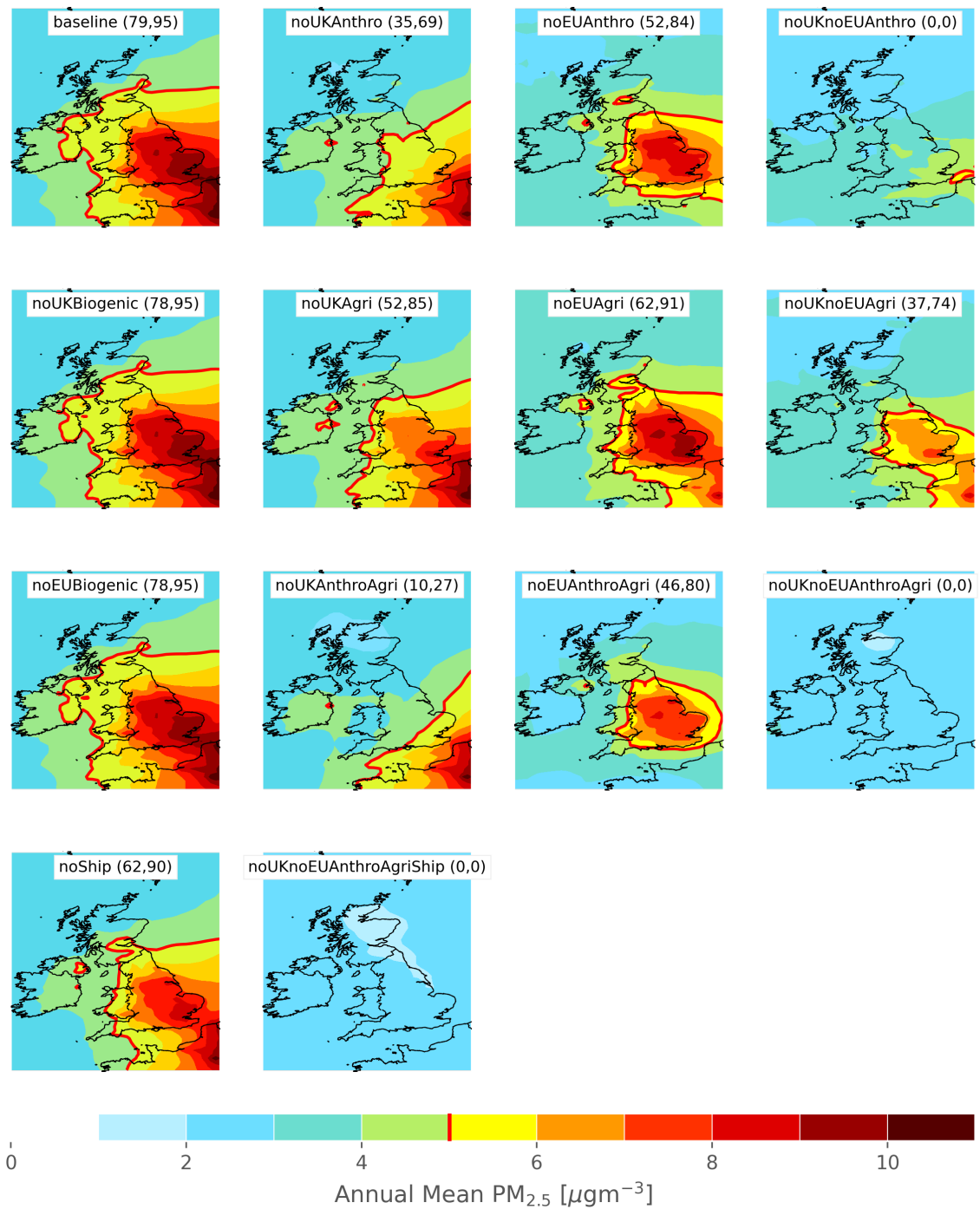
Figure 67: Maps of annual mean concentration of $PM_{2.5}$ for each emission scenario, overlayed with the boundary marking the WHO 5 μgm^{-3} guideline (red line). Annotations show (area of UK exceeding guideline (%), population of UK exceeding guideline(%)).

With no emission changes, the model estimates 79% of the UK area and 95% of the population lived in locations exceeding the WHO guideline of 5 μgm^{-3} for annual mean $PM_{2.5}$.

Removal of anthropogenic emissions from the UK and EU reduced the area of the UK above 5 μgm^{-3} from 79% to 35% (UK emissions) and 52% (EU emissions). The fraction of the population living in areas exceeding the limit also reduced from 95% to 69% (UK emissions) and 84% (EU emissions). The combined impact of removal of both UK and EU emissions leads to all areas being compliant.

Removal of agricultural emissions (predominantly ammonia) had a smaller but substantial impact on limit exceedance reducing the area out of compliance to 52% for UK emissions and 62% for EU. However, the impact on population exposure is small with the removal of agricultural emissions. Switching off UK agricultural emissions reduces the fraction of the population out of compliance from 95% to 85%. An equivalent reduction in European Agricultural emissions only changes the fraction from 95% to 91%.

Although several previous studies stressed the large role of agricultural NH_3 emissions in particulate matter pollution (e.g McDuffie et al. (2021); Wyer et al. (2022); Gu et al. (2021), they have typically compared against individual anthropogenic sectors (transport, energy generation, industry, shipping). This work has instead grouped the anthropogenic emissions sectors together, which is likely why the agricultural impact was smaller.

Biogenic emission changes led to almost not changes in the concentrations with both area and population weighting, indicating a low sensitivity of UK SOA and $PM_{2.5}$ to biogenic emissions in the model.

The removal of shipping emissions lead the area out of compliance to reduce from 79% to 62% but the fraction of the population out of compliance changed much less, going from 95% to 90%. This is consistent with the 4.6% contribution of shipping emission on PM$_{2.5}$-associated mortalities in Europe reported by Gu et al. (2023).

Unlike the case for O$_3$, reducing emissions from anthropogenic, agriculture or shipping emissions only leads to improved air quality. Further, the background air flowing into the UK is compliant with the PM$_{2.5}$ standard. However, reaching the 5 μgm^{-3} standard will still be difficult for the UK. Removing all anthropogenic emissions from the UK substantially improves the outcome, reducing the fraction of people exceeding the standard from 95% to 69%. But this still results in more than 50% of the population being exposed to unhealthy air. Even removing UK anthropogenic and agricultural emissions leads to 27% of the population being exposed to unhealthy concentrations due to transport from Europe and Shipping sources. In order for the UK to reach compliance these model studies suggest that there would need to be an equivalent effort to reduce pollution from the EU as there is from the UK.

4.5   Emission Change Linearity

The response of pollutants such as O$_3$ and PM$_{2.5}$ to emission changes is not always linear due to the non-linearity of chemical and physical processes (Sillman et al., 1990; Clappier et al., 2021). This can present challenges when trying to infer the combined effects of sensitivity scenarios. For example, is the impact of changing anthropogenic emissions and agricultural emissions together the linear sum of changing the anthropogenic emissions and the agricultural emissions separately?

Figures 68 and 69 explore this linearity. The methodology follows that of Thu-

nis et al. (2021) who analysed the non-linearities of $PM_{2.5}$ concentrations in response to 25% reductions of NO_x and NH_3 emissions in the Po Basin, Italy. In this sense, a "linear" response would suggest that the change in concentration in a simulation that removed two components would be the same as the sum of the changes in concentration that changed those two components individually.
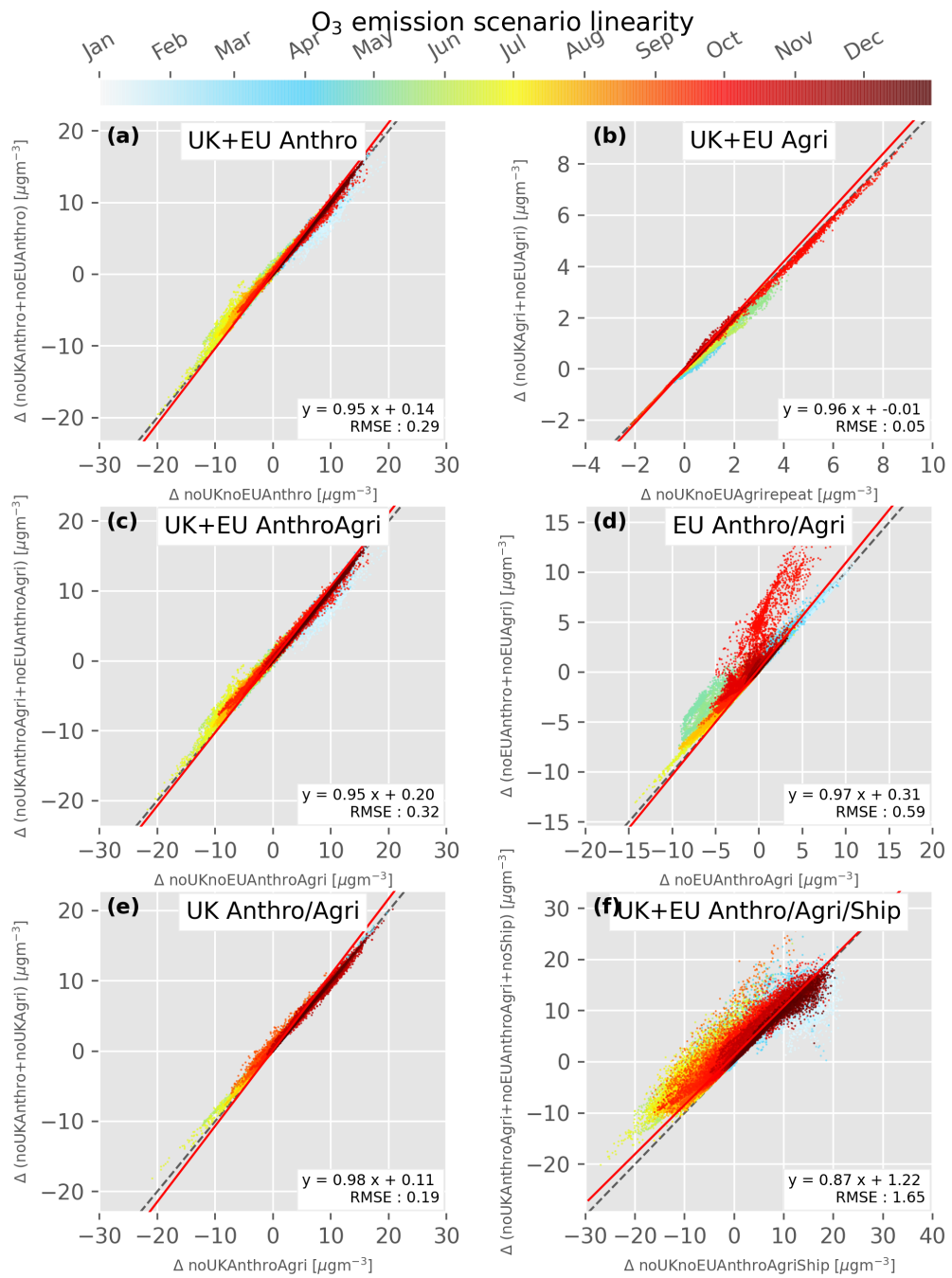
Figure 68: Linearity of O_3 changes. Points show the changes in daily mean species concentration compared to the baseline UK model grid boxes for a scenario implementing two or more emission reductions simultaneously (x-axis) or as the sum of the changes from the individual reduction scenarios (y-axis), coloured by time of the year. The points were fit by orthogonal distance regression (red line). The dashed line indicates a "1:1" perfectly linear relationship.

Ozone changes over the UK were very close to linear for each combination of UK and EU emissions from anthropogenic, agricultural and shipping sources. For most of the combinations the RMSE was less than 1 μgm^{-3} which is small compared to the magnitude of the variations seen. This suggests that despite O$_3$ chemistry being non-linear, over the range of concentrations usually explored, a linear assumption is reasonable. Two of the combinations showed larger RMSEs - EU Agriculture and Anthropogenics (RMSE of 0.59 μgm^{-3}), and the combined impact of all emissions (RMSE of 1.65 μgm^{-3}). In October, the EU Anthro and Agri simulation led to higher O$_3$ concentration than what you would expect from the sum of the two simulations (Figure 68d). It is unclear why this may be the case but likely reflects under certain conditions the non-linearity in the balance between sulfate, nitrate and ammonia as represented by the model's ISORROPIA module (Fountoukis and Nenes, 2007). Additional changes for shipping (Figure 68f) appear to create a substantial reduction in the linearity of the model. This may be due to non-linear responses from the model's use of the PARANOx module's handling of shipping NO$_x$ and O$_3$ emissions (Vinken et al., 2011; Holmes et al., 2014) which included non-linear functions in its emissions. Further work should be done to explore the suitability of PARANOx for these kinds of analyses.

Unlike O$_3$, the impact of emissions changes on PM$_{2.5}$ showed much less linear dependence (Figure 69). There are two features of note here. Firstly lines which do not fit on the 1:1 line, and secondly noise around the lines that are formed.
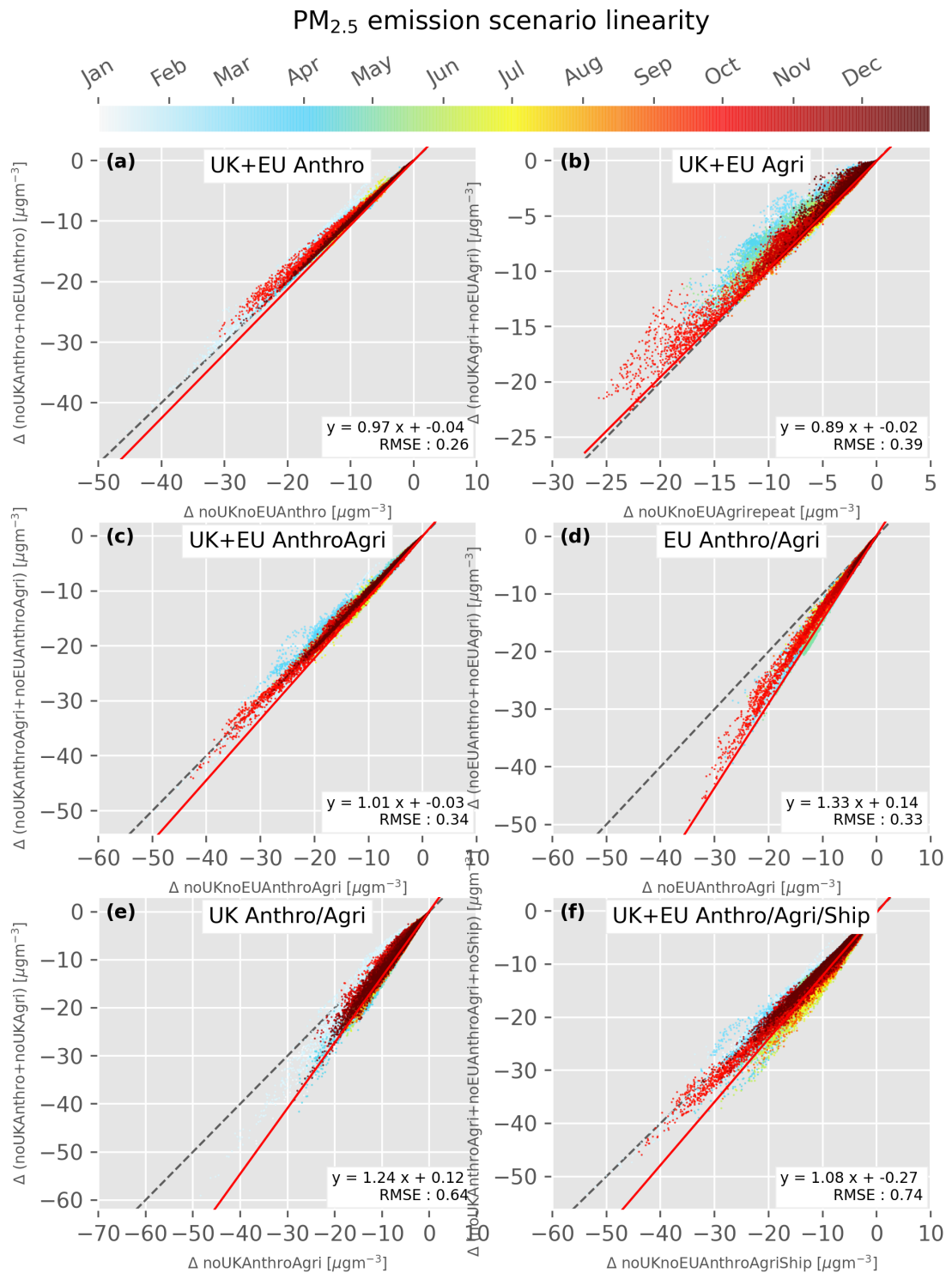
Figure 69: Linearity of PM$_{2.5}$ changes. Points show the changes in daily mean species concentration compared to the baseline UK model grid boxes for a scenario implementing two or more emission reductions simultaneously (x-axis) or as the sum of the changes from the individual reduction scenarios (y-axis), coloured by time of the year. The points were fit by orthogonal distance regression (red line). The dashed line indicates a "1:1" perfectly linear relationship.

Concurrent agricultural emission reductions from both regions showed greater UK concentration reductions than they did independently (Figure 69b), suggesting there is some enhancement of UK ammonium aerosol formation (($NH_4)_2SO_4$ and NH_4NO_3) concentrations by European NH_3 sources. This is consistent with findings from Jonson et al. (2022), which showed larger NH_3 emission reductions led to increasing efficiency to curb PM$_{2.5}$ levels when SO_x and NO_x emissions were much higher than NH_3. The opposite response occurred when anthropogenic and agricultural emissions reduced in the same region (Figure 69d,e for the EU and UK), producing 24-33% smaller PM$_{2.5}$ reductions than expected if the response were linear. As ammonium nitrate tends to be the major component of European inorganic aerosols, and there is evidence to suggest ammonia is the predominant limiting factor (e.g Vieno et al. (2015); Jones et al. (2021)), it follows that a lack of available ammonia for nitrate uptake limits the formation of inorganic aerosols and leaves only natural sources of NH_3 (e.g plant decomposition, emission from soils and oceans). This limiting factor would not be reflected in the independent simulations, leading to overestimates if they were summed to extrapolate results. Alternatively, it can be considered as the simultaneous effect of reductions of both NO_3^- and NH_4^+ in response to reductions in NO_x and NH_3, which would be smaller if only one precursor was removed.

Separating changes due to anthropogenic emissions or anthropogenic and agricultural emissions between the UK and EU did show a strong linear response (Figure 69a,c), supporting the independence of the model responses from these sources i.e PM$_{2.5}$ changes from removing anthropogenic and agricultural emissions from the EU do not affect the same changes from removing UK anthropogenic and agricultural emissions. However, removing shipping emissions alongside UK and EU Anthropogenic and Agricultural emissions (Figure 69f) moved the response further from linear as summertime decreases become smaller in the combined scenario than the individual scenario. This non-linearity may be a response due to the in-plume production of HNO_3-a precursor of aerosol nitrate-

from shipping NO_x emissions in the model PARANOx module.

These results show that the response of UK O_3 concentrations to UK and EU emission changes is mostly linear, with an exception in the summer for shipping emissions. This provides further reason to evaluate the sensitivity to shipping emission changes around the UK, as well as the handling of PARANOx emissions of O_3 and NO_x in non-remote ocean regions at high resolution. In contrast, for $PM_{2.5}$ the response strays from linearity due to the balance between availability of NH_3, NO_x and SO_x. The linearity comparisons provide further evidence about how European sources affect UK O_3 and $PM_{2.5}$: European contributions primarily affect global background O_3 levels which consequently impact the UK, and for both O_3 and $PM_{2.5}$ and $PM_{2.5}$ there is a contribution from From the context of sensitivity studies this emphasises the need for additional modelling studies to be performed, rather than the results of independent simulations being combined, particularly for simulations with particulate matter.

4.6   Conclusions

This chapter has assessed the sensitivity of O_3 and $PM_{2.5}$ concentrations in the UK to complete removal of emissions from anthropogenic, agricultural, biogenic and international shipping emissions from the UK and the EU. Although emission reductions of this magnitude are unlikely to occur, they can inform the modelling community and policy makers of an "upper bound" of the possible changes that could be achieved by reducing emissions from these regions and sources.

Anthropogenic emissions from the UK had the largest effect on O_3 concentration of any source region-sector scenario implemented here. Their removal increased concentrations by an average of 1.4 ppbv over the UK, with larger increases over cities. A smaller increase of 0.4 ppbv followed the removal of shipping emissions within the model domain. On the other hand, European an-

thropogenic emission reductions led to 0.9 ppbv decreases over the UK. The O$_3$ changes due to anthropogenic emission reductions were driven by decreases in NO$_x$ emissions which resulted in local wintertime O$_3$ from reduced NO$_x$ titration, and summertime decreases due to reductions in photochemically produced O$_3$. The response due to shipping emissions removal shared the same seasonality due to changes in the direct emissions of O$_3$ from shipping in high or low NO$_x$ conditions. European emission changes impacted the UK through the north hemisphere background. The seasonal variability of the O$_3$ response to emission changes highlights the importance of carefully choosing an exposure/pollution metric or considering multiple metrics (such as annual mean and peak season concentration), to obtain a comprehensive understanding of the results. Failure to do so can lead to a simplification of a complex system (e.g noUKnoEUAnthro in Figure 47). The model results suggest that changes to biogenic or agricultural emissions from either the UK or the EU would have a <0.5 ppbv impact on UK O$_3$ concentrations. The impact of the regional emission changes implemented was generally small in comparison to the boundary condition contribution. Although nested grid simulations without boundary conditions were not possible to implement with this model configuration, the effect of emission changes further afield on the long-range transport contribution could be further evaluated as in similar sensitivity work by Fu et al. (2012) for East Asia.

Without any emission changes, this work found 22% of the population of the UK to be living in areas exceeding the WHO 60μgm^{-3} guideline for O$_3$. Removing just UK anthropogenic and agricultural emissions or international shipping, this fraction increased to 65% for UK anthropogenic emissions, and 25% for UK agriculture and international shipping. This should be a cause for concern given the existing trend of NO$_x$ emission reductions in the UK. European anthropogenic emissions removal reduced UK exceedance due to the global background reduction, whereas European agricultural emissions produced a small increase. Biogenic emission reductions lowered exposure exceedance fractions to 18% and

13% for the UK and EU biogenics, respectively. The noUKnoEUAnthroAgriShip scenario was the only case where no exceedances of the WHO guideline for O$_3$. This highlights the difficulty of achieving the WHO guideline for O$_3$ in the UK without substantial emission reductions, notably in regions outside of the UK.

Surface PM$_{2.5}$ in the UK showed a much higher sensitivity to reductions from UK or European emissions sources than for O$_3$. The model response to EU emission removal mostly affected SE England and quickly decreased moving northwest as the amount of transported inorganic aerosol dropped. Decreases from removing anthropogenic (27%) or agricultural (15%) UK emissions resembled the spatial distribution of the precursor emissions. Central England saw the largest decreases of 5.0 μgm^{-3} (45%) and 2.9 μgm^{-3} (25 %), respectively. Biogenic emission removal from the UK or EU resulted in PM$_{2.5}$ decreases of up to 1% due to SOA decreases, indicating only a minor contribution of biogenic sources on UK PM$_{2.5}$.

Without changes to the emissions, 95% of the UK population were estimated to live in areas exceeding the WHO annual mean guideline for PM$_{2.5}$ of 5μgm^{-3}. Biogenic emissions had a negligible effect on PM$_{2.5}$ and the population exposed above this guideline. Although anthropogenic emission reductions from the UK or EU separately reduced average concentration substantially, the fraction of the population exceeding was still above 50%. Emissions scenarios involving the removal of UK and EU anthropogenic emissions (noUKnoEUAnthro, noUKnoEUAnthroAgri, noUKnoEUAnthroAgriShip) resulted in none of the UK population residing above the WHO 5 μgm^{-3} guideline.

The model O$_3$ response to emission changes was highly linear for a range of combinations of UK and EU anthropogenic and agricultural emission reductions. This indicates that the results from different scenarios can be added together and still make a reasonable approximation of the result from modelling both hypotheti-

cal cases simultaneously. For modellers, this reduces the computational cost and time of additional simulations, and for policy makers this provides a faster route to potentially relevant information. On the other hand, PM$_{2.5}$ responses showed less linearity, likely because of the sensitivity of inorganic aerosol levels to the variable ratio of NH$_3$ to NO$_x$ and SO$_x$ following emission reductions. The deviation from linearity was largest for agricultural emission changes because of the large NH$_3$ component. As a result, it's recommended to conduct additional sensitivity simulations when making further changes to model emissions.

Although NO$_2$ is also a pollutant of concern in the UK, these experiments did not investigate its sensitivity to emission reductions, crucially because of the large model underestimate identified in the previous chapter. The WHO target value for NO$_2$ is an annual mean of 10 μgm^{-3}, which the model simulated was exceeded in large English cities (Figure 109). However, the model underestimated concentrations to be substantially below the UK's legislative limit value for NO$_2$ is 40 μgm^{-3}, which was exceeded in 37 of 43 monitoring zones in 2017 (DEFRA, 2018). One proposed cause for the underestimate was the model horizontal resolution (Chapter 3). An alternative version of the GEOS-Chem CTM, GEOS-Chem High Performance (GCHP) has the capability to model at higher resolutions. The next chapter will evaluate the potential improvements of increasing the model horizontal resolution.

5 The Effect of Horizontal Resolution on Model Performance for NO$_x$, O$_3$ and PM$_{2.5}$

5.1 Introduction

Coarse model horizontal resolutions relative to spatial emissions variability can affect model bias through the dilution of species concentrations over model grid boxes. This effect for short-lived species such as NO$_x$ was discussed in Section 3.4.3. This chapter will build upon that discussion by exploring the resolution sensitivity of NO, NO$_2$, O$_3$ and PM$_{2.5}$ with GEOS-Chem simulations over the UK in Summer 2021, assessing how model performance varies with increased resolution.

5.1.1 Previous Work

Previous studies have investigated the impact of model horizontal resolution on air pollutant concentrations, usually focusing on densely populated areas to better understand the impact on human health. Improved understanding of resolution dependencies in these areas can facilitate model improvement and improve confidence in model estimates.

Schaap et al. (2015) evaluated the performance of several regional CTMs for NO$_2$, O$_3$ and PM$_{10}$ over 30 urban areas in Europe, comparing four resolutions between 56 and 14 km. They found the impact of horizontal resolution to be significant in regions with high emission rates such as urban areas, resulting in intensified urban signals with decreased model grid size. This effect was more pronounced for NO$_2$ than PM$_{10}$, as PM$_{10}$ mass consisted of secondary components unaffected by resolution. O$_3$ was shown to be less sensitive to resolution changes than NO$_2$ and PM$_{10}$, but was affected by spatial mixing which varied with grid resolution. Despite the lower sensitivity of O$_3$, increased model resolution re-

duced model bias in urban regions for O$_3$, NO$_2$ and PM$_{10}$. Spatial correlations improved for NO$_2$ but became worse for O$_3$ and PM$_{10}$.

Fenech et al. (2018) looked at the seasonal effects of two different model resolutions on the HadGEM3–UKCA chemistry–climate model (140 and 50 km resolution) on O$_3$ and PM$_{2.5}$ over Europe. At the coarser resolution, simulated O$_3$ concentrations were higher on average in the Winter (10%) and Spring (6%), and lower in the Summer (1%) and Autumn (4%). This seasonal resolution-sensitivity was attributed to NO$_2$ concentrations, which at fine resolution were higher in the the winter and spring and lower in the summer and autumn. The inverse trend was identified for PM$_{2.5}$. Compared to the fine resolution model, concentrations in the coarse resolution were lower in the Winter (8%) and Spring (6%), and higher in the summer and autumn (29%) and (8%). They attributed these differences to a combination of differences in the planetary boundary layer height (PBL) and wet deposition loss via simulated precipitation between the two resolutions.

Schwantes et al. (2022) explored the effect of horizontal resolution and updates to isoprene and terpene chemistry on O$_3$ and its precursors over the contiguous US (CONUS), comparing against measurements from flight campaigns in 2013. O$_3$ precursors showed a higher sensitivity to model resolution, and updates to chemistry were more pronounced at higher resolutions, indicating the combined importance of balancing resolution increases with improvement of model physical and chemical processes. Despite resolution reducing ozone biases, inaccuracies in modelled meteorological processes like temperature, water vapour and PBLH also had an impact on ozone bias.

Tie et al. (2010) evaluated WRF-Chem estimates for CO, NO$_x$ and O$_3$ in Mexico City at 3, 6, 12 and 24 km. Finer resolutions could reasonably simulate species diurnals, but coarser simulations underestimated concentrations. Alongside the spatial distribution of emissions, calculated meteorology and ozone production

were affected by horizontal resolutions. They proposed 12 km resolution as the threshold for reasonably simulating O$_3$ and its precursors in urban environments.

Recently, Zhang et al. (2023) reported differences in the source sector contributions and population exposure of NO$_2$ and PM$_{2.5}$ over the Global South from 1-year GEOS-Chem High Performance (GCHP, see Section 5.2) simulations at C360 (25 km) and C48 (200 km). Higher resolutions showed more pronounced spatial heterogeneity, particularly for NO$_2$ and primary components of PM$_{2.5}$. The relative contribution of open fires to Urban pollution exposure decreased at high resolution, whilst contributions from anthropogenic sectors were enhanced. NO$_2$ enhancements were particularly large due to its high spatial heterogeneity at fine resolutions. For PM$_{2.5}$, the relative importance of specific anthropogenic sectors for primary components such as BC more closely followed the spatial distribution of emission sources.For example, industrial contributions increased relative to power plants due the the higher population collocation extent of industrial factories. They estimated that the spatial heterogeneity of PM$_{2.5}$ in the Global South was 1.3 times greater than the global average.

High emissions regions such as urban areas have been found to show greater resolution sensitivity than low emission regions. This particularly impacts primary species such as NO$_x$, and related species like O$_3$, but has less of an impact on particulate matter. Increasing model resolution tends to improve performance in urban environments up to a point, where either model bias from other sources e.g chemical complexity, accuracy of meteorology have a greater effect, or the increased computational demands cannot be justified. However, reported thresholds vary between models and species of interest, and one has not been reported for the UK or with GEOS-Chem chemistry. The resolution sensitivity of particulate matter can vary based on the balance between different source sectors (Zhang et al., 2023), but currently has not been investigated for the UK.

This chapter will explore the effect of resolution on the ability of GCHP to simulate surface concentrations of NO, NO$_2$, O$_3$ and PM$_{2.5}$ over the UK between 1st June and 31st July 2021. Models will share the same emissions, chemistry and meteorology but vary the horizontal resolution from 200 km (C48) to 14 km (C120S6) using the GCHP stretched grid functionality. Much of the previous literature has focused on the resolution effect in urban areas, this work will make comparisons with DEFRA AURN network measurements for both urban ("Non-Rural") and rural environments. The impact of horizontal resolution on biases for these species in the UK will be explored, using available high resolution (1×1 km) NAEI emissions to propose the threshold where emissions resolution becomes a minor factor. Finally, an approach to identify suitable GCHP resolutions for simulating UK air quality will be suggested, taking into account the resource costs of high resolution stretched grid simulations.

5.2 GEOS-Chem High Performance

GEOS-Chem High Performance (GCHP), first described by Eastham et al. (2018) is a grid-independent implementation of GEOS-Chem designed to distribute computation over massively parallel architectures. Message Passing Interface (MPI) paralellisation enables global high resolution simulations which were previously prohibited due to memory and time constraints on a single node. GCHP incorporates a cubed-sphere grid discretization (see Figure 70) used by GEOS data assimilation system (DAS) as opposed to a rectilinear latitude-longitude grid. It also uses the Finite-Volume Cubed-Sphere Dynamical Core (FV3) advection algorithm as it has been optimised for higher scalability and efficiency (Putman and Lin, 2007). The local term in the continuity equation (which describes the local net production and loss of a species) is handled by code identical to that of GEOS-Chem Classic, such that only the advection processes differ from the GEOS-Chem Classic processes. The atmosphere is divided into independent atmospheric columns, with subsets of these being assigned to individual compu-

tational cores and with advection between boundaries handled by communication with the MPI, Open-MPI (https://www.open-mpi.org/; last access 05/07/2023).

5.2.1   The GCHP Model Grid

The process for creating a cubed-sphere grid is shown in Figure 70. The cubed sphere grid discretization splits the surface of a sphere into six equal faces, which are subdivided into approximately equal sized cells representing atmospheric columns. Each face is divided at the edges into N equal segments, connected to generate a regular mesh. The N parameter is used to describe the resolution of the cubed-sphere grid in the format CN e.g C48, with higher values of N indicating finer grid discretization and resulting model resolution. Global resolution can be approximated as 10,000/N km, such that C48 is roughly 200 km horizontal resolution.
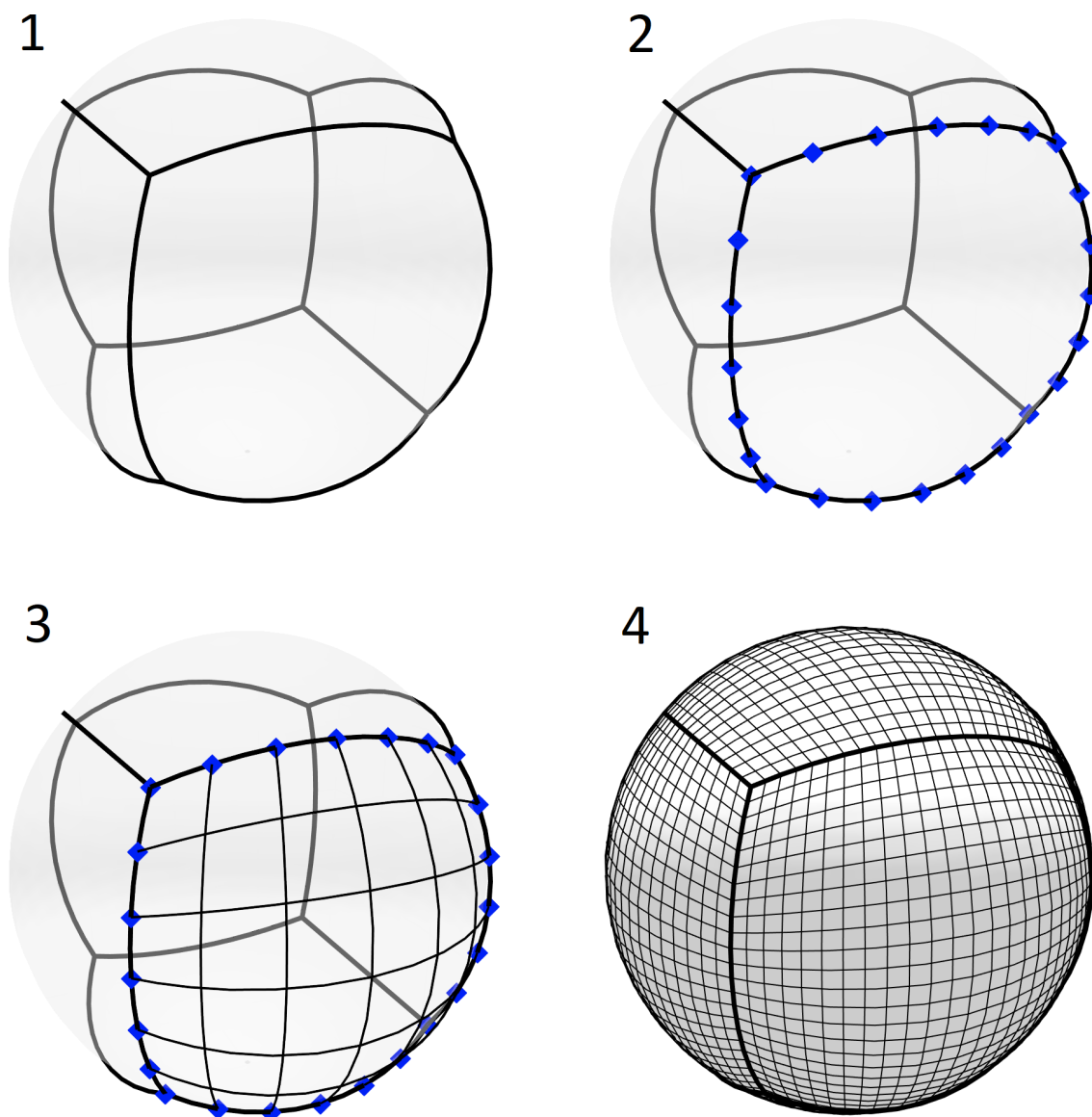
Figure 70: Illustration of the processes used to generate a gnomic cubed-sphere grid. Grids 1-3 are C6, and grid 4 is C24. Reproduced from Eastham et al. (2018). Demonstration available interactively at `https://geos-chem.seas.harvard.edu/cubespherestep-step` (last access: 05/07/2023).

5.2.2   Stretched Grid Simulations

Stretched-grid simulations (Bindle et al., 2021b) allow resolution enhancement over a user-defined region. The stretched grid simulations shrink a "target face" (the cubed sphere face covering the area of user interest) by a stretch-factor (see Figure 71). Stretched grids are described in the format C*N*S*M*, where C48S6 would refer to a C48 cubed-sphere grid with a stretch factor of 6. One benefit of this approach versus nested grids like those used in the GCClassic simulations in Chapters 3 and 4 is that it removes the need for lateral boundary conditions, al-

lowing regional feedbacks from within the refined domain (see Figure 71, center).
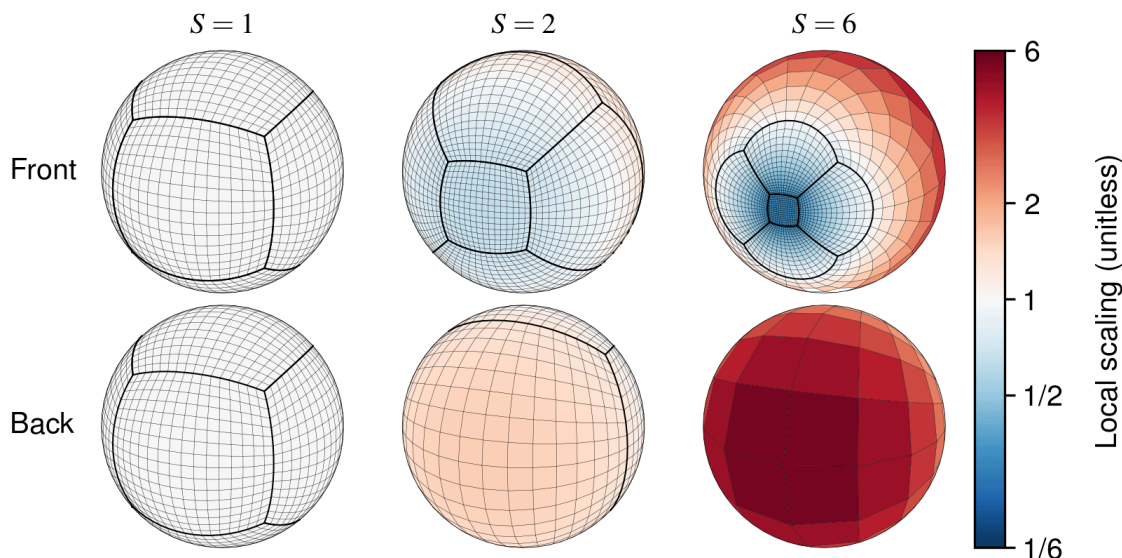
Figure 71: Three stretched grids that illustrate the effect of the stretch factor *S* on stretching and local scaling on a C16 cubed sphere Reproduced from Bindle et al. (2021b). Demonstration available interactively at `https://geos-chem.seas.harvard.edu/cubespherestep-step` (last access: 26/06/2021)

The procedure for grid-stretching uses the methodology of Harris et al. (2016), which is a simplified form of the Schmidt (1977) transform for gnomic cubed-sphere grids. The primary face of the grid is at the South Pole, and grid coordinates are attracted towards the South Pole along meridians according to the stretch factor, before re-centering the refinement about a set of user-defined target coordinates. Stretching results in a grid which approximately has a resolution at the centre of the target face *S* times finer than the unstretched grid, and at the antipode, *S* times coarser. The smallest of the gridboxes of the target face are closest to the edges. For specific grid boxes, the change in size from stretching is referred to as the "local scaling". As derived by Bindle et al. (2021a), the local scaling as a function of arclength from a target position, *y*, to the South Pole, $\ominus$, with stretch factor, *S*, is given by Equation 9:

$$L(\ominus; S) = \frac{1 + cos\ominus + S^2(1 - cos\ominus)}{2S} \qquad (9)$$

Within the target face, local scaling is nearly constant and approximately 1/S, but in the remaining 5 cubed-sphere faces, will vary as a function of distance from the target point. An illustrative grid-stretching example from Bindle et al. (2021b) is shown in Figure 71.

5.2.3   Previous work using GCHP

Currently, only a small number of studies have used the GCHP stretched grid functionality (Martin et al., 2022; Nowlan et al., 2023; Chatterjee et al., 2023), and only one has used it to investigate resolution sensitivity. Li et al. (2023a) investigated the factors contributing to NO$_x$ resolution effects over the Great Lakes (GL) and Southern States (SS) of the eastern United States using GCHP stretched grid simulations between 13 and 181 km resolution. The strong localisation of NO$_x$ emissions near their sources at high resolutions decreased NO$_x$ lifetime in NO$_x$-limited regimes and increased it in NO$_x$-saturated regimes respectively. This resulted in coarser resolutions having NO$_x$ mixing ratios which were 16% lower in the NO$_x$-saturated GL region and 7% higher in the NO$_x$-limited SS. They also made comparisons with satellite NO$_2$ column density, finding negative summertime biases over the GL and positive biases over the SS in July due to HO$_x$ enhancements intruding into the upper troposphere.

5.3   Experiment Setup

5.3.1   GCHP simulations in this Chapter

This work used v13.4.0 of GCHP (GCHP13.4.0, 2022). Initial spin up for GCHP simulations used a C48 simulation with the same emissions configuration, run from 1st May 2020 to 1st June 2021. Then, initial conditions for each GCHP simulation were obtained by regridding at a C48 model restart to the stretched grid

resolutions, and simulating globally from 20th May 2021 to 1st August 2021, discarding the first 11 days as model spin-up.

Table 12 shows the simulations performed in this Chapter, their resolutions, chemistry and transport operator timesteps, and the average number of simulated days per real-world day (model throughput). The finest resolution simulation (C120S6 results in a regridding of the 0.25°×0.3125° GEOS-FP meteorology to a finer resolution than the native resolution. Without increasing resource needs, an increased cubed sphere *N* leads to larger computational demands and slower model runs. Stretched grid simulations bring an additional resource burden further slowing them down (scaling as approximately N^2. However, there is little-to-no difference in the runtime for stretched grid models with the same value of *N* (e.g C80S6 versus C80S3), because although the target face resolution has increased, the total number of gridboxes remains the same and the computational burden of applying a stretch is similar. Figure 72 and 73 compares several model resolutions globally and over the UK.

Table 12: Approximate resolution (in square kilometres), length of chemistry and transport timestep (in minutes), and model throughput (in days per day, to the nearest day) of the GCHP simulations compared in this chapter.   All simulations used the same amount of resources (72 cores split equally across 3 nodes).   Node hardware description available at `https://www.york.ac.uk/it-services/services/viking-computing-cluster/`; last access 13/09/2023.

Model	Resolution [km^2]	Chemistry/Transport [mins]	Throughput [days day^{-1}]
C48	200	20 / 10	65
C80S1.5	83	20 / 10	25
C60S2	83	20 / 10	41
C48S3	69	20 / 10	39
C48S4	52	10 / 5	39
C80S3	42	10 / 5	16
C60S4	42	10 / 5	27
C48S5	42	10 / 5	39
C48S6	34	10 / 5	39
C80S6	21	10 / 5	16
C100S5	21	10 / 5	10
C120S6	14	10 / 5	7
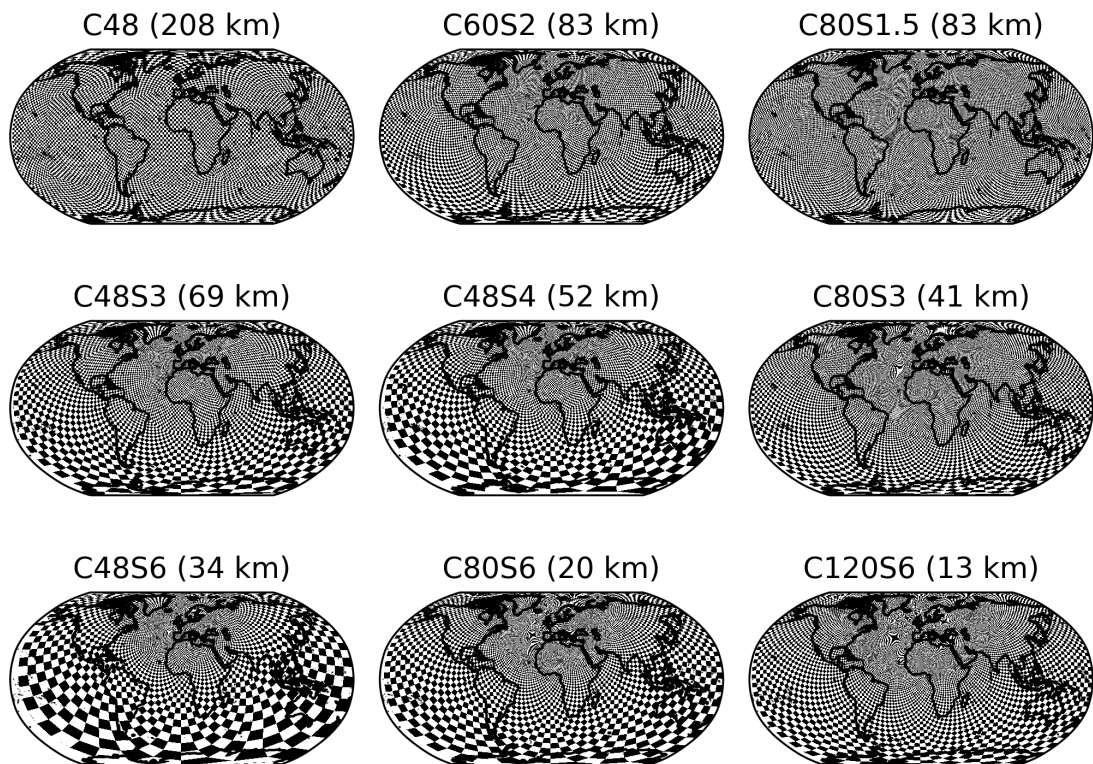
Figure 72: Global comparison of model resolutions for C48, C60S2, C80S1.5, C48S3, C48S4, C80S3, C48S6, C80S6 and C120S6. Alternating gridboxes are coloured white and black to highlight gridbox sizes.
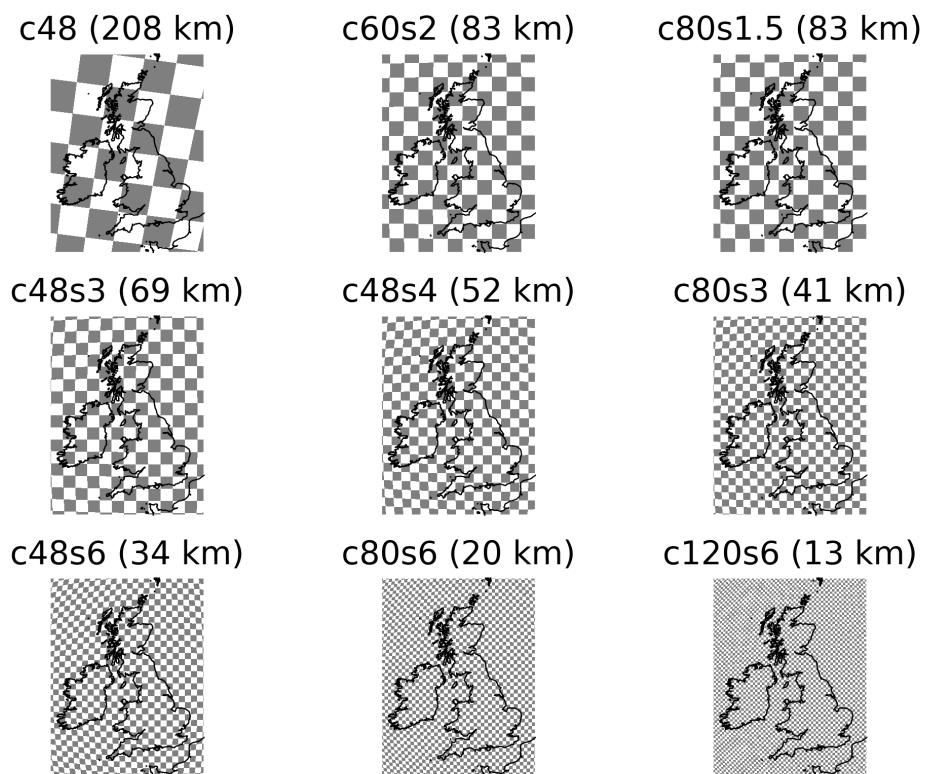
Figure 73: Comparison of model resolutions centred over the UK for the same stretched grid configurations shown in Figure 72. Alternating gridboxes are coloured white and black to highlight gridbox sizes.

5.3.2   Emissions

We replace the default model CEDS anthropogenic emissions land-based over the UK with emissions from the UK National Atmospheric Emissions Inventory (NAEI) for 2017. Over the rest of Europe (30W-90E 30N-82N) the EMEP anthropogenic emissions for 2017 are used (as in Chapters 3 and 4). Whilst the anthropogenic emissions used are not for the same year as the model simulates, their spatial distribution should be comparable to the actual emissions. Using anthropogenic emissions at a finer horizontal resolution than the models assessed avoids the effect of artificial dilution when regridding to lower resolutions (e.g EMEP at 0.1°×0.1°), whilst also facilitating the separation of rural and urban sites which at low resolution might share emissions in the same grid cell. To illustrate this, Figure 74 shows a comparison of NO$_x$ emissions over the UK from three anthropogenic emissions inventories at different resolutions.
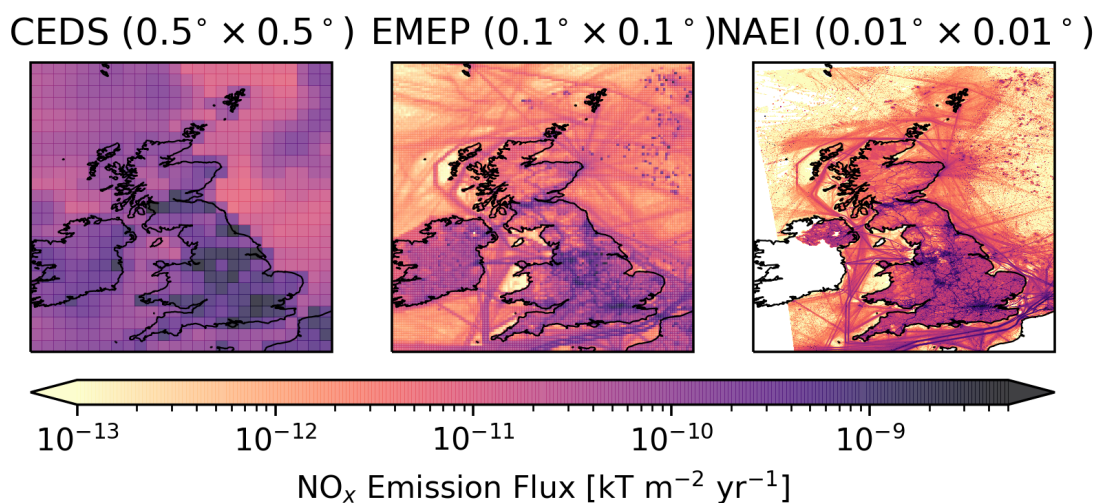
Figure 74: Comparison of 2017 anthropogenic NO$_x$ emissions from the CEDS (left panel) , EMEP (center panel) and NAEI (right panel) inventories. Note: CEDS anthropogenic emissions do not include shipping emissions here, and CEDS and EMEP emissions were conservatively regridded to 0.01°×0.01° for this comparison.

5.3.3   Observations

This work used observations for NO, NO$_2$, O$_3$ and PM$_{2.5}$ for 159 measurement sites from 01/06/2021 to 31/07/2021 from the DEFRA AURN monitoring network, and additional O$_3$ measurements from Mace Head. Monitoring site locations for each species are shown in 75. Measurements were obtained using the `openair` R package, and the measurement methods are as described in Table 6. As in Chapter 3, measurements from Urban Traffic sites were excluded as these environments cannot be accurately resolved by the model even at the highest resolution implemented in this work. NO and NO$_2$ measurement sites were included only if they also recorded measurements for O$_3$, so comparisons for these species were at the same locations Sites with less than 90% of the maximum number of total measurements over the two month period were excluded. This results in the exclusion of 9 of 60 measurement sites for NO, NO$_2$ and O$_3$ (as we only compare for sites which measure all three species) and 6 of 55 sites for PM$_{2.5}$. Observed concentrations were compared to modelled concentrations at the lowest model vertical level.
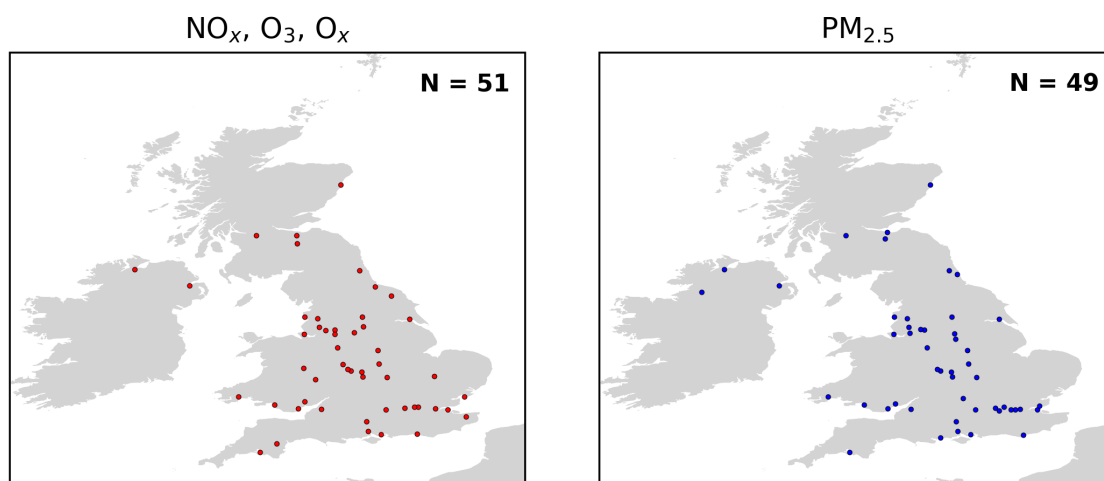
Figure 75: DEFRA AURN measurement site locations used in this work for NO, NO$_2$, O$_3$ and PM$_{2.5}$. The number of sites available for each species is given in the top-right.

We analyse model predictions using varying GCHP horizontal resolutions and compare them to AURN measurements of NO, NO$_2$, O$_3$, and PM$_{2.5}$. The compar-

isons are conducted at two timescales: daily averaged measurements and the average diurnal cycle. In addition, we differentiate the assessments based on site type, categorising them as either Rural and Non-Rural. Non-Rural sites include the Urban Industrial category from the AURN. The spatial coverage of measurement sites in these two categories limits this analysis. This aims to assess the potential enhancement of model performance through increased resolution. Comparisons of model-observation NMB and Pearson's *r* are shown in Figures 80, 81, 87 and 103.

5.4   The Resolution Sensitivity of UK NO$_x$

5.4.1   NO$_x$ changes with resolution at AURN sites

Figure 76 compares the mean diurnals from June 1st - July 31st at each model resolution and the observations for NO, NO$_2$ and NO$_x$. Increasing spatial resolution increased concentrations for NO, NO$_2$ and NO$_x$. Model response to changing resolution was consistent between Rural and Non-Rural environments. However, Non-Rural changes were larger due to larger NO$_x$ enhancements from higher emissions (more localised sources) at fine resolutions in these areas (Tie et al., 2010). Comparison of the input anthropogenic NO$_x$ emissions with modelled NO$_x$ at a coarse resolution (C48S5, 41 km) and fine resolution (C120S6, 13 km) in Figure 77 supported this.
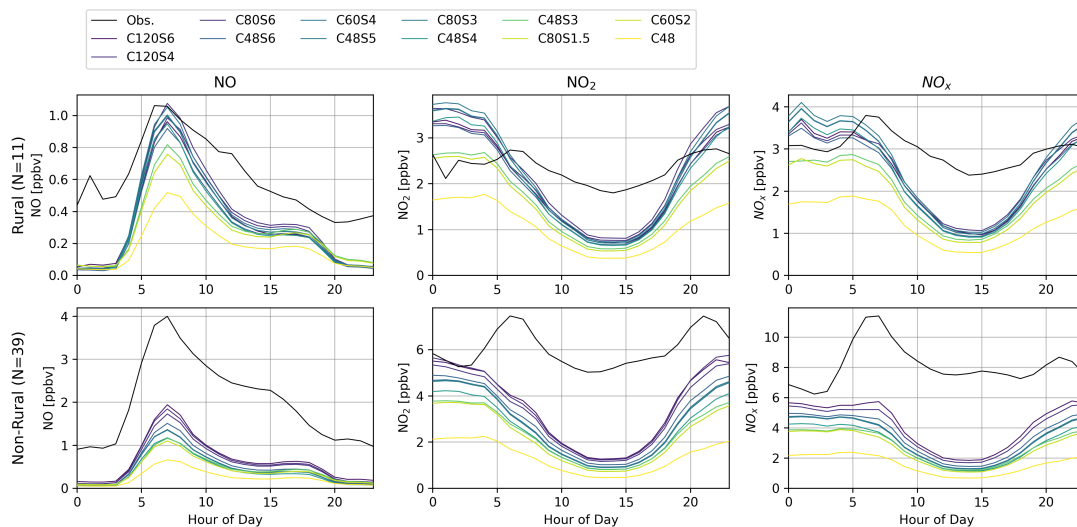
Figure 76: Mean surface observed (black) and modelled diurnal (coloured lines by resolution) of NO, NO_2 and NO_x at Rural (upper) and Non-Rural sites (lower), from 1st June 2021 to 31st July 2021, in ppbv.
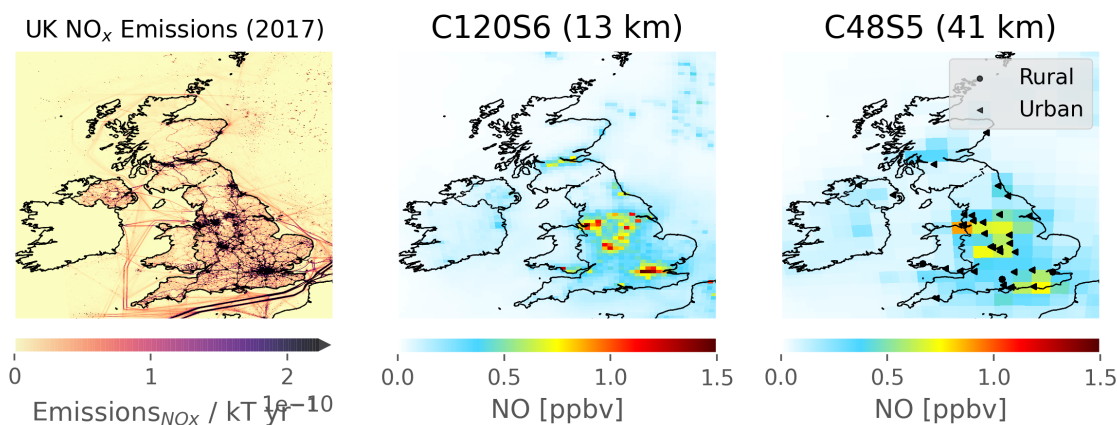
Figure 77: The annuak anthropogenic NO_x emissions for 2017 at 1 km^2 used as model input (left, source `https://naei.beis.gov.uk/data/`, last access 16/06/2023), and mean modelled surface NO concentrations from the C120S6 (centre) and C48S5 (right) simulations, in ppbv. NO measurement site locations are shown over the C48S5 panel for Rural sites (black circles) and Urban sites (black triangles).

In the higher resolution simulations, there were increases in the modelled NO morning maximum, and the NO$_2$ and NO$_x$ daytime minimum and nighttime maximum. Whilst responses appeared larger at night, relative differences showed them to be similar at all times of day. Despite improvements with resolution increases, in both Rural and Non-Rural environments the NO daytime maximum was still substantially underestimated, and the diurnal profiles were still poorly represented for NO$_2$ and NO$_x$. At Rural sites the C48S5, C60S4 and C80S3 simulations estimated higher NO$_x$ concentrations than at C120S6. This was identified to be due to higher modelled emissions at the Rural sites at these resolutions because of gridbox position. Further resolution increases may improve the model bias. However, the concentration-resolution trends suggest diminishing improvements will be achieved. Therefore, it is more likely that the model bias is due to sources other than resolution e.g underestimated NO emissions, supported by numerous previous studies (e.g Derwent et al. (2017); Vaughan et al. (2016); Karl et al. (2017)).

Modelled concentrations are compared with observations at the daily timescale for NO in Figure 78 and for NO$_2$ in Figure 79. As resolution increased, observed features in the daily means were better captured for both species. The model occasionally overestimated concentrations at Rural sites, and increased resolution made these overestimates worse. There was a more distinct and constant separation between modelled concentrations at Non-Rural sites.
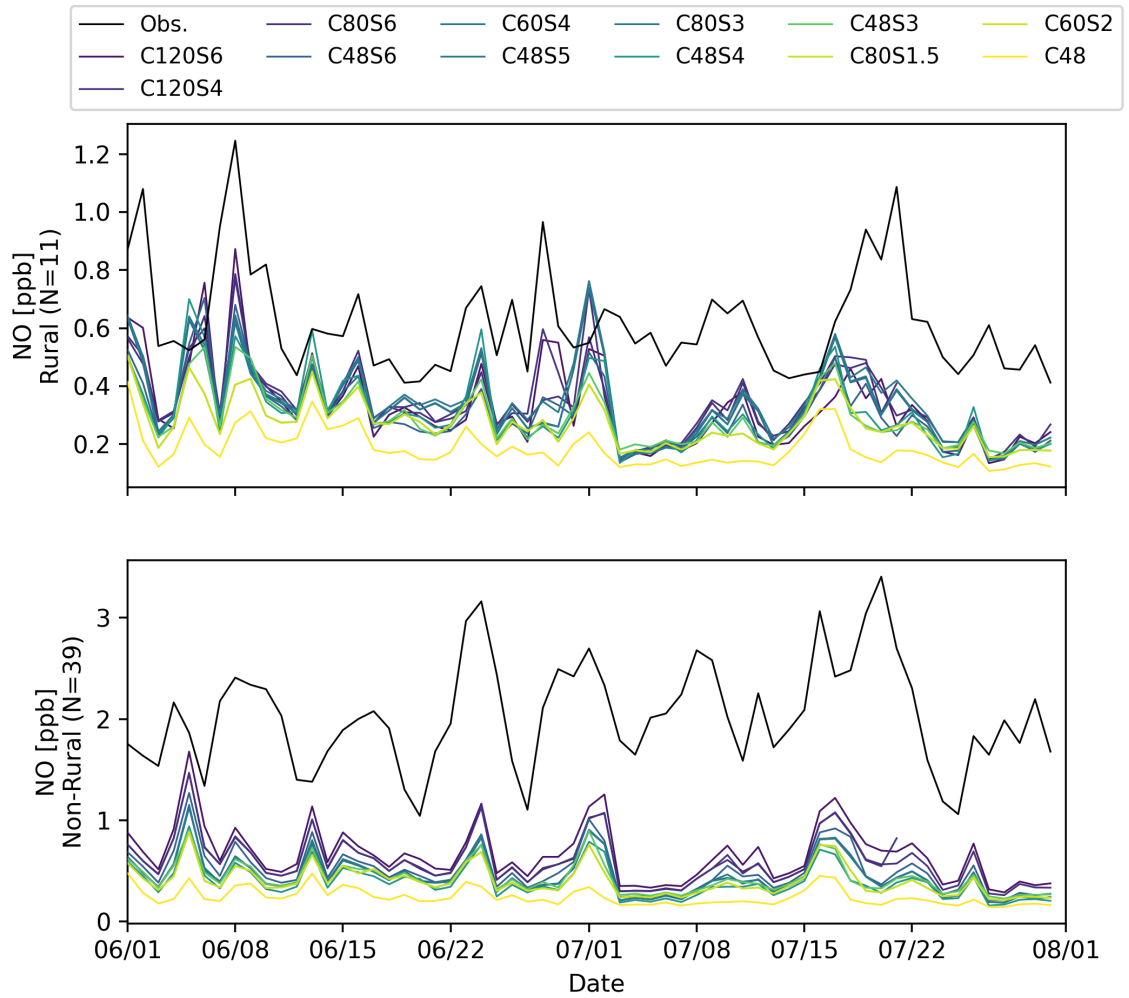
Figure 78: Daily average modelled (coloured lines) and observed (black line) NO concentration at Rural (top panel) and Non-Rural (bottom) sites, in ppbv.
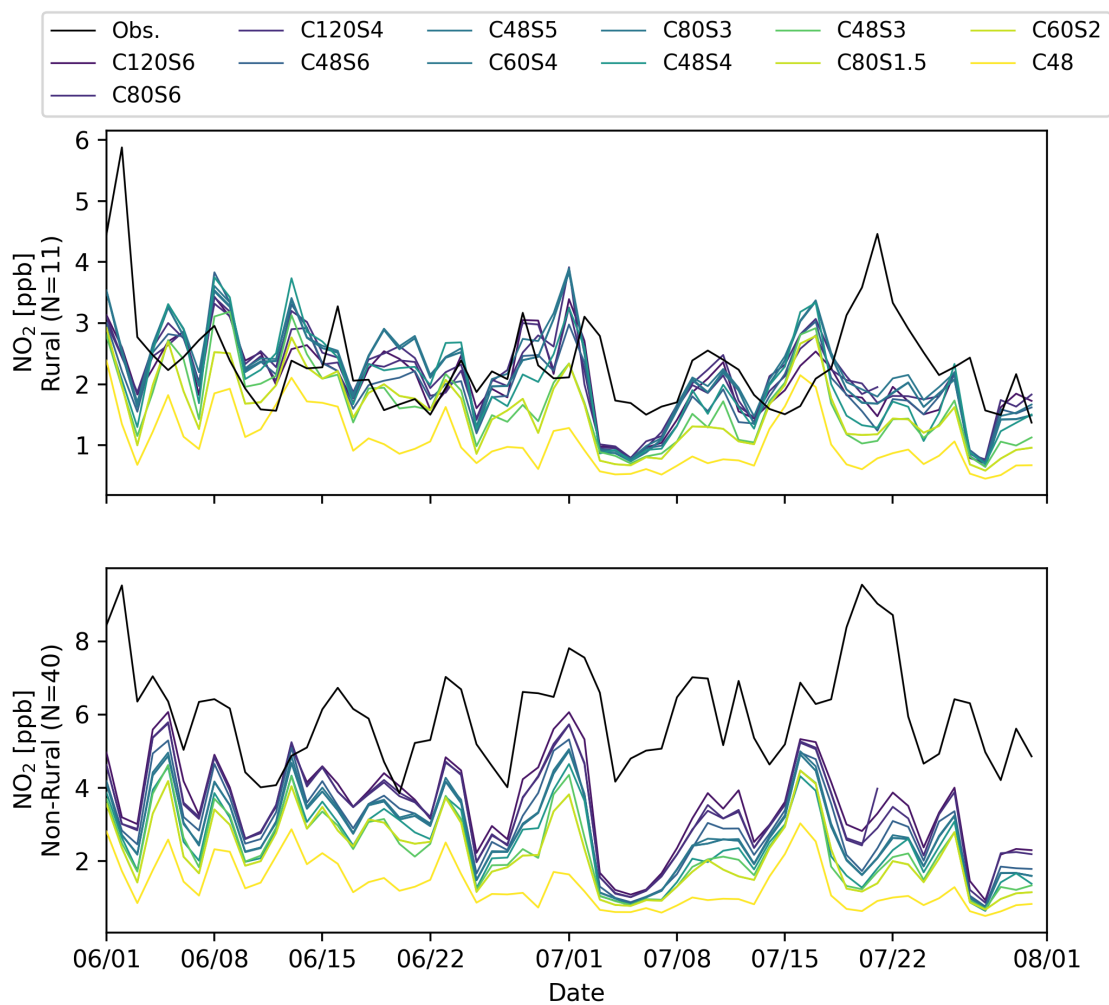
Figure 79: Daily average modelled (coloured lines) and observed (black line) NO$_2$ concentration at Rural (top panel) and Non-Rural (bottom) sites, in ppbv.

5.4.2   The Effect of Resolution on NMB and correlation for NO$_x$ at AURN Sites

We will now evaluate how model estimates for NO and NO$_2$ changed with resolution by assessing with Pearson's *r* correlation and NMB metrics at daily and hourly (diurnal) timescales. Model performance with these metrics is compared for NO in Figure 80 and for NO$_2$ in Figure 81, separating between Rural and Non-Rural site types.
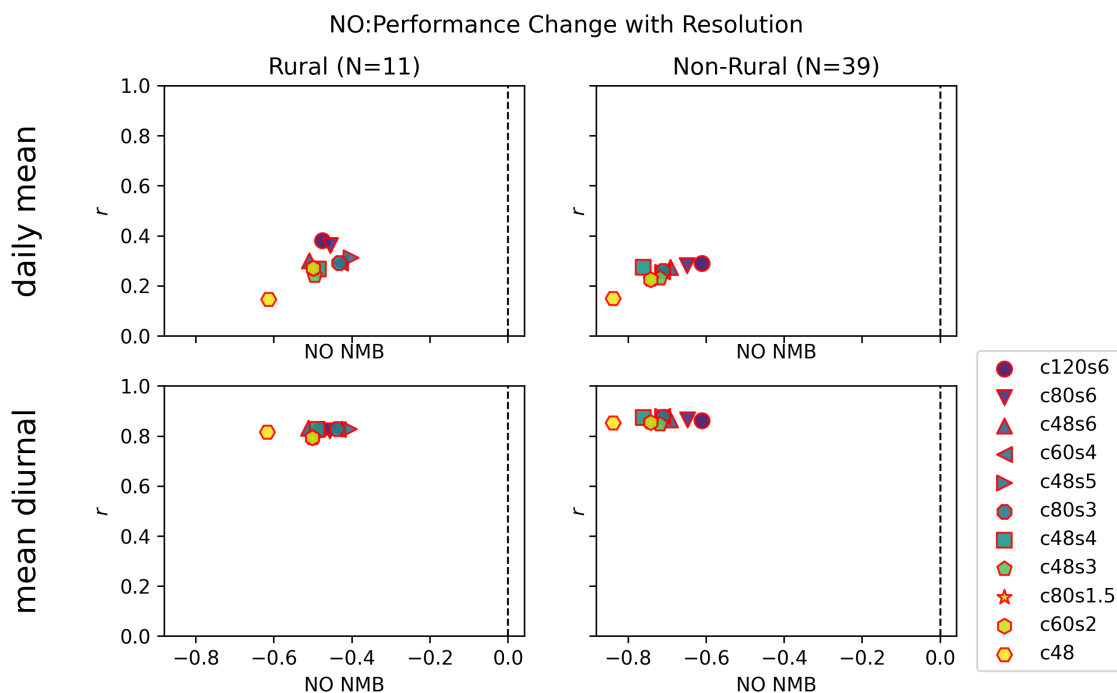
Figure 80: NO NMB and Pearson's *r* for each model (coloured points, according to resolution) compared to observations at Rural sites (left) and Non-Rural sites (right) for daily mean (top row) and hourly mean (bottom row) measurements.NMB is optimised towards the right and *r* towards the top, so optimal performance is at the top right of the diagram.
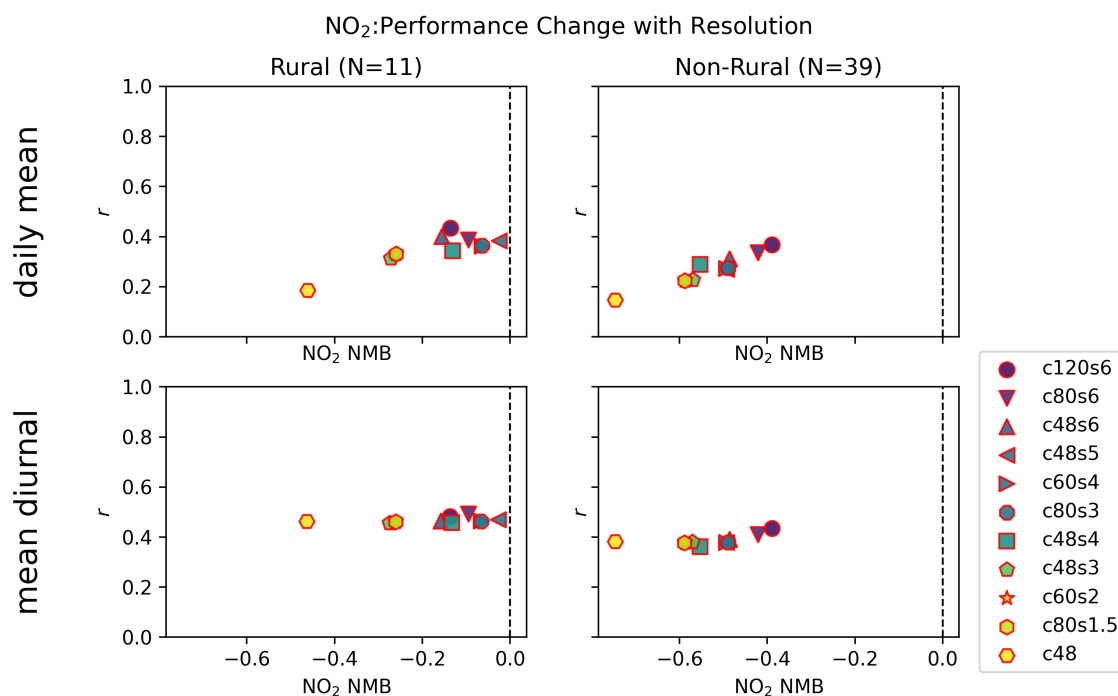
Figure 81: NO$_2$ NMB and Pearson's *r* for each model (coloured points, according to resolution) compared to observations at Rural sites (left) and Non-Rural sites (right) for daily mean (top row) and hourly mean (bottom row) measurements. NMB is optimised towards the right, and *r* towards the top, so optimal performance is at the top right of the diagram.

Higher resolution reduced NO underestimates by up to 21% at Rural sites and 24% at Non-Rural sites, but correlation improvements were larger at Rural sites (Δr=0.24) than Non-Rural sites (Δr=0.12). Bias reductions were more substantial for NO$_2$: 44% at Rural sites, and 38% at Non-Rural sites. The reductions in Rural underestimates for NO$_2$ brought the model average concentration nearly into agreement with the Rural measurements. However, Non-Rural estimates were still underestimated by nearly 40% at C120S6.

For NO, there was almost no difference (± 0.03) in model-observation diurnal correlations in either environment type. However, daily averages had maximum increases of 0.23 at Rural sites and 0.14 at Non-Rural sites. There were similar correlation improvements improvements for NO$_2$ at the daily timescale: by up to 0.25 at Rural sites and by up to 0.22 at Non-Rural sites. NO$_2$ also showed small improvements of up to 0.04 at Rural sites and up to 0.07 at Non-Rural sites. Given all simulations used the same emission profiles and chemistry schemes,

these changes can be attributed to improvements in the transport and better spatial respresentativity of local emissions.

5.4.3 NO$_x$ changes with resolution over the UK

Whilst comparing modelled concentrations to measurements data is helpful to assess its performance in areas of interest, it may not be representative of the whole country. To expand on this, we now look at the impact of horizontal resolution over the whole of UK for the June-July period. Figure 82 compares the mean modelled surface NO concentrations at C120S6 with C48, C80S1.5, C48S5, C80S4 and C80S6 resolutions, and Figure 83 performs the same comparison for NO$_2$.

NO and NO$_2$ differences compared to C120S6 had similar spatial distributions, as might be expected given their close chemical relationship. In areas where C120S6 estimated high concentrations for either species e.g Liverpool, Birmingham and Manchester, coarser simulations estimated lower concentrations than C120S6 (indicated by blue on the figures) and concentrations over the rest of the UK were higher at coarser resolution. However, the relative positive bias was larger for NO than for NO$_2$, potentially due to the longer lifetime of NO$_2$, which lead to a different trend in the UK average percentage differences as resolution changed. In agreement with the previous section, NO$_x$ measurement sites were predominantly located in these urban, populated regions. However, remaining parts of the UK estimated concentrations which were higher than C120S6 for NO, by up to 16.5% at C80S1.6, which would suggest a localisation of emissions sources could be responsible for the areas where C120S6 showed higher concentrations. This also highlights that the perspective gained from the comparison at the AURN measurement sites was not representative of the UK as a whole.
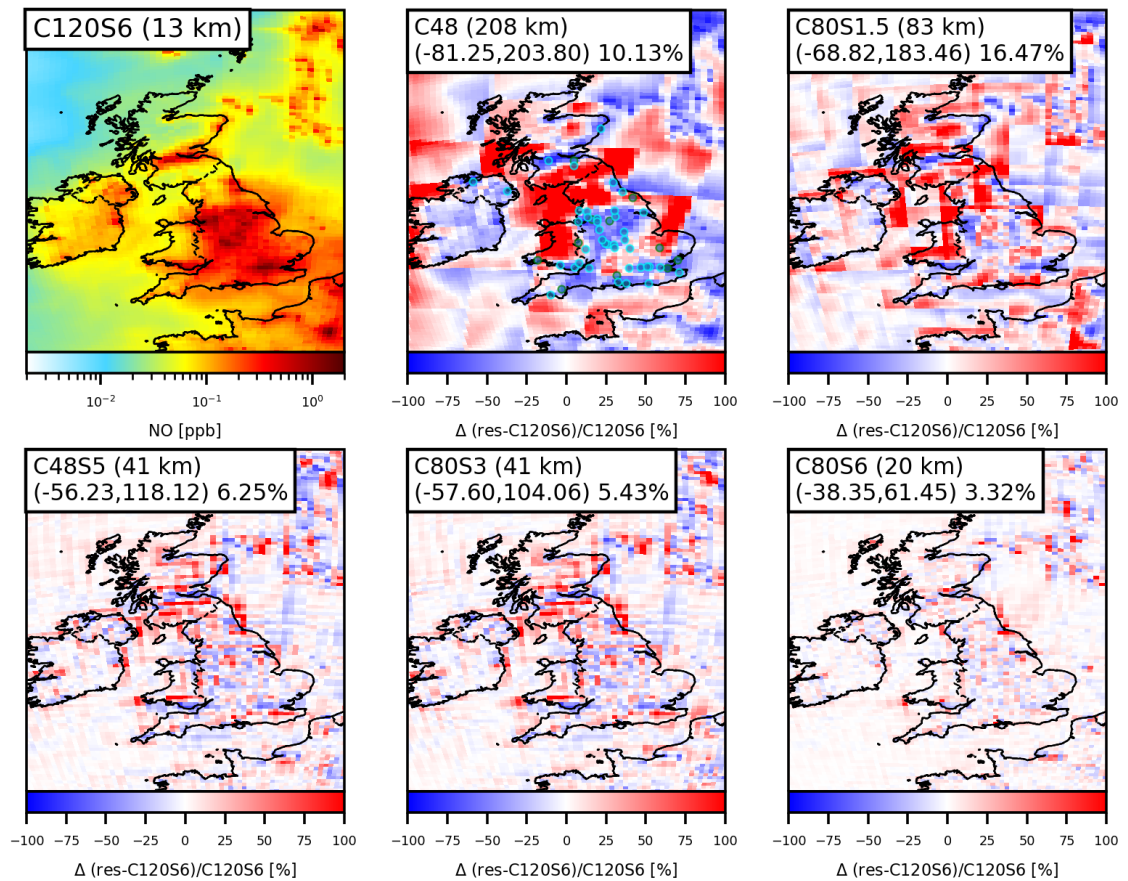
Figure 82: Mean surface NO concentration for the C120S6 simulation (top left, in ppbv) and percentage difference of the C120S6 simulation compared to the C48, C80S1.5, C48S5, C80S3 and C80S6 simulations regridded to the finest resolution. Captions indicate the 5th and 95th quantiles, and UK mean percentage differences over UK gridboxes. Measurement site locations used for comparisons in Section 5.4.1 are shown over the C48 plot (top center panel)
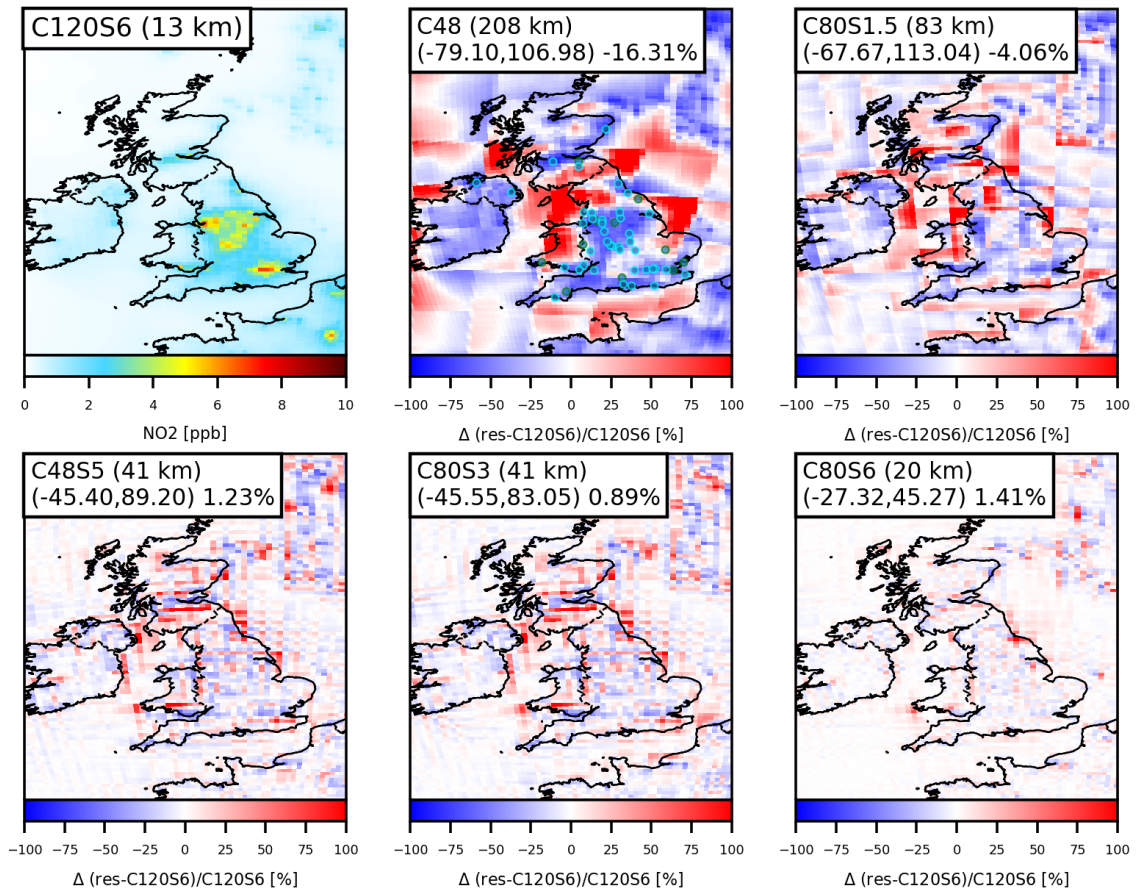
Figure 83: Mean surface NO$_2$ concentration for the C120S6 simulation (top left, in ppbv) and percentage difference of the C120S6 simulation compared to the C48, C80S1.5, C48S5, C80S3 and C80S6 simulations regridded to the finest resolution. Captions indicate the 5th and 95th quantiles, and UK mean percentage differences over UK gridboxes.Measurement site locations used for comparisons in Section 5.4.1 are shown over the C48 plot (top center panel)

5.5   The Resolution Sensitivity of UK Ozone

This section will explore how modelled O$_3$ concentrations change as resolution increases, and how those changes affect the model-observation performance (NMB and correlation) at AURN sites. To facilitate the comparison, we also look at modelled O$_x$ (O$_x$ = O$_3$ + NO$_2$).

5.5.1   Ozone changes with varying model resolution at AURN sites

Figure 84 compare O$_3$ and O$_x$ diurnal cycles with AURN observations at Rural and Non-Rural sites. Higher resolution concentrations reduced concentrations by more for O$_3$ ($\Delta_{(C48-C120S6)}$=-4.37 ppbv) than for O$_x$ ($\Delta_{(C48-C120S6)}$=-2.44 ppbv). All model resolutions produced a similar diurnal profile for both O$_3$ and O$_x$, where the daytime increase occurred at around 0700 compared to 0500 in the observations. The O$_3$ decreases at higher resolution were larger at Non-Rural sites ($\Delta_{C48-C120S6} = -4.5$ ppbv) than at Rural sites ($\Delta_{C48-C120S6} = -3.8$ ppbv).
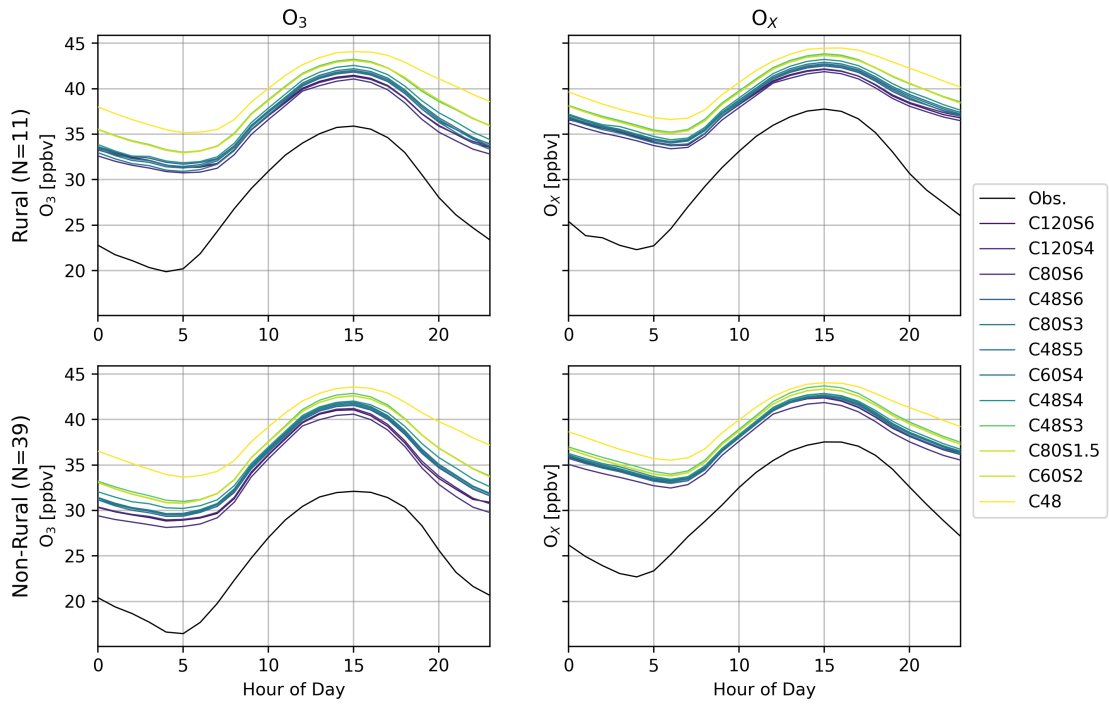
Figure 84: Mean surface observed (black) and modelled diurnal (coloured lines by resolution) of O$_3$ and O$_x$ at Rural and Non-Rural sites, from 1st June 2021 to 31st July 2021, in ppbv.

Modelled daily mean concentrations are compared with observations at Rural and Non-Rural sites for O$_3$ in Figure 85 and for O$_x$ in Figure 86. General features in the observations were captured by all the models, with differences only in their relative amplitudes, where coarse resolutions overestimated the most and failed to capture smaller features. Some features which were not captured at C48 but were simulated at all other resolutions.
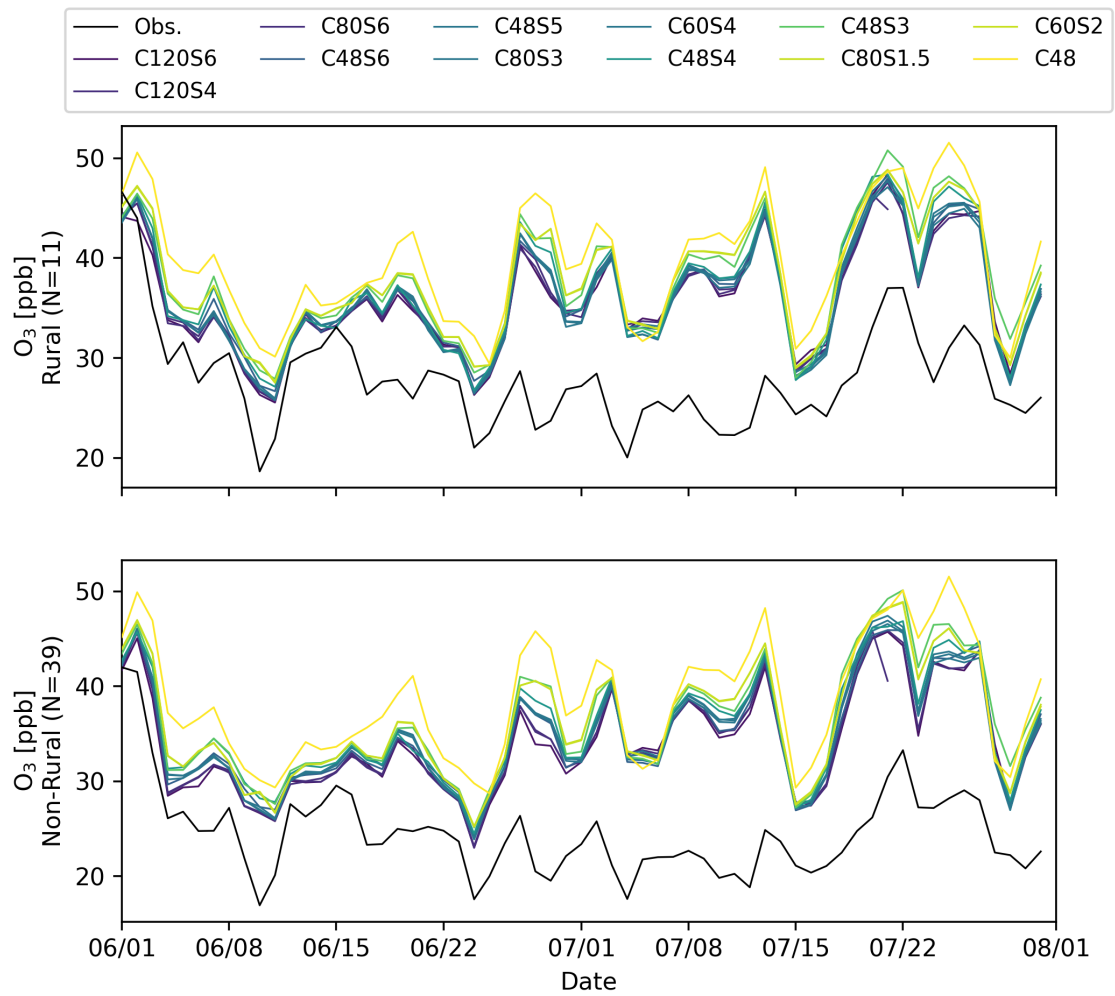
Figure 85: Daily mean surface observed (black line) and modelled (coloured lines by resolution) O$_3$ at Rural sites (top panel) and Non-Rural (bottom panel) sites from 1st June 2021 to 31st July 2021, in ppbv.
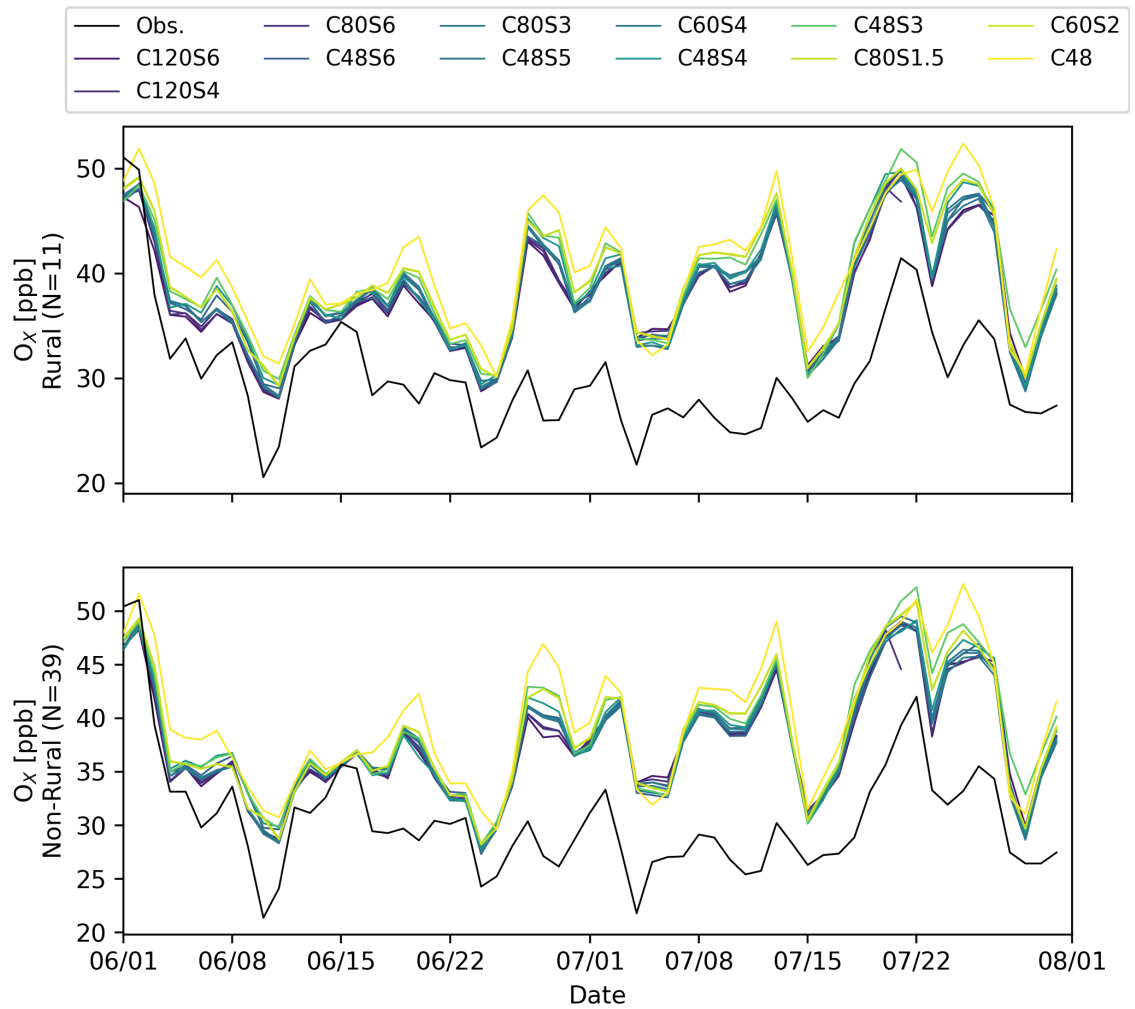
Figure 86: Daily mean surface observed (black line) and modelled (coloured lines by resolution) O_x at Rural sites (top panel) and Non-Rural (bottom panel) sites from 1st June 2021 to 31st July 2021, in ppbv.

A higher resolution sensitivity for O$_3$ than for O$_x$ suggests an increase in NO$_x$ titration because of the higher NO$_x$ concentrations at higher resolution(Section 5.4). However, this does not explain why there were also O$_x$ reductions, so there are multiple factors affecting O$_3$ resolution sensitivity. We first look at whether there are differences in transported contributions passing over the UK, then how O$_3$ production rate over the UK varies with resolution.

Transport of air masses over the UK from the Atlantic can have a large effect on UK O$_3$ (Romero-Alvarez et al., 2022), and O$_3$ concentration in these air masses could differ due to differences in resolution between stretched grid configurations. To determine if this had significant effect at varying resolutions, the performance (model-observation NMB and correlation) of each model at Mace Head was compared (Table 13), as the region is considered representative of the incoming Western airflow (Jennings et al., 2003). Mean O$_3$ concentration, model-observation correlation and NMB were similar for all the model resolutions, except for C48. For C48, O$_3$ concentrations were around 2 ppbv lower, resulting in a slightly smaller model overestimate (NMB$_{C48}$=0.09 compared to around 0.15 for the remaining simulations), but a comparable correlation to other results. We note that the centre of the nearest model gridbox for the C48 simulation is considerably further away from Mace Head than other resolutions. In addition, the coarse resolution means the gridbox concentration will reflect conditions over a much larger area than the other resolutions assessed and may be including some NO$_x$ titration not observed by other models in the same gridbox. The strong similarities between the remaining model resolutions at Mace Head confirm that O$_3$ performance differences between models are not due to boundary condition effects, and that estimates of this contribution are very similar between GCHP simulations between 14 and 83 km horizontal resolution.

Table 13: Comparison of model gridbox centre - Mace Head distance, mean modelled O$_3$ concentrations (in ppbv) at Mace Head, Pearson's *r* and NMB compared to Mace Head O$_3$ measurements for each GCHP simulation.

Model	Distance [km]	Mean O$_3$ [ppbv]	*r*	NMB
C48	115.9	33.47	0.64	0.09
C80S1.5	12.5	35.68	0.62	0.17
C60S2	11.7	35.66	0.63	0.17
C48S3	16.1	35.51	0.67	0.16
C48S4	13.6	35.58	0.67	0.16
C48S5	27.0	34.01	0.66	0.11
C60S4	24.2	34.25	0.65	0.12
C80S3	22.1	34.45	0.65	0.13
C48S6	17.3	35.48	0.68	0.16
C80S6	9.2	35.32	0.66	0.15
C120S6	4.1	35.54	0.65	0.16

Reductions in O$_3$ production might also explain the O$_3$ and O$_x$ resolution sensitivities. To assess this, the average rate of O$_3$ production for the NO+HO$_2$ reaction over the UK and at the O$_3$ measurement sites was calculated for the first month (Table 14). Over the whole of the UK, the coarsest resolution (C48) estimated roughly 20% higher production rates than the finer resolutions. However, the finer resolutions showed only minor differences in rates between them. The differences become much larger when focusing on the AURN measurement site locations, with coarse resolutions estimating substantially higher rates of daytime O$_3$ production. Production rates being significantly higher at coarse resolutions might explain why the C48 simulation showed higher average estimates at the measurement sites despite underestimating the background contribution by 2 ppb. Therefore, we can attribute O$_3$ decreases at finer resolution to a combination of local NO$_x$ titration effects and O$_3$ production decreases.

Table 14: Mean daytime (0600-1800) modelled O$_3$ production rates over the whole of the UK ("UK Rate") and only at gridboxes nearest to the AURN O$_3$ measurement sites ("Site Rate") in June 2021. Rate was calculated as k[NO][HO$_2$], with $k_{\mathrm{HO2+NO}}$ (298 K) = 8.2 cm^{3}molecule^{-1}s^{-1} (Burkholder et al., 2020). Rates were calculated from conservatively regridded data for each model at C120S6 and a UK mask at the same resolution. We do not attempt to calculate production via RO$_2$+NO reactions.

Model	Resolution [km^2]	UK Rate [molecules s^{-1}]	Site Rate [molecules s^{-1}]
C48	208	1.434×10^5	1.250×10^5
C80S1.5	83	1.219×10^5	8.860×10^4
C60S2	83	1.222×10^5	8.875×10^4
C48S4	52	1.257×10^5	8.521×10^4
C80S3	42	1.188×10^5	7.260×10^4
C60S4	42	1.200×10^5	7.325×10^4
C48S5	42	1.221×10^5	7.445×10^4
C48S6	34	1.279×10^5	7.189×10^4
C80S6	21	1.186×10^5	6.797×10^4
C120S6	14	1.210×10^5	6.024×10^4

5.5.2   The Effect of Resolution on NMB and correlation for Ozone at AURN Sites

Figure 87 compares the NMB and correlation coefficient for O$_3$ at Rural and Non-Rural measurement sites for each model resolution. O$_3$ overestimates are reduced by 14% at Rural sites and by 23% at Non-Rural sites at higher resolution. Section 5.5.1 showed that modelled O$_3$ diurnal profiles were similar for all resolutions in both environment types, which reflects that there were only minor improvements in correlations with observed diurnals beyond the +0.04 achieved increasing from C48 to C80S1.5. Similarly to NO and NO$_2$, correlation improvements were larger for daily means: increasing by up to 0.06 (from 0.48 at C48 to 0.54 at C120S6) at Rural sites and 0.04 at Non-Rural sites (from 0.43 at C48 to 0.47 at C120S6). Further, the trend in increased correlations with daily means at Rural sites suggests that even finer resolutions may further improve correlations. However, the same cannot be said for model bias, which showed incrementally smaller improvements as resolution increased. From this we can conclude that resolution increases can reduce model O$_3$ bias to an extent, and that higher resolution improves correlations at the daily mean timescale, but not

at diurnal timescale, where processes other than resolution are likely responsible for model-observation differences.
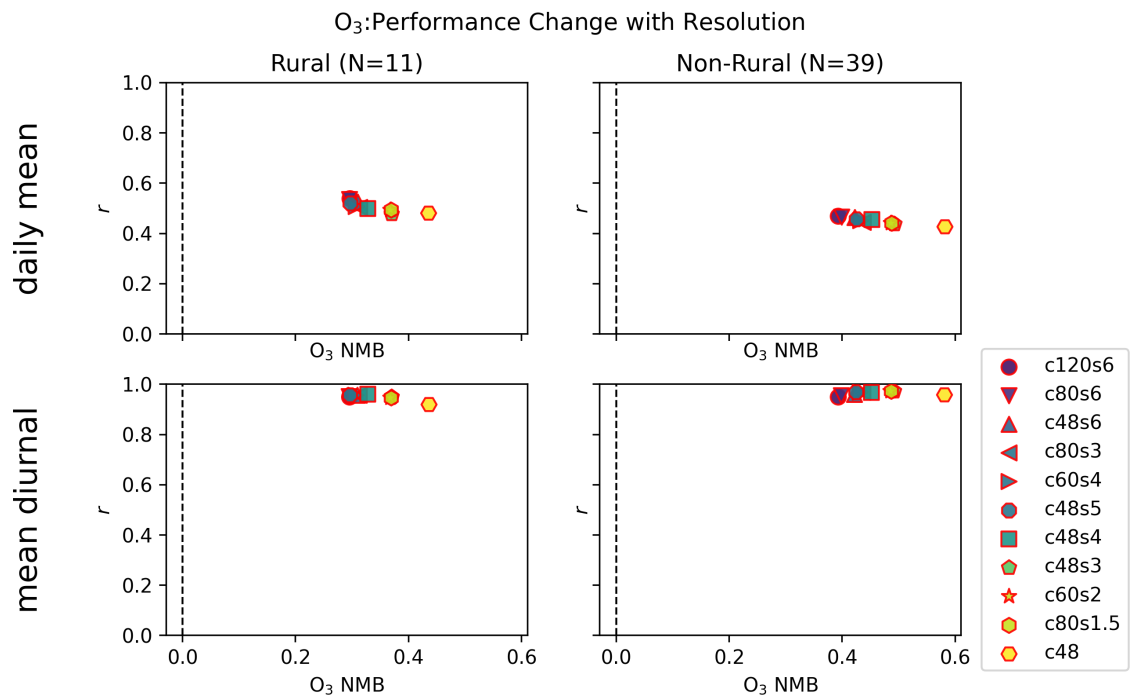
Figure 87: O$_3$ NMB and Pearson's *r* for each model (coloured points, according to resolution) compared to observations at Rural sites (left) and Non-Rural sites (right) for daily mean (top row) and hourly mean (bottom row) measurements. NMB is optimised towards the left, and *r* towards the top, so optimal performance is at the top left of the diagram.

5.5.3   Ozone and O$_x$ changes with resolution over the UK

Figure 88 and 89 compare mean O$_3$ and O$_x$ concentration differences in the same way as Section 5.4.3 did for NO and NO$_2$. O$_3$ and O$_x$ concentrations at C120S6 showed a trend of increasing concentrations moving South East from the North of Scotland to South East England, with reduced O$_3$ concentrations over Manchester/Liverpool, Birmingham and London-areas which showed NO$_x$ increases at higher resolutions (Figure 82, 83). At higher resolution the gridboxes surrounding these areas showed similar underestimates for O$_3$ but not for O$_x$, suggesting that they are the result of local NO$_x$ emission and titration enhancement. Coarser resolutions estimated concentrations which were 7.65% higher for O$_3$ and 6% higher for O$_x$ at C48 over the UK as a whole. As resolution increased, the positive bias at coarser resolutions decreased, until at 20 km resolution (C80S6) the UK average difference is slightly negative (-0.23% for O$_3$ and -0.26% for O$_x$). This change is likely due to small differences in between the original model grid at C80S6 and its regridded counterpart.
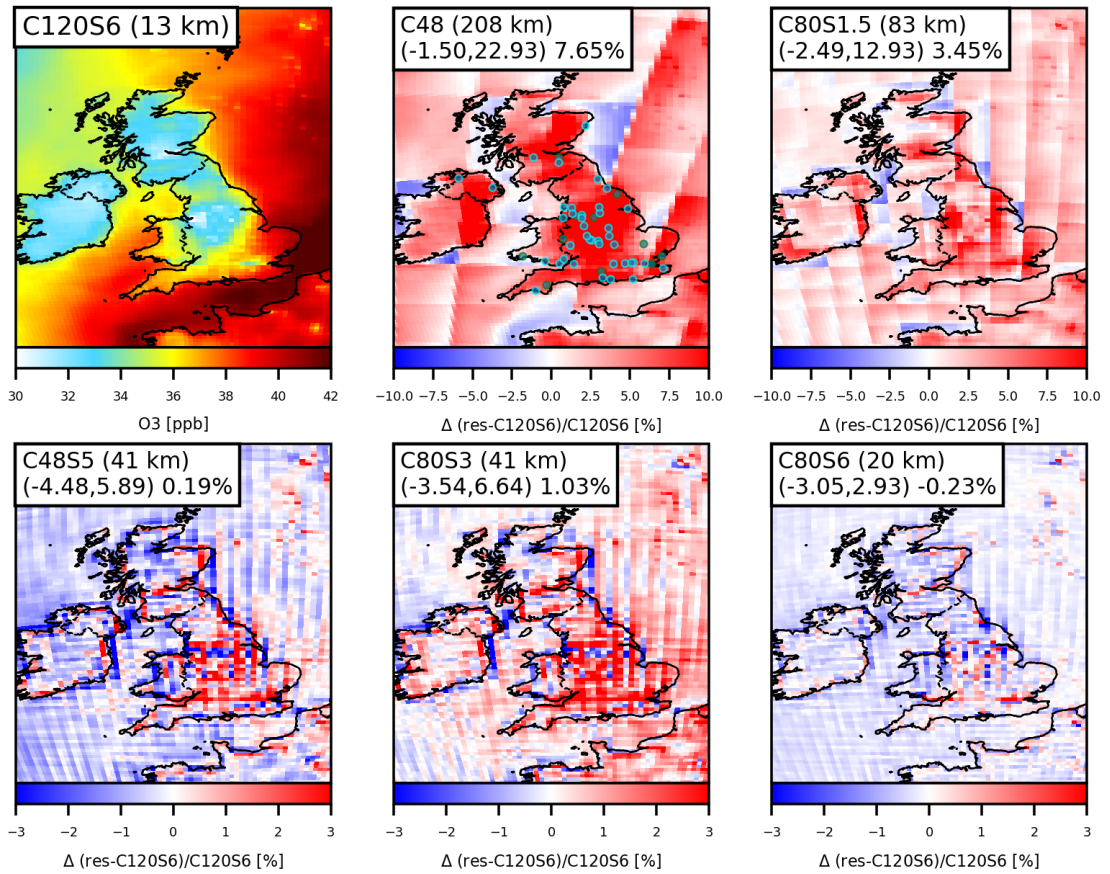
Figure 88: Mean surface O$_3$ concentration for the C120S6 simulation (top left, in ppbv) and percentage difference of the C120S6 simulation compared to the C48, C80S1.5, C48S5, C80S3 and C80S6 simulations regridded to the finest resolution. Captions indicate the 5th and 95th quantiles, and UK mean percentage differences over UK gridboxes. Measurement site locations used for comparisons in Section 5.4.1 are shown over the C48 plot (top center panel)
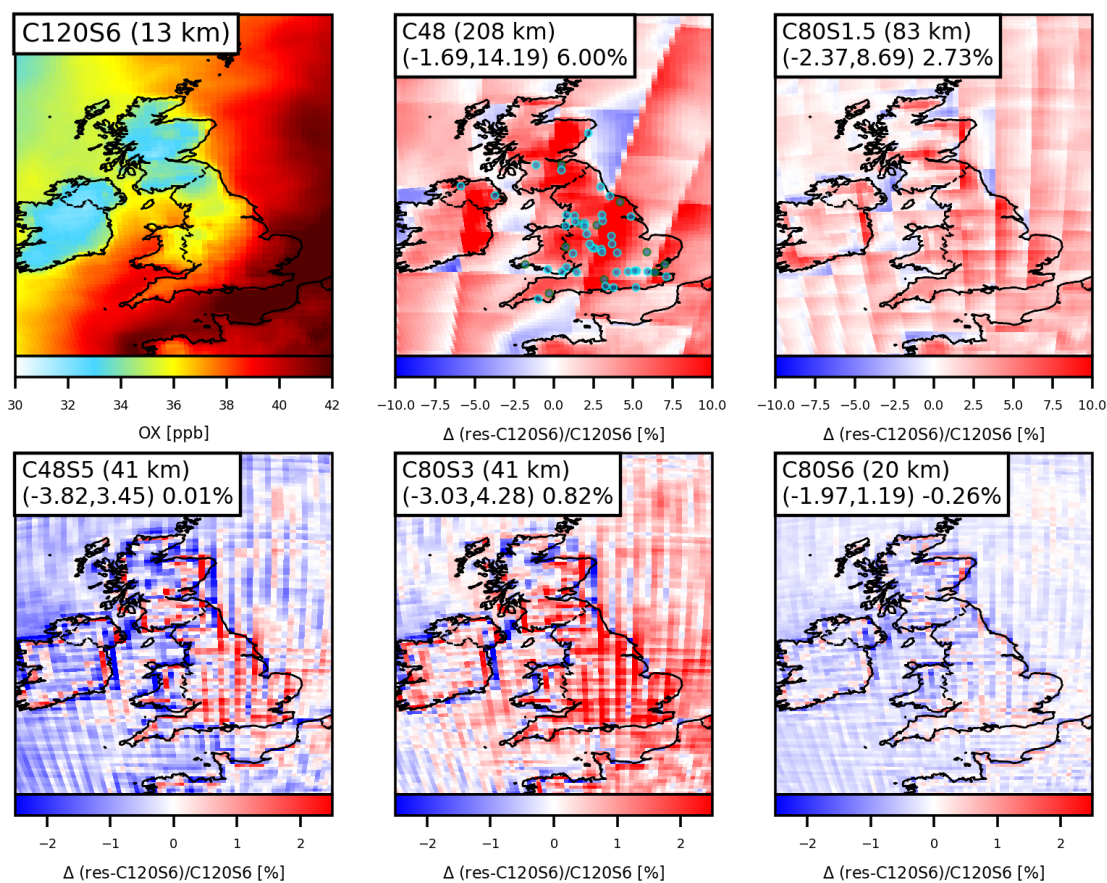
Figure 89: Mean surface O$_x$ concentration for the C120S6 simulation (top left, in ppbv) and percentage difference of the C120S6 simulation compared to the C48, C80S1.5, C48S5, C80S3 and C80S6 simulations regridded to the finest resolution. Captions indicate the 5th and 95th quantiles, and UK mean percentage differences over UK gridboxes. Measurement site locations used for comparisons in Section 5.4.1 are shown over the C48 plot (top center panel)

5.6 The Resolution Sensitivity of UK PM$_{2.5}$

5.6.1 PM$_{2.5}$ and PM$_{2.5}$ Component concentration changes with resolution at AURN sites

Figure 90 and 91 compare the mean concentration from 1st June to 31st July 2021 for PM$_{2.5}$ and its components at each model resolution at the Rural and Non-Rural measurement sites for PM$_{2.5}$. There was no visible trend in the resolution-sensitivity of mean PM$_{2.5}$ at Rural sites, as concentrations both increased and decreased at higher resolutions. This may be due to a combination of grid overlap differences between resolutions and the complex composition of PM$_{2.5}$. At Non-Rural sites, although there were similar irregularitiesthere was a clearer trend of increased PM$_{2.5}$ concentration at higher resolution - concentrations at 13 km (C120S6) were 1.77 μgm^{-3}(19.6%) larger than at 200 km (C48). This increase is broadly consistent with the 29% increase in Summer PM$_{2.5}$ at fine resolution over Europe reported by Fenech et al. (2018) for comparisons of a 50 km (fine) and 140 km (coarse) resolution model.
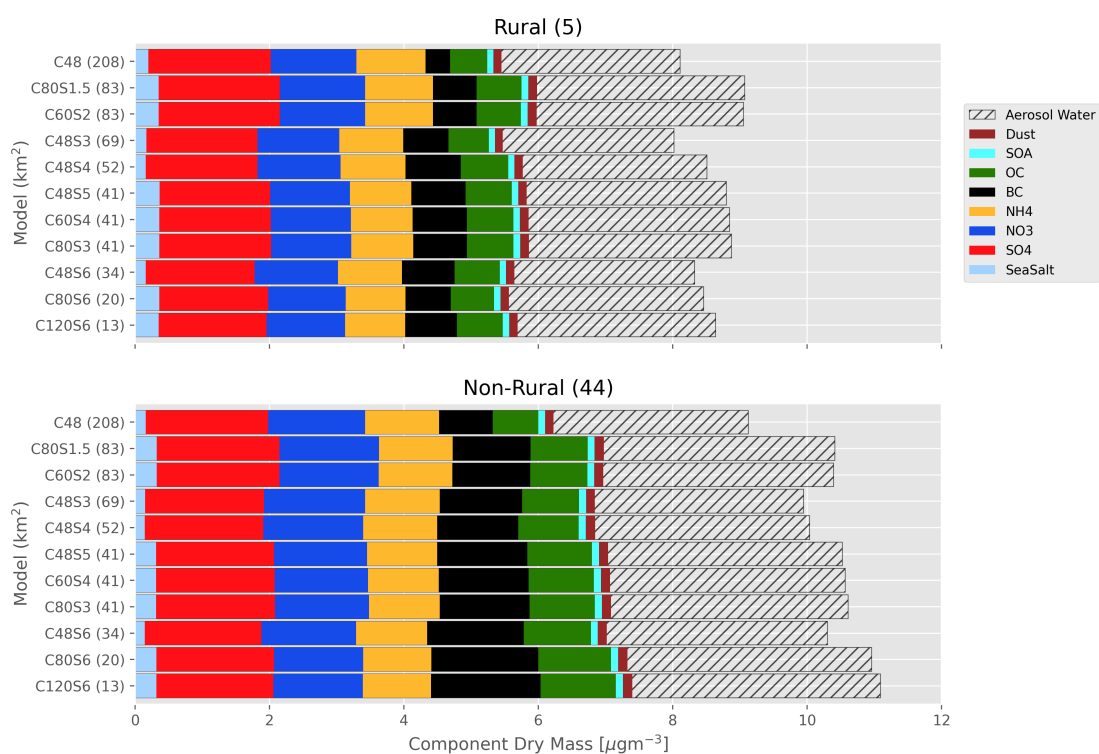
Figure 90: Mean concentration of aerosol water in PM$_{2.5}$ (hatched), calculated at 50% relative humidity, and (dry) concentration of PM$_{2.5}$ components, Sea Salt, SO$_4^{2-}$, NO$_3^-$, NH$_4^+$, BC, OC, SOA, Dust, at Rural and Non-Rural PM$_{2.5}$ measurement sites from 1st June 2021 to 31st July 2021. Bracketed numbers in the panel titles indicate the number of measurement sites for each environment type.
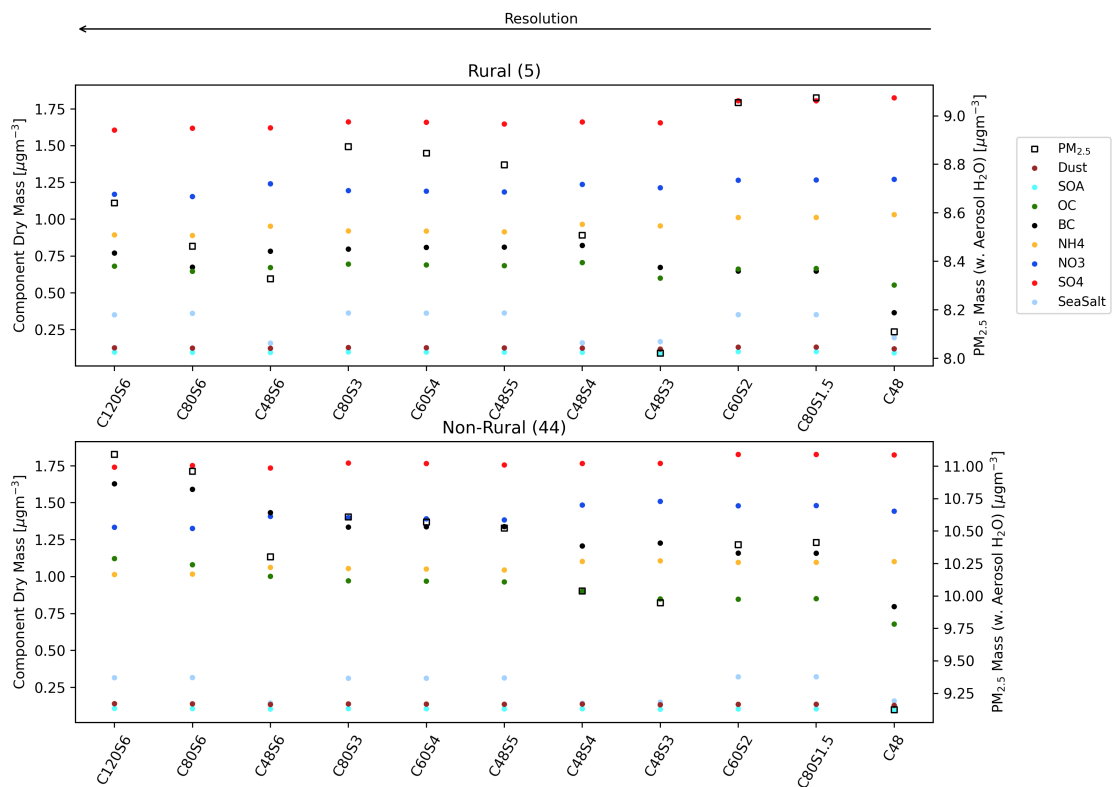
Figure 91: Mean dry concentration of PM$_{2.5}$ components, and PM$_{2.5}$ accounting for aerosol water (black square) at Rural (top) and Non-Rural (bottom) measurement sites from 1st June 2021 to 31st July 2021. Bracketed numbers in the panel titles indicate the number of measurement sites for each environment type.

For all the sites (Rural and Non-Rural), the higher concentrations of PM$_{2.5}$ at finer resolutions were due to increases in concentration of BC (0.77 μg m^{-3}, 103.4 %) and OC (0.41 μg m^{-3}, 61.1%) concentrations. Sea Salt concentrations varied by $\pm$50% between simulations, but were identical for simulations at the same resolution (e.g C60S4 and C48S5), suggesting the cause for variability is gridbox placement. Dust concentrations increased by 0.23 μg m^{-3}(44.0%) at C120S6 compared to C48. SOA did not show a resolution dependence. Increases in resolution had a small negative impact on concentrations of SO$_4^{2-}$ (-0.10 μg m^{-3}-5.4%), NO$_3^-$ (-0.12 μg m^{-3}, -8.3 %) and NH$_4^+$ (-0.10 μg m^{-3}, -8.8%).

The sample of measurement sites used for these comparisons are likely not representative of the UK as a whole, and may lead the interpreter to alternative conclusions about what is happening. So the next section will compare concentrations of PM$_{2.5}$ and its components over the whole of the UK.

5.6.2   PM$_{2.5}$ and PM$_{2.5}$ Component Changes with resolution over the whole of the UK

Figure 92 compares the mean surface PM$_{2.5}$ concentration at resolutions from C48 to C120S6 from June-July 2021. Peak UK concentrations are lower at coarser spatial resolutions. As resolution increases the model starts to resolve spatial features like higher concentrations over large urban areas, particularly in central and South East England. Figure 93 shows the percentage difference in PM$_{2.5}$ concentration at several resolutions relative to C120S6, with the AURN measurement site locations shown over the C48 panel. There was a generally even mix of areas where concentrations at a given resolution were higher than at C120S6 (red) and those which were lower than at C120S6(blue). The highest resolution model usually had higher PM$_{2.5}$ concentrations than lower resolution simulations at Non-Rural site locations, whilst Rural site locations experienced a mix of higher and lower concentrations. This accounts for why Rural sites didn't

show a resolution sensitivity trend for PM$_{2.5}$ in Figure 90. It also shows that the conclusion that PM$_{2.5}$ concentrations increased at higher resolution is skewed by the measurement site locations.
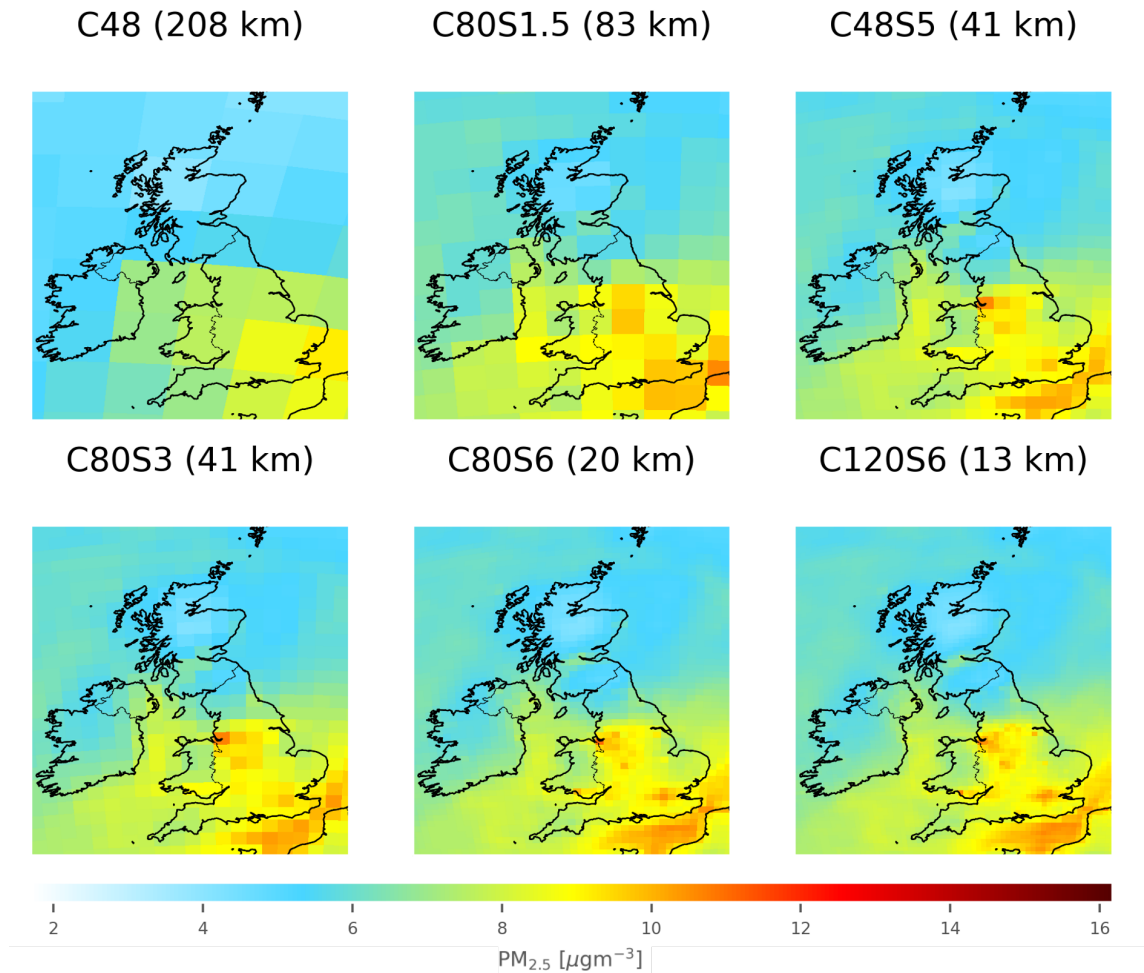
Figure 92: Mean surface PM$_{2.5}$ concentration from 1st June 2021 to 31st July 2021 at C48, C80S1.5, C48S5, C80S3, C80S6 and C120S6, in μgm^{-3}. The locations of Rural (green circles) and Non-Rural (cyan circles) are shown over the C48 for reference.
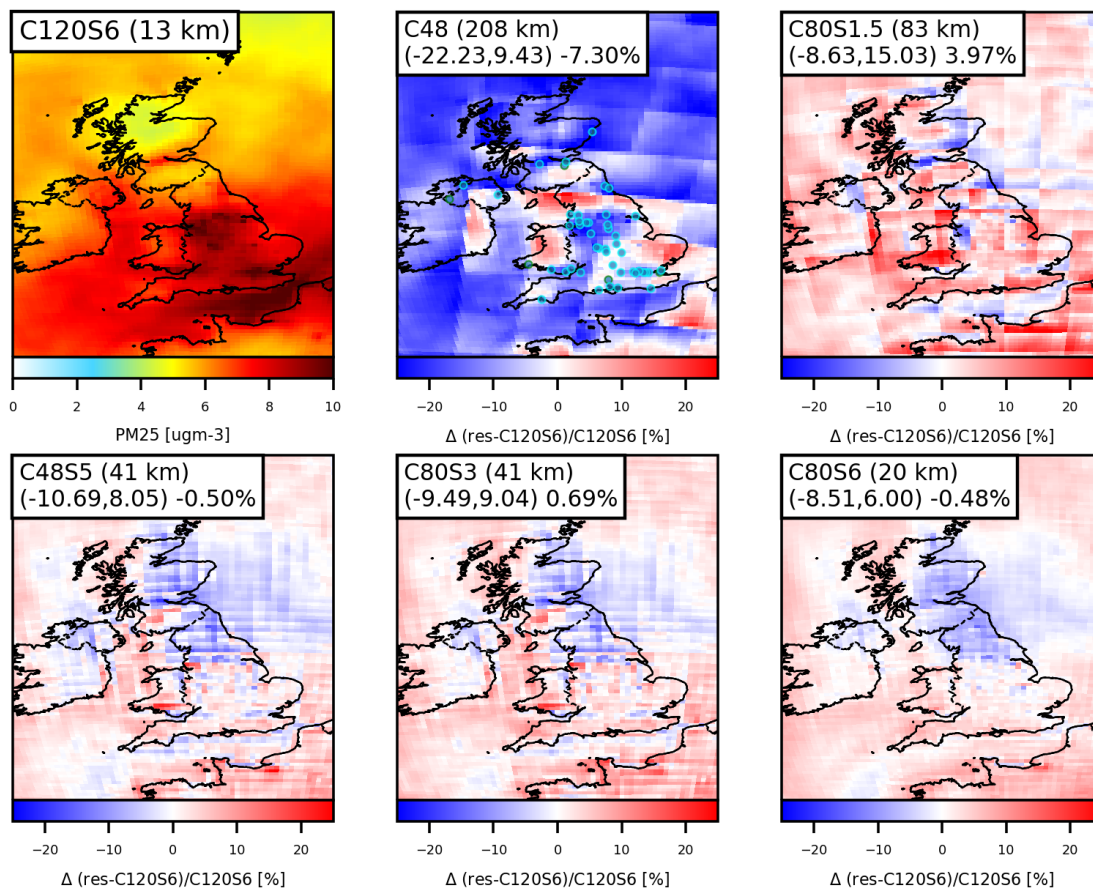
Figure 93: Mean surface $PM_{2.5}$ concentration from 1st June 2021 to 31st July 2021 at C48, C80S1.5, C48S5, C80S3, C80S6 and C120S6, in μgm^{-3}. Locations of Rural (green circles) and Non-Rural (cyan circles) measurement sites are shown over C48 for reference.

Section 5.6.1 showed large increases in the concentrations of BC and OC were responsible for the trend of $PM_{2.5}$ increases at the measurement sites at higher resolutions. In the same way as for $PM_{2.5}$ in Figure 93, the percentage differences are shown for BC in Figure 94 and OC in Figure 95. Higher concentrations at higher resolutions occurred over populated Urban regions, with nearby areas showing opposite trends, which would indicate increased local emissions. This is consistent with the prior study by Zhang et al. (2023) which found increased sectoral contributions for BC from residential combustion, industry, energy and transport in the Global South at higher model resolution. The same work found a combination of both positive and negative effects on $PM_{2.5}$ components at varying resolutions. Given anthropogenic emissions of BC and OC are based off the same data, it follows that they would respond similarly to increased reso-

lutions.
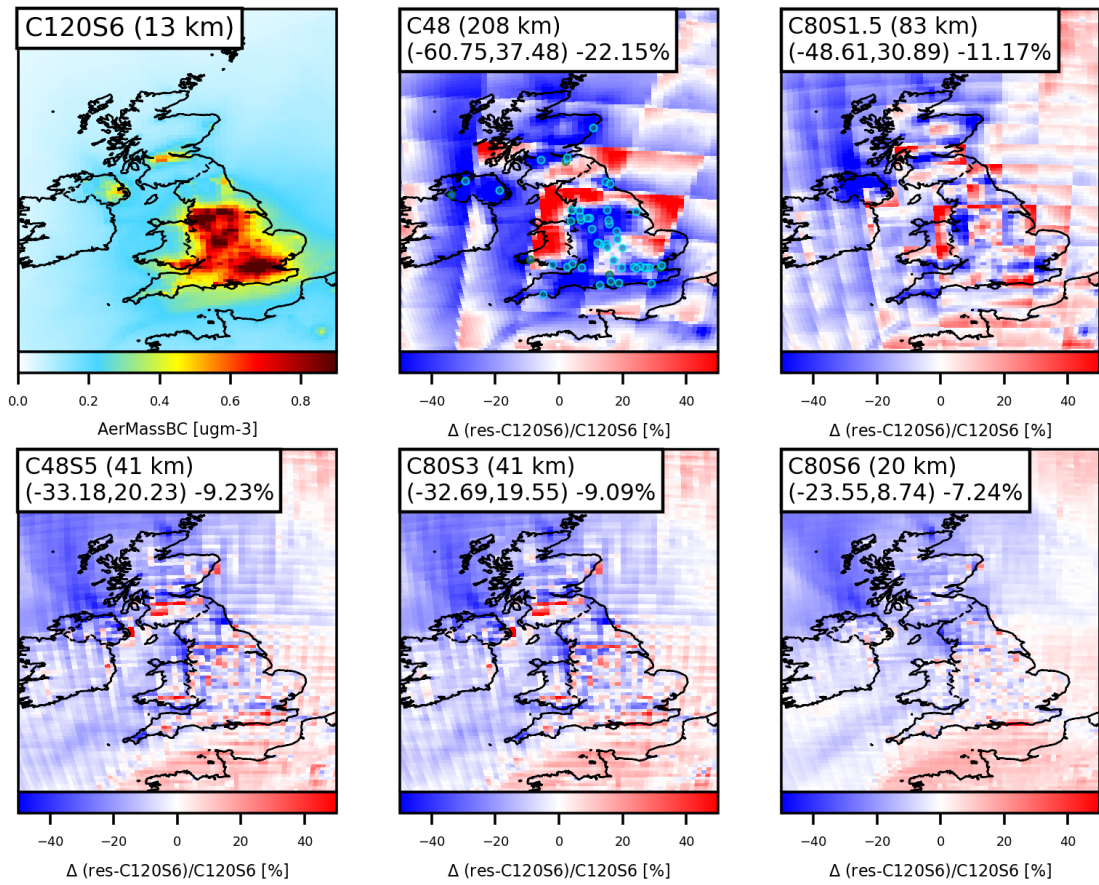
Figure 94: Mean concentration of BC at C120S6 (top left), compared with the percentage difference versus C48, C80S1.5, C48S5, C80S3 and C80S6.Locations of Rural (green circles) and Non-Rural (cyan circles) measurement sites are shown over C48 for reference.
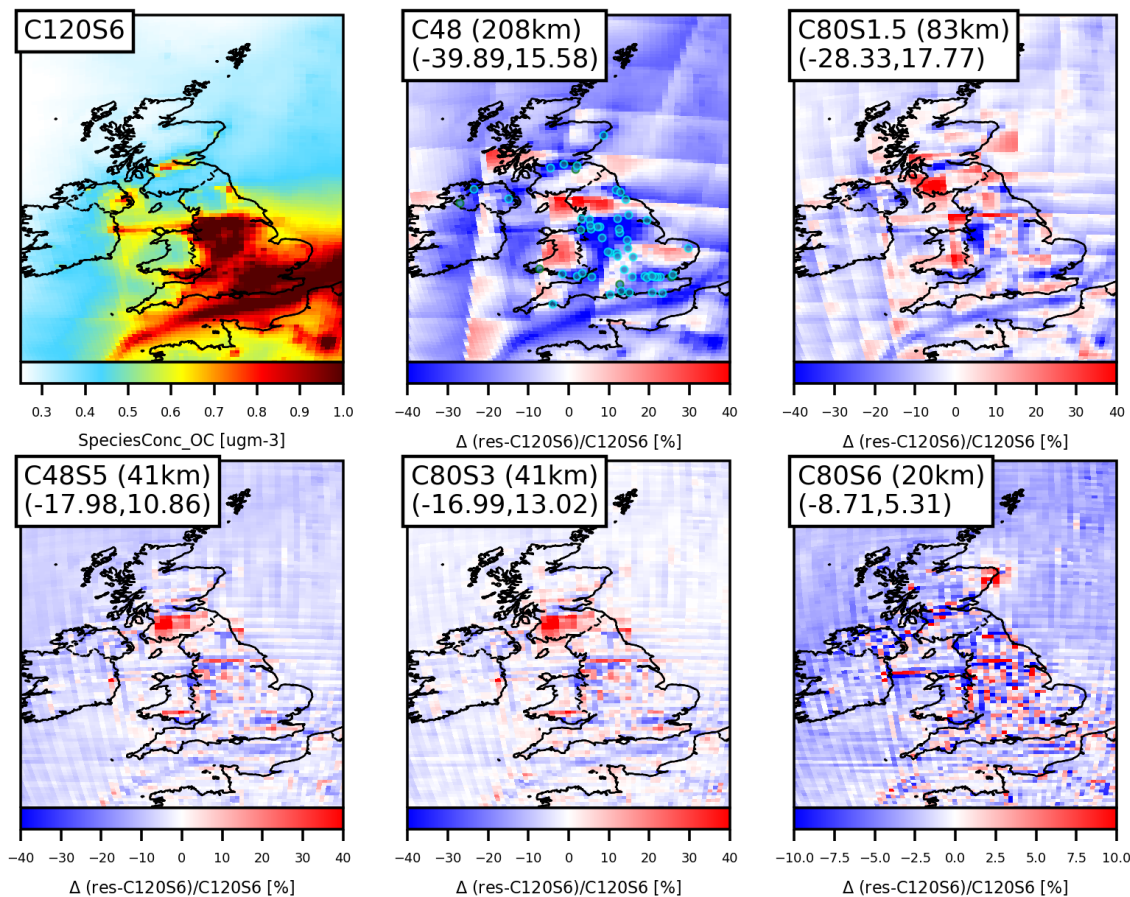
Figure 95: Mean concentration of OC at C120S6 (top left), compared with the percentage difference versus C48, C80S1.5, C48S5, C80S3 and C80S6.Locations of Rural (green circles) and Non-Rural (cyan circles) measurement sites are shown over C48 for reference.

Sea Salt concentrations didn't show a resolution dependence but showed a lot of variability between different resolutions (Section 5.6.1). Sea Salt emissions in GEOS-Chem use offline grid-independent emissions, so in theory should be identical regardless of resolution. Global emissions of Sea Salt showed similar spatial distributions and global totals, with one exception for C48 which was approximately 5% lower than other estimates and may indicate an error in the regridding, which we do not investigate further. As emissions for the remaining resolutions are the same, this would suggest the differences relate to gridbox location relative to the AURN site sampled. Figure 96 compares the percentage differences in average Sea Salt concentration over the UK for the modelled period. Over most of the UK, the C48 simulations shows a systematic underestimate compared to higher resolutions, which was accounted for by the global emissions deficit. The

remaining resolutions showed a mix of higher and lower concentrations relative to C120S6 along coastlines, which were comparable in magnitude to the percentage differences between Sea Salt concentrations seen in Figure 90. Therefore we can conclude that the inter-model differences were due to measurement site locations rather than changes in Sea Salt concentrations as a whole.

Like Sea Salt, natural Dust in GEOS-Chem also uses grid-independent emissions for soil/desert sources of dust, and the toxicity of naturally occurring is typically lower than those from anthropogenic sources (Park et al., 2018). However, there are additional sources from anthropogenic emissions. Figure 97 compares the mean Dust concentration at C120S6 with coarser resolutions as in 96. There were large increases (blue, i.e C120S6 is higher concentration) in individual grid-boxes around Hull, Port Talbot and Liverpool, and smaller increases over the Greater London area, corresponding to significant point sources and large area sources of PM$_{2.5}$ emissions, which will be speciated into Dust. Therefore, the Dust increases are associated with more localised primary emissions.
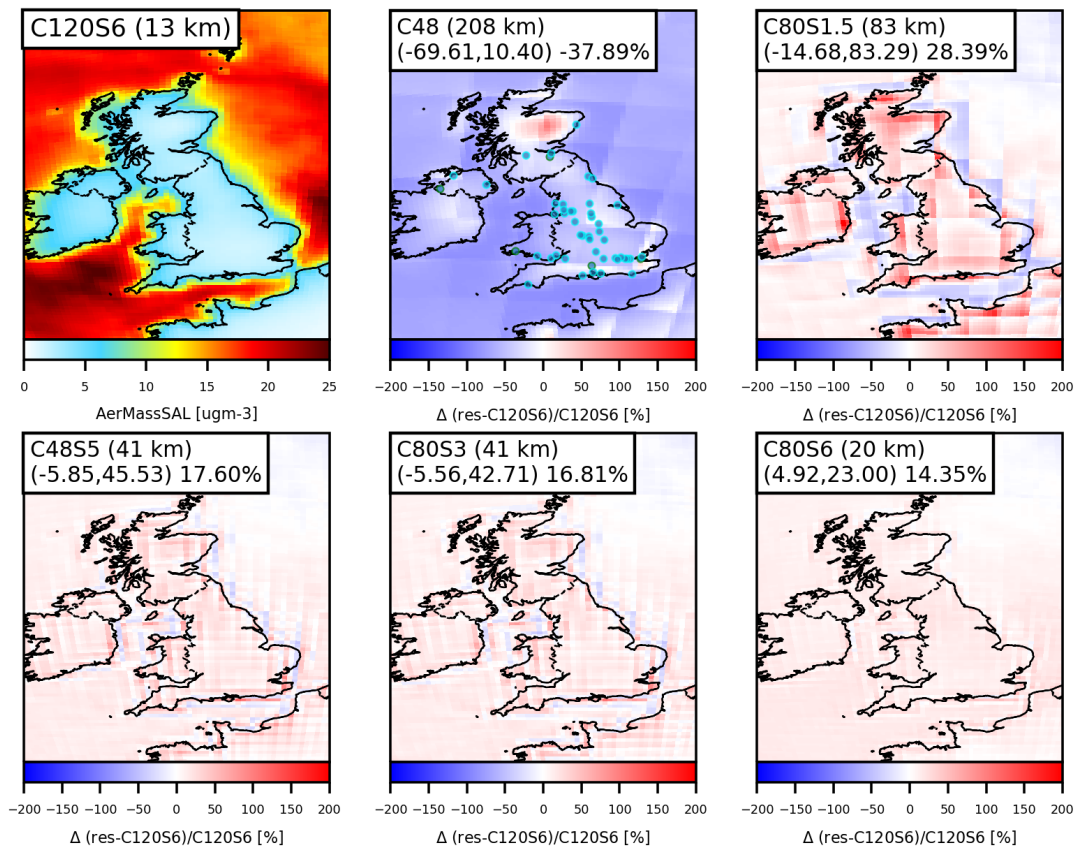
Figure 96: Mean surface Sea Salt concentration from 1st June 2021 to 31st July 2021 at C48, C80S1.5, C48S5, C80S3, C80S6 and C120S6, in $\mu\mathrm{g\,m}^{-3}$. Locations of Rural (green circles) and Non-Rural (cyan circles) measurement sites are shown over C48 for reference.
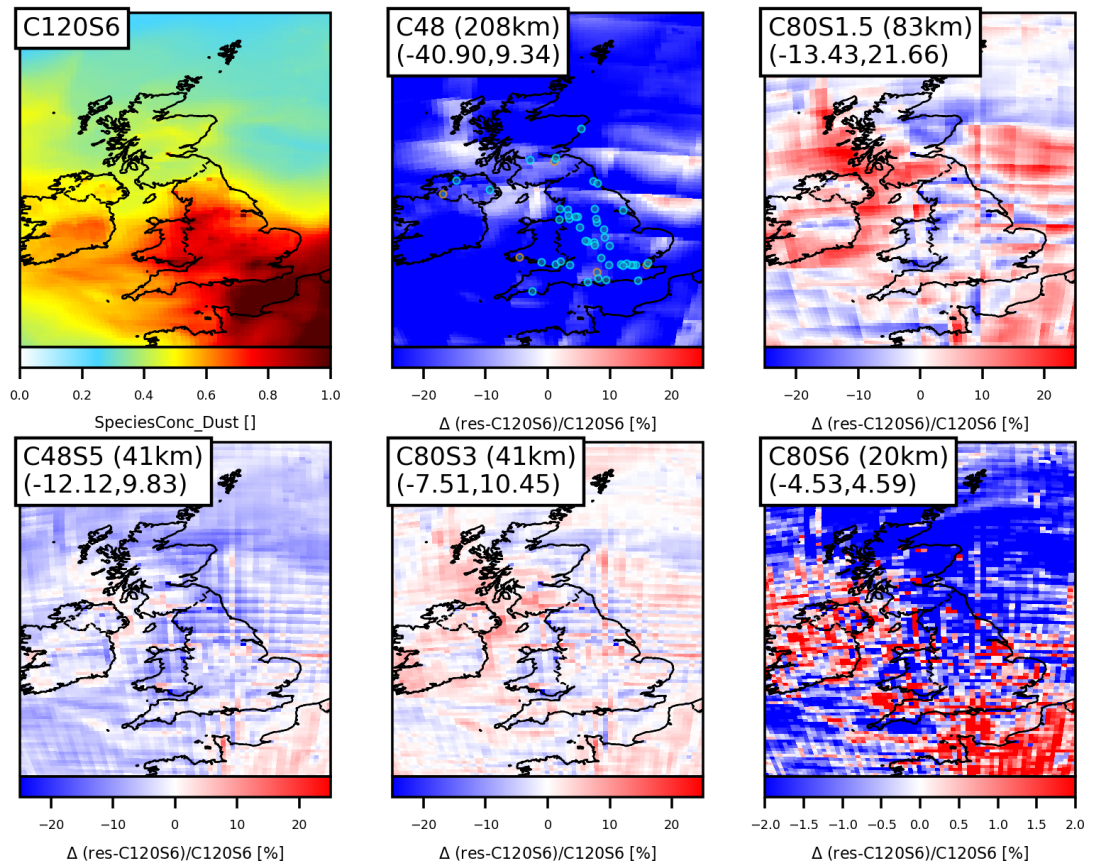
Figure 97: Mean dust (Dust = DST1+0.3×DST2) concentration at C120S6 (top right) and percentage differences compared to C48, C80S1.5, C48S5, C80S3, C80S6 for June 2021. Locations of Rural (green circles) and Non-Rural (cyan circles) measurement sites are shown over C48 for reference.

Figures 98-100 compare the average spatial differences for SO$_4^{2-}$, NO$_3^-$ and NH$_4^+$ over the UK versus the C120S6 simulation. The highest concentrations at C120S6 occurred at known point sources such as a steel works in Scunthorpe and a brickworks in Peterborough (`https://naei.beis.gov.uk/emissionsapp`,last access 14/07/2023). Coarser simulations calculate lower concentration at these locations. Over the whole of the UK, aerosol SO$_4^{2-}$ concentration at coarser resolutions was higher than at C120S6-by 11% at C48. As resolution increased, Eastern parts of the UK begin to show lower concentrations than at C120S6. The predominantly Non-Rural monitoring sites for PM$_{2.5}$ tended to be in areas which opposed the trend over the whole of the UK by having lower concentrations than at C120S6, likely due to higher local concentrations in these gridboxes at higher resolution.
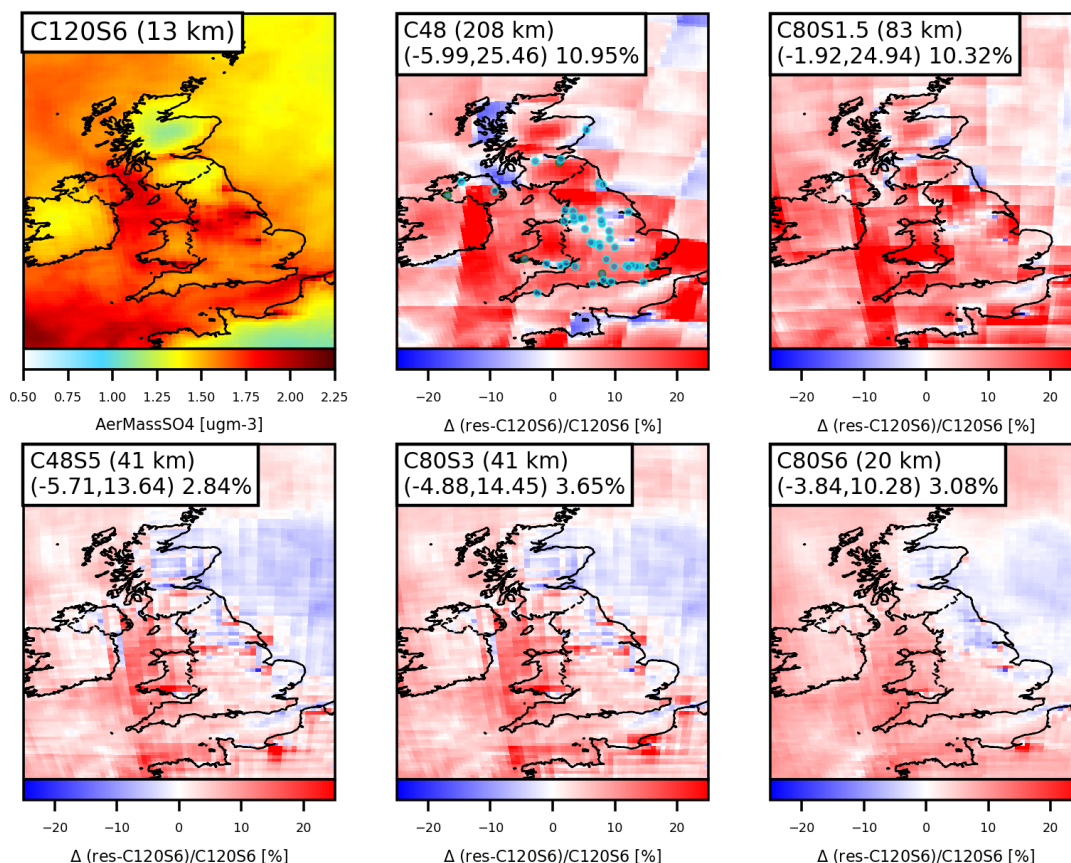
Figure 98: Mean aerosol SO_4^{2-} concentration at C120S6 from 2021/06/01-2021/07/31 (top left), and percentage difference compared to the C48, C80S1.5, C48S5, C80S3 and C80S6 simulations. The 5th and 95th quantiles of for percentage differences are shown in brackets for each difference plot. Note the smaller scale for differences at C80S6. Locations of Rural (green circles) and Non-Rural (cyan circles) measurement sites are shown over C48 for reference.

Aerosol NO_3^- concentrations in coarser simulations were 10-17% lower over the whole of the UK than at C120S6. However, the coarsest resolutions also predicted concentrations which were up to 18% higher at C48 and 10% higher at C80S1.5 over most of South East England and Wales. At slightly higher resolutions like C48S1.5 and C80S3, this overprediction had disappeared, which could indicate a threshold where aerosol NO_3^- production increases at coarse resolution as concentrations are diluted over larger areas. PM$_{2.5}$ measurement sites were located in a mixture of areas which were higher and lower than C120S6 at coarser resolutions, but overall the effect was an underestimate across these locations.
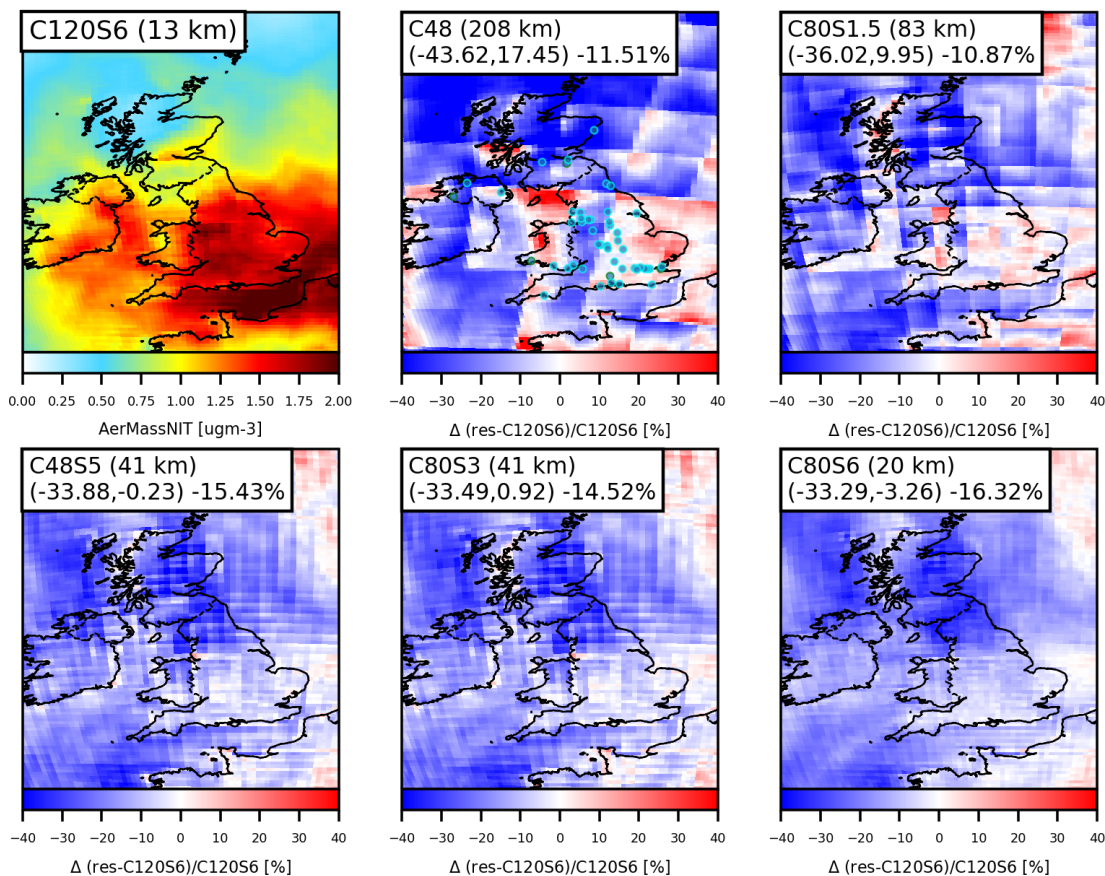
Figure 99: Mean aerosol NO$_3^-$ concentration at C120S6 from 2021/06/01-2021/07/31 (top left), and percentage difference compared to the C48, C80S1.5, C48S5, C80S3 and C80S6 simulations. The 5th and 95th quantiles of for percentage differences are shown in brackets for each difference plot. Note the smaller scale for differences at C80S6. Locations of Rural (green circles) and Non-Rural (cyan circles) measurement sites are shown over C48 for reference.

Northern parts of the UK, where aerosol NH$_4$ concentrations were low, coarse simulations estimated lower concentrations. England and Wales showed a mixture of overestimates and underestimates in similar locations to aerosol NO$_3^-$, supporting that the concentrations changes result from aerosol production instead of transport. Given this, we attribute the small inorganic aerosol reductions at fine resolutions to increases in the spatial segregation (reduced spatial dilution) of aerosol precursors hindering formation, consistent with the recent resolution sensitivity study by Zhang et al. (2023).
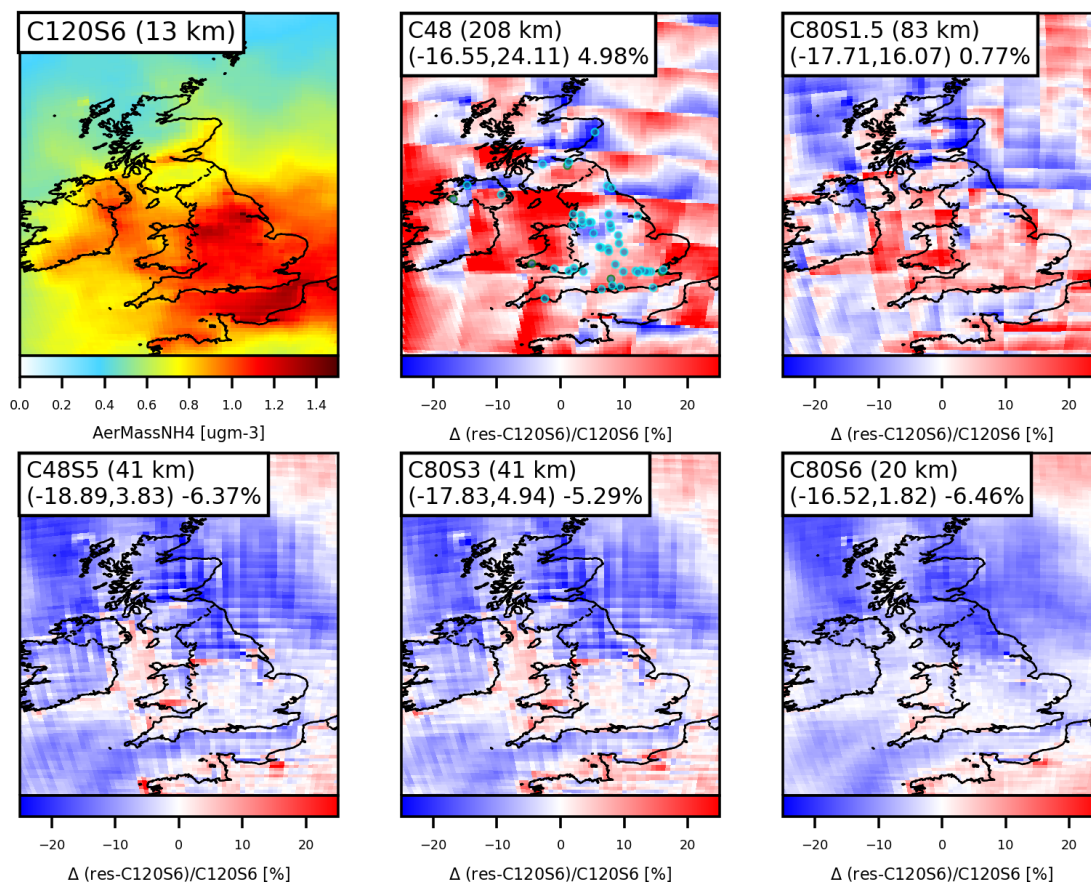
Figure 100: Mean aerosol NH$_4^+$ concentration at C120S6 from 2021/06/01-2021/07/31 (top left), and percentage difference compared to the C48, C80S1.5, C48S5, C80S3 and C80S6 simulations. The 5th and 95th quantiles of for percentage differences are shown in brackets for each difference plot. Note the smaller scale for differences at C80S6.

Comparing the spatial distribution of PM$_{2.5}$ and its components has shown firstly that the changes in model concentrations at measurement sites provide only a partial explanation for the changes that are happening, as comparable opposing changes often occur in other parts of the UK. Thus, when we conclude that concentrations at AURN sites increase with model resolution, this is only a snapshot of the whole response, occurring because the majority of those sites are in areas experiencing higher local emissions of PM$_{2.5}$ components (e.g BC, OC, Dust) or their precursors (NO$_x$, SO$_x$, NH$_3$).

5.6.3   The Effect of Resolution on NMB and correlation for PM$_{2.5}$ at AURN sites

Modelled PM$_{2.5}$ concentrations at each resolution are compared with daily mean and hourly mean (diurnal) values in Figure 101 and 102, and the correlation (Pearson's *r*) and NMB for each model and environment type and averaging period are plotted in in Figure 103. Daily mean estimates were around 2 μgm^{-3} lower at Rural sites than at Non-Rural ones, but generally shared the same profile throughout the 2-month period. Model estimates at resolutions between 14-60 km showed similar estimates, whilst coarser resolutions (C48, C80S1.5 and C60S2) displayed lager differences. Observed features were slightly better represented at Non-Rural sites, than at Rural sites. Increasing grid resolution improved this, with a maximum correlation increase of 0.12 (from 0.32 at C48 to 0.44 at C120S6) at Rural sites and 0.15 (from 0.31 at C48 to 0.46 at C120S6) at Non-Rural sites. Despite performance improvements following resolution changes, all model resolutions failed to capture some features in the observations for either environment type.
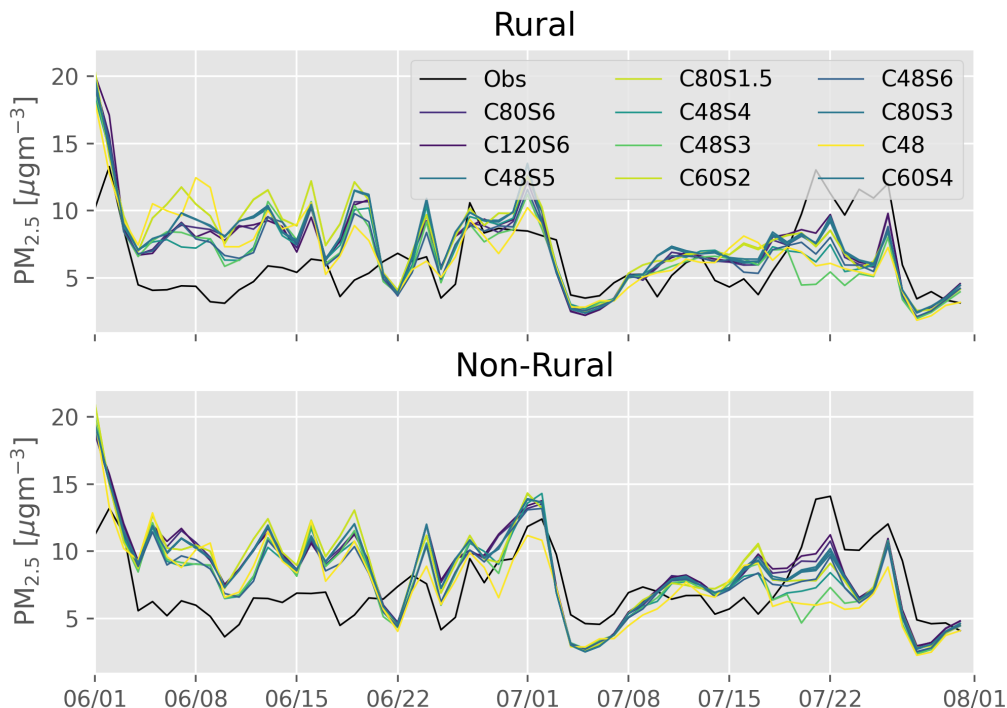
Figure 101: Daily mean observed (black lines) and surface PM$_{2.5}$ concentration from 1st June 2021 to 31st July 2021 at C80S1.5, C48S6, C80S6, C48S5, C48S4, C48S3, C60S2, C80S3, C48, C60S4 and C120S6 (coloured lines).

Modelled PM$_{2.5}$ diurnals (Figure 102) in both environments showed larger amplitude than the measurements, overestimating concentrations at night and up the morning increase at around 0500. The morning increase was present only in observations for Non-Rural sites. In both environments, finer resolution simulations more closely captured the afternoon minimum at around 1500. Chapter 3 proposed that some of the discrepancy in the diurnal profile came from biases in the modelled planetary boundary layer height. Li et al. (2023b) showed that with observationally derived adjustments to GEOS-Chem PBLH inputs reduced bias in simulated PM$_{2.5}$ diurnal amplitude by 8%. They also further extended the improvements demonstrated by adjusting for concentration gradients in Chapter 3, by estimating concentrations at 2 m above the surface. All simulations here used the same input meteorology data, which are regridded to model resolution, so differences in PBLH may have arisen due to differences in model horizontal grids.
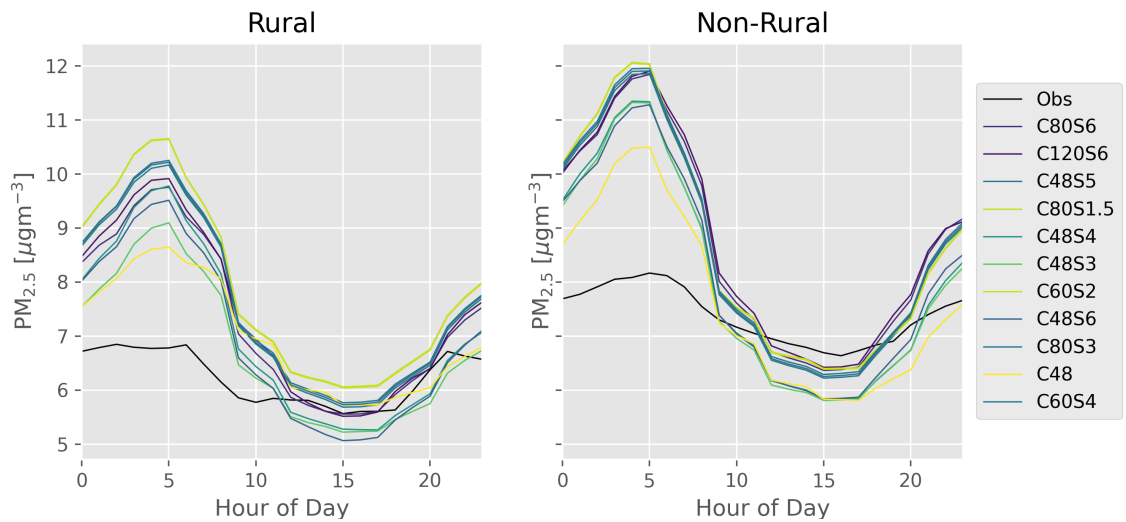
Figure 102: Mean Rural (left) and Non-Rural (right) $PM_{2.5}$ diurnal from 1st June 2021 to 31st July 2021 at C80S1.5, C48S6, C80S6, C48S5, C48S4, C48S3, C60S2, C80S3, C48, C60S4 and C120S6 (coloured lines).

Increases in Non-Rural $PM_{2.5}$ concentrations produced overestimates which were up to 17% larger than the coarsest resolution. Although the model bias was high by 18-34% at Rural sites, there was no clear relationship between resolution and bias, which may be due to the locations of the limited number of Rural sites here.
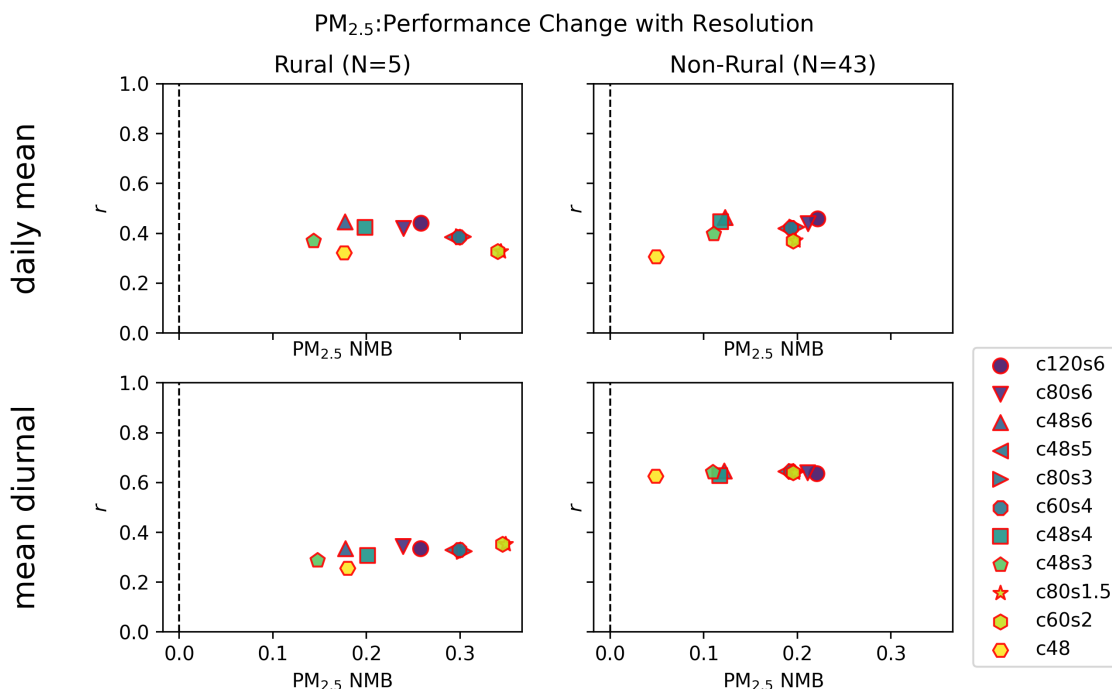
Figure 103: PM$_{2.5}$ NMB and Pearson's *r* for each model (coloured points, according to resolution) compared to observations at Rural sites (left) and Non-Rural sites (right) for daily mean (top row) and hourly mean (bottom row) measurements. NMB is optimised towards the left, and *r* towards the top, so optimal performance is at the top left of the diagram.

5.7 The relationship between emissions resolution and model-measurement NMB

The previous sections and several previous studies (e.g (Fountoukis et al., 2013)) have highlighted the importance of emissions resolution on model performance. The dilution of emissions from small sources over larger areas as the model grid becomes coarser can contribute to systematic bias for species estimates. However, the spatial heterogeneity of emissions sources can make assessing the contribution of emissions to bias challenging. To investigate how UK emissions heterogeneity varies with model resolution, we calculate an Emission Ratio, *ER*, at resolutions from 1-100 km^2, based on regridding of the 1 km^2 UK anthropogenic emissions from NAEI used as model input for the simulations (Section 5.3.2). *ER* for a given species,*S*, and site, *X*, is given by 10:

$$ER_{S,X} = \frac{E_{S,X,\text{target}}}{E_{S,X,\text{ref}}} \qquad (10)$$

where E_{target} and E_{ref} are the nearest emissions to the site at the target resolution and reference resolutions (1 km $\times$ 1 km), respectively. We conservatively regrid the NAEI emissions to each target resolution. We consider *ER* to be a metric which provides some information about the heterogeneity of emissions near a measurement site of interest. A positive *ER* indicates that for that site at the target resolution, emissions are greater than at the reference resolution. Figure 104 presents a comparison of the *ER* for NO$_x$, SO$_2$, NH$_3$ and VOCs UK anthropogenic emissions at the NO$_2$ measurement sites from 1-100 km^2.
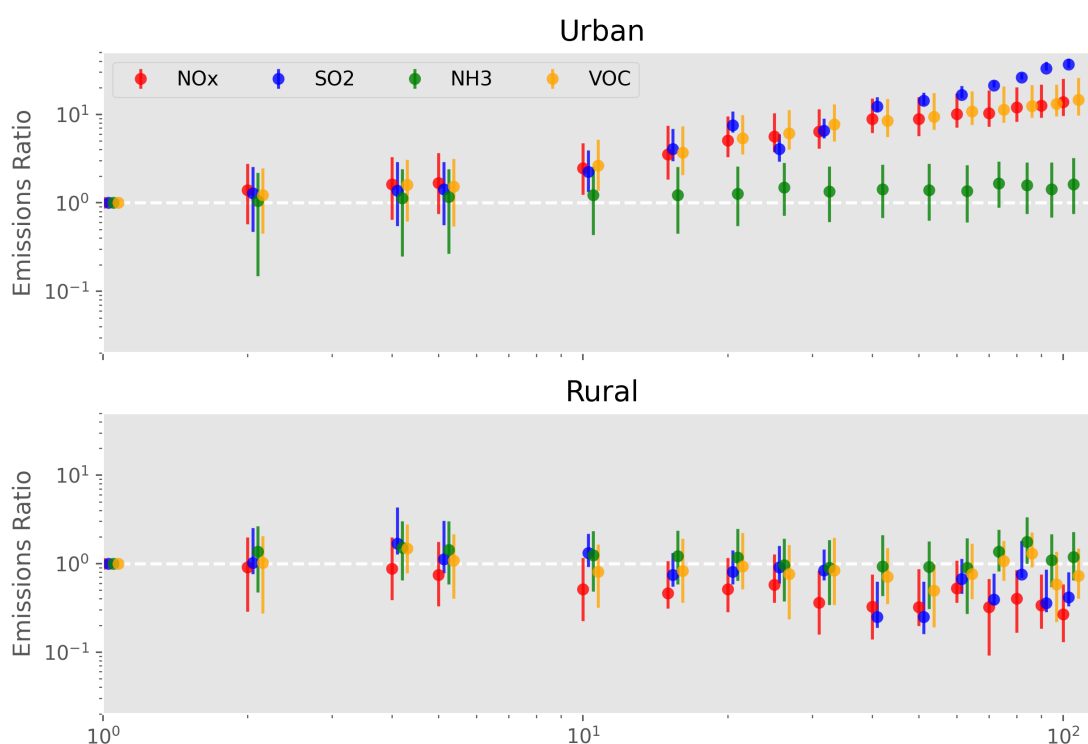
Figure 104: Emissions Ratios for NO$_x$,SO$_2$,NH$_3$ and VOCs at Urban (N=62) and Rural (N=12) NO$_2$ measurement sites, based on regridded 1 km^2 UK NAEI anthropogenic emissions. Mean averages for all the sites are the coloured points, and the vertical show the ER range for all sites at that resolution.

The trends for each species align with our understanding of their primary emission sources. For example, NH$_3$ emissions from agriculture tend to cover expansive areas, resulting in less variability as the emissions become coarser at larger resolutions. However, as detailed by Marais et al. (2021), NAEI agricultural emissions for NH$_3$ are calculated at 5 km resolution, which may explain the minimal changes seen for ER_{NH3} at the finest resolutions. On the other hand,

SO$_2$ emissions often stem from concentrated point sources such as power plants and industrial combustion. Whilst the grids of the GCHP simulations in this Chapter (Table 12) won't align perfectly with the regridded NAEI emissions here, their spatial variability should be reasonably similar. As a result, this shows the trend of how emissions local to NO$_2$ measurement sites will change with increases in model resolution: At coarse resolutions, the measurement sites are likely to experience emissions several times smaller than the "true" emissions near a site, and this represents a systematic bias in how the model emissions are represented.

We'll now relate these emission trends to the model performance changes with resolution by comparing the mean NMB for Rural and Non-Rural sites for NO, NO$_2$ and O$_3$ and PM$_{2.5}$ with the emission ratio in Figure 105. As resolution increased up to 14 km, the rate of NMB reduction decreased for NO, NO$_2$ and O$_3$. This trend was stronger at Non-Rural than at Rural environments. For a species affected by the resolution of emissions these features would be expected, and are consistent with resolution - emissions heterogeneity relationship (for NO$_x$ and VOCs) shown in Figure 104. However, the slowing of bias reductions at finer resolution suggests further resolution enhancement would bring negligible improvements. Given this, there is a threshold where other processes impacting model bias (e.g transport, diffusion, chemistry) are dominant. Whilst the assessment here did not go to such fine resolutions, the trends are consistent with the conclusions of Falasca and Curci (2018), who reported enhancement beyond 4 km horizontal resolution was not justified for simulating air quality in two cities in Italy.
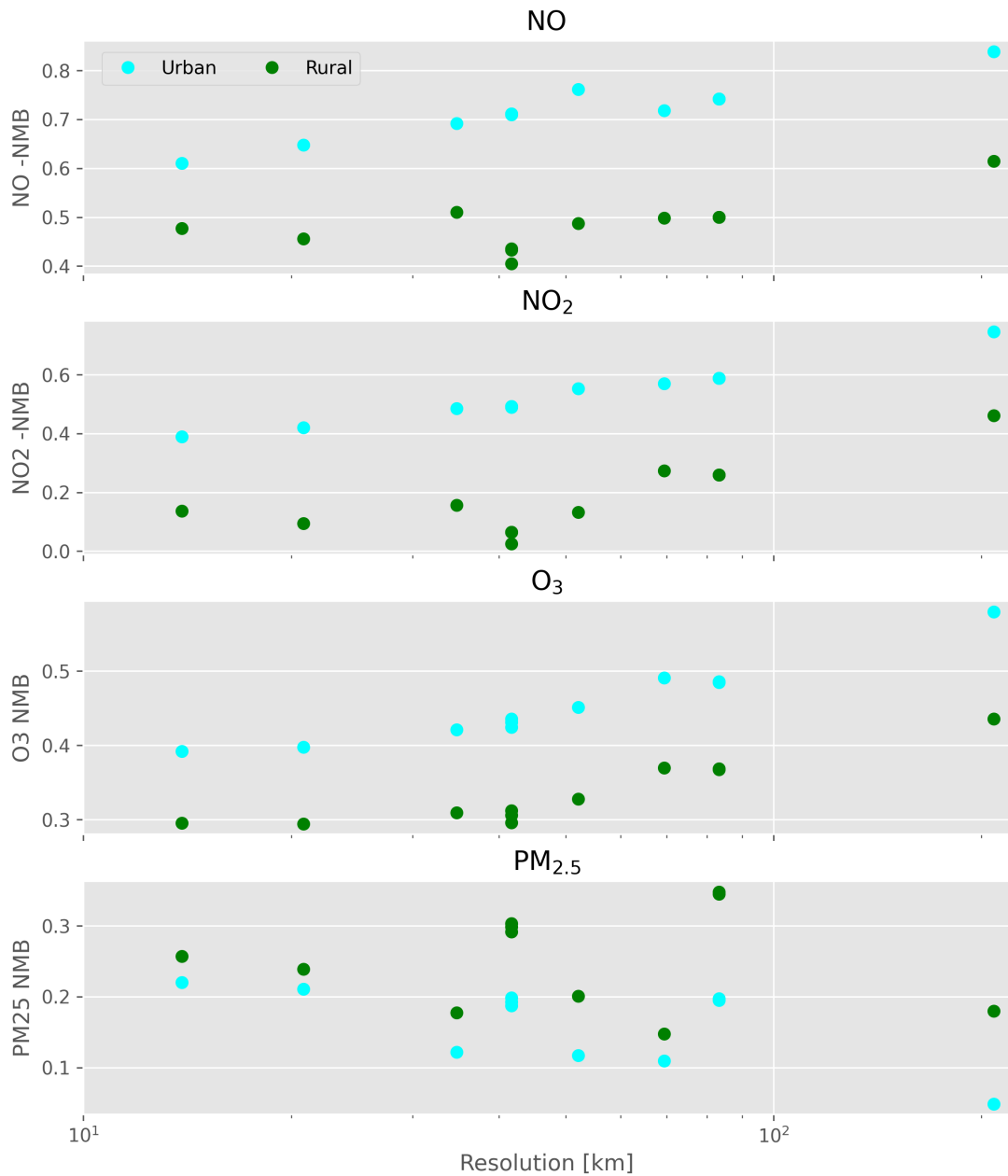
Figure 105: The resolution dependence of NMB at Non-Rural sites (cyan points) and Rural sites (green points) for NO, NO$_2$, O$_3$ and PM$_{2.5}$ from 1st June 2021 to 31st July 2021. NO, NO$_2$ and O$_3$ NMB was calculated at 11 Rural and 40 Non-Rural NO$_2$ measurement sites, and at 5 Rural and 43 Non-Rural PM$_{2.5}$ measurement sites for PM$_{2.5}$. Note: the x-axis is on a log scale, and extends farther than in Figure 104 to include NMB for the C48 simulation.

PM$_{2.5}$ doesn't show a trend similar to NO$_x$ or O$_3$ in either environment. This is likely because the variety of its sources and its chemistry leads to a less direct impact of emissions. There may be a weak trend of around 10% bias reduction in Rural sites and a small (few percent) bias increase in Non-Rural sites at finer resolutions, but the C48S3 (69 km) and C48S6 (34 km) simulations buck this trend. Overall, higher resolutions beyond 34 km seems to give benefits for NO$_x$ and O$_3$ but not for PM$_{2.5}$.

5.8   Proposing the optimal resolution for GCHP simulations

The previous sections in this chapter have highlighted some of the improvements in model-observation bias and correlations that can come from using GCHP simulations at higher resolutions. However, higher resolutions can be computationally expensive, and the improvements should be weighed against their computational costs. These costs may not be of interest for some users (e.g researchers at large institutions with large amounts of computational resources), whereas for others it may be a limiting factor. Thus, we propose a metric which aims to incorporate the cost-performance trade-offs for a given user and modelling situation, and to suggest a grid configuration. This approach is similar to that used by Philip et al. (2016) to propose optimal chemical and transport operator duration in GCClassic simulations. The cost-adjusted normalised error, CANE, is calculated as in Equation 11 for each species, s, and resolution, *x*, relative to a reference resolution, *ref*:

$$CANE = \frac{E_x^s - E_{ref}^s}{E_{ref}^s} \times \left(\frac{t_x}{t_{ref}} \right)^k \tag{11}$$

CANE is the product of the change in a given performance metric, *E*, and throughputs, *t*, for the target and reference resolutions. An additional factor, *k*, is added to account for the variable importance of throughput for a user. *k* less than 1 means throughput is less important than model bias, and above one places a greater importance on throughput. CANE has the flexibility of being able to use different metrics based on the user's goals. For example, if model-obs bias is not a priority, the user can use model-obs correlation. CANE was calculated for NO, NO$_2$

and O$_3$ with k=0.1 using NMB and r at each resolution (Figure 106). The optimal resolution with CANE$_{NMB}$ is the minimum, and with CANE$_r$ is the maximum. The recommended resolutions for each species and metric are shown in Table 15. With NMB as a metric, CANE was optimised at C120S6 (14 km, the highest resolution) for NO, NO$_2$ and O$_3$, in agreement with the NMB being minimised at the highest resolution for each of these. In contrast, the recommended resolution for PM$_{2.5}$ was C48S3 (69 km), as resolution increases tended to increase the model overestimate. With Pearson's r as a metric, CANE improved steadily for NO$_2$ as resolution increased, resulting in C120S6 (14 km) being recommended, as the relative improvements outweigh the additional throughput costs. The recommended resolutions were lower for NO (C48S5, 42 km), O$_3$ (C48S6, 35 km) and PM$_{2.5}$ (C48S6, 35 km) due to their diminishing improvements in r at even finer resolutions.

Table 15: Recommended GCHP configurations to simulate NO, NO$_2$, O$_3$ and PM$_{2.5}$ for UK observational comparisons based on optimising CANE for varying values of k, for either NMB or r

Metric	Species	k				
		0.01	0.1	0.5	1	1.5
CANE$_{NMB}$	NO	C120S6	C120S6	C48S6	C48S6	C48S6
	NO$_2$	C120S6	C80S6	C48S6	C48S6	C48S6
	O$_3$	C120S6	C80S6	C48S5	C48S5	C48S5
	PM$_{2.5}$	C48S3	C48S3	C48S3	C120S6	C120S6
CANE$_r$	NO	C48S5	C48S5	C48S5	C48S5	C48S5
	NO$_2$	C120S6	C120S6	C48S6	C48S6	C48S6
	O$_3$	C48S6	C48S6	C48S6	C48S6	C48S6
	PM$_{2.5}$	C48S6	C48S6	C48S6	C48S6	C48S6
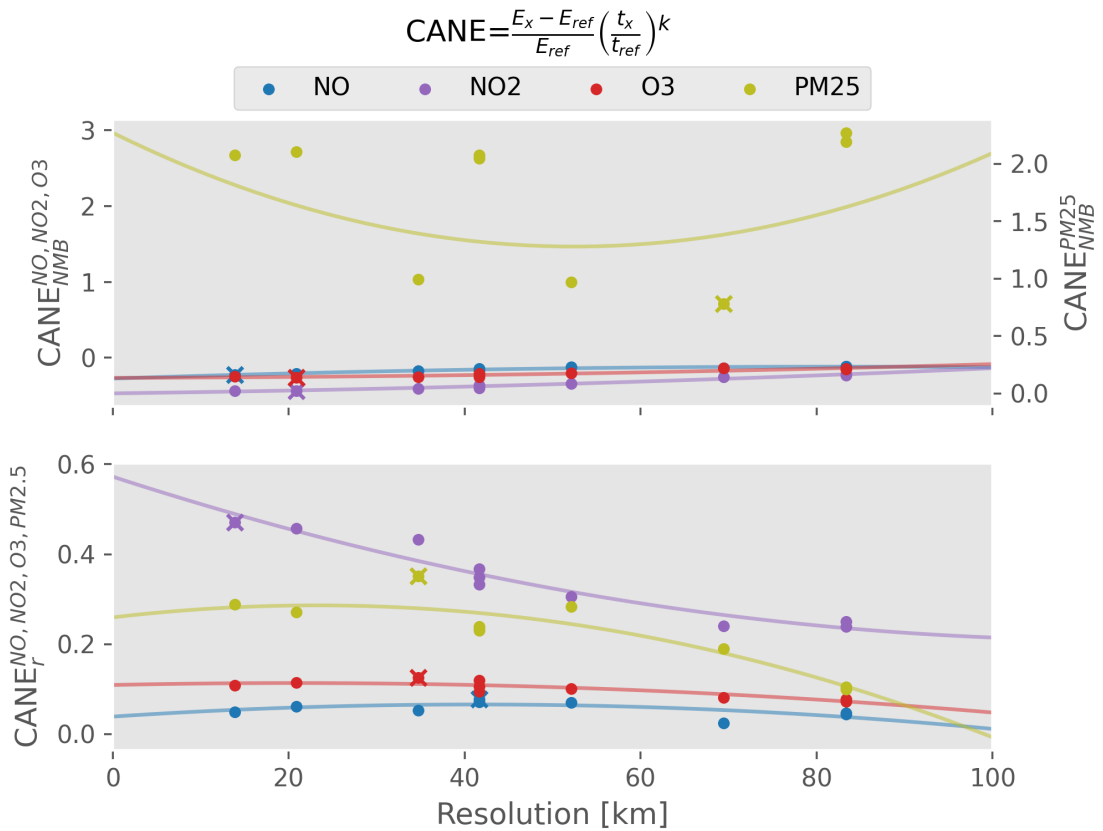
Figure 106: CANE calculated at each resolution (C48, C60S2, C80S1.5, C48S3, C48S4, C48S5, C60S4, C80S3, C48S6, C80S6, C120S6) with NMB (top panel) and r (bottom pane) for NO (blue points), NO$_2$ (purple points), O$_3$ (red points) and PM$_{2.5}$ (green points). The optimal values are highlighted with a cross. k was set to 0.1. Note: CANE should be minimised and maximised for NMB and r, respectively.

As in illustrative example, Figure 107 shows the effect of vaying k on CANE^{NO} with for NMB and r metrics. With small values of k (< 0.5), CANE found no minimum within this range of resolutions for NMB or r, which may motivate further increases in resolution before the resource costs outweigh the performance improvements.
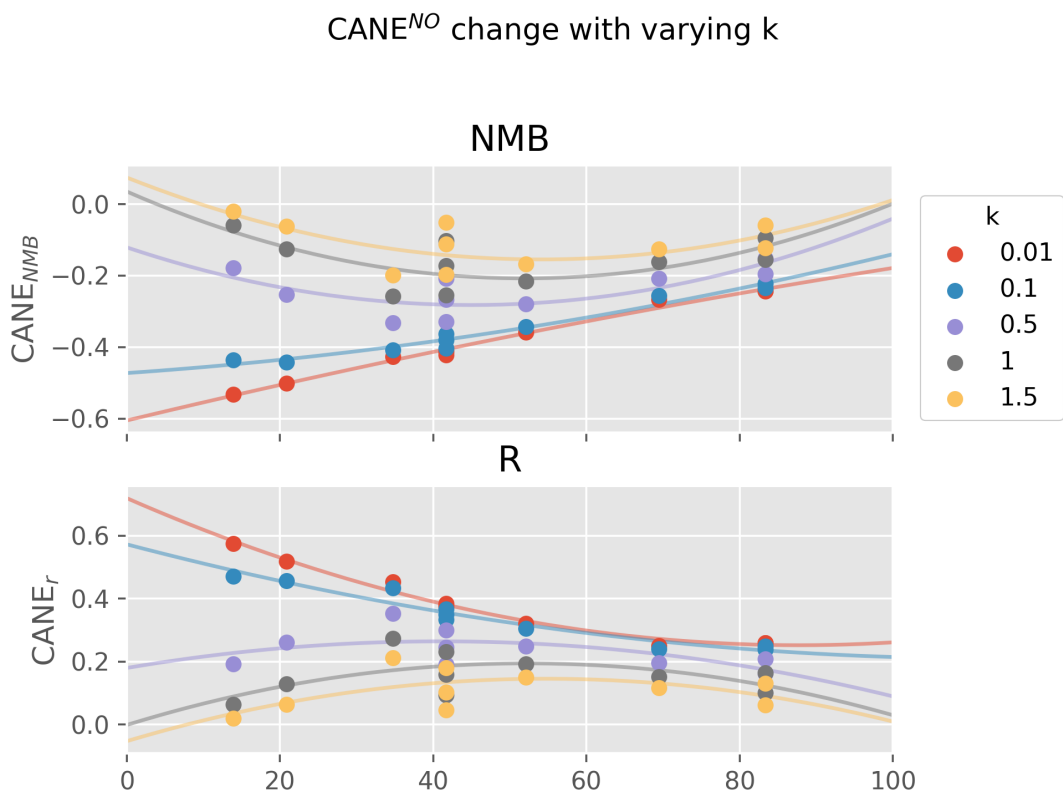
Figure 107: Change in CANE$^{NO}_{NMB}$ and CANE$^{NO}_{NMB}$ for k = 0.01, 0.1, 0.5, 1, and 1.5. For NMB (top panel) the optimum value is towards the bottom of the panel, and for *r* (bottom panel) it is towards the top of the panel. Optimum values are given in Table 15

It should be noted that the error metrics used here were determined against a sample that is inherently non-representative of the model performance over the whole of the UK as measurement sites are not spatially homogeneous, and comparisons were only made for a 2-month period. In addition, resolution sensitivities can vary seasonally (Fenech et al., 2018), so other times of year may come to different conclusions. As a result, the optimal resolutions determined using CANE will vary depending on the region of interest and sample sites available, as well as the performance metrics and chosen *k* for a user.

5.9   Conclusions

This Chapter has explored the resolution sensitivity of UK NO, NO$_2$, O$_3$ and PM$_{2.5}$ over the UK in summer 2021. Whilst there is some improvement by going to

higher resolution, it varies for different species. There are still some aspects of the model which don't improve as resolution increases, so model resolution is not an all encompassing explanation for model error.

Increasing model resolution from 208 km to 14 km reduced biases substantially in both rural and non-rural environments for NO, NO$_2$ and O$_3$. Unexpectedly, resolution increases produced larger bias reductions for NO$_2$ in Rural environments than in Non-Rural environments. Improvements in the spatial representativity of NO$_x$ emissions were responsible for the NO and NO$_x$ bias reductions. O$_3$ bias reductions at higher resolution were due to a combined effect of NO$_x$ titration enhancements and reduced O$_3$ production rates. Stock et al. (2014) proposed a similar resolution sensitivity for ozone production over Europe in the winter, where coarser models couldn't distinguish between NO$_x$ and VOC-limited environments. Whilst they found only small differences in O$_3$ production between resolutions in the summer, their comparison was limited to only one UK site and O$_3$ production regimes in the UK are not necessarily the same as the rest of continental Europe (Ivatt et al., 2022). PM$_{2.5}$ concentrations and biases increased at higher resolution, and showed a more variable resolution dependence due to its relatively complex composition. Local emission enhancements impacted BC, OC and Dust components, leading to higher concentrations, whereas concentrations of secondary inorganic aerosols decreased due to increases in the spatial segregation of their precursors. Secondary organic aerosol showed almost no change with resolution. Trends in the resolution sensitivity of NO, NO$_2$ and O$_3$ biases were similar to emissions heterogeneity trends for NO$_x$ and VOCs, but reductions become smaller at high resolutions as other processes become more important.

For NO, NO$_2$, O$_3$ and PM$_{2.5}$ correlation improvements at higher resolutions primarily impacted processes at the daily timescale. This indicates that inaccuracies in other model processes such as emissions and meteorology are important sources of error. Correlation improvements were largest for NO and NO$_2$ in Non-

Rural environments, for O$_3$ in Non-Rural environments and similar for PM$_{2.5}$ in both environments.

A new metric has been shown (CANE), which balances the trade-off between model performance and computation costs for specific use cases. It encompasses the relationship between model resolution and performance for a specific species and performance metric, whilst allowing flexibility for users with different resources available. When the objective is to minimise model bias compared to observations, CANE indicated that the highest resolution model (C120S6) was the best resolution to run with when NO, NO$_2$ and O$_3$ concentrations are of interest, whereas for PM$_{2.5}$, a coarser (C48S3, 69 km) resolution was recommended because of trade-off of increasing PM$_{2.5}$ concentrations at higher resolutions. However, if we are more concerned with how well the model is capturing changes in species over the period looked at, CANE can be calculated using correlation. In this respect, CANE proposes that the higher resolution simulations tended to be worth their resource costs for NO (C48S5),NO$_2$(C120S6),O$_3$(C48S6) and PM$_{2.5}$(C48S6). CANE proposed the finest resolution (C120S6) for NO$_2$ as correlations increased steadily at finer resolutions. Whereas for NO, O$_3$ and PM$_{2.5}$, there were still small correlation improvements at finer resolutions, but these weren't justified by the resource usage.

Further work could aim to build upon some of the limitations of this study by exploring the improvements from using even higher resolution (C720) meteorological fields. Resolution effects over the whole of the UK were often different to the effects at monitoring site locations, so future evaluations should consider that a sample of monitoring sites is likely to be unrepresentative of the whole model region. In addition, Chapter 4 proposed that there may be uncertainties with the PARANOX module for shipping emissions at $0.25° \times 0.3125°$. These uncertainties could be further exacerbated with resolution increases, and this was not explored.

6   Conclusions

This thesis has explored the modelling of UK air pollutants, specifically NO_x, O_3 and $PM_{2.5}$, with some work to look at the simulation of their precursors. It has used an offline atmospheric chemistry transport model and explored the fidelity of the base model run at a relatively high resolution (around 25km resolution), the impact of the different emission sources on UK pollutant concentrations and the impact of resolution. There are several key conclusions that can be made from this work.

GEOS-Chem is a well established atmospheric chemistry transport model. Historically it has focused on global simulations, but it is increasingly being used for regional applications, either through the nested grid or stretched grid versions. For this work both the European scale EMEP ($0.1\,^\circ \times 0.1\,^\circ$) and the UK scale NAEI ($1\,\mathrm{km} \times 1\,\mathrm{km}$) emission inventories were incorporated into the model through the HEMCO module. Although these emissions inventories provide useful information on an annual basis, they are not complete. These annual emissions need to be temporally scaled to provide the sub-hourly emissions used in the model (Figure 6). Lumped species such as VOCs need to be speciated into appropriate model tracers (Table 3). They need to be scaled vertically to provide appropriate height information (Figure 7). Rather coarse assumptions on these scalings are used to exploit these data-sets, likely adding significant uncertainties to the emissions used in the model. Much of this information is probably held by the organisations providing the emissions inventory but is not made available. It would be very useful for there to be better alignment between the groups producing these emission inventories and the modelling groups using them to ensure that appropriate information is available to fully use these inventories.

The model systematically underestimates NO_x in non-rural sites, but performs better at the rural sites (Figure 11). Previous studies have highlighted likely NO_x

underestimates in the emissions inventory. However, at the grid resolution used here, a model underestimate would seem inherent. By analysing the $1\,\mathrm{km} \times 1\,\mathrm{km}$ NAEI emissions, the NO_x emissions local to the measurement sites was found to be systematically higher than the average used in the associated model 25 km$\times$31 km model grid (Figure 104). Given the short lifetime of NO_x, a systematic underestimate of concentrations by the model would therefore seem inevitable, even if the model emissions were perfect. Care thus needs to be given to the conclusions of an underestimate in UK NOx emissions from model-measurement comparisons. Given this conclusion, process-based modelling of NO_x concentrations at a scale useful for human exposure and comparison to the observational network is likely to be difficult. Spatial scales of 1 km or smaller would seem to be needed, at least an order of magnitude finer than the simulations performed here. This will be challenging both computationally (at least 2 orders of magnitude more computationally intensive than these studies) and from the perspective of providing appropriate driving meteorology, land surface data, emissions data etc.

Non-rural O_3 concentration suffer from a similar problem to NO_x. The rapid cycling between O_3, NO and NO_2 leads to a close coupling between model errors in those species. An underestimate in NO_x concentrations will likely lead to an overestimate in O_3 concentrations due to a lack of titration of O_3 by NO. The use of O_X (O_3+NO_2) in the model-measurement comparison (Figure 40) can, to some extent, remove this sensitivity and provide an alternative perspective on the model performance for O_3.

This work again highlighted the importance of the hemispheric background concentration of O_3 flowing into the UK in determining UK O_X and O_3 concentrations, estimating 78% of the UK O_X being outside of the UK's direct control. The model low bias in the hemispheric background (Figure 37) lead to a low bias in rural sites (Figure 23). At non-rural sites this was compensated for by the NO_x resolu-

tion issue underestimating O_3 titration.

UK NO_x emissions have decreased substantially over the last few decades. If they continue to do so there are questions about how this will impact human exposure of NO_x and O_3. NO_x concentrations are strongly linked to emissions so it would seem likely that the concentration of NO_x will decrease as emissions do. The impact of O_3 is more complex. During the winter months there is little to no O_3 production over the UK, so if NO_x emissions were to continue to drop, O_3 concentrations can be expected to increase as titration is reduced. During the summer months the pattern is more complex. Figure 42 shows the diagnosed photochemical regimes seasonally. In the summer months most of the UK is in a NO_x limited regime (green), thus reductions in NO_x emissions would likely reduce O_3 concentrations. Urban areas though, such the South East of England, the Midlands, the Liverpool-Hull corridor, the Scottish central belt etc. are in a VOC limited regime (yellow and red) and so a decrease in the NO_x emissions could cause an increase in the O_3 production. Overall, on an area weighted basis, a reduction in NO_x emissions in the summertime in the UK leads to a reduction in O_3 concentrations (Figure 50). Summer UK O_3 production rates are surprisingly uncorrelated to the model resolution (once the model has reached a 100 km resolution) with most resolutions after this point simulating very similar O_3 production rates over the UK as a whole (Table 14). Locally, at the AURN site locations, higher resolutions produce lower O_3 production rates, likely reflecting many of those sites being in a VOC-limited regions. However, overall for the UK as a whole, the summer time O_3 production shows little resolution dependence.

Shipping is an important source of NO_x in coastal atmosphere and ports. The current configuration of the model uses PARANOx to process these emissions, which was designed for use in the global version of the model. In the regional version of the model, NO_x concentrations get much higher, which leads to some unusual features in the simulated O_3 response to shipping NO_x (Figure 56). It

may be that in the highly polluted marine environments around the UK this parameterization is not suitable, and it would be better to direct emitt shipping NO_x into the atmosphere rather than parameterizing it with PARANOx.

The model overestimates $PM_{2.5}$ (Figure 26), with much of this associated with an overestimate in sulfate, nitrate and ammonium (Figure 28). Ammonia concentrations do not correlate well in the model against observations (Figure 21) but average modelled concentrations appear consistent with observations (Figure 22). Previous studies have suggested an overestimate in the sulfur emissions in the model. The model shows overestimates at some sites (Figure 13) but overall there is a good level of consistency between average concentration in the model and observations (Figure 14). Altering the emission height of the industrial component of SO_2 emissions reduces SO_2 concentration in the model but did little to reduce the positive bias for sulfate or $PM_{2.5}$ (Figure 41). The chemistry and physics of the inorganic aerosol is complex and it is unclear whether this bias is due to errors in the emissions of precursors, their chemical processing, the partitioning of material between the gas and aerosol phase, or the loss of aerosol to clouds and the surface.

The UK has proposed a bill aiming to move its $PM_{2.5}$ standard to an annual average of 10 μgm^{-3} (`https://bills.parliament.uk/bills/3161`; last access 18/01/2024), with the WHO suggesting 5 μgm^{-3} as a target. These concentrations are challenging for the UK to achieve. On an area weighted basis, the modelled UK average $PM_{2.5}$ is below the 10 μgm^{-3} limit but above the 5 μgm^{-3} limit (Figure 60). However, on a population weighted basis the UK violates both standards (Figure 61). Reductions in emissions on either a UK or EU basis lead to a reduction in exposure, however substantial reductions are required to get to compliance with the 5 μgm^{-3} standard. Switching off UK anthropogenic emissions entirely in the model only reduces the fraction of the population exceeding the 5 μgm^{-3} standard from 95% to 69% (Figure 67). Switching off both the

UK's anthropogenic and agricultural emissions moves that number to 27% with a substantial fraction of those people in areas exceeding the standard being in the South East of England. A pan-European effort on both anthropogenic and agriculture would though lead to complete compliance. Reductions on this scale would however have significant impacts on society.

$PM_{2.5}$ concentrations tended to increase at higher resolutions at both Rural and Non-Rural sites, but with a weaker resolution sensitivity than NO_x and O_3 due to contrasting responses of its components. Whilst higher resolutions tended to increase model $PM_{2.5}$ bias, correlation with measurements continued to improve as resolution increased up to 14 km.

6.1   Future steps in understanding UK air quality

Measurements from Urban Traffic sites have been excluded here as the high local emissions were poorly represented in simulations at comparatively coarse resolutions. However, higher resolution simulations might more accurately capture the conditions in these environments. This may be achievable with simulations using the highest resolution meteorology currently available for GCHP (C720, 12 km^2), or with online approaches for meteorology such as WRF-GC (Lin et al., 2020). Resolution increases gave minimal improvements to model diurnal performance in Chapter 5, and would indicate other sources of model error are responsible. Further work to establish these sources could make use of measurements for additional species. In particular, measurements of OH and HO_2 from recent measurement campaigns in Manchester as part of the Integrated Research Observation System for Clean Air (OSCA) project (`https://gtr.ukri.org/projects?ref=NE%2FT001984%2F1`; last access 17/09/2023) could provide valuable insights into the underlying causes of model error.

Supporting Figures for Chapter 4
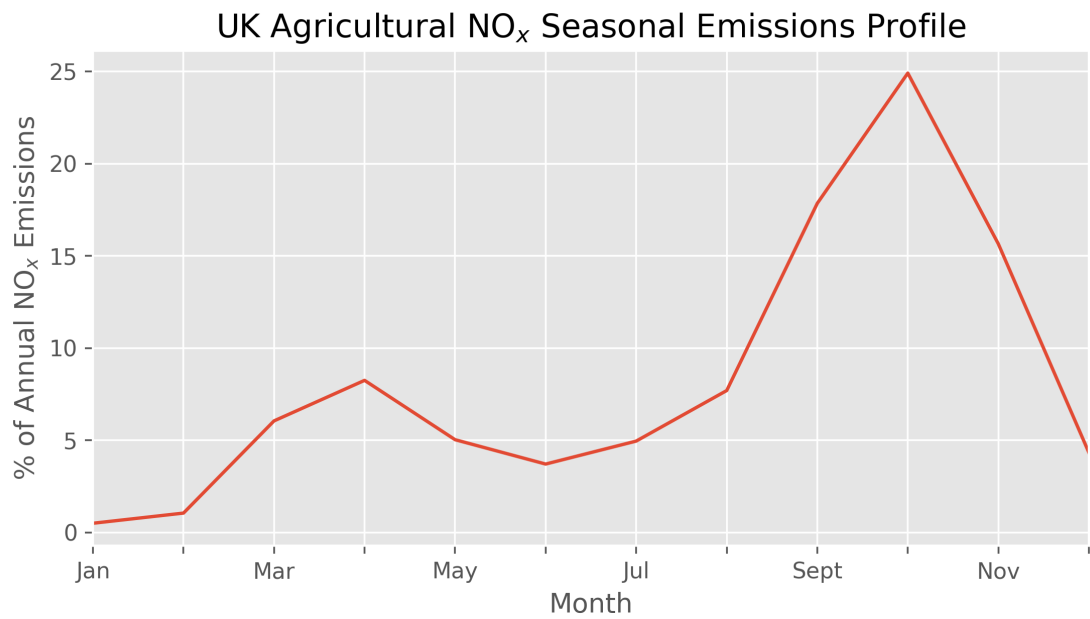
Figure 108: Model input seasonality for NO_x emissions from agriculture in 2017
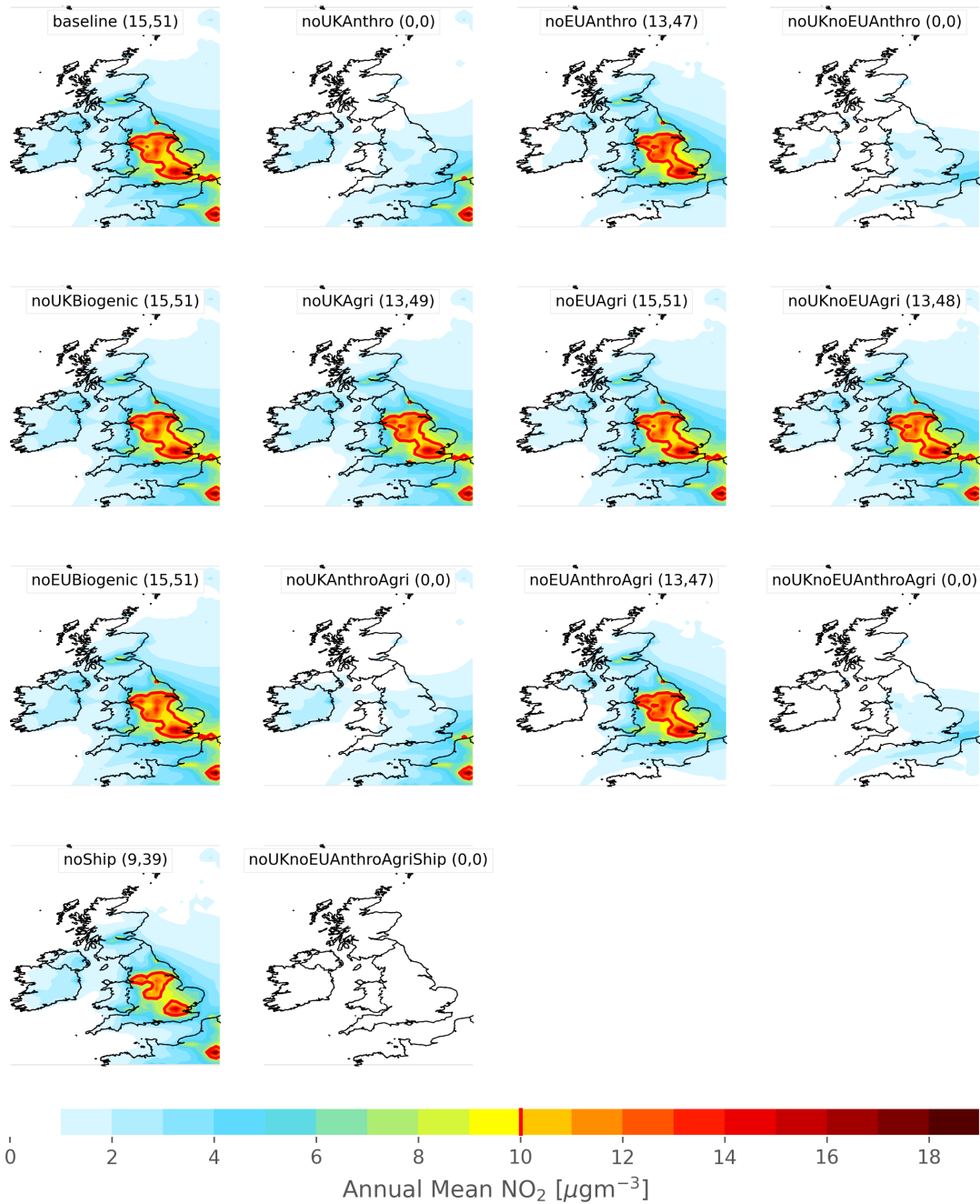
Figure 109: NO$_2$ exceedances of the WHO guideline for each emission scenario.. The number in brackets indicates the percentage of the UK area exceeding the WHO 10 μgm^{-3} guideline for NO$_2$. The red contour distinguishes the boundary between area's exceeding and below the guideline.

Supporting Tables for Chapter 4

Table 16: Change in Annual Mean and Peak Season O_3 concentration at Mace Head for each scenario compared to the model baseline, in μgm^{-3}. For reference, concentrations in the baseline were 63.06 μgm^{-3} and 135.36 μgm^{-3} for annual mean and peak season, respectively.

	Annual Mean	Peak Season
noUKAnthro	0.09 (-0.15%)	-0.18 (-0.27%)
noEUAnthro	-1.55 (-2.46%)	-1.89 (-2.79%)
noUKnoEUAnthro	-1.91 (-3.02%)	-2.38 (-3.51%)
noUKBiogenic	-0.09 (-0.14%)	-0.10 (-0.15%)
noUKAgri	0.03 (0.04%)	0.04 (0.06%)
noEUAgri	0.36 (0.58%)	0.34 (0.50%)
noUKnoEUAgri	0.44 (0.70%)	0.43 (0.64%)
noShip	-1.33 (-2.11%)	-2.23 (-3.30%)
noEUBiogenic	-0.58 (-0.93%)	-0.63 (-0.93%)
noUKAnthroAgri	-0.09 (-0.14%)	-0.18 (-0.26%)
noEUAnthroAgri	-1.63 (-2.58%)	-2.02 (-2.99%)
noUKnoEUAnthroAgri	-2.11 (-3.34%)	-2.65 (-3.91%)
noUKnoEUAnthroAgriShip	-4.35 (-6.89%)	-5.71 (-8.43%)

Table 17: Annual mean area and population weighted absolute, minimum, maximum and percentage O_3 changes over the UK for each emission scenario compared to the baseline

Species (units)	Scenario	Area Weighted ΔConc. (min-max)	Δ%	Population Weighted ΔConc. (min-max)	Δ(%)
O_3 (μgm^{-3})	noUKAnthro	3.32 (-0.17-14.97)	7.18	7.16 (-0.03-352.88)	16.52
	noEUAnthro	-1.74 (-2.16–0.47)	-3.37	-1.63 (-37.64-0.01)	-3.55
	noUKnoEUAnthro	1.36 (-2.38-13.27)	3.40	5.37 (-2.20-312.89)	12.63
	noUKBiogenic	-0.34 (-0.75–0.08)	-0.69	-0.47 (-15.71–0.00)	-1.05
	noEUBiogenic	-0.88 (-1.76–0.60)	-1.74	-0.96 (-29.15–0.00)	-2.11
	noUKAgri	0.24 (0.05-0.56)	0.50	0.30 (0.00-7.60)	0.66
	noEUAgri	0.39 (0.27-0.77)	0.77	0.38 (0.00-10.11)	0.84
	noUKnoEUAgri	0.70 (0.49-1.16)	1.39	0.74 (0.00-18.98)	1.62
	noUKAnthroAgri	3.40 (-0.18-15.07)	7.35	7.29 (-0.03-355.24)	16.80
	noEUAnthroAgri	-2.03 (-2.57–0.51)	-3.94	-1.93 (-45.20-0.00)	-4.21
	noUKnoEUAnthroAgri	1.02 (-2.90-12.89)	2.74	5.06 (-3.28-303.84)	11.95
	noShip	0.83 (-1.82-6.63)	1.88	2.00 (-1.31-51.67)	4.56
	noUKnoEUAnthroAgriShip	-0.33 (-6.99-12.01)	0.25	4.33 (-9.90-283.12)	10.48

Species (units)	Scenario	Area Weighted		Population Weighted	
		ΔConc. (min-max)	Δ%	ΔConc. (min-max)	Δ(%)
$O_X(\mu gm^{-3})$	noUKAnthro	-0.67 (-1.37-0.43)	-1.18	-0.65 (-20.99-2.16)	-1.16
	noEUAnthro	-2.04 (-2.40–1.70)	-3.56	-2.00 (-52.25–0.00)	-3.56
	noUKnoEUAnthro	-2.95 (-3.65–1.46)	-5.18	-2.86 (-78.33–0.00)	-5.10
	noUKBiogenic	-0.31 (-0.69–0.07)	-0.54	-0.43 (-14.92–0.00)	-0.77
	noEUBiogenic	-0.85 (-1.60–0.59)	-1.48	-0.92 (-28.72–0.00)	-1.64
	noUKAgri	0.10 (0.02-0.23)	0.18	0.13 (0.00-4.18)	0.22
	noEUAgri	0.35 (0.17-0.53)	0.61	0.35 (0.00-10.09)	0.63
	noUKnoEUAgri	0.51 (0.25-0.83)	0.90	0.54 (0.00-15.75)	0.96
	noUKAnthroAgri	-0.75 (-1.51-0.45)	-1.31	-0.72 (-23.54-2.18)	-1.28
	noEUAnthroAgri	-2.36 (-2.84–1.88)	-4.13	-2.33 (-60.76–0.00)	-4.16
	noUKnoEUAnthroAgri	-3.49 (-4.30–1.73)	-6.11	-3.40 (-92.90–0.00)	-6.06
	noShip	0.10 (-2.38-3.56)	0.21	0.89 (-2.22-28.91)	1.62
	noUKnoEUAnthroAgriShip	-5.50 (-8.11–1.74)	-9.61	-5.26 (-141.00–0.00)	-9.35

Table 18: Annual mean area and population weighted absolute, minimum, maximum and percentage $PM_{2.5}$ changes over the UK for each emission scenario compared to the baseline

Species (units)	Scenario	Area Weighted ΔConc. (min-max)	Δ%	Population Weighted ΔConc. (min-max)	Δ(%)
$PM_{2.5}(\mu gm^{-3})$	noUKAnthro	-2.32 (-5.02–0.34)	-30.89	-3.36 (-113.44–0.00)	-37.41
	noEUAnthro	-1.31 (-3.27–0.47)	-18.57	-1.62 (-53.51–0.00)	-18.29
	noUKnoEUAnthro	-3.72 (-7.12–0.88)	-50.83	-5.05 (-167.95–0.00)	-56.69
	noUKBiogenic	-0.03 (-0.06–0.00)	-0.40	-0.04 (-1.41–0.00)	-0.47
	noEUBiogenic	-0.06 (-0.19–0.01)	-0.73	-0.08 (-3.07–0.00)	-0.88
	noUKAgri	-1.33 (-2.92–0.17)	-18.26	-1.65 (-39.16–0.00)	-18.71
	noEUAgri	-0.82 (-2.43–0.33)	-11.81	-0.99 (-32.15–0.00)	-11.26
	noUKnoEUAgri	-2.40 (-4.43–0.59)	-33.54	-2.92 (-77.89–0.00)	-33.30
	noUKAnthroAgri	-3.04 (-6.13–0.48)	-40.63	-4.32 (-137.69–0.00)	-48.30
	noEUAnthroAgri	-1.71 (-4.49–0.63)	-24.41	-2.11 (-68.63–0.00)	-23.89
	noUKnoEUAnthroAgri	-4.68 (-9.01–1.08)	-63.95	-6.35 (-204.60–0.00)	-71.30
	noShip	-0.85 (-2.00–0.19)	-11.82	-1.12 (-29.62–0.00)	-12.76
	noUKnoEUAnthroAgriShip	-4.93 (-9.46–1.18)	-67.44	-6.67 (-213.55–0.00)	-74.89

Table 19: Annual mean area and population weighted absolute, minimum, maximum and percentage NO_3^- aerosol changes over the UK for each emission scenario compared to the baseline

Species (units)	Scenario	Area Weighted		Population Weighted	
		ΔConc. (min-max)	Δ%	ΔConc. (min-max)	Δ(%)
NO_3^- (μgm^{-3})	noUKAnthro	-0.45 (-0.85–0.09)	-28.65	-0.57 (-18.90–0.00)	-28.46
	noEUAnthro	-0.35 (-0.84–0.10)	-22.91	-0.45 (-15.34–0.00)	-22.40
	noUKnoEUAnthro	-0.80 (-1.51–0.20)	-52.35	-1.01 (-33.41–0.00)	-50.63
	noUKBiogenic	0.00 (-0.02-0.01)	0.22	-0.01 (-0.39-0.04)	-0.27
	noEUBiogenic	-0.02 (-0.08-0.00)	-0.95	-0.03 (-1.26-0.00)	-1.44
	noUKAgri	-0.55 (-1.11–0.08)	-35.83	-0.64 (-14.52–0.00)	-32.71
	noEUAgri	-0.41 (-1.29–0.17)	-27.68	-0.49 (-16.04–0.00)	-24.64
	noUKnoEUAgri	-1.08 (-2.24–0.30)	-71.43	-1.28 (-34.04–0.00)	-64.90
	noUKAnthroAgri	-0.82 (-1.52–0.16)	-52.29	-1.08 (-32.19–0.00)	-54.43
	noEUAnthroAgri	-0.56 (-1.52–0.18)	-37.09	-0.70 (-23.26–0.00)	-35.14
	noUKnoEUAnthroAgri	-1.33 (-2.67–0.31)	-85.25	-1.73 (-54.10–0.00)	-86.52
	noShip	-0.39 (-0.97–0.08)	-24.36	-0.53 (-14.87–0.00)	-26.51
	noUKnoEUAnthroAgriShip	-1.46 (-2.92–0.35)	-93.65	-1.91 (-59.34–0.00)	-95.38

Table 20: Annual mean area and population weighted absolute, minimum, maximum and percentage NH_4^+ changes over the UK for each emission scenario compared to the baseline

Species (units)	Scenario	Area Weighted		Population Weighted	
		ΔConc. (min-max)	Δ%	ΔConc. (min-max)	Δ(%)
NH_4^+ (μgm^{-3})	noUKAnthro	-0.25 (-0.58–0.04)	-35.71	-0.35 (-10.95–0.00)	-39.24
	noEUAnthro	-0.16 (-0.37–0.05)	-24.83	-0.20 (-6.31–0.00)	-22.77
	noUKnoEUAnthro	-0.43 (-0.80–0.10)	-63.82	-0.56 (-17.54–0.00)	-64.39
	noUKBiogenic	0.00 (-0.00-0.00)	0.17	-0.00 (-0.09-0.01)	-0.12
	noEUBiogenic	-0.00 (-0.02-0.00)	-0.51	-0.01 (-0.30-0.00)	-0.78
	noUKAgri	-0.26 (-0.60–0.03)	-38.18	-0.33 (-7.85–0.00)	-37.88
	noEUAgri	-0.14 (-0.42–0.06)	-23.18	-0.17 (-5.62–0.00)	-20.45
	noUKnoEUAgri	-0.46 (-0.85–0.11)	-68.81	-0.56 (-14.71–0.00)	-64.94
	noUKAnthroAgri	-0.38 (-0.84–0.06)	-55.10	-0.52 (-15.31–0.00)	-59.48
	noEUAnthroAgri	-0.23 (-0.55–0.08)	-36.00	-0.28 (-8.85–0.00)	-32.61
	noUKnoEUAnthroAgri	-0.60 (-1.11–0.14)	-88.94	-0.78 (-23.81–0.00)	-90.36
	noShip	-0.12 (-0.26–0.02)	-18.64	-0.16 (-4.03–0.00)	-18.41
	noUKnoEUAnthroAgriShip	-0.63 (-1.16–0.15)	-93.92	-0.83 (-25.07–0.00)	-95.27

Table 21: Annual mean area and population weighted absolute, minimum, maximum and percentage SO_4^{2-} changes over the UK for each emission scenario compared to the baseline

Species (units)	Scenario	Area Weighted		Population Weighted	
		ΔConc. (min-max)	Δ%	ΔConc. (min-max)	Δ(%)
SO_4^{2-} (μgm^{-3})	noUKAnthro	-0.27 (-0.87–0.04)	-39.01	-0.40 (-11.94–0.00)	-48.69
	noEUAnthro	-0.13 (-0.29–0.06)	-21.83	-0.15 (-4.50–0.00)	-19.98
	noUKnoEUAnthro	-0.44 (-1.06–0.11)	-66.03	-0.59 (-17.46–0.00)	-73.89
	noUKBiogenic	0.00 (-0.00-0.00)	0.06	0.00 (-0.00-0.01)	0.05
	noEUBiogenic	0.00 (-0.00-0.00)	0.02	0.00 (-0.00-0.02)	0.06
	noUKAgri	-0.20 (-0.63–0.02)	-27.70	-0.28 (-7.55–0.00)	-34.45
	noEUAgri	-0.07 (-0.15–0.02)	-10.99	-0.09 (-2.83–0.00)	-11.18
	noUKnoEUAgri	-0.28 (-0.74–0.04)	-41.62	-0.39 (-10.77–0.00)	-48.35
	noUKAnthroAgri	-0.30 (-0.90–0.04)	-42.87	-0.43 (-12.66–0.00)	-52.62
	noEUAnthroAgri	-0.16 (-0.31–0.07)	-25.42	-0.18 (-5.34–0.00)	-23.60
	noUKnoEUAnthroAgri	-0.46 (-1.08–0.11)	-69.06	-0.61 (-18.07–0.00)	-76.67
	noShip	-0.05 (-0.13-0.03)	-8.76	-0.04 (-0.62-0.09)	-5.42
	noUKnoEUAnthroAgriShip	-0.48 (-1.10–0.13)	-73.49	-0.63 (-18.49–0.00)	-79.79

Table 22: Annual mean area and population weighted absolute, minimum, maximum and percentage Sea Salt changes over the UK for each emission scenario compared to the baseline

| Species (units) | Scenario | Area Weighted | | Population Weighted | |
		ΔConc. (min-max)	Δ%	ΔConc. (min-max)	Δ(%)
Sea Salt(μgm^{-3})	noUKAnthro	0.00 (0.00-0.00)	0.00	0.00 (0.00-0.00)	0.00
	noEUAnthro	0.00 (0.00-0.00)	0.00	0.00 (0.00-0.00)	0.00
	noUKnoEUAnthro	0.00 (0.00-0.00)	0.00	0.00 (0.00-0.00)	0.00
	noUKBiogenic	0.00 (0.00-0.00)	0.00	0.00 (0.00-0.00)	0.00
	noEUBiogenic	0.00 (0.00-0.00)	0.00	0.00 (0.00-0.00)	0.00
	noUKAgri	0.00 (0.00-0.00)	0.00	0.00 (0.00-0.00)	0.00
	noEUAgri	0.00 (0.00-0.00)	0.00	0.00 (0.00-0.00)	0.00
	noUKnoEUAgri	0.00 (-0.00-0.00)	0.00	0.00 (-0.00-0.00)	0.00
	noUKAnthroAgri	0.00 (0.00-0.00)	0.00	0.00 (0.00-0.00)	0.00
	noEUAnthroAgri	0.00 (0.00-0.00)	0.00	0.00 (0.00-0.00)	0.00
	noUKnoEUAnthroAgri	0.00 (0.00-0.00)	0.00	0.00 (0.00-0.00)	0.00
	noShip	0.00 (0.00-0.00)	0.00	0.00 (0.00-0.00)	0.00
	noUKnoEUAnthroAgriShip	0.00 (0.00-0.00)	0.00	0.00 (0.00-0.00)	0.00

Table 23: Annual mean area and population weighted absolute, minimum, maximum and percentage BC changes over the UK for each emission scenario compared to the baseline

Species (units)	Scenario	Area Weighted		Population Weighted	
		ΔConc. (min-max)	$\Delta\%$	ΔConc. (min-max)	$\Delta(\%)$
BC(μgm^{-3})	noUKAnthro	-0.14 (-0.37–0.01)	-65.98	-0.23 (-8.61–0.00)	-74.86
	noEUAnthro	-0.04 (-0.13–0.02)	-25.03	-0.06 (-1.81–0.00)	-19.19
	noUKnoEUAnthro	-0.19 (-0.44–0.03)	-91.58	-0.29 (-10.44–0.00)	-94.40
	noUKBiogenic	0.00 (0.00-0.00)	0.00	0.00 (0.00-0.00)	0.00
	noEUBiogenic	0.00 (0.00-0.00)	0.00	0.00 (0.00-0.00)	0.00
	noUKAgri	-0.00 (-0.01–0.00)	-2.02	-0.00 (-0.11–0.00)	-1.70
	noEUAgri	-0.00 (-0.01–0.00)	-1.07	-0.00 (-0.07–0.00)	-0.78
	noUKnoEUAgri	-0.01 (-0.01–0.00)	-3.11	-0.01 (-0.18–0.00)	-2.49
	noUKAnthroAgri	-0.15 (-0.37–0.01)	-68.01	-0.24 (-8.72–0.00)	-76.56
	noEUAnthroAgri	-0.05 (-0.14–0.02)	-26.09	-0.06 (-1.88–0.00)	-19.96
	noUKnoEUAnthroAgri	-0.19 (-0.45–0.03)	-94.69	-0.30 (-10.62–0.00)	-96.89
	noShip	-0.02 (-0.06–0.00)	-9.90	-0.03 (-0.71–0.00)	-9.26
	noUKnoEUAnthroAgriShip	-0.19 (-0.45–0.03)	-95.39	-0.30 (-10.64–0.00)	-97.25

Table 24: Annual mean area and population weighted absolute, minimum, maximum and percentage OC changes over the UK for each emission scenario compared to the baseline

Species (units)	Scenario	Area Weighted		Population Weighted	
		ΔConc. (min-max)	Δ%	ΔConc. (min-max)	Δ(%)
OC(μgm^{-3})	noUKAnthro	-0.30 (-0.75–0.03)	-61.85	-0.49 (-17.70–0.00)	-71.45
	noEUAnthro	-0.10 (-0.30–0.04)	-24.04	-0.12 (-4.00–0.00)	-19.37
	noUKnoEUAnthro	-0.41 (-0.92–0.07)	-86.40	-0.61 (-21.76–0.00)	-91.15
	noUKBiogenic	0.00 (0.00-0.00)	0.00	0.00 (0.00-0.00)	0.00
	noEUBiogenic	0.00 (0.00-0.00)	0.00	0.00 (0.00-0.00)	0.00
	noUKAgri	-0.01 (-0.02–0.00)	-1.76	-0.01 (-0.22–0.00)	-1.55
	noEUAgri	-0.00 (-0.01–0.00)	-0.93	-0.00 (-0.14–0.00)	-0.71
	noUKnoEUAgri	-0.01 (-0.02–0.00)	-2.71	-0.01 (-0.37–0.00)	-2.26
	noUKAnthroAgri	-0.31 (-0.76–0.03)	-63.61	-0.50 (-17.92–0.00)	-73.00
	noEUAnthroAgri	-0.10 (-0.30–0.04)	-24.96	-0.13 (-4.14–0.00)	-20.07
	noUKnoEUAnthroAgri	-0.42 (-0.94–0.07)	-89.11	-0.63 (-22.13–0.00)	-93.41
	noShip	-0.04 (-0.14–0.01)	-9.82	-0.06 (-1.69–0.00)	-9.84
	noUKnoEUAnthroAgriShip	-0.42 (-0.94–0.07)	-89.32	-0.63 (-22.14–0.00)	-93.53

References

AEA Group: Automatic Urban & Rural Network: Assessment of Siting Criteria, 2009.

Aguado, E. and Burt, J.: Understanding Weather and Climate, Pearson, URL `https://books.google.co.uk/books?id=zOE2ygAACAAJ`, 2013.

Ahsan, H., Wang, H., Wu, J., Wu, M., Smith, S. J., Bauer, S., Suchyta, H., Olivié, D., Myhre, G., Matsui, H., Bian, H., Lamarque, J.-F., Carslaw, K., Horowitz, L., Regayre, L., Chin, M., Schulz, M., Skeie, R. B., Takemura, T., and Naik, V.: The Emissions Model Intercomparison Project (Emissions-MIP): quantifying model sensitivity to emission characteristics, EGUsphere, pp. 1–29, https://doi.org/10.5194/egusphere-2023-604, URL `https://egusphere.copernicus.org/preprints/2023/egusphere-2023-604/`, publisher: Copernicus GmbH, 2023.

Alexander, B., Park, R. J., Jacob, D. J., Li, Q. B., Yantosca, R. M., Savarino, J., Lee, C. C. W., and Thiemens, M. H.: Sulfate formation in sea-salt aerosols: Constraints from oxygen isotopes, Journal of Geophysical Research: Atmospheres, 110, https://doi.org/10.1029/2004JD005659, URL `https://onlinelibrary.wiley.com/doi/abs/10.1029/2004JD005659`, _eprint: https://onlinelibrary.wiley.com/doi/pdf/10.1029/2004JD005659, 2005.

Amos, H. M., Jacob, D. J., Holmes, C. D., Fisher, J. A., Wang, Q., Yantosca, R. M., Corbitt, E. S., Galarneau, E., Rutter, A. P., Gustin, M. S., Steffen, A., Schauer, J. J., Graydon, J. A., Louis, V. L. S., Talbot, R. W., Edgerton, E. S., Zhang, Y., and Sunderland, E. M.: Gas-particle partitioning of atmospheric Hg(II) and its effect on global mercury deposition, Atmospheric Chemistry and Physics, 12, 591–603, https://doi.org/10.5194/acp-12-591-2012, URL `https://acp.copernicus.org/articles/12/591/2012/acp-12-591-2012.html`, publisher: Copernicus GmbH, 2012.

Andreae, M. O. and Rosenfeld, D.: Aerosol–cloud–precipitation interactions. Part 1. The nature and sources of cloud-active aerosols, Earth-Science Reviews,

89, 13–41, https://doi.org/10.1016/j.earscirev.2008.03.001, URL `https://www.sc iencedirect.com/science/article/pii/S0012825208000317`, 2008.

Aneja, V. P., Roelle, P. A., Murray, G. C., Southerland, J., Erisman, J. W., Fowler, D., Asman, W. A. H., and Patni, N.: Atmospheric nitrogen compounds II: emissions, transport, transformation, deposition and assessment, Atmospheric Environment, 35, 1903–1911, https://doi.org/10.1016/S1352-2310(00)00543-4, URL `https://www.sciencedirect.com/science/article/pii/S135223100000543 4`, 2001.

Aneja, V. P., Schlesinger, W. H., and Erisman, J. W.: Farming pollution, Nature Geoscience, 1, 409–411, publisher: Nature Publishing Group UK London, 2008.

AQEG: Measurements of isoprene at UK sites-anthropogenic and biogenic contributions, `https://uk-air.defra.gov.uk/assets/documents/reports/cat 11/0903231104_Monitoring-Data-Mike-Jenkin.pdf`, accessed: 2022-06-21, 2009.

AQEG: Mitigation of United Kingdom PM2.5 Concentrations, Tech. rep., DEFRA, URL `https://uk-air.defra.gov.uk/assets/documents/reports/cat11/150 8060903_DEF-PB14161_Mitigation_of_UK_PM25.pdf`, 2015.

AQEG: Ozone in the UK: Recent Trends and Future Projections, `https://uk-air .defra.gov.uk/assets/documents/reports/cat09/2112200932_Ozone_in_t he_UK_Recent_Trends_and_Future_Projections.pdf`, accessed: 2023-03-07, 2021.

AQEG: Air Pollution in the UK 2021-Compliance Assessment Summary, `https: //uk-air.defra.gov.uk/library/annualreport/assets/documents/annual report/air_pollution_uk_2021_Compliance_Assessment_Summary_Issue1. pdf`, accessed: 2023-03-07, 2022.

Atkinson, R.: Atmospheric chemistry of VOCs and NOx, Atmospheric Environment, 34, 2063–2101, https://doi.org/10.1016/S1352-2310(99)00460-4, URL `ht`

tps://www.sciencedirect.com/science/article/pii/S1352231099004604, 2000.

Bates, K. H. and Jacob, D. J.: A new model mechanism for atmospheric oxidation of isoprene: global effects on oxidants, nitrogen oxides, organic products, and secondary organic aerosol, Atmospheric Chemistry and Physics, 19, 9613–9640, 2019.

Bates, K. H., Jacob, D. J., Wang, S., Hornbrook, R. S., Apel, E. C., Kim, M. J., Millet, D. B., Wells, K. C., Chen, X., Brewer, J. F., and others: The global budget of atmospheric methanol: new constraints on secondary, oceanic, and terrestrial sources, Journal of Geophysical Research: Atmospheres, 126, e2020JD033 439, publisher: Wiley Online Library, 2021.

Behera, S. N. and Sharma, M.: Investigating the potential role of ammonia in ion chemistry of fine particulate matter formation for an urban environment, Science of The Total Environment, 408, 3569–3575, https://doi.org/10.1016/j.sc itotenv.2010.04.017, URL https://www.sciencedirect.com/science/article/ pii/S0048969710003955, 2010.

Behera, S. N., Sharma, M., Aneja, V. P., and Balasubramanian, R.: Ammonia in the atmosphere: a review on emission sources, atmospheric chemistry and deposition on terrestrial bodies, Environmental Science and Pollution Research, 20, 8092–8131, https://doi.org/10.1007/s11356-013-2051-9, URL https://doi.org/10.1007/s11356-013-2051-9, 2013.

Bey, I., Jacob, D. J., Yantosca, R. M., Logan, J. A., Field, B. D., Fiore, A. M., Li, Q., Liu, H. Y., Mickley, L. J., and Schultz, M. G.: Global modeling of tropospheric chemistry with assimilated meteorology: Model description and evaluation, Journal of Geophysical Research Atmospheres, 106, 23 073–23 095, https://doi.org/10.1029/2001JD000807, publisher: Blackwell Publishing Ltd, 2001.

Bian, H. and Prather, M. J.: Fast-J2: Accurate simulation of stratospheric photoly-

sis in global chemical models, Journal of Atmospheric Chemistry, 41, 281–296, publisher: Springer, 2002.

Bindle, L., Martin, R. V., Cooper, M. J., Lundgren, E. W., Eastham, S. D., Auer, B. M., Clune, T. L., Weng, H., Lin, J., Murray, L. T., Meng, J., Keller, A., Putman, W. M., Pawson, S., and Jacob, D. J.: Atmospheric Chemistry Model, pp. 5977–5997, 2021a.

Bindle, L., Martin, R. V., Cooper, M. J., Lundgren, E. W., Eastham, S. D., Auer, B. M., Clune, T. L., Weng, H., Lin, J., Murray, L. T., Meng, J., Keller, C. A., Putman, W. M., Pawson, S., and Jacob, D. J.: Grid-stretching capability for the GEOS-Chem 13.0.0 atmospheric chemistry model, Geoscientific Model Development, 14, 5977–5997, https://doi.org/10.5194/gmd-14-5977-2021, URL https://gmd.copernicus.org/articles/14/5977/2021/, 2021b.

Bouwman, A. F., Lee, D. S., Asman, W. a. H., Dentener, F. J., Van Der Hoek, K. W., and Olivier, J. G. J.: A global high-resolution emission inventory for ammonia, Global Biogeochemical Cycles, 11, 561–587, https://doi.org/10.1029/97GB0226 6, URL https://onlinelibrary.wiley.com/doi/abs/10.1029/97GB02266, _eprint: https://onlinelibrary.wiley.com/doi/pdf/10.1029/97GB02266, 1997.

Brasseur, G. P. and Jacob, D. J.: Modeling of atmospheric chemistry, Cambridge University Press, 2017.

Brasseur, G. P., Hauglustaine, D. A., Walters, S., Rasch, P. J., Müller, J.-F., Granier, C., and Tie, X. X.: MOZART, a global chemical transport model for ozone and related chemical tracers: 1. Model description, Journal of Geophysical Research: Atmospheres, 103, 28 265–28 289, https://doi.org/10.1029/98JD 02397, URL https://onlinelibrary.wiley.com/doi/abs/10.1029/98JD0239 7, _eprint: https://onlinelibrary.wiley.com/doi/pdf/10.1029/98JD02397, 1998.

Breider, T. J., Mickley, L. J., Jacob, D. J., Ge, C., Wang, J., Payer Sulprizio, M., Croft, B., Ridley, D. A., McConnell, J. R., Sharma, S., Husain, L., Dutkiewicz, V. A., Eleftheriadis, K., Skov, H., and Hopke, P. K.: Multidecadal trends in

aerosol radiative forcing over the Arctic: Contribution of changes in anthropogenic aerosol to Arctic warming since 1980, Journal of Geophysical Research: Atmospheres, 122, 3573–3594, https://doi.org/10.1002/2016JD025321, URL `https://onlinelibrary.wiley.com/doi/abs/10.1002/2016JD025321`, _eprint: https://onlinelibrary.wiley.com/doi/pdf/10.1002/2016JD025321, 2017.

Burkholder, J., Sander, S., Abbatt, J., Barker, J., Cappa, C., Crounse, J., Dibble, T., Huie, R., Kolb, C., Kurylo, M., and others: Chemical kinetics and photochemical data for use in atmospheric studies; evaluation number 19, Tech. rep., Pasadena, CA: Jet Propulsion Laboratory, National Aeronautics and Space . . . , 2020.

Byun, D.: Science algorithms of the EPA Models-3 community multiscale air quality (CMAQ) modeling system, EPA/600/R-99/030, 1999.

Carslaw, D. C. and Ropkins, K.: Openair—an R package for air quality data analysis, Environmental Modelling & Software, 27, 52–61, 2012.

Chameides, W. and Davis, D.: Iodine: Its possible role in tropospheric photochemistry, Journal of Geophysical Research: Oceans, 85, 7383–7398, publisher: Wiley Online Library, 1980.

Charlson, R. J., Schwartz, S., Hales, J., Cess, R. D., Coakley Jr, J., Hansen, J., and Hofmann, D.: Climate forcing by anthropogenic aerosols, Science, 255, 423–430, publisher: American Association for the Advancement of Science, 1992.

Chatterjee, D., McDuffie, E. E., Smith, S. J., Bindle, L., van Donkelaar, A., Hammer, M. S., Venkataraman, C., Brauer, M., and Martin, R. V.: Source Contributions to Fine Particulate Matter and Attributable Mortality in India and the Surrounding Region, Environmental Science & Technology, publisher: ACS Publications, 2023.

Chemel, C., Sokhi, R. S., Yu, Y., Hayman, G. D., Vincent, K. J., Dore, A. J., Tang, Y. S., Prain, H. D., and Fisher, B. E. A.: Evaluation of a CMAQ simulation at high

resolution over the UK for the calendar year 2003, Atmospheric Environment, 44, 2927–2939, https://doi.org/10.1016/j.atmosenv.2010.03.029, URL `https://www.sciencedirect.com/science/article/pii/S1352231010002402`, 2010.

Chen, Q., Schmidt, J., Shah, V., Jaeglé, L., Sherwen, T., and Alexander, B.: Sulfate production by reactive bromine: Implications for the global sulfur and reactive bromine budgets, Geophysical Research Letters, 44, 7069–7078, publisher: Wiley Online Library, 2017.

Chin, M., Rood, R. B., Lin, S. J., Müller, J. F., and Thompson, A. M.: Atmospheric sulfur cycle simulated in the global model GOCART: Model description and global properties, Journal of Geophysical Research Atmospheres, 105, 24 671–24 687, https://doi.org/10.1029/2000JD900384, publisher: Blackwell Publishing Ltd, 2000.

Ciarelli, G., Theobald, M. R., Vivanco, M. G., Beekmann, M., Aas, W., Andersson, C., Bergström, R., Manders-Groot, A., Couvidat, F., Mircea, M., Tsyro, S., Fagerli, H., Mar, K., Raffort, V., Roustan, Y., Pay, M. T., Schaap, M., Kranenburg, R., Adani, M., Briganti, G., Cappelletti, A., D'Isidoro, M., Cuvelier, C., Cholakian, A., Bessagnet, B., Wind, P., and Colette, A.: Trends of inorganic and organic aerosols and precursor gases in Europe: Insights from the EURODELTA multi-model experiment over the 1990-2010 period, Geoscientific Model Development, 12, 4923–4954, https://doi.org/10.5194/gmd-12-4923-2019, 2019.

Clappier, A., Thunis, P., Beekmann, M., Putaud, J. P., and de Meij, A.: Impact of SOx, NOx and NH3 emission reductions on PM2.5 concentrations across Europe: Hints for future measure development, Environment International, 156, 106 699, https://doi.org/10.1016/j.envint.2021.106699, URL `https://www.sciencedirect.com/science/article/pii/S016041202100324X`, 2021.

Cooper, O. R., Parrish, D. D., Ziemke, J., Balashov, N. V., Cupeiro, M., Galbally, I. E., Gilge, S., Horowitz, L., Jensen, N. R., Lamarque, J.-F., Naik, V., Oltmans, S. J., Schwab, J., Shindell, D. T., Thompson, A. M., Thouret, V., Wang, Y.,

and Zbinden, R. M.: Global distribution and trends of tropospheric ozone: An observation-based review, Elementa: Science of the Anthropocene, 2, 000 029, https://doi.org/10.12952/journal.elementa.000029, URL https://doi.org/10.129 52/journal.elementa.000029, 2014.

Croft, B., Wentworth, G. R., Martin, R. V., Leaitch, W. R., Murphy, J. G., Murphy, B. N., Kodros, J. K., Abbatt, J. P. D., and Pierce, J. R.: Contribution of Arctic seabird-colony ammonia to atmospheric particles and cloud-albedo radiative effect, Nature Communications, 7, 13 444, https://doi.org/10.1038/ncomms13 444, URL https://www.nature.com/articles/ncomms13444, number: 1 Publisher: Nature Publishing Group, 2016.

Cullis, C. and Hirschler, M.: Atmospheric sulphur: natural and man-made sources, Atmospheric Environment (1967), 14, 1263–1278, publisher: Elsevier, 1980.

Daellenbach, K. R., Uzu, G., Jiang, J., Cassagnes, L.-E., Leni, Z., Vlachou, A., Stefenelli, G., Canonaco, F., Weber, S., Segers, A., Kuenen, J. J. P., Schaap, M., Favez, O., Albinet, A., Aksoyoglu, S., Dommen, J., Baltensperger, U., Geiser, M., El Haddad, I., Jaffrezo, J.-L., and Prévôt, A. S. H.: Sources of particulate-matter air pollution and its oxidative potential in Europe, Nature, 587, 414–419, https://doi.org/10.1038/s41586-020-2902-8, URL https://www.nature.com/articles/s41586-020-2902-8, number: 7834 Publisher: Nature Publishing Group, 2020.

Dai, J. and Wang, T.: Impact of international shipping emissions on ozone and $PM_{2.5}$ in East Asia during summer: the important role of HONO and $ClNO_2$, Atmospheric Chemistry and Physics, 21, 8747–8759, https://doi.org/10.5194/acp-21-8747-2021, URL https://acp.copernicus.org/articles/21/8747/2021/, publisher: Copernicus GmbH, 2021.

Dals øren, S. B., Myhre, G., Hodnebrog, o. i., Myhre, C. L., Stohl, A., Pisso, I., Schwietzke, S., H ö glund Isaksson, L., Helmig, D., Reimann, S., Sauvage, S., Schmidbauer, N., Read, K. A., Carpenter, L. J., Lewis, A. C., Punjabi,

S., and Wallasch, M.: Discrepancy between simulated and observed ethane and propane levels explained by underestimated fossil emissions, Nature Geoscience, 11, 178–184, https://doi.org/10.1038/s41561-018-0073-0, 2018.

Damian, V., Sandu, A., Damian, M., Potra, F., and Carmichael, G. R.: The kinetic preprocessor KPP-a software environment for solving chemical kinetics, Computers & Chemical Engineering, 26, 1567–1579, https://doi.org/10.1016/S0098-1354(02)00128-X, URL https://www.sciencedirect.com/science/article/pii/S009813540200128X, 2002.

Davis, D. D., Grodzinsky, G., Kasibhatla, P., Crawford, J., Chen, G., Liu, S., Bandy, A., Thornton, D., Guan, H., and Sandholm, S.: Impact of ship emissions on marine boundary layer NOx and SO2 Distributions over the Pacific Basin, Geophysical Research Letters, 28, 235–238, https://doi.org/10.1029/2000GL012013, URL https://onlinelibrary.wiley.com/doi/abs/10.1029/2000GL012013, _eprint: https://onlinelibrary.wiley.com/doi/pdf/10.1029/2000GL012013, 2001.

Davison, A. and Barnes, J.: Effects of ozone on wild plants, The New Phytologist, 139, 135–151, publisher: Cambridge University Press, 1998.

De Meij, A., Krol, M., Dentener, F., Vignati, E., Cuvelier, C., and Thunis, P.: The sensitivity of aerosol in Europe to two different emission inventories and temporal distribution of emissions, Atmospheric Chemistry and Physics, 6, 4287–4309, publisher: Copernicus GmbH, 2006.

DEFRA: DEFRA AURN monitoring methods and EU standards (last accessed 15/06/2021), URL https://uk-air.defra.gov.uk/networks/monitoring-methods?view=eu-standards.

DEFRA: M8 Monitoring Ambient Air Environment Agency, URL www.mcerts.net, 2011.

DEFRA: Non-Methane Volatile Organic Compounds in the UK, https://uk-air.defra.gov.uk/assets/documents/reports/cat09/2006240803_Non_Meth

ane_Volatile_Organic_Compounds_in_the_UK.pdf, accessed: 2023-02-17, 2015.

DEFRA: Air Pollution in the UK 2017, URL `https://uk-air.defra.gov.uk/assets/documents/annualreport/air_pollution_uk_2017_issue_1.pdf`, 2018.

DEFRA: Air Pollution in the UK 2017: Compliance Assessement Summary, URL `https://uk-air.defra.gov.uk/library/annualreport/assets/documents/annualreport/air_pollution_uk_2017_Compliance_Assessment_Summary_Issue1.pdf`, 2018.

DEFRA: Air Pollution in the UK 2020, Annual Report 2020 Issue 1, URL `https://uk-air.defra.gov.uk/library/annualreport`, 2021.

DEFRA: Air Pollution in the UK 2021, URL `https://uk-air.defra.gov.uk/library/annualreport/viewonline?year=2021_issue_1#report_pdf`, 2022a.

DEFRA: Statistical Digest of Rural England; August 2022 edition, URL `https://assets.publishing.service.gov.uk/media/630620558fa8f5536c077dcc/07_Statistical_Digest_of_Rural_England_2022_August_edition.pdf`, 2022b.

Delmas, R., Serça, D., and Jambert, C.: Global inventory of NOx sources, Nutrient Cycling in Agroecosystems, 48, 51–60, https://doi.org/10.1023/A:1009793806086, URL `https://doi.org/10.1023/A:1009793806086`, 1997.

Dentener, F. J. and Crutzen, P. J.: Reaction of N2O5 on tropospheric aerosols: Impact on the global distributions of NO x, O3, and OH, Journal of Geophysical Research: Atmospheres, 98, 7149–7163, publisher: Wiley Online Library, 1993.

Derwent, R. G. and Parrish, D. D.: Analysis and assessment of the observed long-term changes over three decades in ground-level ozone across north-west Europe from 1989 - 2018, Atmospheric Environment, 286, 119 222, https://doi.org/10.1016/j.atmosenv.2022.119222, URL `https://doi.org/10.1016/j.atmosenv.2022.119222`, publisher: Elsevier Ltd, 2022.

Derwent, R. G., Jenkin, M. E., Utembe, S. R., Shallcross, D. E., Murrells, T. P., and Passant, N. R.: Secondary organic aerosol formation from a large number of reactive man-made organic compounds, Science of The Total Environment, 408, 3374–3381, https://doi.org/10.1016/j.scitotenv.2010.04.013, URL `https://www.sciencedirect.com/science/article/pii/S0048969710003918`, 2010.

Derwent, R. G., Field, R. A., Dumitrean, P., Murrells, T. P., and Telling, S. P.: Origins and trends in ethane and propane in the United Kingdom from 1993 to 2012, Atmospheric Environment, 156, 15–23, https://doi.org/10.1016/j.atmosenv.2017.02.030, URL `http://dx.doi.org/10.1016/j.atmosenv.2017.02.030`, publisher: Elsevier Ltd, 2017.

Deutsch, F., Vankerkom, J., Janssen, L., Janssen, S., Bencs, L., Van Grieken, R., Fierens, F., Dumont, G., and Mensink, C.: Modelling concentrations of airborne primary and secondary PM10 and PM2.5 with the BelEUROS-model in Belgium, Ecological Modelling, 217, 230–239, https://doi.org/10.1016/j.ecolmodel.2008.06.003, URL `https://www.sciencedirect.com/science/article/pii/S0304380008002561`, 2008.

Donahue, N. M., Robinson, A. L., and Pandis, S. N.: Atmospheric organic particulate matter: From smoke to secondary organic aerosol, Atmospheric Environment, 43, 94–106, https://doi.org/10.1016/j.atmosenv.2008.09.055, URL `https://www.sciencedirect.com/science/article/pii/S1352231008009229`, 2009.

Dore, A. J., Carslaw, D. C., Braban, C., Cain, M., Chemel, C., Conolly, C., Derwent, R. G., Griffiths, S. J., Hall, J., Hayman, G., Lawrence, S., Metcalfe, S. E., Redington, A., Simpson, D., Sutton, M. A., Sutton, P., Tang, Y. S., Vieno, M., Werner, M., and Whyatt, J. D.: Evaluation of the performance of different atmospheric chemical transport models and inter-comparison of nitrogen and sulphur deposition estimates for the UK, Atmospheric Environment, 119, 131–143, https://doi.org/10.1016/j.atmosenv.2015.08.008, 2015.

Du, Q., Zhao, C., Zhang, M., Dong, X., Chen, Y., Liu, Z., Hu, Z., Zhang, Q., Li, Y., and Miao, S.: Modeling diurnal variation of surface PM2.5 concentrations

over East China with WRF-Chem: Impacts from boundary-layer mixing and anthropogenic emission, Atmospheric Chemistry and Physics, 20, 2839–2863, https://doi.org/10.5194/ACP-20-2839-2020, publisher: Copernicus GmbH, 2020.

Duncan Fairlie, T., Jacob, D. J., and Park, R. J.: The impact of transpacific transport of mineral dust in the United States, Atmospheric Environment, 41, 1251–1266, https://doi.org/10.1016/j.atmosenv.2006.09.048, URL https://www.sciencedirect.com/science/article/pii/S1352231006009915, 2007.

Dytłow, S. and Górka-Kostrubiec, B.: Concentration of heavy metals in street dust: an implication of using different geochemical background data in estimating the level of heavy metal pollution, Environmental Geochemistry and Health, 43, 521–535, https://doi.org/10.1007/s10653-020-00726-9, URL https://www.ncbi.nlm.nih.gov/pmc/articles/PMC7847877/, 2021.

Eastham, S. D., Weisenstein, D. K., and Barrett, S. R. H.: Development and evaluation of the unified tropospheric–stratospheric chemistry extension (UCX) for the global chemistry-transport model GEOS-Chem, Atmospheric Environment, 89, 52–63, https://doi.org/10.1016/j.atmosenv.2014.02.001, URL https://www.sciencedirect.com/science/article/pii/S1352231014000971, 2014.

Eastham, S. D., Long, M. S., Keller, C. A., Lundgren, E., Yantosca, R. M., Zhuang, J., Li, C., Lee, C. J., Yannetti, M., Auer, B. M., Clune, T. L., Kouatchou, J., Putman, W. M., Thompson, M. A., Trayanov, A. L., Molod, A. M., Martin, R. V., and Jacob, D. J.: GEOS-Chem high performance (GCHP v11-02c): A next-generation implementation of the GEOS-Chem chemical transport model for massively parallel applications, Geoscientific Model Development, 11, 2941–2953, https://doi.org/10.5194/gmd-11-2941-2018, 2018.

Ehhalt, D. and Drummond, J.: The tropospheric cycle of NOx, in: Chemistry of the Unpolluted and Polluted Troposphere: Proceedings of the NATO Advanced Study Institute held on the Island of Corfu, Greece, September 28–October 10, 1981, pp. 219–251, Springer, 1982.

EMEP: EMEP Status Report 1/2019: Transboundary particulate matter, photo-oxidants, acidifying and eutrophying components, Tech. rep., EMEP, URL `https://emep.int/publ/reports/2019/EMEP_Status_Report_1_2019.pdf`, 2019.

EMEP MSC-W: Open Source EMEP/MSC-W model rv4.34 (202001), https://doi.org/10.5281/zenodo.3647990, URL `https://doi.org/10.5281/zenodo.3647990`, 2020.

Emerson, E. W., Hodshire, A. L., DeBolt, H. M., Bilsback, K. R., Pierce, J. R., McMeeking, G. R., and Farmer, D. K.: Revisiting particle dry deposition and its role in radiative effect estimates, Proceedings of the National Academy of Sciences, 117, 26 076–26 082, publisher: National Acad Sciences, 2020.

Emmons, L. K., Walters, S., Hess, P. G., Lamarque, J.-F., Pfister, G. G., Fillmore, D., Granier, C., Guenther, A., Kinnison, D., Laepple, T., et al.: Description and evaluation of the Model for Ozone and Related chemical Tracers, version 4 (MOZART-4), Geoscientific Model Development, 3, 43–67, 2010.

EPA: Nitrogen Oxides (NOx), Why and How They are Controlled, Tech. rep., Enivronment Protection Agency, 1999.

Etiope, G. and Ciccioli, P.: Earth's Degassing: A Missing Ethane and Propane Source, Science, 323, 478–478, https://doi.org/10.1126/science.1165904, URL `https://www.science.org/doi/full/10.1126/science.1165904`, publisher: American Association for the Advancement of Science, 2009.

Falasca, S. and Curci, G.: High-resolution air quality modeling: Sensitivity tests to horizontal resolution and urban canopy with WRF-CHIMERE, Atmospheric Environment, 187, 241–254, https://doi.org/10.1016/j.atmosenv.2018.05.048, URL `https://www.sciencedirect.com/science/article/pii/S1352231018303583`, 2018.

Faloona, I.: Sulfur processing in the marine atmospheric boundary layer: A review and critical assessment of modeling uncertainties, Atmospheric Environment,

43, 2841–2854, https://doi.org/10.1016/j.atmosenv.2009.02.043, URL `https://www.sciencedirect.com/science/article/pii/S1352231009001630`, 2009.

Fenech, S., Doherty, R. M., Heaviside, C., Vardoulakis, S., Macintyre, H. L., and O'Connor, F. M.: The influence of model spatial resolution on simulated ozone and fine particulate matter for Europe: implications for health impact assessments, Atmospheric Chemistry and Physics, 18, 5765–5784, https://doi.org/10.5194/acp-18-5765-2018, URL `https://acp.copernicus.org/articles/18/5765/2018/`, publisher: Copernicus GmbH, 2018.

Fisher, J. A., Jacob, D. J., Wang, Q., Bahreini, R., Carouge, C. C., Cubison, M. J., Dibb, J. E., Diehl, T., Jimenez, J. L., Leibensperger, E. M., Lu, Z., Meinders, M. B. J., Pye, H. O. T., Quinn, P. K., Sharma, S., Streets, D. G., van Donkelaar, A., and Yantosca, R. M.: Sources, distribution, and acidity of sulfate–ammonium aerosol in the Arctic in winter–spring, Atmospheric Environment, 45, 7301–7318, https://doi.org/10.1016/j.atmosenv.2011.08.030, URL `https://www.sciencedirect.com/science/article/pii/S1352231011008545`, 2011.

Forster, P., Ramaswamy, V., Artaxo, P., Berntsen, T., Betts, R., Fahey, D. W., Haywood, J., Lean, J., Lowe, D. C., Myhre, G., and others: Changes in atmospheric constituents and in radiative forcing, Climate Change 2007: The Physical Science Basis. Contribution of Working Group I to the 4th Assessment Report of the Intergovernmental Panel on Climate Change, publisher: Cambridge University Press, Cambridge, United Kingdom and New York, USA, 2007.

Fountoukis, C. and Nenes, A.: ISORROPIAII: A computationally efficient thermodynamic equilibrium model for K+-Ca2+-Mg2+-NH4+-Na+-SO42–NO3–Cl–H2O aerosols, Atmospheric Chemistry and Physics, 7, 4639–4659, https://doi.org/10.5194/acp-7-4639-2007, 2007.

Fountoukis, C., Koraj, D., Denier van der Gon, H. A. C., Charalampidis, P. E., Pilinis, C., and Pandis, S. N.: Impact of grid resolution on the predicted fine PM by a regional 3-D chemical transport model, Atmospheric Environment, 68,

24–32, https://doi.org/10.1016/j.atmosenv.2012.11.008, URL `https://www.scie ncedirect.com/science/article/pii/S1352231012010539`, 2013.

Fu, J. S., Dong, X., Gao, Y., Wong, D. C., and Lam, Y. F.: Sensitivity and linearity analysis of ozone in East Asia: The effects of domestic emission and intercontinental transport, Journal of the Air & Waste Management Association, 62, 1102–1114, https://doi.org/10.1080/10962247.2012.699014, URL `https://doi.org/10.1080/10962247.2012.699014`, publisher: Taylor & Francis _eprint: https://doi.org/10.1080/10962247.2012.699014, 2012.

Gabusi, V. and Volta, M.: Seasonal modelling assessment of ozone sensitivity to precursors in northern Italy, Atmospheric Environment, 39, 2795–2804, https://doi.org/10.1016/j.atmosenv.2004.07.041, URL `https://www.sciencedir ect.com/science/article/pii/S1352231005001627`, 2005.

Gaffney, J. S. and Marley, N. A.: The impacts of combustion emissions on air quality and climate – From coal to biofuels and beyond, Atmospheric Environment, 43, 23–36, https://doi.org/10.1016/j.atmosenv.2008.09.016, URL `https://www.sciencedirect.com/science/article/pii/S1352231008009175`, 2009.

Gantt, B., Johnson, M. S., Crippa, M., Prévôt, A. S. H., and Meskhidze, N.: Implementing marine organic aerosols into the GEOS-Chem model, Geoscientific Model Development, 8, 619–629, https://doi.org/10.5194/gmd-8-619-2015, URL `https://gmd.copernicus.org/articles/8/619/2015/`, publisher: Copernicus GmbH, 2015.

Garstin, T. J.: An Air Quality Assessment of the European Nested Grid of the GEOS-Chem Model and the Influence of the Agricultural Sector, Ph.D. thesis, University of York, URL `http://etheses.whiterose.ac.uk/20960/`, 2017.

GC13.1.1: geoschem/geos-chem: GEOS-Chem 13.1.1, https://doi.org/10.5281/ze nodo.5014891, URL `https://doi.org/10.5281/zenodo.5014891`, Please see the LICENSE.txt and AUTHORS.txt files in the root folder for the GEOS-Chem license description (based on the MIT license) and a complete list of authors.

For more information about GEOS-Chem in general, please see www.geos-chem.org and wiki.geos-chem.org., 2021.

GCHP13.4.0: geoschem/GCHP: GCHP 13.4.0, https://doi.org/10.5281/zenodo.6512251, URL `https://zenodo.org/record/6512251`, Please see the LICENSE.txt and AUTHORS.txt files in the root folder for the GEOS-Chem license description (based on the MIT license) and a complete list of authors. For more information about GEOS-Chem in general, please see www.geos- chem.org and wiki.geos-chem.org., 2022.

GCv13.1.2, T. I. G.-C. U.: GEOS-Chem 13.1.2 (GCClassic), https://doi.org/10.5281/ZENODO.5075847, URL `https://zenodo.org/record/5075847`, 2021.

Ge, W., Liu, J., Yi, K., Xu, J., Zhang, Y., Hu, X., Ma, J., Wang, X., Wan, Y., Hu, J., Zhang, Z., Wang, X., and Tao, S.: Influence of atmospheric in-cloud aqueous-phase chemistry on global simulation of SO<sub>2</sub> in CESM2, Atmospheric Chemistry and Physics, pp. 1–35, https://doi.org/10.5194/acp-2021-406, 2021a.

Ge, Y., Heal, M. R., Stevenson, D. S., Wind, P., and Vieno, M.: Evaluation of global EMEP MSC-W (rv4.34) WRF (v3.9.1.1) model surface concentrations and wet deposition of reactive N and S with measurements, Geoscientific Model Development, 14, 7021–7046, https://doi.org/10.5194/gmd-14-7021-2021, URL `https://gmd.copernicus.org/articles/14/7021/2021/`, publisher: Copernicus GmbH, 2021b.

GEOS-Chem Steering Committee: GEOS-Chem Steering Committee Telecon, 23 Febrary 2022, pp. 1–2, URL `https://geos-chem.seas.harvard.edu/files/acmg-geos/files/gcsc_minutes_23feb2022_01.pdf`, 2022.

Gillani, N. V. and Godowitch, J. M.: Plume-In-Grid Treatment of Major Point Source Emissions, in: SCIENCE ALGORITHMS OF THE EPA MODELS-3 COMMUNITY MULTISCALE AIR QUALITY (CMAQ) MODELING SYSTEM, pp.

1–40, U.S. Environmental Protection Agency, URL `https://cfpub.epa.gov/ si/si_public_record_report.cfm?dirEntryId=63400&Lab=NERL`, 1999.

Goldstein, A. H. and Galbally, I. E.: Known and unknown organic constituents in the Earth's atmosphere, Environmental Science & Technology, 41, 1514–1521, https://doi.org/10.1021/es072476p, 2007.

Goldstein, A. H., Koven, C. D., Heald, C. L., and Fung, I. Y.: Biogenic carbon and anthropogenic pollutants combine to form a cooling haze over the southeastern United States, Proceedings of the National Academy of Sciences, 106, 8835–8840, publisher: National Acad Sciences, 2009.

Goroch, A. K. and Geernaert, G.: Coastal Aerosol Workshop Proceedings Held, 23-24 May 1994, 1995.

Graham, A. M.: Simulation and Evaluation of Regional Air Quality in the UK, PhD Thesis, University of Leeds, 2021.

Graham, A. M., Pringle, K. J., Arnold, S. R., Pope, R. J., Vieno, M., Butt, E. W., Conibear, L., Stirling, E. L., and McQuaid, J. B.: Impact of weather types on UK ambient particulate matter concentrations, Atmospheric Environment: X, 5, 100 061, https://doi.org/10.1016/j.aeaoa.2019.100061, URL `https://www.scienc edirect.com/science/article/pii/S2590162119300644`, 2020.

Grell, G. and Baklanov, A.: Integrated modeling for forecasting weather and air quality: A call for fully coupled approaches, Atmospheric Environment, 45, 6845–6851, https://doi.org/10.1016/j.atmosenv.2011.01.017, URL `https: //linkinghub.elsevier.com/retrieve/pii/S1352231011000240`, 2011.

Grell, G. A., Peckham, S. E., Schmitz, R., McKeen, S. A., Frost, G., Skamarock, W. C., and Eder, B.: Fully coupled "online" chemistry within the WRF model, Atmospheric Environment, 39, 6957–6975, https://doi.org/10.1016/j.atmosenv.2 005.04.027, URL `https://www.sciencedirect.com/science/article/pii/S1 352231005003560`, 2005.

Gu, B., Zhang, L., Van Dingenen, R., Vieno, M., Van Grinsven, H. J., Zhang, X., Zhang, S., Chen, Y., Wang, S., Ren, C., Rao, S., Holland, M., Winiwarter, W., Chen, D., Xu, J., and Sutton, M. A.: Abating ammonia is more cost-effective than nitrogen oxides for mitigating PM2.5 air pollution, Science (New York, N.Y.), 374, 758–762, https://doi.org/10.1126/science.abf8623, 2021.

Gu, Y., Henze, D. K., Nawaz, M. O., Cao, H., and Wagner, U. J.: Sources of PM2.5-Associated Health Risks in Europe and Corresponding Emission-Induced Changes During 2005–2015, GeoHealth, 7, e2022GH000 767, https://doi.org/10.1029/2022GH000767, URL https://onlineli brary.wiley.com/doi/abs/10.1029/2022GH000767, _eprint: https://onlinelibrary.wiley.com/doi/pdf/10.1029/2022GH000767, 2023.

Guenther, A.: Seasonal and Spatial Variations in Natural Volatile Organic Compound Emissions, Ecological Applications, 7, 34–45, https://doi.org/10.1890/10 51-0761(1997)007[0034:SASVIN]2.0.CO;2, URL https://onlinelibrary.wi ley.com/doi/abs/10.1890/1051-0761%281997%29007%5B0034%3ASASVIN %5D2.0.CO%3B2, _eprint: https://onlinelibrary.wiley.com/doi/pdf/10.1890/1051-0761%281997%29007%5B0034%3ASASVIN%5D2.0.CO%3B2, 1997.

Guenther, A. B., Jiang, X., Heald, C. L., Sakulyanontvittaya, T., Duhl, T., Emmons, L. K., and Wang, X.: The model of emissions of gases and aerosols from nature version 2.1 (MEGAN2.1): An extended and updated framework for modeling biogenic emissions, Geoscientific Model Development, 5, 1471–1492, https://doi.org/10.5194/GMD-5-1471-2012, 2012.

Guevara, M., Soret, A., Arévalo, G., Martínez, F., and Baldasano, J. M.: Implementation of plume rise and its impacts on emissions and air quality modelling, Atmospheric Environment, 99, 618–629, https://doi.org/10.1016/J.ATMOSENV .2014.10.029, publisher: Pergamon, 2014.

Hall, S. J., Matson, P. A., and Roth, P. M.: NOx EMISSIONS FROM SOIL: Implications for Air Quality Modeling in Agricultural Regions, Annual Review of Energy and the Environment, 21, 311–346, https://doi.org/10.1146/annurev.en

ergy.21.1.311, URL https://doi.org/10.1146/annurev.energy.21.1.311, _eprint: https://doi.org/10.1146/annurev.energy.21.1.311, 1996.

Hardacre, C., Mulcahy, J. P., Pope, R. J., Jones, C. G., Rumbold, S. T., Li, C., Johnson, C., and Turnock, S. T.: Evaluation of SO2, SO42-and an updated SO2dry deposition parameterization in the United Kingdom Earth System Model, Atmospheric Chemistry and Physics, 21, 18 465–18 497, https://doi.org/10.5194/acp-21-18465-2021, 2021.

Harley, R. A., Hannigan, M. P., and Cass, G. R.: Respeciation of organic gas emissions and the detection of excess unburned gasoline in the atmosphere, Environmental Science & Technology, 26, 2395–2408, publisher: ACS Publications, 1992.

Harris, L. M., Lin, S.-J., and Tu, C.: High-resolution climate simulations using GFDL HiRAM with a stretched global grid, Journal of Climate, 29, 4293–4314, 2016.

Harrison, R. M., Vu, T. V., Jafar, H., and Shi, Z.: More mileage in reducing urban air pollution from road traffic, Environment International, 149, 106 329, https://doi.org/10.1016/j.envint.2020.106329, URL https://www.sciencedirect.com/science/article/pii/S0160412020322844, 2021.

Hellsten, S., Dragosits, U., Place, C. J., Misselbrook, T. H., Tang, Y. S., and Sutton, M. A.: Modelling seasonal dynamics from temporal variation in agricultural practices in the UK ammonia emission inventory, Water, Air, and Soil Pollution: Focus, 7, 3–13, https://doi.org/10.1007/S11267-006-9087-5/FIGURES/6, URL https://link.springer.com/article/10.1007/s11267-006-9087-5, publisher: Springer, 2007.

Hellsten, S., Dragosits, U., Place, C. J., Vieno, M., Dore, A. J., Misselbrook, T. H., Tang, Y. S., and Sutton, M. A.: Modelling the spatial distribution of ammonia emissions in the UK, Environmental Pollution, 154, 370–379, https://doi.org/10.1016/J.ENVPOL.2008.02.017, publisher: Elsevier, 2008.

Henriksen, T., Dahlback, A., Larsen, S. H., and Moan, J.: ULTRAVIOLET-RADIATION and SKIN CANCER. EFFECT OF AN OZONE LAYER DEPLETION, Photochemistry and Photobiology, 51, 579–582, https://doi.org/10.1111/j.1751-1097.1990.tb01968.x, URL https://onlinelibrary.wiley.com/doi/abs/10.1111/j.1751-1097.1990.tb01968.x, _eprint: https://onlinelibrary.wiley.com/doi/pdf/10.1111/j.1751-1097.1990.tb01968.x, 1990.

Hogrefe, C., Isukapalli, S. S., Tang, X., Georgopoulos, P. G., He, S., Zalewsky, E. E., Hao, W., Ku, J.-Y., Key, T., and Sistla, G.: Impact of Biogenic Emission Uncertainties on the Simulated Response of Ozone and Fine Particulate Matter to Anthropogenic Emission Reductions, Journal of the Air & Waste Management Association (1995), 61, 92–108, URL https://www.ncbi.nlm.nih.gov/pmc/articles/PMC3079461/, 2011.

Holmes, C. D., Prather, M. J., and Vinken, G. C. M.: The climate impact of ship NO_x emissions: an improved estimate accounting for plume chemistry, Atmospheric Chemistry and Physics, 14, 6801–6812, https://doi.org/10.5194/acp-14-6801-2014, URL https://acp.copernicus.org/articles/14/6801/2014/, publisher: Copernicus GmbH, 2014.

Holton, J. R., Haynes, P. H., McIntyre, M. E., Douglass, A. R., Rood, R. B., and Pfister, L.: Stratosphere-troposphere exchange, Reviews of Geophysics, 33, 403–439, https://doi.org/10.1029/95RG02097, URL https://onlinelibrary.wiley.com/doi/abs/10.1029/95RG02097, _eprint: https://onlinelibrary.wiley.com/doi/pdf/10.1029/95RG02097, 1995.

Hood, C., MacKenzie, I., Stocker, J., Johnson, K., Carruthers, D., Vieno, M., and Doherty, R.: Air quality simulations for London using a coupled regional-to-local modelling system, Atmospheric Chemistry and Physics, 18, 11 221–11 245, https://doi.org/10.5194/acp-18-11221-2018, URL https://acp.copernicus.org/articles/18/11221/2018/, 2018.

Horowitz, H. M., Holmes, C., Wright, A., Sherwen, T., Wang, X., Evans, M.,

Huang, J., Jaeglé, L., Chen, Q., Zhai, S., and Alexander, B.: Effects of Sea Salt Aerosol Emissions for Marine Cloud Brightening on Atmospheric Chemistry: Implications for Radiative Forcing, Geophysical Research Letters, 47, e2019GL085 838, https://doi.org/10.1029/2019GL085838, URL `https://onlinelibrary.wiley.com/doi/abs/10.1029/2019GL085838`, _eprint: https://onlinelibrary.wiley.com/doi/pdf/10.1029/2019GL085838, 2020.

House of Lords: Clean Air (Human Rights) Bill [HL Bill 69] 2022, `https://bills.parliament.uk/publications/48605/documents/2487`, accessed: 2023-03-07, 2022.

Ivatt, P. D., Evans, M. J., and Lewis, A. C.: Suppression of surface ozone by an aerosol-inhibited photochemical ozone regime, Nature Geoscience, https://doi.org/10.1038/S41561-022-00972-9, URL `https://www.nature.com/articles/s41561-022-00972-9`, 2022.

Jacob, D. J.: Introduction to atmospheric chemistry, Princeton university press, 1999.

Jacob, D. J.: Heterogeneous chemistry and tropospheric ozone, Atmospheric Environment, 34, 2131–2159, https://doi.org/10.1016/S1352-2310(99)00462-8, 2000.

Jaeglé, L., Jacob, D. J., Brune, W. H., Tan, D., Faloona, I. C., Weinheimer, A. J., Ridley, B. A., Campos, T. L., and Sachse, G. W.: Sources of HOx and production of ozone in the upper troposphere over the United States, Geophysical Research Letters, 25, 1709–1712, https://doi.org/10.1029/98GL00041, URL `https://onlinelibrary.wiley.com/doi/abs/10.1029/98GL00041`, _eprint: https://onlinelibrary.wiley.com/doi/pdf/10.1029/98GL00041, 1998.

Jaeglé, L., Quinn, P. K., Bates, T. S., Alexander, B., and Lin, J.-T.: Global distribution of sea salt aerosols: new constraints from in situ and remote sensing observations, Atmospheric Chemistry and Physics, 11, 3137–3157, https://doi.org/

10.5194/acp-11-3137-2011, URL `https://acp.copernicus.org/articles/11/3137/2011/`, publisher: Copernicus GmbH, 2011.

Jaeglé, L., Shah, V., Thornton, J. A., Lopez-Hilfiker, F. D., Lee, B. H., Mc-Duffie, E. E., Fibiger, D., Brown, S. S., Veres, P., Sparks, T. L., Ebben, C. J., Wooldridge, P. J., Kenagy, H. S., Cohen, R. C., Weinheimer, A. J., Campos, T. L., Montzka, D. D., Digangi, J. P., Wolfe, G. M., Hanisco, T., Schroder, J. C., Campuzano-Jost, P., Day, D. A., Jimenez, J. L., Sullivan, A. P., Guo, H., and Weber, R. J.: Nitrogen Oxides Emissions, Chemistry, Deposition, and Export Over the Northeast United States During the WINTER Aircraft Campaign, Journal of Geophysical Research: Atmospheres, 123, 12,368–12,393, https://doi.org/10.1029/2018JD029133, URL `https://onlinelibrary.wiley.com/doi/abs/10.1029/2018JD029133`, _eprint: https://onlinelibrary.wiley.com/doi/pdf/10.1029/2018JD029133, 2018.

Jenkin, M. E.: Trends in ozone concentration distributions in the UK since 1990: Local, regional and global influences, Atmospheric Environment, 42, 5434–5445, https://doi.org/10.1016/j.atmosenv.2008.02.036, URL `https://www.sciencedirect.com/science/article/pii/S135223100800191X`, 2008.

Jenkin, M. E., Valorso, R., Aumont, B., and Rickard, A. R.: Estimation of rate coefficients and branching ratios for reactions of organic peroxy radicals for use in automated mechanism construction, Atmospheric Chemistry and Physics, 19, 7691–7717, https://doi.org/10.5194/acp-19-7691-2019, URL `https://acp.copernicus.org/articles/19/7691/2019/`, 2019.

Jennings, S. G., Kleefeld, C., O Dowd, C. D., Junker, C., Spain, T. G., O Brien, P., Roddy, A. F., and O Connor, T. C.: Mace Head Atmospheric Research Station-characterization of aerosol radiative parameters, Boreal environment research, 8, 303–314, 2003.

Jones, A. C., Hill, A., Remy, S., Abraham, N. L., Dalvi, M., Hardacre, C., Hewitt, A. J., Johnson, B., Mulcahy, J. P., and Turnock, S. T.: Exploring the sensitivity of

atmospheric nitrate concentrations to nitric acid uptake rate using the Met Office's Unified Model, Atmospheric Chemistry and Physics, 21, 15 901–15 927, https://doi.org/10.5194/acp-21-15901-2021, URL https://acp.copernicus.org/articles/21/15901/2021/, publisher: Copernicus GmbH, 2021.

Jones, W. H. S., Withington, E. T., Potter, P., Smith, W. D., and others: Hippocrates Volume III, vol. 3, Harvard University Press, 1927.

Jonson, J. E., Gauss, M., Schulz, M., Jalkanen, J.-P., and Fagerli, H.: Effects of global ship emissions on European air pollution levels, Atmospheric Chemistry and Physics, 20, 11 399–11 422, https://doi.org/10.5194/acp-20-11399-2020, URL https://acp.copernicus.org/articles/20/11399/2020/, publisher: Copernicus GmbH, 2020.

Jonson, J. E., Fagerli, H., Scheuschner, T., and Tsyro, S.: Modelling changes in secondary inorganic aerosol formation and nitrogen deposition in Europe from 2005 to 2030, Atmospheric Chemistry and Physics, 22, 1311–1331, https://doi.org/10.5194/acp-22-1311-2022, URL https://acp.copernicus.org/articles/22/1311/2022/, publisher: Copernicus GmbH, 2022.

Kanakidou, M., Tsigaridis, K., Dentener, F. J., and Crutzen, P. J.: Human-activity-enhanced formation of organic aerosols by biogenic hydrocarbon oxidation, Journal of Geophysical Research: Atmospheres, 105, 9243–9354, https://doi.org/10.1029/1999JD901148, URL https://onlinelibrary.wiley.com/doi/abs/10.1029/1999JD901148, _eprint: https://onlinelibrary.wiley.com/doi/pdf/10.1029/1999JD901148, 2000.

Karl, T., Graus, M., Striednig, M., Lamprecht, C., Hammerle, A., Wohlfahrt, G., Held, A., Von Der Heyden, L., Deventer, M. J., Krismer, A., Haun, C., Feichter, R., and Lee, J.: Urban eddy covariance measurements reveal significant missing NO x emissions in Central Europe, Scientific Reports, 7, 1–9, https://doi.org/10.1038/s41598-017-02699-9, publisher: Springer US, 2017.

Keller, C. A., Long, M. S., Yantosca, R. M., Da Silva, A. M., Pawson, S., and Jacob,

D. J.: HEMCO v1.0: a versatile, ESMF-compliant component for calculating emissions in atmospheric models, Geoscientific Model Development, 7, 1409–1417, https://doi.org/10.5194/gmd-7-1409-2014, URL `https://gmd.copernicus.org/articles/7/1409/2014/gmd-7-1409-2014.html`, publisher: Copernicus GmbH, 2014.

Kelly, J. M., Marais, E. A., Lu, G., Obszynska, J., Mace, M., White, J., and Leigh, R. J.: Diagnosing domestic and transboundary sources of fine particulate matter (PM2.5) in UK cities using GEOS-Chem, City and Environment Interactions, 18, 100 100, https://doi.org/10.1016/j.cacint.2023.100100, URL `https://www.sciencedirect.com/science/article/pii/S2590252023000028`, 2023.

Khalil, M. A. and Rasmussen, R. A.: The global cycle of carbon monoxide: Trends and mass balance, Chemosphere, 20, 227–242, https://doi.org/10.1016/0045-6535(90)90098-E, publisher: Pergamon, 1990.

Khan, M. A. H., Schlich, B.-L., Jenkin, M. E., Shallcross, B. M. A., Moseley, K., Walker, C., Morris, W. C., Derwent, R. G., Percival, C. J., and Shallcross, D. E.: A Two-Decade Anthropogenic and Biogenic Isoprene Emissions Study in a London Urban Background and a London Urban Traffic Site, Atmosphere, 9, 387, https://doi.org/10.3390/atmos9100387, URL `https://www.mdpi.com/2073-4433/9/10/387`, number: 10 Publisher: Multidisciplinary Digital Publishing Institute, 2018.

Kiehl, J. and Briegleb, B.: The relative roles of sulfate aerosols and greenhouse gases in climate forcing, Science, 260, 311–314, publisher: American Association for the Advancement of Science, 1993.

Kristensen, K., Bilde, M., Aalto, P. P., Petäjä, T., and Glasius, M.: Denuder/filter sampling of organic acids and organosulfates at urban and boreal forest sites: Gas/particle distribution and possible sampling artifacts, Atmospheric Environment, 130, 36–53, https://doi.org/10.1016/J.ATMOSENV.2015.10.046, publisher: Pergamon, 2016.

Kuik, F., Kerschbaumer, A., Lauer, A., Lupascu, A., Von Schneidemesser, E., and Butler, T. M.: Top-down quantification of NOx emissions from traffic in an urban area using a high-resolution regional atmospheric chemistry model, Atmospheric Chemistry and Physics, 18, 8203–8225, https://doi.org/10.5194/acp-18-8203-2018, 2018.

Kushta, J., Pozzer, A., and Lelieveld, J.: Uncertainties in estimates of mortality attributable to ambient PM2.5 in Europe, Environmental Research Letters, 13, 064 029, https://doi.org/10.1088/1748-9326/aabf29, URL https://dx.doi.org/10.1088/1748-9326/aabf29, publisher: IOP Publishing, 2018.

Latimer, R. N. and Martin, R. V.: Interpretation of measured aerosol mass scattering efficiency over North America using a chemical transport model, Atmospheric Chemistry and Physics, 19, 2635–2653, publisher: Copernicus GmbH, 2019.

Lawrence, M. G. and Crutzen, P. J.: Influence of NOx emissions from ships on tropospheric photochemistry and climate, Nature, 402, 167–170, URL https://ideas.repec.org//a/nat/nature/v402y1999i6758d10.1038_46013.html, publisher: Nature, 1999.

Lelieveld, J. and Crutzen, P. J.: Influences of cloud photochemical processes on tropospheric ozone, Nature, 343, 227–233, https://doi.org/10.1038/343227a0, URL https://www.nature.com/articles/343227a0, number: 6255 Publisher: Nature Publishing Group, 1990.

Lelieveld, J., Evans, J. S., Fnais, M., Giannadaki, D., and Pozzer, A.: The contribution of outdoor air pollution sources to premature mortality on a global scale, Nature, 525, 367–371, https://doi.org/10.1038/nature15371, URL https://www.nature.com/articles/nature15371, number: 7569 Publisher: Nature Publishing Group, 2015.

Li, C., Martin, R. V., Cohen, R. C., Bindle, L., Zhang, D., Chatterjee, D., Weng, H., and Lin, J.: Variable effects of spatial resolution on modeling of nitrogen

oxides, Atmospheric Chemistry and Physics, 23, 3031–3049, https://doi.org/10.5194/acp-23-3031-2023, URL https://acp.copernicus.org/articles/23/3031/2023/, publisher: Copernicus GmbH, 2023a.

Li, Y., Martin, R. V., Li, C., Boys, B. L., Van Donkelaar, A., Meng, J., and Pierce, J. R.: Development and evaluation of processes affecting simulation of diel fine particulate matter variation in the GEOS-Chem model, preprint, Aerosols/Atmospheric Modelling and Data Analysis/Troposphere/Chemistry (chemical composition and reactions), https://doi.org/10.5194/egusphere-2023-704, URL https://egusphere.copernicus.org/preprints/2023/egusphere-2023-704/, 2023b.

Lin, C., Heal, M. R., Vieno, M., MacKenzie, I. A., Armstrong, B. G., Butland, B. K., Milojevic, A., Chalabi, Z., Atkinson, R. W., Stevenson, D. S., Doherty, R. M., and Wilkinson, P.: Spatiotemporal evaluation of EMEP4UK-WRF v4.3 atmospheric chemistry transport simulations of health-related metrics for NO2, O3, PM10, and PM2.5 for 2001-2010, Geoscientific Model Development, 10, 1767–1787, https://doi.org/10.5194/gmd-10-1767-2017, 2017.

Lin, H., Feng, X., Fu, T.-M., Tian, H., Ma, Y., Zhang, L., Jacob, D. J., Yantosca, R. M., Sulprizio, M. P., Lundgren, E. W., Zhuang, J., Zhang, Q., Lu, X., Zhang, L., Shen, L., Guo, J., Eastham, S. D., and Keller, C. A.: WRF-GC (v1.0): online coupling of WRF (v3.9.1.1) and GEOS-Chem (v12.2.1) for regional atmospheric chemistry modeling – Part 1: Description of the one-way model, Geoscientific Model Development, 13, 3241–3265, https://doi.org/10.5194/gmd-13-3241-2020, URL https://gmd.copernicus.org/articles/13/3241/2020/, publisher: Copernicus GmbH, 2020.

Lin, H., Jacob, D. J., Lundgren, E. W., Sulprizio, M. P., Keller, C. A., Fritz, T. M., Eastham, S. D., Emmons, L. K., Campbell, P. C., Baker, B., Saylor, R. D., and Montuoro, R.: Harmonized Emissions Component (HEMCO) 3.0 as a versatile emissions component for atmospheric models: application in the GEOS-Chem, NASA GEOS, WRF-GC, CESM2, NOAA GEFS-Aerosol,

and NOAA UFS models, Geoscientific Model Development, 14, 5487–5506, https://doi.org/10.5194/gmd-14-5487-2021, URL https://gmd.copernicus.org/articles/14/5487/2021/, publisher: Copernicus GmbH, 2021.

Lin, H., Long, M. S., Sander, R., Sandu, A., Yantosca, R. M., Estrada, L. A., Shen, L., and Jacob, D. J.: An Adaptive Auto-Reduction Solver for Speeding Up Integration of Chemical Kinetics in Atmospheric Chemistry Models: Implementation and Evaluation in the Kinetic Pre-Processor (KPP) Version 3.0.0, Journal of Advances in Modeling Earth Systems, 15, e2022MS003 293, https://doi.org/https://doi.org/10.1029/2022MS003293, URL https://agupubs.onlinelibrary.wiley.com/doi/abs/10.1029/2022MS003293, e2022MS003293 2022MS003293, 2023.

Lin, J.-T. and McElroy, M. B.: Impacts of boundary layer mixing on pollutant vertical profiles in the lower troposphere: Implications to satellite remote sensing, Atmospheric Environment, 44, 1726–1739, https://doi.org/10.1016/j.atmosenv.2010.02.009, URL https://www.sciencedirect.com/science/article/pii/S1352231010001147, 2010.

Lin, J.-T., Youn, D., Liang, X.-Z., and Wuebbles, D. J.: Global model simulation of summertime US ozone diurnal cycle and its sensitivity to PBL mixing, spatial resolution, and emissions, Atmospheric Environment, 42, 8470–8483, 2008.

Lin, S.-J. and Rood, R. B.: Multidimensional flux-form semi-Lagrangian transport schemes, Monthly Weather Review, 124, 2046–2070, 1996.

Liu, H., Jacob, D. J., Bey, I., and Yantosca, R. M.: Constraints from 210Pb and 7Be on wet deposition and transport in a global three-dimensional chemical tracer model driven by assimilated meteorological fields, Journal of Geophysical Research: Atmospheres, 106, 12 109–12 128, https://doi.org/10.1029/2000JD900839, URL https://onlinelibrary.wiley.com/doi/abs/10.1029/2000JD900839, _eprint: https://onlinelibrary.wiley.com/doi/pdf/10.1029/2000JD900839, 2001.

Liu, H., Crawford, J. H., Pierce, R. B., Norris, P., Platnick, S. E., Chen, G., Logan, J. A., Yantosca, R. M., Evans, M. J., Kittaka, C., and others: Radiative effect of clouds on tropospheric chemistry in a global three-dimensional chemical transport model, Journal of Geophysical Research: Atmospheres, 111, publisher: Wiley Online Library, 2006.

Liu, H., Crawford, J. H., Considine, D. B., Platnick, S., Norris, P. M., Duncan, B. N., Pierce, R. B., Chen, G., and Yantosca, R. M.: Sensitivity of photolysis frequencies and key tropospheric oxidants in a global model to cloud vertical distributions and optical properties, Journal of Geophysical Research: Atmospheres, 114, publisher: Wiley Online Library, 2009.

Liu, S. and Liang, X.-Z.: Observed Diurnal Cycle Climatology of Planetary Boundary Layer Height, Journal of Climate, 23, 5790–5809, https://doi.org/10.1175/2010JCLI3552.1, URL https://journals.ametsoc.org/view/journals/clim/23/21/2010jcli3552.1.xml, publisher: American Meteorological Society Section: Journal of Climate, 2010.

Liu, Z.: Investigating tropospheric and surface ozone sensitivity from present day to future, Ph.D. thesis, https://doi.org/10.7488/era/2293, URL https://era.ed.ac.uk/handle/1842/39042, accepted: 2022-06-07T10:07:40Z Publisher: The University of Edinburgh, 2022.

Logan, J. A.: Tropospheric ozone: Seasonal behavior, trends, and anthropogenic influence, Journal of Geophysical Research: Atmospheres, 90, 10 463–10 482, publisher: Wiley Online Library, 1985.

Mailler, S., Khvorostyanov, D., and Menut, L.: Impact of the vertical emission profiles on background gas-phase pollution simulated from the EMEP emissions over Europe, Atmospheric Chemistry and Physics, 13, 5987–5998, https://doi.org/10.5194/ACP-13-5987-2013, 2013.

Manabe, S. and Strickler, R. F.: Thermal Equilibrium of the Atmosphere with a Convective Adjustment, Journal of the Atmospheric Sciences, 21, 361–385,

https://doi.org/10.1175/1520-0469(1964)021<0361:TEOTAW>2.0.CO;2, URL `https://journals.ametsoc.org/view/journals/atsc/21/4/1520-0469_1964_021_0361_teotaw_2_0_co_2.xml`, publisher: American Meteorological Society Section: Journal of the Atmospheric Sciences, 1964.

Manisalidis, I., Stavropoulou, E., Stavropoulos, A., and Bezirtzoglou, E.: Environmental and Health Impacts of Air Pollution: A Review, Frontiers in Public Health, 8, 14, https://doi.org/10.3389/fpubh.2020.00014, URL `https://www.ncbi.nlm.nih.gov/pmc/articles/PMC7044178/`, 2020.

Mao, J., Jacob, D. J., Evans, M. J., Olson, J. R., Ren, X., Brune, W. H., Clair, J. M. S., Crounse, J. D., Spencer, K. M., Beaver, M. R., Wennberg, P. O., Cubison, M. J., Jimenez, J. L., Fried, A., Weibring, P., Walega, J. G., Hall, S. R., Weinheimer, A. J., Cohen, R. C., Chen, G., Crawford, J. H., McNaughton, C., Clarke, A. D., Jaeglé, L., Fisher, J. A., Yantosca, R. M., Le Sager, P., and Carouge, C.: Chemistry of hydrogen oxide radicals (HO_x) in the Arctic troposphere in spring, Atmospheric Chemistry and Physics, 10, 5823–5838, https://doi.org/10.5194/acp-10-5823-2010, URL `https://acp.copernicus.org/articles/10/5823/2010/acp-10-5823-2010.html`, publisher: Copernicus GmbH, 2010.

Marais, E. A., Jacob, D. J., Jimenez, J. L., Campuzano-Jost, P., Day, D. A., Hu, W., Krechmer, J., Zhu, L., Kim, P. S., Miller, C. C., Fisher, J. A., Travis, K., Yu, K., Hanisco, T. F., Wolfe, G. M., Arkinson, H. L., Pye, H. O. T., Froyd, K. D., Liao, J., and McNeill, V. F.: Aqueous-phase mechanism for secondary organic aerosol formation from isoprene: application to the southeast United States and co-benefit of SO_2 emission controls, Atmospheric Chemistry and Physics, 16, 1603–1618, https://doi.org/10.5194/acp-16-1603-2016, URL `https://acp.copernicus.org/articles/16/1603/2016/`, publisher: Copernicus GmbH, 2016.

Marais, E. A., Pandey, A. K., Van Damme, M., Clarisse, L., Coheur, P. F., Shephard, M. W., Cady-Pereira, K. E., Misselbrook, T., Zhu, L., Luo, G., and Yu, F.: UK Ammonia Emissions Estimated With Satellite Observations and GEOS-

Chem, Journal of Geophysical Research: Atmospheres, 126, https://doi.org/10.1029/2021JD035237, 2021.

Martin, R. V., Eastham, S. D., Bindle, L., Lundgren, E. W., Clune, T. L., Keller, C. A., Downs, W., Zhang, D., Lucchesi, R. A., Sulprizio, M. P., and others: Improved advection, resolution, performance, and community access in the new generation (version 13) of the high-performance GEOS-Chem global atmospheric chemistry model (GCHP), Geoscientific model development, 15, 8731–8748, publisher: Copernicus GmbH, 2022.

Matsui, H., Koike, M., Takegawa, N., Kondo, Y., Griffin, R. J., Miyazaki, Y., Yokouchi, Y., and Ohara, T.: Secondary organic aerosol formation in urban air: Temporal variations and possible contributions from unidentified hydrocarbons, Journal of Geophysical Research: Atmospheres, 114, https://doi.org/10.1029/2008JD010164, URL https://onlinelibrary.wiley.com/doi/abs/10.1029/2008JD010164, _eprint: https://onlinelibrary.wiley.com/doi/pdf/10.1029/2008JD010164, 2009.

McDuffie, E. E., Smith, S. J., O'Rourke, P., Tibrewal, K., Venkataraman, C., Marais, E. A., Zheng, B., Crippa, M., Brauer, M., and Martin, R. V.: A global anthropogenic emission inventory of atmospheric pollutants from sector- And fuel-specific sources (1970-2017): An application of the Community Emissions Data System (CEDS), Earth System Science Data, 12, 3413–3442, https://doi.org/10.5194/essd-12-3413-2020, 2020.

McDuffie, E. E., Martin, R. V., Spadaro, J. V., Burnett, R., Smith, S. J., O'Rourke, P., Hammer, M. S., van Donkelaar, A., Bindle, L., Shah, V., Jaeglé, L., Luo, G., Yu, F., Adeniran, J. A., Lin, J., and Brauer, M.: Source sector and fuel contributions to ambient PM2.5 and attributable mortality across multiple spatial scales, Nature Communications, 12, 3594, https://doi.org/10.1038/s41467-021-23853-y, URL https://www.nature.com/articles/s41467-021-23853-y, number: 1 Publisher: Nature Publishing Group, 2021.

Mellouki, A., Wallington, T., and Chen, J.: Atmospheric chemistry of oxygenated

volatile organic compounds: impacts on air quality and climate, Chemical reviews, 115, 3984–4014, 2015.

Meng, J., Martin, R. V., Ginoux, P., Hammer, M., Sulprizio, M. P., Ridley, D. A., and van Donkelaar, A.: Grid-independent high-resolution dust emissions (v1.0) for chemical transport models: application to GEOS-Chem (12.5.0), Geoscientific Model Development, 14, 4249–4260, https://doi.org/10.5194/gmd-14-4249-2021, URL `https://gmd.copernicus.org/articles/14/4249/2021/`, publisher: Copernicus GmbH, 2021.

Millet, D. B., Guenther, A., Siegel, D. A., Nelson, N. B., Singh, H. B., de Gouw, J. A., Warneke, C., Williams, J., Eerdekens, G., Sinha, V., Karl, T., Flocke, F., Apel, E., Riemer, D. D., Palmer, P. I., and Barkley, M.: Global atmospheric budget of acetaldehyde: 3-D model analysis and constraints from in-situ and satellite observations, Atmospheric Chemistry and Physics, 10, 3405–3425, https://doi.org/10.5194/acp-10-3405-2010, URL `https://acp.copernicus.org/articles/10/3405/2010/acp-10-3405-2010.html`, publisher: Copernicus GmbH, 2010.

Millet, D. B., Baasandorj, M., Farmer, D. K., Thornton, J. A., Baumann, K., Brophy, P., Chaliyakunnel, S., de Gouw, J. A., Graus, M., Hu, L., and others: A large and ubiquitous source of atmospheric formic acid, Atmospheric Chemistry and Physics, 15, 6283–6304, publisher: Copernicus GmbH, 2015.

Mircea, M., Bessagnet, B., D'Isidoro, M., Pirovano, G., Aksoyoglu, S., Ciarelli, G., Tsyro, S., Manders, A., Bieser, J., Stern, R., Vivanco, M. G., Cuvelier, C., Aas, W., Prévôt, A. S. H., Aulinger, A., Briganti, G., Calori, G., Cappelletti, A., Colette, A., Couvidat, F., Fagerli, H., Finardi, S., Kranenburg, R., Rouïl, L., Silibello, C., Spindler, G., Poulain, L., Herrmann, H., Jimenez, J. L., Day, D. A., Tiitta, P., and Carbone, S.: EURODELTA III exercise: An evaluation of air quality models' capacity to reproduce the carbonaceous aerosol, Atmospheric Environment: X, 2, 100 018, https://doi.org/10.1016/j.aeaoa.2019.100018, URL `ht`

tps://www.sciencedirect.com/science/article/pii/S2590162119300218, 2019.

Monahan, E. C., Spiel, D. E., and Davidson, K. L.: A Model of Marine Aerosol Generation Via Whitecaps and Wave Disruption, in: Oceanic Whitecaps: And Their Role in Air-Sea Exchange Processes, edited by Monahan, E. C. and Niocaill, G. M., Oceanographic Sciences Library, pp. 167–174, Springer Netherlands, Dordrecht, https://doi.org/10.1007/978-94-009-4668-2_16, URL https://doi.org/10.1007/978-94-009-4668-2_16, 1986.

Monks, P. S.: A review of the observations and origins of the spring ozone maximum, Atmospheric Environment, 34, 3545–3561, https://doi.org/10.1016/S1352-2310(00)00129-1, iSBN: 4411625237, 2000.

Monson, R. K., Jaeger, C. H., Adams, III, W. W., Driggers, E. M., Silver, G. M., and Fall, R.: Relationships among Isoprene Emission Rate, Photosynthesis, and Isoprene Synthase Activity as Influenced by Temperature 1, Plant Physiology, 98, 1175–1180, https://doi.org/10.1104/pp.98.3.1175, URL https://doi.org/10.1104/pp.98.3.1175, 1992.

Murray, L. T., Jacob, D. J., Logan, J. A., Hudman, R. C., and Koshak, W. J.: Optimized regional and interannual variability of lightning in a global chemical transport model constrained by LIS/OTD satellite data, Journal of Geophysical Research: Atmospheres, 117, https://doi.org/10.1029/2012JD017934, URL https://onlinelibrary.wiley.com/doi/abs/10.1029/2012JD017934, _eprint: https://onlinelibrary.wiley.com/doi/pdf/10.1029/2012JD017934, 2012.

National Research Council: Rethinking the Ozone Problem in Urban and Regional Air Pollution, National Academies Press, google-Books-ID: J2MSJI7LY2AC, 1992.

Nawaz, M. O., Henze, D. K., Anenberg, S. C., Braun, C., Miller, J., and Pronk, E.: A Source Apportionment and Emission Scenario Assessment of PM2.5- and O3-Related Health Impacts in G20 Countries, GeoHealth,

7, e2022GH000 713, https://doi.org/10.1029/2022GH000713, URL `https://onlinelibrary.wiley.com/doi/abs/10.1029/2022GH000713`, _eprint: https://onlinelibrary.wiley.com/doi/pdf/10.1029/2022GH000713, 2023.

Nowlan, C. R., González Abad, G., Kwon, H.-A., Ayazpour, Z., Chan Miller, C., Chance, K., Chong, H., Liu, X., O'Sullivan, E., Wang, H., and others: Global Formaldehyde Products From the Ozone Mapping and Profiler Suite (OMPS) Nadir Mappers on Suomi NPP and NOAA-20, Earth and Space Science, 10, e2022EA002 643, publisher: Wiley Online Library, 2023.

Oikonomakis, E., Aksoyoglu, S., Ciarelli, G., Baltensperger, U., and Prévôt, A. S. H.: Low modeled ozone production suggests underestimation of precursor emissions (especially NOx) in Europe, Atmospheric Chemistry and Physics, 18, 2175–2198, https://doi.org/10.5194/acp-18-2175-2018, 2018.

Orellano, P., Reynoso, J., and Quaranta, N.: Short-term exposure to sulphur dioxide (SO2) and all-cause and respiratory mortality: A systematic review and meta-analysis, Environment International, 150, 106 434, https://doi.org/10.1016/j.envint.2021.106434, URL `https://www.ncbi.nlm.nih.gov/pmc/articles/PMC7937788/`, 2021.

Organization, W. H.: WHO global air quality guidelines: particulate matter (PM2.5 and PM10), ozone, nitrogen dioxide, sulfur dioxide and carbon monoxide, Tech. rep., World Health Organization, type: Publications, 2021.

Pai, S. J., Heald, C. L., Pierce, J. R., Farina, S. C., Marais, E. A., Jimenez, J. L., Campuzano-Jost, P., Nault, B. A., Middlebrook, A. M., Coe, H., Shilling, J. E., Bahreini, R., Dingle, J. H., and Vu, K.: An evaluation of global organic aerosol schemes using airborne observations, Atmospheric Chemistry and Physics, 20, 2637–2665, https://doi.org/10.5194/acp-20-2637-2020, iSBN: 2026372020, 2020.

Pandey, P. and Yadav, R.: A review on volatile organic compounds (VOCs) as

environmental pollutants: fate and distribution, International Journal of Plant and Environment, 4, 2018.

Park, M., Joo, H. S., Lee, K., Jang, M., Kim, S. D., Kim, I., Borlaza, L. J. S., Lim, H., Shin, H., Chung, K. H., et al.: Differential toxicities of fine particulate matters from various sources, Scientific reports, 8, 17 007, 2018.

Park, R. J., Jacob, D. J., Field, B. D., Yantosca, R. M., and Chin, M.: Natural and transboundary pollution influences on sulfate-nitrate-ammonium aerosols in the United States: Implications for policy, Journal of Geophysical Research: Atmospheres, 109, https://doi.org/10.1029/2003JD004473, URL `https://online library.wiley.com/doi/full/10.1029/2003JD004473`, publisher: John Wiley & Sons, Ltd, 2004.

Parrish, D. D., Law, K. S., Staehelin, J., Derwent, R., Cooper, O. R., Tanimoto, H., Volz-Thomas, A., Gilge, S., Scheel, H.-E., Steinbacher, M., and Chan, E.: Lower tropospheric ozone at northern midlatitudes: Changing seasonal cycle, Geophysical Research Letters, 40, 1631–1636, https://doi.org/10.1002/grl.5030 3, URL `https://onlinelibrary.wiley.com/doi/abs/10.1002/grl.50303`, _eprint: https://onlinelibrary.wiley.com/doi/pdf/10.1002/grl.50303, 2013.

Passant, N.: Speciation of UK emissions of non-methane volatile organic compounds, AEA Technology, URL `https://uk-air.defra.gov.uk/assets/docum ents/reports/empire/AEAT_ENV_0545_final_v2.pdf`, 2002.

Philip, S., Martin, R. V., and Keller, C. A.: Sensitivity of chemistry-transport model simulations to the duration of chemical and transport operators: a case study with GEOS-Chem v10-01, Geoscientific Model Development, 9, 1683–1695, https://doi.org/10.5194/gmd-9-1683-2016, URL `https://gmd.copernicus.org/a rticles/9/1683/2016/gmd-9-1683-2016.html`, publisher: Copernicus GmbH, 2016.

Philip, S., Martin, R. V., Snider, G., Weagle, C. L., Donkelaar, A. v., Brauer, M., Henze, D. K., Klimont, Z., Venkataraman, C., Guttikunda, S. K., and Zhang,

Q.: Anthropogenic fugitive, combustion and industrial dust is a significant, underrepresented fine particulate matter source in global atmospheric models, Environmental Research Letters, 12, 044 018, https://doi.org/10.1088/1748-9326/aa65a4, URL `https://dx.doi.org/10.1088/1748-9326/aa65a4`, publisher: IOP Publishing, 2017.

Pope, R. J., Butt, E. W., Chipperfield, M. P., Doherty, R. M., Fenech, S., Schmidt, A., Arnold, S. R., and Savage, N. H.: The impact of synoptic weather on UK surface ozone and implications for premature mortality, Environmental Research Letters, 11, 124 004, https://doi.org/10.1088/1748-9326/11/12/124004, URL `https://dx.doi.org/10.1088/1748-9326/11/12/124004`, publisher: IOP Publishing, 2016.

Pound, R. J., Sherwen, T., Helmig, D., Carpenter, L. J., and Evans, M. J.: Influences of oceanic ozone deposition on tropospheric photochemistry, Atmospheric Chemistry and Physics, 20, 4227–4239, publisher: Copernicus GmbH, 2020.

Pregger, T. and Friedrich, R.: Effective pollutant emission heights for atmospheric transport modelling based on real-world information, Environmental Pollution, 157, 552–560, publisher: Elsevier, 2009.

Prinn, R. G., Weiss, R. F., Arduini, J., Arnold, T., DeWitt, H. L., Fraser, P. J., Ganesan, A. L., Gasore, J., Harth, C. M., Hermansen, O., et al.: History of chemically and radiatively important atmospheric gases from the Advanced Global Atmospheric Gases Experiment (AGAGE), Earth System Science Data, 10, 985–1018, 2018.

Pun, B. K., Wu, S.-Y., Seigneur, C., Seinfeld, J. H., Griffin, R. J., and Pandis, S. N.: Uncertainties in Modeling Secondary Organic Aerosols: Three-Dimensional Modeling Studies in Nashville/Western Tennessee, Environmental Science & Technology, 37, 3647–3661, https://doi.org/10.1021/es0341541, URL `https://doi.org/10.1021/es0341541`, publisher: American Chemical Society, 2003.

Putman, W. M. and Lin, S.-J.: Finite-volume transport on various cubed-sphere grids, Journal of Computational Physics, 227, 55–78, https://doi.org/10.1016/j.jcp.2007.07.022, URL `https://linkinghub.elsevier.com/retrieve/pii/S0021999107003105`, 2007.

Pye, H., Chan, A., Barkley, M., and Seinfeld, J.: Global modeling of organic aerosol: the importance of reactive nitrogen (NO x and NO 3), Atmospheric Chemistry and Physics, 10, 11 261–11 276, publisher: Copernicus GmbH, 2010.

Pöschl, U.: Atmospheric aerosols: composition, transformation, climate and health effects, Angewandte Chemie (International Ed. in English), 44, 7520–7540, https://doi.org/10.1002/anie.200501122, 2005.

Randerson, J., Van Der Wef, G., Giglio, L., Collatz, G., and Kasibhatla, P.: Global Fire Emissions Database, Version 4.1 (GFEDv4), https://doi.org/10.3334/ORNL DAAC/1293, URL `https://daac.ornl.gov/cgi-bin/dsviewer.pl?ds_id=1293`, 2017.

Redington, A. L. and Derwent, R. G.: Modelling secondary organic aerosol in the United Kingdom, Atmospheric Environment, 64, 349–357, https://doi.org/10.1016/j.atmosenv.2012.09.074, URL `https://www.sciencedirect.com/science/article/pii/S135223101200951X`, 2013.

Redington, A. L., Derwent, R. G., Witham, C. S., and Manning, A. J.: Sensitivity of modelled sulphate and nitrate aerosol to cloud, pH and ammonia emissions, Atmospheric Environment, 43, 3227–3234, https://doi.org/10.1016/j.atmosenv.2009.03.041, URL `https://www.sciencedirect.com/science/article/pii/S1352231009002544`, 2009.

Ricardo: AURN QAQC Annual Technical Report 2021, 2021.

Romero-Alvarez, J., Lupaşcu, A., Lowe, D., Badia, A., Acher-nicholls, S., Dorling, S., Reeves, C. E., and Butler, T.: Sources of Surface O 3 in the UK : Tagging

O 3 within WRF-Chem, Atmospheric Chemistry and Physics Discussions, pp. 1–34, 2022.

Rosen, H., Hansen, A., Gundel, L., and Novakov, T.: Identification of the optically absorbing component in urban aerosols, Applied Optics, 17, 3859–3861, publisher: Optica Publishing Group, 1978.

Sakamoto, Y., Sadanaga, Y., Li, J., Matsuoka, K., Takemura, M., Fujii, T., Nakagawa, M., Kohno, N., Nakashima, Y., Sato, K., et al.: Relative and absolute sensitivity analysis on ozone production in Tsukuba, a city in Japan, Environmental science & technology, 53, 13 629–13 635, 2019.

Samaké, A., Bonin, A., Jaffrezo, J.-L., Taberlet, P., Weber, S., Uzu, G., Jacob, V., Conil, S., and Martins, J. M. F.: High levels of primary biogenic organic aerosols are driven by only a few plant-associated microbial taxa, Atmospheric Chemistry and Physics, 20, 5609–5628, https://doi.org/10.5194/acp-20-5609-2020, URL https://acp.copernicus.org/articles/20/5609/2020/, publisher: Copernicus GmbH, 2020.

Sandu, A. and Sander, R.: Technical note: Simulating chemical systems in Fortran90 and Matlab with the Kinetic PreProcessor KPP-2.1, Atmospheric Chemistry and Physics, 6, 187–195, https://doi.org/10.5194/acp-6-187-2006, URL https://acp.copernicus.org/articles/6/187/2006/, publisher: Copernicus GmbH, 2006.

Schaap, M., Cuvelier, C., Hendriks, C., Bessagnet, B., Baldasano, J. M., Colette, A., Thunis, P., Karam, D., Fagerli, H., Graff, A., and others: Performance of European chemistry transport models as function of horizontal resolution, Atmospheric Environment, 112, 90–105, publisher: Elsevier, 2015.

Schindlbacher, S., Matthews, B., and Ullrich, B.: Uncertainties and recalculations of emission inventories submitted under CLRTAP, URL https://www.ceip.at/fileadmin/inhalte/ceip/00_pdf_other/2021/uncertainties_and_recalculations_of_emission_inventories_submitted_under_clrtap.pdf, 2021.

Schumann, U. and Huntrieser, H.: The global lightning-induced nitrogen oxides source, Atmospheric Chemistry and Physics, 7, 3823–3907, https://doi.org/10.5194/acp-7-3823-2007, URL `https://acp.copernicus.org/articles/7/3823/2007/`, publisher: Copernicus GmbH, 2007.

Schwantes, R. H., Lacey, F. G., Tilmes, S., Emmons, L. K., Lauritzen, P. H., Walters, S., Callaghan, P., Zarzycki, C. M., Barth, M. C., Jo, D. S., and others: Evaluating the impact of chemical complexity and horizontal resolution on tropospheric ozone over the conterminous US with a global variable resolution chemistry model, Journal of Advances in Modeling Earth Systems, 14, e2021MS002 889, publisher: Wiley Online Library, 2022.

Screpanti, A. and De Marco, A.: Corrosion on cultural heritage buildings in Italy: a role for ozone?, Environmental pollution, 157, 1513–1520, publisher: Elsevier, 2009.

Seinfeld, J. H.: Air pollution: A half century of progress, AIChE Journal, 50, 1096–1108, publisher: Wiley Online Library, 2004.

Sharkey, T. D., Wiberley, A. E., and Donohue, A. R.: Isoprene Emission from Plants: Why and How, Annals of Botany, 101, 5–18, https://doi.org/10.1093/aob/mcm240, URL `https://www.ncbi.nlm.nih.gov/pmc/articles/PMC2701830/`, 2008.

Sharma, M., Kishore, S., Tripathi, S. N., and Behera, S. N.: Role of atmospheric ammonia in the formation of inorganic secondary particulate matter: A study at Kanpur, India, Journal of Atmospheric Chemistry, 58, 1–17, https://doi.org/10.1007/s10874-007-9074-x, URL `https://doi.org/10.1007/s10874-007-9074-x`, 2007.

Shen, L., J. Jacob, D., Santillana, M., Wang, X., and Chen, W.: An adaptive method for speeding up the numerical integration of chemical mechanisms in atmospheric chemistry models: Application to GEOS-Chem ver-

sion 12.0.0, Geoscientific Model Development, 13, 2475–2486, https://doi.org/10.5194/gmd-13-2475-2020, 2020.

Sherwen, T., Schmidt, J. A., Evans, M. J., Carpenter, L. J., Großmann, K., Eastham, S. D., Jacob, D. J., Dix, B., Koenig, T. K., Sinreich, R., et al.: Global impacts of tropospheric halogens (Cl, Br, I) on oxidants and composition in GEOS-Chem, Atmospheric Chemistry and Physics, 16, 12 239–12 271, 2016.

Sillanpää, M., Hillamo, R., Saarikoski, S., Frey, A., Pennanen, A., Makkonen, U., Spolnik, Z., Van Grieken, R., Braniš, M., Brunekreef, B., and others: Chemical composition and mass closure of particulate matter at six urban sites in Europe, Atmospheric Environment, 40, 212–223, publisher: Elsevier, 2006.

Sillman, S.: The use of NO y, H2O2, and HNO3 as indicators for ozone-NO x-hydrocarbon sensitivity in urban locations, Journal of Geophysical Research: Atmospheres, 100, 14 175–14 188, publisher: Wiley Online Library, 1995.

Sillman, S.: The relation between ozone, NOx and hydrocarbons in urban and polluted rural environments, Atmospheric Environment, 33, 1821–1845, https://doi.org/10.1016/S1352-2310(98)00345-8, URL https://www.sciencedirect.com/science/article/pii/S1352231098003458, 1999.

Sillman, S.: Tropospheric Ozone and Photochemical Smog, Treatise on Geochemistry, 9, 612, https://doi.org/10.1016/B0-08-043751-6/09053-8, URL https://ui.adsabs.harvard.edu/abs/2003TrGeo...9..407S, aDS Bibcode: 2003TrGeo...9..407S, 2003.

Sillman, S., Logan, J. A., and Wofsy, S. C.: The sensitivity of ozone to nitrogen oxides and hydrocarbons in regional ozone episodes, Journal of Geophysical Research: Atmospheres, 95, 1837–1851, https://doi.org/10.1029/JD095iD02p01837, URL https://onlinelibrary.wiley.com/doi/abs/10.1029/JD095iD02p01837, _eprint: https://onlinelibrary.wiley.com/doi/pdf/10.1029/JD095iD02p01837, 1990.

Simpson, D., Guenther, A., Hewitt, C. N., and Steinbrecher, R.: Biogenic emissions in Europe: 1. Estimates and uncertainties, Journal of Geophysical Research: Atmospheres, 100, 22 875–22 890, https://doi.org/10.1029/95JD02368, URL `https://onlinelibrary.wiley.com/doi/abs/10.1029/95JD02368`, _eprint: https://onlinelibrary.wiley.com/doi/pdf/10.1029/95JD02368, 1995.

Simpson, D., Fagerli, H., Jonson, J., Tsyro, S., Wind, P., and Tuovinen, J.: The EMEP Unified Eulerian Model. Model Description. EMEP MSC-W Report 1/2003, Norw. Meteorol. Inst., Oslo, Norway.(Available at http://www. emep. int), 2003.

Simpson, D., Benedictow, A., Berge, H., Bergström, R., Emberson, L. D., Fagerli, H., Flechard, C. R., Hayman, G. D., Gauss, M., Jonson, J. E., Jenkin, M. E., Nyúri, A., Richter, C., Semeena, V. S., Tsyro, S., Tuovinen, J. P., Valdebenito, A., and Wind, P.: The EMEP MSC-W chemical transport model – Technical description, Atmospheric Chemistry and Physics, 12, 7825–7865, https://doi.org/10.5194/acp-12-7825-2012, 2012a.

Simpson, D., Benedictow, A., Berge, H., Bergström, R., Emberson, L. D., Fagerli, H., Flechard, C. R., Hayman, G. D., Gauss, M., Jonson, J. E., Jenkin, M. E., Nyúri, A., Richter, C., Semeena, V. S., Tsyro, S., Tuovinen, J. P., Valdebenito, A., and Wind, P.: The EMEP MSC-W chemical transport model – Technical description, Atmospheric Chemistry and Physics, 12, 7825–7865, https://doi.org/10.5194/acp-12-7825-2012, 2012b.

Solazzo, E., Bianconi, R., Hogrefe, C., Curci, G., Tuccella, P., Alyuz, U., Balzarini, A., Baro, R., Bellasio, R., Bieser, J., Brandt, J., Christensen, J. H., Colette, A., Francis, X., Fraser, A., Garcia Vivanco, M., Jiménez-Guerrero, P., Im, U., Manders, A., Nopmongcol, U., Kitwiroon, N., Pirovano, G., Pozzoli, L., Prank, M., Sokhi, R. S., Unal, A., Yarwood, G., and Galmarini, S.: Evaluation and error apportionment of an ensemble of atmospheric chemistry transport modeling systems: Multivariable temporal and spatial breakdown, Atmospheric Chem-

istry and Physics, 17, 3001–3054, https://doi.org/10.5194/acp-17-3001-2017, 2017.

Solazzo, E., Crippa, M., Guizzardi, D., Muntean, M., Choulga, M., and Janssens-Maenhout, G.: Uncertainties in the Emissions Database for Global Atmospheric Research (EDGAR) emission inventory of greenhouse gases, Atmospheric Chemistry and Physics, 21, 5655–5683, https://doi.org/10.5194/acp-21-5655-2021, URL https://acp.copernicus.org/articles/21/5655/2021/, publisher: Copernicus GmbH, 2021.

Song, C. H., Chen, G., Hanna, S. R., Crawford, J., and Davis, D. D.: Dispersion and chemical evolution of ship plumes in the marine boundary layer: Investigation of O3/NOy/HOx chemistry, Journal of Geophysical Research: Atmospheres, 108, https://doi.org/10.1029/2002JD002216, URL https://onlinelibrary.wiley.com/doi/abs/10.1029/2002JD002216, _eprint: https://onlinelibrary.wiley.com/doi/pdf/10.1029/2002JD002216, 2003.

Song, H., Chen, X., Lu, K., Zou, Q., Tan, Z., Fuchs, H., Wiedensohler, A., Moon, D. R., Heard, D. E., Baeza-Romero, M.-T., et al.: Influence of aerosol copper on HO 2 uptake: a novel parameterized equation, Atmospheric Chemistry and Physics, 20, 15 835–15 850, 2020.

Song, H., Lu, K., Dong, H., Tan, Z., Chen, S., Zeng, L., and Zhang, Y.: Reduced Aerosol Uptake of Hydroperoxyl Radical May Increase the Sensitivity of Ozone Production to Volatile Organic Compounds, Environmental Science and Technology Letters, 9, 22–29, https://doi.org/10.1021/acs.estlett.1c00893, 2022.

Stavrakou, T., Müller, J. F., Boersma, K. F., De Smedt, I., and van der A, R. J.: Assessing the distribution and growth rates of NOx emission sources by inverting a 10-year record of NO2 satellite columns, Geophysical Research Letters, 35, 1–5, https://doi.org/10.1029/2008GL033521, 2008.

Stavrakou, T., Müller, J.-F., Boersma, K., Van Der A, R., Kurokawa, J., Ohara, T., and Zhang, Q.: Key chemical NO x sink uncertainties and how they influence

top-down emissions of nitrogen oxides, Atmospheric Chemistry and Physics, 13, 9057–9082, publisher: Copernicus GmbH, 2013.

Steinbacher, M., Zellweger, C., Schwarzenbach, B., Bugmann, S., Buchmann, B., Ordóñez, C., Prevot, A. S., and Hueglin, C.: Nitrogen oxide measurements at rural sites in Switzerland: Bias of conventional measurement techniques, Journal of Geophysical Research Atmospheres, 112, 1–13, https://doi.org/10.1 029/2006JD007971, 2007.

Stettler, M., Eastham, S., and Barrett, S.: Air quality and public health impacts of UK airports. Part I: Emissions, Atmospheric Environment, 45, 5415–5424, https://doi.org/10.1016/j.atmosenv.2011.07.012, URL https://linkinghub.els evier.com/retrieve/pii/S135223101100728X, 2011.

Stewart, H. E., Hewitt, C. N., Bunce, R. G. H., Steinbrecher, R., Smiatek, G., and Schoenemeyer, T.: A highly spatially and temporally resolved inventory for biogenic isoprene and monoterpene emissions: Model description and application to Great Britain, Journal of Geophysical Research: Atmospheres, 108, https://doi.org/10.1029/2002JD002694, URL https://on linelibrary.wiley.com/doi/abs/10.1029/2002JD002694, _eprint: https://onlinelibrary.wiley.com/doi/pdf/10.1029/2002JD002694, 2003.

Stock, Z. S., Russo, M. R., and Pyle, J. A.: Representing ozone extremes in European megacities: the importance of resolution in a global chemistry climate model, Atmospheric Chemistry and Physics, 14, 3899–3912, https://doi.org/ 10.5194/acp-14-3899-2014, URL https://acp.copernicus.org/articles/14/3 899/2014/acp-14-3899-2014.html, publisher: Copernicus GmbH, 2014.

Stull, R. B.: An introduction to boundary layer meteorology, vol. 13, Springer Science & Business Media, 1988.

Sutton, M. A., Reis, S., Riddick, S. N., Dragosits, U., Nemitz, E., Theobald, M. R., Tang, Y. S., Braban, C. F., Vieno, M., Dore, A. J., Mitchell, R. F., Wanless, S., Daunt, F., Fowler, D., Blackall, T. D., Milford, C., Flechard, C. R.,

Loubet, B., Massad, R., Cellier, P., Personne, E., Coheur, P. F., Clarisse, L., Van Damme, M., Ngadi, Y., Clerbaux, C., Skjøth, C. A., Geels, C., Hertel, O., Wichink Kruit, R. J., Pinder, R. W., Bash, J. O., Walker, J. T., Simpson, D., Horváth, L., Misselbrook, T. H., Bleeker, A., Dentener, F., and de Vries, W.: Towards a climate-dependent paradigm of ammonia emission and deposition, Philosophical Transactions of the Royal Society B: Biological Sciences, 368, 20130 166, https://doi.org/10.1098/rstb.2013.0166, URL `https://royalsocietypublishing.org/doi/10.1098/rstb.2013.0166`, publisher: Royal Society, 2013.

Syrakov, D., Prodanova, M., Georgieva, E., Etropolska, I., and Slavov, K.: Simulation of European air quality by WRF–CMAQ models using AQMEII-2 infrastructure, Journal of Computational and Applied Mathematics, 293, 232–245, https://doi.org/10.1016/j.cam.2015.01.032, URL `https://www.sciencedirect.com/science/article/pii/S0377042715000448`, 2016.

Tang, Y., Cape, J., Leith, I., Twigg, M., Coyle, M., Kentisbeer, J., Leeson, S., Di Marco, C., Nemitz, E., Bealey, W., et al.: UK Eutrophying and Acidifying Atmospheric Pollutants Monitoring networks UKEAP, 2013.

Thomas, F. W., Carpenter, S. B., and Gartrell, F. E.: Stacks-How High?, Journal of the Air Pollution Control Association, 13, 198–204, https://doi.org/10.1080/00022470.1963.10468165, URL `http://www.tandfonline.com/doi/abs/10.1080/00022470.1963.10468165`, 1963.

Thunis, P., Clappier, A., Beekmann, M., Putaud, J. P., Cuvelier, C., Madrazo, J., and de Meij, A.: Non-linear response of PM$_{2.5}$ to changes in NO$_x$ and NH$_3$ emissions in the Po basin (Italy): consequences for air quality plans, Atmospheric Chemistry and Physics, 21, 9309–9327, https://doi.org/10.5194/acp-21-9309-2021, URL `https://acp.copernicus.org/articles/21/9309/2021/`, publisher: Copernicus GmbH, 2021.

Tie, X., Wu, D., and Brasseur, G.: Lung cancer mortality and exposure to atmospheric aerosol particles in Guangzhou, China, Atmospheric Environment,

43, 2375–2377, https://doi.org/10.1016/j.atmosenv.2009.01.036, URL `https://www.sciencedirect.com/science/article/pii/S1352231009000661`, 2009.

Tie, X., Brasseur, G., and Ying, Z.: Impact of model resolution on chemical ozone formation in Mexico City: application of the WRF-Chem model, Atmospheric Chemistry and Physics, 10, 8983–8995, https://doi.org/10.5194/acp-10-8983-2010, URL `https://acp.copernicus.org/articles/10/8983/2010/acp-10-8983-2010.html`, publisher: Copernicus GmbH, 2010.

Tran, T., Kumar, N., and Knipping, E.: Investigating sensitivity of ozone to emission reductions in the New York City (NYC) metropolitan and downwind areas, Atmospheric Environment, 301, 119 675, https://doi.org/10.1016/j.atmosenv.2023.119675, URL `https://www.sciencedirect.com/science/article/pii/S1352231023001012`, 2023.

Travis, K. and Jacob, D.: Systematic bias in evaluating chemical transport models with maximum daily 8-hour average (MDA8) surface ozone for air quality applications, Geoscientific Model Development Discussions, pp. 1–13, https://doi.org/10.5194/gmd-2019-78, 2019.

Twigg, M. M., Ilyinskaya, E., Beccaceci, S., Green, D. C., Jones, M. R., Langford, B., Leeson, S. R., Lingard, J. J., Pereira, G. M., Carter, H., et al.: Impacts of the 2014–2015 Holuhraun eruption on the UK atmosphere, Atmospheric Chemistry and Physics, 16, 11 415–11 431, 2016.

Tzompa-Sosa, Z. A., Mahieu, E., Franco, B., Keller, C. A., Turner, A. J., Helmig, D., Fried, A., Richter, D., Weibring, P., Walega, J., Yacovitch, T. I., Herndon, S. C., Blake, D. R., Hase, F., Hannigan, J. W., Conway, S., Strong, K., Schneider, M., and Fischer, E. V.: Revisiting global fossil fuel and biofuel emissions of ethane, Journal of Geophysical Research, 122, 2493–2512, https://doi.org/10.1002/2016JD025767, 2017.

Vaughan, A. R., Lee, J. D., Misztal, P. K., Metzger, S., Shaw, M. D., Lewis, A. C., Purvis, R. M., Carslaw, D. C., Goldstein, A. H., Hewitt, C. N., Davison, B.,

Beevers, S. D., and Karl, T. G.: Spatially resolved flux measurements of NOX from London suggest significantly higher emissions than predicted by inventories, Faraday Discussions, 189, 455–472, https://doi.org/10.1039/c5fd00170f, publisher: Royal Society of Chemistry, 2016.

Vieno, M., Wind, P., Weston, K. J., Dore, A. J., Tarrasón, L., and Sutton, M. A.: Fine scale application of the EMEP unified air pollution model to the United Kingdom, in: 10th Harmonisation conference proceedings, Crete.< http://www. harmo. org/harmo10, 2005.

Vieno, M., Heal, M. R., Hallsworth, S., Famulari, D., Doherty, R. M., Dore, A. J., Tang, Y. S., Braban, C. F., Leaver, D., Sutton, M. A., and Reis, S.: The role of long-range transport and domestic emissions in determining atmospheric secondary inorganic particle concentrations across the UK, Atmospheric Chemistry and Physics, 14, 8435–8447, https://doi.org/10.5194/acp-14-8435-2014, URL https://acp.copernicus.org/articles/14/8435/2014/acp-14-8435-2014.html, publisher: Copernicus GmbH, 2014.

Vieno, M., Heal, M. R., Williams, M. L., Carnell, E. J., Stedman, J. R., and Reis, S.: Sensitivities of UK PM2.5 concentrations to emissions reductions, preprint, Aerosols/Atmospheric Modelling/Troposphere/Chemistry (chemical composition and reactions), https://doi.org/10.5194/acpd-15-20881-2015, URL https://acp.copernicus.org/preprints/15/20881/2015/acpd-15-20881-2015.pdf, 2015.

Vieno, M., Heal, M. R., Twigg, M. M., MacKenzie, I. A., Braban, C. F., Lingard, J. J., Ritchie, S., Beck, R. C., Móring, A., Ots, R., Di Marco, C. F., Nemitz, E., Sutton, M. A., and Reis, S.: The UK particulate matter air pollution episode of March-April 2014: More than Saharan dust, Environmental Research Letters, 11, https://doi.org/10.1088/1748-9326/11/4/044004, publisher: IOP Publishing, 2016a.

Vieno, M., Heal, M. R., Williams, M. L., Carnell, E. J., Nemitz, E., Stedman, J. R., and Reis, S.: The sensitivities of emissions reductions for the mitigation of

UK PM2.5, Atmospheric Chemistry and Physics, 16, 265–276, https://doi.org/10.5194/acp-16-265-2016, URL `https://acp.copernicus.org/articles/16/265/2016/`, 2016b.

Vijayaraghavan, K., Snell, H. E., and Seigneur, C.: Practical Aspects of Using Satellite Data in Air Quality Modeling, Environmental Science & Technology, 42, 8187–8192, https://doi.org/10.1021/es7031339, URL `https://doi.org/10.1021/es7031339`, publisher: American Chemical Society, 2008.

Vinken, G. C. M., Boersma, K. F., Jacob, D. J., and Meijer, E. W.: Accounting for non-linear chemistry of ship plumes in the GEOS-Chem global chemistry transport model, Atmospheric Chemistry and Physics, 11, 11 707–11 722, https://doi.org/10.5194/acp-11-11707-2011, URL `https://acp.copernicus.org/articles/11/11707/2011/acp-11-11707-2011.html`, publisher: Copernicus GmbH, 2011.

Volz, A. and Kley, D.: Evaluation of the Montsouris series of ozone measurements made in the nineteenth century, Nature, 332, 240–242, publisher: Nature Publishing Group UK London, 1988.

Wagner, P. and Kuttler, W.: Biogenic and anthropogenic isoprene in the near-surface urban atmosphere — A case study in Essen, Germany, Science of The Total Environment, 475, 104–115, https://doi.org/10.1016/J.SCITOTENV.2013.12.026, publisher: Elsevier, 2014.

Walker, H. L., Heal, M. R., Braban, C. F., Ritchie, S., Conolly, C., Sanocka, A., Dragosits, U., and Twigg, M. M.: Changing supersites: assessing the impact of the southern UK EMEP supersite relocation on measured atmospheric composition, Environmental Research Communications, 1, 041 001, 2019.

Wang, H., Lu, X., Jacob, D. J., Cooper, O. R., Chang, K.-L., Li, K., Gao, M., Liu, Y., Sheng, B., Wu, K., Wu, T., Zhang, J., Sauvage, B., Nédélec, P., Blot, R., and Fan, S.: Global tropospheric ozone trends, attributions, and radiative impacts in 1995–2017: an integrated analysis using aircraft (IA-

GOS) observations, ozonesonde, and multi-decadal chemical model simulations, Atmospheric Chemistry and Physics, 22, 13 753–13 782, https://doi.org/10.5194/acp-22-13753-2022, URL `https://acp.copernicus.org/articles/22/13753/2022/`, publisher: Copernicus GmbH, 2022.

Wang, X., Jacob, D. J., Downs, W., Zhai, S., Zhu, L., Shah, V., Holmes, C. D., Sherwen, T., Alexander, B., Evans, M. J., et al.: Global tropospheric halogen (Cl, Br, I) chemistry and its impact on oxidants, Atmospheric Chemistry and Physics, 21, 13 973–13 996, 2021.

Wang, Y., Jacob, D. J., and Logan, J. A.: Global simulation of tropospheric O3-NOx-hydrocarbon chemistry - 1. Model formulation, Journal of Geophysical Research: Atmospheres, 103, 10 713–10 725, https://doi.org/10.1029/98JD00158, publisher: Blackwell Publishing Ltd, 1998.

Wang, Y., Ma, Y.-F., Muñoz-Esparza, D., Dai, J., Li, C. W. Y., Lichtig, P., Tsang, R. C.-W., Liu, C.-H., Wang, T., and Brasseur, G. P.: Coupled mesoscale–microscale modeling of air quality in a polluted city using WRF-LES-Chem, Atmospheric Chemistry and Physics, 23, 5905–5927, https://doi.org/10.5194/acp-23-5905-2023, URL `https://acp.copernicus.org/articles/23/5905/2023/`, publisher: Copernicus GmbH, 2023.

Wang, Y. X., McElroy, M. B., Jacob, D. J., and Yantosca, R. M.: A nested grid formulation for chemical transport over Asia: Applications to CO, Journal of Geophysical Research: Atmospheres, 109, https://doi.org/10.1029/2004JD005237, URL `https://onlinelibrary.wiley.com/doi/abs/10.1029/2004JD005237`, _eprint: https://onlinelibrary.wiley.com/doi/pdf/10.1029/2004JD005237, 2004.

Weng, H., Lin, J., Martin, R., Millet, D. B., Jaeglé, L., Ridley, D., Keller, C., Li, C., Du, M., and Meng, J.: Global high-resolution emissions of soil NOx, sea salt aerosols, and biogenic volatile organic compounds, Scientific Data, 7, 148, https://doi.org/10.1038/s41597-020-0488-5, URL `https://www.nature.com/articles/s41597-020-0488-5`, number: 1 Publisher: Nature Publishing Group, 2020.

WHO: Ambient air pollution: A global assessment of exposure and burden of disease, Tech. rep., World Health Organization, publisher: World Health Organization, 2016.

WHO: Global ambient air pollution attributable deaths (update 2018), URL `www.who.int/data/gho/data/indicators/indicator-details/GHO/ambient-air-pollution-attributable-deaths`, 2018.

WHO: WHO global air quality guidelines: particulate matter (PM2.5 and PM10), ozone, nitrogen dioxide, sulfur dioxide and carbon monoxide, URL `https://www.who.int/publications/i/item/9789240034228`, 2021.

Wilson, S., Farren, N. J., Rose, R. A., Wilde, S. E., Davison, J., Wareham, J. V., Lee, J. D., and Carslaw, D. C.: The impact on passenger car emissions associated with the promotion and demise of diesel fuel, Environment International, 182, 108 330, 2023.

Wolfe, A. H. and Patz, J. A.: Reactive nitrogen and human health: acute and long-term implications, Ambio: A journal of the human environment, 31, 120–125, publisher: BioOne, 2002.

Wu, S., Mickley, L. J., Jacob, D. J., Logan, J. A., Yantosca, R. M., and Rind, D.: Why are there large differences between models in global budgets of tropospheric ozone?, Journal of Geophysical Research: Atmospheres, 112, https://doi.org/10.1029/2006JD007801, URL `https://onlinelibrary.wiley.com/doi/abs/10.1029/2006JD007801`, _eprint: https://onlinelibrary.wiley.com/doi/pdf/10.1029/2006JD007801, 2007.

Wyer, K. E., Kelleghan, D. B., Blanes-Vidal, V., Schauberger, G., and Curran, T. P.: Ammonia emissions from agriculture and their contribution to fine particulate matter: A review of implications for human health, Journal of Environmental Management, 323, 116 285, https://doi.org/10.1016/j.jenvman.2022.116285, URL `https://www.sciencedirect.com/science/article/pii/S0301479722018588`, 2022.

Xia, W., Wang, Y., Chen, S., Huang, J., Wang, B., Zhang, G. J., Zhang, Y., Liu, X., Ma, J., Gong, P., Jiang, Y., Wu, M., Xue, J., Wei, L., and Zhang, T.: Double Trouble of Air Pollution by Anthropogenic Dust, Environmental Science & Technology, 56, 761–769, https://doi.org/10.1021/acs.est.1c04779, URL https://doi.org/10.1021/acs.est.1c04779, publisher: American Chemical Society, 2022.

Xiao, Y., Logan, J. A., Jacob, D. J., Hudman, R. C., Yantosca, R., and Blake, D. R.: Global budget of ethane and regional constraints on U.S. sources, Journal of Geophysical Research Atmospheres, 113, 1–13, https://doi.org/10.1029/2007JD009415, 2008.

Xu, J.-W., Martin, R. V., Henderson, B. H., Meng, J., Öztaner, Y. B., Hand, J. L., Hakami, A., Strum, M., and Phillips, S. B.: Simulation of airborne trace metals in fine particulate matter over North America, Atmospheric Environment, 214, 116 883, publisher: Elsevier, 2019.

Yang, Y., Russell, L. M., Lou, S., Liao, H., Guo, J., Liu, Y., Singh, B., and Ghan, S. J.: Dust-wind interactions can intensify aerosol pollution over eastern China, Nature Communications, 8, 15 333, https://doi.org/10.1038/ncomms15333, URL https://www.nature.com/articles/ncomms15333, number: 1 Publisher: Nature Publishing Group, 2017.

Yang, Y., Smith, S. J., Wang, H., Lou, S., and Rasch, P. J.: Impact of Anthropogenic Emission Injection Height Uncertainty on Global Sulfur Dioxide and Aerosol Distribution, Journal of Geophysical Research: Atmospheres, 124, 4812–4826, https://doi.org/10.1029/2018JD030001, URL https://onlinelibrary.wiley.com/doi/full/10.1029/2018JD030001, publisher: John Wiley & Sons, Ltd, 2019.

Yin, J. and Harrison, R. M.: Pragmatic mass closure study for PM1.0, PM2.5 and PM10 at roadside, urban background and rural sites, Atmospheric Environment, 42, 980–988, https://doi.org/10.1016/j.atmosenv.2007.10.005, URL https://www.sciencedirect.com/science/article/pii/S1352231007008989, 2008.

Young, P., Archibald, A., Bowman, K., Lamarque, J.-F., Naik, V., Stevenson, D., Tilmes, S., Voulgarakis, A., Wild, O., Bergmann, D., and others: Pre-industrial to end 21st century projections of tropospheric ozone from the Atmospheric Chemistry and Climate Model Intercomparison Project (ACCMIP), Atmospheric Chemistry and Physics, 13, 2063–2090, publisher: Copernicus GmbH, 2013.

Yu, Y., Sokhi, R. S., Kitwiroon, N., Middleton, D. R., and Fisher, B.: Performance characteristics of MM5–SMOKE–CMAQ for a summer photochemical episode in southeast England, United Kingdom, Atmospheric Environment, 42, 4870–4883, https://doi.org/10.1016/j.atmosenv.2008.02.051, URL `https://www.sciencedirect.com/science/article/pii/S1352231008001830`, 2008.

Zhai, S., Jacob, D. J., Brewer, J. F., Li, K., Moch, J. M., Kim, J., Lee, S., Lim, H., Lee, H. C., Kuk, S. K., Park, R. J., Jeong, J. I., Wang, X., Liu, P., Luo, G., Yu, F., Meng, J., Martin, R. V., Travis, K. R., Hair, J. W., Anderson, B. E., Dibb, J. E., Jimenez, J. L., Campuzano-Jost, P., Nault, B. A., Woo, J.-H., Kim, Y., Zhang, Q., and Liao, H.: Interpretation of geostationary satellite aerosol optical depth (AOD) over East Asia in relation to fine particulate matter (PM$_{2.5}$): insights from the KORUS-AQ aircraft campaign and seasonality, preprint, Aerosols/Remote Sensing/Troposphere/Physics (physical properties and processes), https://doi.org/10.5194/acp-2021-413, URL `https://acp.copernicus.org/preprints/acp-2021-413/acp-2021-413.pdf`, 2021.

Zhang, C. and Stevenson, D.: Characteristic changes of ozone and its precursors in London during COVID-19 lockdown and the ozone surge reason analysis, Atmospheric Environment (Oxford, England : 1994), 273, 118 980, https://doi.org/10.1016/j.atmosenv.2022.118980, URL `https://www.ncbi.nlm.nih.gov/pmc/articles/PMC8815197/`, 2022.

Zhang, D., Martin, R. V., Bindle, L., Li, C., Eastham, S. D., van Donkelaar, A., and Gallardo, L.: Advances in Simulating the Global Spatial Heterogeneity of Air Quality and Source Sector Contributions: Insights into the Global South,

Environmental Science & Technology, 57, 6955–6964, https://doi.org/10.1021/acs.est.2c07253, URL https://doi.org/10.1021/acs.est.2c07253, publisher: American Chemical Society, 2023.

Zhang, L., Gong, S., Padro, J., and Barrie, L.: A size-segregated particle dry deposition scheme for an atmospheric aerosol module, Atmospheric environment, 35, 549–560, publisher: Elsevier, 2001.

Zhang, L., Jacob, D. J., Knipping, E. M., Kumar, N., Munger, J. W., Carouge, C. C., Van Donkelaar, A., Wang, Y. X., and Chen, D.: Nitrogen deposition to the United States: Distribution, sources, and processes, Atmospheric Chemistry and Physics, 12, 4539–4554, https://doi.org/10.5194/acp-12-4539-2012, 2012a.

Zhang, R., Khalizov, A., Wang, L., Hu, M., and Xu, W.: Nucleation and growth of nanoparticles in the atmosphere, Chemical reviews, 112, 1957–2011, 2012b.

Zhang, Y., Huang, J.-P., Henze, D. K., and Seinfeld, J. H.: Role of isoprene in secondary organic aerosol formation on a regional scale, Journal of Geophysical Research: Atmospheres, 112, https://doi.org/10.1029/2007JD008675, URL https://onlinelibrary.wiley.com/doi/abs/10.1029/2007JD008675, _eprint: https://onlinelibrary.wiley.com/doi/pdf/10.1029/2007JD008675, 2007.